ACOUSTIC EMISSION SIGNAL ANALYSIS

by

John Michael Carlyle

A thesis submitted for the degree of
Doctor of Philosophy in Physics
at Brunel University,
Uxbridge, England

1982

ABSTRACT

An extension of acoustic emission technology was made which permits identification of probable source mechanisms for signals emitted during the failure of metals. This was achieved through the construction of a unique instrument and the development of special computer programs. The instrument permitted wideband digital waveform recordings to be made of both acoustic emission signals generated during the failure of a specimen, as well as calibration signals derived from a helium gas jet. These recordings were then processed by the computer programs to yield power spectra insensitive to specimen geometry, thus allowing the direct comparison of acoustic emissions from different specimens. A series of experiments conducted to test the instrument and the programs resulted in the conclusion that, at the 95% confidence level, acoustic emission caused by brittle particle fracture in 7039 aluminum could be differentiated from acoustic emission caused by the discontinuous movement of a crack in 4340 steel. Detailed descriptions of acoustic emission source modeling, transducer operating principles, calibration techniques and digital signal processing provide the necessary theoretical background for the reported technology extension, while a comprehensive review of the literature of acoustic emission places the experimental work into the proper context.

ACKNOWLEDGEMENTS

During the period while this research was being performed I was employed at the Naval Air Development Center, Warminster, Pennsylvania. Without the financial support of this organization and the active encouragement of many people in the Aircraft and Crew System Technology Directorate this thesis would not exist. I wish to express to them my grateful appreciation for their efforts.

Special thanks is due to Dr. G.J. London for the role he played in motivating me to write this thesis. It is certain that without his support it could not have been done. My thanks also to my external advisor, Dr. W.R. Scott, my internal advisor, Dr. J. Blitz, and my friend, Prof. J. Awerbuch, for their helpful advice and constructive criticisms. Their guidance has assisted me in writing a more lucid thesis. I would also like to acknowledge the artistic assistance given to me by Mr. R.H. Dalrymple.

Finally, I wish to thank my family for their understanding during the last seven years. My concentration was aided considerably because for the most part their complaints were not acoustically emitted.

J.M.C.

TABLE OF CONTENTS

ABSTRACT ii

ACKNOWLEDGEMENTS iii

CHAPTER 1. INTRODUCTION

1.1 Problem Identification 1
1.2 Historical Review 5

CHAPTER 2. FUNDAMENTALS

2.1 Sources of Acoustic Emission 16
2.2 Source Models 30
2.3 Propagation Effects 48
2.4 Signal Detection 58

CHAPTER 3. CALIBRATION TECHNIQUES

3.1 Transducer Calibration 71
3.2 System Calibration 86

CHAPTER 4. SIGNAL PROCESSING CONCEPTS

4.1 Data Acquisition 96
4.2 Spectral Analysis 109

CHAPTER 5. INSTRUMENTATION CONSTRUCTION

5.1 Hardware 116
5.2 Software 134

CHAPTER 6. SIGNAL ANALYSIS RESEARCH

6.1 Objective 155
6.2 Experimental Design 157
6.3 Results 164
6.4 Data Analysis 181

CHAPTER 7. SUMMATION

7.1 General 200
7.2 Observations 205
7.3 Conclusions 206

APPENDICES

A. Fast Fourier Transform Theory 208
B. Computer Program Source Code 218

REFERENCES 303

CHAPTER 1

INTRODUCTION

This chapter identifies a problem in the current acoustic emission technology, namely, that there is no method for distinguishing among the probable source mechanisms of signals emitted during the failure of metals. A review of the literature of acoustic emission shows that development of such a signal discrimination technique would extend the applicability of acoustic emission monitoring.

1.1 Problem Identification

Nondestructive testing is an area of technology whose function is to characterize materials and structures without rendering them unfit for their intended purpose. Most commonly, nondestructive testing is utilized for detecting the presence of defects which would cause a component or structure to fail prematurely during its service life, but many other applications exist as well. These include the measurement of basic material properties such as density, speed of sound, elastic modulus, electrical conductivity and magnetic permeability as well as process control variables such as coating thickness, degree of heat treatment and amount of surface roughness. As might be expected from the diverse nature of these measurements, many different methods of nondestructive testing exist. For the primary task of detecting defects, however, the most popular nondestructive testing techniques are liquid penetrant, magnetic particle, penetrating radiation, eddy current, ultrasound and acoustic emission.

Acoustic emission is the youngest nondestructive testing technique, although as is shown in Section 1.2 the phenomenon itself has been recognized for centuries. Specifically, acoustic emission is the name given to stress waves emitted when a material reacts to decrease its internal energy. The fact that a lowering of internal energy can result in stress waves is a consequence of the first law of thermodynamics (energy is conserved). Conservation of energy, however, does not guarantee that acoustic emission will occur when a potentially dangerous defect grows in a material that is being loaded because the mode of energy partitioning can vary. Indeed, the first question that must be answered by a nondestructive testing engineer attempting to apply acoustic emission is whether the phenomenon may be expected to occur prior to the fracture of the article which is to be monitored. An important point to notice is that because of the manner in which the signals are generated acoustic emission monitoring is generally partially destructive, e.g., the specimen must suffer some degree of damage if emissions are to be produced.

The fact that acoustic emission is the result of processes occurring within a material has enormous practical significance which sets it apart from the other nondestructive defect detection methods mentioned previously. The other methods require that the article to be inspected be placed in an artificial environment in which an energy field is created for the purpose of establishing specific material-energy interactions which are perturbed by the presence of defects. Acoustic emission nondestructive testing, on the other hand, occurs in real-time and can be applied to an in-service article in its normal environment. Another important advantage is that the stress waves from the internal material processes can travel many meters (depending on the attenuation characteristics and geometry of the component). These two attributes theoretically permit all portions of a large structure in normal service to be continuously monitored for the presence of growing defects.

One fundamental problem exists which prevents the technique of acoustic emission from being applied on a routine basis for the continuous detection of flaws in important structures. This problem is that the technology that is currently used for processing acoustic emission signals cannot discriminate between signals in a fashion that will allow the positive identification of the material process which is the source of the acoustic emission. In view of this difficulty it is reasonable to ask why acoustic emission monitoring is considered useful at all. The answer is that acoustic emission monitoring is so sensitive that it can detect the presence of a crack long before it would be possible to do so with any other nondestructive testing method. For example, Carlyle and Scott [Ref 1] were able to detect the presence of a fatigue crack in a laboratory specimen by its acoustic emissions 100,000 cycles before it could be confirmed visually. This was accomplished in spite of the fact that acoustic emission from the testing machine's loading mechanism interfered with the acoustic emission from the crack. Carlyle and Scott did not discriminate between individual signals, but rather circumstantially associated a group of acoustic emission signals with the crack by using an instrument which they later patented [Ref 2].

There are, however, many situations in which continuous detection of defects is desirable and circumstances preclude the application of signal association methods. An example is the detection of cracks in the tubes of operating boilers. Such tubes typically become coated in service with a scale which cracks under the same conditions which can cause cracking of the tube itself. Another example is the detection of cracking in critical areas of aircraft structure. Cracks commonly start at fastener holes, but the same loading which causes cracks to form will usually cause fastener fretting first. Fretting is essentially harmless and is quite common, but the acoustic emission it generates cannot be readily differentiated from that caused by cracking. Without some means of signal source identification it would be impractical to apply acoustic emission monitoring in either of these example cases, since the boiler or aircraft would most probably be removed from service because of a benign process rather than a genuine crack which would warrant repair or retirement.

The intent of the work described herein was to extend the technology of acoustic emission nondestructive testing by developing methods for discriminating between acoustic emission signals, thereby permitting the identification of the material processes which caused the emitted acoustic emission signal. Such a technological extension would conceivably make economically feasible continuous defect detection in important structures, and thus prevent their possible catastrophic failure due to rarely occurring dangerous defects. Acoustic emission signal discrimination methods were developed by adapting digital signal processing techniques to the needs of acoustic emission technology. Since this had never been done before, it was necessary to build a unique acoustic emission system to acquire, digitize and record the signals. It was also necessary to write signal processing programs which yielded the desired discrimination. Finally, of course, it was necessary to prove through experimentation that the developed techniques worked. These major accomplishments are documented in Chapters 5 and 6, while the remainder of the thesis provides the reader with the requisite theoretical background.

1.2 Historical Review

A brief history of acoustic emission (taken from the author's master's thesis [Ref 3]) is appropriate to show the wide variety of situations in which the technique has been found useful. Applications for acoustic emission have been on the increase ever since 1950 when Josef Kaiser [Ref 4] published his pioneering work, but the phenomenon itself has been observed for hundreds of years. Tinsmiths have heard "tin cry" which is produced when the metal twins ever since ancient times, and steel workers have long noted audible clicks caused by martensitic transformations. Mine workers know well the ominous creaking sounds heard immediately prior to a cave-in, while construction workers are familiar with the crackling sound associated with the impending failure of overloaded wooden structures. The most dramatic example of acoustic emission occurs in the field of seismology, though, where stress waves are used to characterize fault movement (earthquakes) in terms of energy release, location and depth.

In materials research, the earliest mention of acoustic emission occurred in 1923 when the French metallurgists Portevin and LeChatelier [Ref 5] were studying the effects of large deformations on aluminum alloys. They noted that load drops which were accompanied by a Luder's line formation coincided with a specimen emitted noise; the "Portevin-LeChatelier effect" was subsequently found to occur in other metals which formed Luder's lines. Some time later Joffe and Ehrenfest [Ref 6] reported hearing noises from zinc and heated rock salt. They were studying shear deformation and discovered that as shear progressed in each material with a series of small jumps a noise like the tick of a clock was heard. Each tick could be correlated to a load drop and it was found that the rate of ticking was proportional to the applied load, with thousands of ticks occurring during a single test.

The next reported experiment involving acoustic emission occurred in 1948 when Mason, McSkimin and Shockley [Ref 7] undertook the investigation of dislocation movements induced by twinning tin. Their work is well worth noting for the simple fact that it remains today as one of the only observations of what is perhaps a true acoustic emission waveform. This feat was achieved through careful experimental design in which an acoustically matched sample and transducer were compressed between specially designed clamps to obtain an essentially broadband (resonance free) system. Their results are shown in Figure 1.1. Mason, McSkimin and Shockley concluded that the fine structure of the traces was characteristic of the twinning process, caused by the successive passage of twinning dislocations across the specimen at the speed of sound. This has never been confirmed, possibly because of the problems encountered in obtaining detectable signals with their system when using metals which do not twin as extensively as tin.

Josef Kaiser's research [Ref 4], published in 1950, is generally conceded to be the beginning of the present era in acoustic emission study because his work was the first investigation into the phenomenon of acoustic emission for its own sake. He employed transducers, amplifiers and oscilloscopes to study the faint noises he discovered to be present in polycrystalline zinc, steel, tin, brass, aluminum, copper and lead samples undergoing tensile tests. His conclusion that the emissions were produced primarily by grain boundary sliding has since been disproven, while his observation that the emissions were of two types, a low amplitude continuous sound with high amplitude bursts superimposed, has been confirmed many times. He also observed that the amplitude and frequency of the emissions were characteristic of the material and stress level. But perhaps his greatest contribution was the observation that acoustic emission activity appeared to be irreversible. Kaiser found that when a previously loaded sample was reloaded, no emissions were generated until the stress level exceeded its previous high. This behavior has been named the "Kaiser effect",

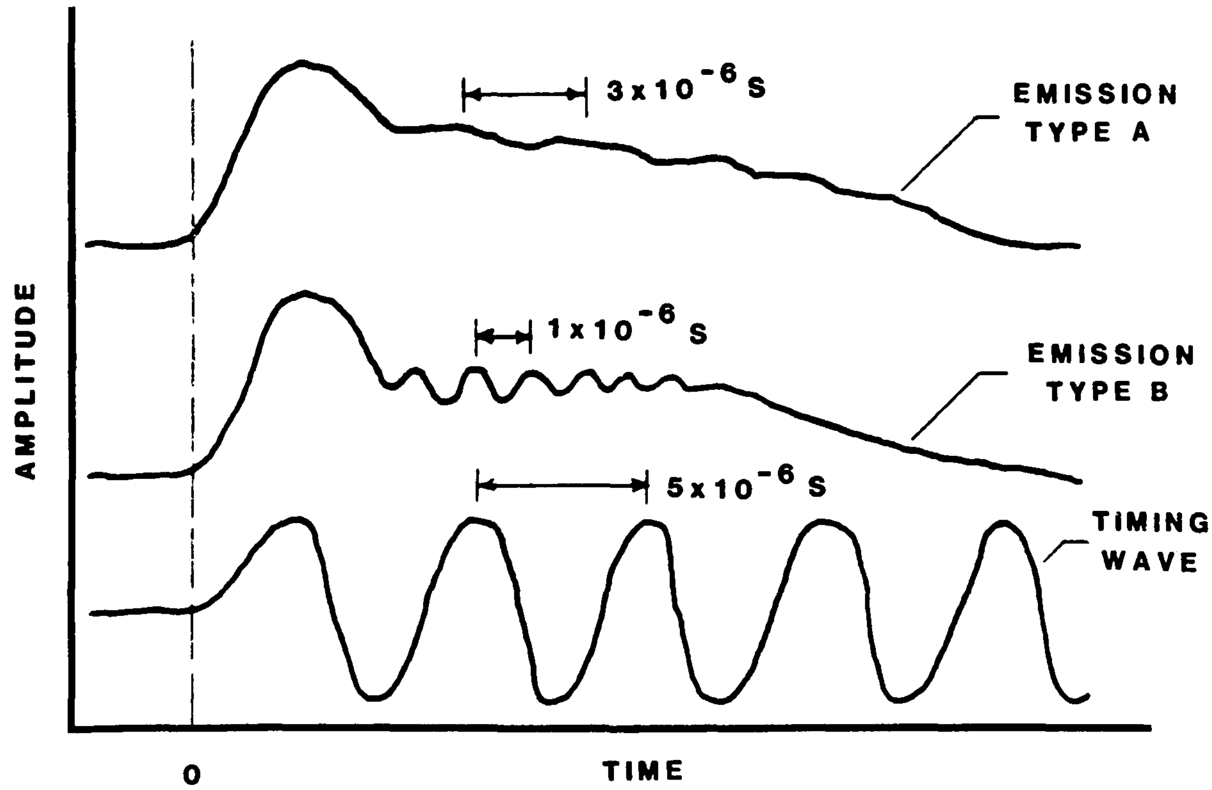

Figure 1.1. Characteristic emissions produced by the twinning of tin [Ref 7].

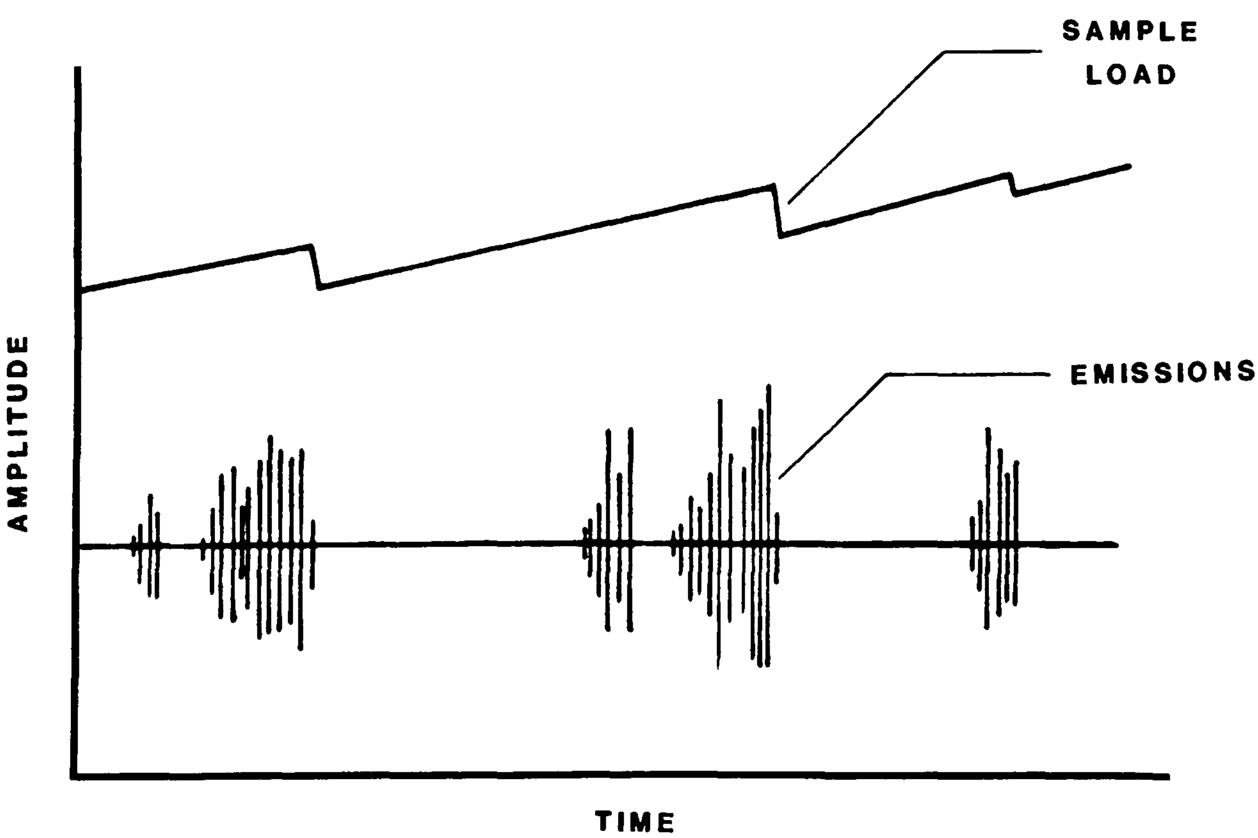

Figure 1.2. Emissions produced by Luder's line formation in soft steel [Ref 10].

and although a few materials (mainly composites) have since been found in which the effect does not occur, it is widely applicable and has been successfully utilized in determining the stresses which structures have undergone in service [Ref 8 and 9].

Kaiser's work was furthered in 1958 when the French metallurgists Lean, Plateau, Bachet and Crussard [Ref 10] reinvestigated the Portevin-LeChatelier effect using electronic instrumentation to record acoustic emission. They concluded that in soft steel emissions were generated at an early stage in Luder's line formation, since the noise was found to precede load drops by milliseconds as Figure 1.2 shows. Somewhat later Schofield [Ref 11] and Tatro [Ref 12] initiated research in the United States in an attempt to identify the sources of acoustic emission. Schofield [Ref 13] discovered that grain boundaries were not the sole sources of emissions since single crystals also emitted noise under stress. Further investigations using anodic etching techniques with polarity reversals and acoustic monitoring during twin formation lead him to conclude that dislocation motion was responsible for acoustic emission. Tatro and Liptai [Ref 14] supported this, suggesting that emission activity was related to the pile-up and breakaway of dislocations. They also reported that barriers to dislocation movement, such as surface oxide layers, changed the emission spectra.

In the meanwhile, geologists had discovered that acoustic emission could be used to detect impending mine collapse [Ref 15]. A series of studies was carried out in the United States in the early 1940's in an attempt to prevent rock bursts through better mining techniques, and similar studies were initiated in Russia in the late 1940's. The U.S. research efforts were discontinued around 1945, but in Russia the acoustic emission technique was adopted as standard mining practice and was used to identify geologically weak areas by the increase in emissions when a weak area was penetrated. The technique resulted in considerable economic benefits in the shoring requirements of mines, and improved operating safety at the same time. However, little interchange of information took place between materials engineers and geologists and it was not until 1964 that the "new" technique of acoustic emission was used to test the integrity of an engineering structure. This occurred when Green, Lockman and Steele [Ref 16] noticed that audible popping noises were emitted during routine hydraulic proof testing of Polaris rocket motors. Using accelerometers and frequency analysis equipment they devised two methods whereby the failure pressure of a rocket motor could be predicted. In the first method an average amplitude for the emissions which occurred during the first proof cycle was calculated and plotted against the burst pressure of the motor obtained during the second proof cycle. After a sufficient number of samples had been tested a curve was obtained which could be used to nondestructively determine the failure pressure of the rocket using only one proof cycle. Since there was a considerable amount of scatter in this method a second procedure was developed whereby a three-dimensional plot of emission amplitude at different frequencies as a function of hydraulic pressure was made during a proof test. This plot, coined a "missile-print" because of its close association with the voice-prints used in law enforcement, enabled better predictions of failure pressure to be made.

More significantly, it enabled Green, Lockman and Steele to predict the type of failure which would ultimately destroy the rocket by the patterns created in the plot.

Acoustic emission applications developed rapidly from this point, partly because of the relative simplicity of the instrumentation needed, but also because the inherent sensitivity of the technique (detection thresholds on the order of femtometers for displacement and milli-Pascals for pressure) enabled many microscopic processes occurring in materials to be studied. Metallurgists used the phenomenon to study martensitic transformations [Ref 17], where they found that martensite plates forming in microseconds could be detected. Flawed materials undergoing fracture toughness tests were monitored acoustically to detect pop-in [Ref 18], a condition in which a crack suddenly forms in the highly stressed region around a flaw. Acoustic emission detection of pop-in is relatively easy as it is composed of high amplitude emissions, and the technique was welcomed by experimenters who were trying to accurately determine the driving force necessary to initiate failure in high strength materials. Plastic deformation at crack tips and other highly stressed regions was also studied, with one experiment [Ref 19] reporting that strain increments as small as 0.1 microstrain produced detectable emissions. Dislocation movements were studied as well and there is now considerable evidence that the cooperative movement of numbers of dislocations are needed to produce detectable stress waves [Ref 20].

A very important application for acoustic emission testing is the detection of growing flaws. Laboratory studies have revealed that growing cracks occurring during hydrogen embrittlement, stress corrosion cracking, welding and low cycle fatigue can all be detected by continuous monitoring of acoustic emission. Moreover, in some cases it has proved possible to directly infer the amount of crack growth from the acoustic emission data [Ref 21]. Dunegan [Ref 22] has shown that flawed steel pressure vessels will generate emissions much earlier than unflawed ones, and has been able to diagnose the presence of potentially dangerous flaws at low stresses and make reasonably accurate failure pressure predictions at roughly 70% of the final failure pressure. This has enabled companies to evaluate pressure vessels during their working life by occasionally submitting them to a proof test, thus preventing accidents due to catastrophic failure.

The atomic energy industry is particularly interested in the capability of acoustic emission to remotely detect flaws well before they become dangerous. Extensive research [Ref 23] has been performed in developing transducers which will operate in the hostile environment of a operating reactor and in determining whether or not growing flaws can be detected through the high background noise usually present. Several useful side effects of acoustic emission monitoring emerged from this research when it was found that boiling core coolant could easily be discerned, thus leading to better control of the reactor. Further, it was found that there was a sonic "signature" associated with each reactor that could be used to determine whether normal operation was prevailing. Having proved the feasibility and usefulness of the technique, considerable effort was then expended upon building systems which could locate emission sources inside a reactor. Parry [Ref 24] reported the development of a four transducer system which utilized a computer to process emission arrival data into a location on the surface of a pressure vessel. His equipment could handle a million emissions per hour and was capable of locating sources with an accuracy of 2 centimeters on vessels having a capacity of 25 kiloliters.

Industrial applications for acoustic emission testing have also been reported. The work of Jolly [Ref 25] demonstrated the feasibility of in-process monitoring of welds. He was able to show sensitivity to weld cracking caused by contamination as well as being able to detect slag inclusions in submerged arc welds. Prine [Ref 26] successfully monitored production line submerged arc welds in steel tank cars. His acoustic emission results gave excellent correlation with radiographs on both artificially induced and natural defects even when noise from the welding arc and cracking slag caused some interference. In another area Hutton [Ref 27] proved that acoustic emission could provide process control information on metal drawing operations. His data on the forming of metal jackets for small arms bullets showed that the emission pattern was sensitive to a number of process variations which affected the final quality of the product.

A large amount of work has been expended upon acoustic emission monitoring in composites since they were found to be copious emitters of acoustic emission. Rathbun, Beattie and Hiles [Ref 28] reported that in filament wound pressure vessels emissions were generated in areas where structural damage took place and specifically where filaments were broken. Unlike the experience of Green, Lockman and Steele with the Polaris rockets mentioned previously, however, Rathbun, Beattie and Hiles concluded that there was no definite indicator in the emission pattern which would allow a prediction to be made of the burst pressure. Liptai [Ref 29], investigating tensile failures of filament wound rings, concluded that the failure followed a cumulative damage mode which could be studied with acoustic emission. Pattnaik and Lawley [Ref 30] reported that in $Al-CuAl_2$ composites emissions were the result of premature cracking of the $CuAl_2$ phase, but they were unable to develop a quantitative correlation between the amount of damage and the total acoustic emission. Harris, Tetelman and Darwish [Ref 31] on the other hand, were able to find such a correlation in their work on $Al-Al_3Ni$. Starting with the knowledge of the number of cracked fibers as a function of strain (which was determined by optical examination of the surfaces of strained samples), they derived an equation relating the number of acoustic emission counts to the strain in the specimen. Balderston [Ref 32], working with boron fiber reinforced plastic, reported success in predicting the lifetimes of tensile specimens through observation of the acoustic emission count rate during the test. Carlyle [Ref 33] was able to predict the failure of graphite fiber reinforced plastic tensile specimens through the sudden reduction in the acoustic emission count rate. This was found to be caused by the cessation of one of two simultaneously occurring failure mechanisms immediately prior to final fracture. Mullin and Mehan [Ref 34] performed preliminary experiments in boron fiber reinforced plastic in an attempt to develop a relationship between dominant frequencies observed in emissions from the material and particular failure mechanisms. Speake and Curtis [Ref 35] extended this work by using a foil transducer which reportedly had a flat response over the frequency range of 10 kHz to 5 MHz. They concluded that while some correlation between dominant frequencies and specific failure mechanisms did exist, more work was required to eliminate the extensive effects of material and geometry upon the emissions.

Clearly, acoustic emission testing has applications in a variety of fields, from basic research into the properties of materials to flaw detection in large engineering structures. However, as was stated in Section 1.1, the fundamental problem of not being able to identify the failure mechanism which caused the acoustic emission signal prevents the technique from being more widely utilized. The remainder of this thesis is devoted to developing signal processing techniques which will allow this problem to be overcome.

CHAPTER 2

FUNDAMENTALS

This chapter develops the theoretical background for acoustic emission. Material processes which generate acoustic emission are described, models which predict the specimen surface response resulting from the operation of such sources are reviewed, signal propagation effects which modify the acoustic emission waveform are examined and the operating principles of transducers are discussed.

2.1 Sources of Acoustic Emission

As was made clear in the previous chapter, the phenomenon of acoustic emission occurs in many different materials. What has not been pointed out is that the amount of acoustic emission generated by a material is highly dependent upon parameters such as composition, grain size, impurity content, the deformation process, the fracture mode, and even its prior stress history. Indeed, the amount of acoustic emission received from a specimen can be dependent upon the direction in which it is stressed [Ref 36]. The explanation for this behavior lies in the nature of the microscopic processes which are ultimately responsible for the creation of acoustic emission, and in the fact that more than one process can contribute to the observed acoustic emission output during a test.

Single crystals have been investigated by several workers with regard to their acoustic emission response. The advantage of working with single crystals is that there are no grain boundaries to complicate data interpretation, and as long as care is taken to merely plastically deform the specimen and not to fail it, the acoustic emission activity can only be caused by dislocation movements. Schofield [Ref 13] studied aluminum single crystals and concluded that the source of acoustic emission was the unpinning of dislocation pileups. His experiments indicated that barriers to dislocation movement such as oxide surfaces significantly increased acoustic emission activity, and that a minimum energy release was required via dislocation unpinning to produce an acoustic emission signal. Fisher and Lally [Ref 19] showed a strain rate dependence for the acoustic emission from magnesium single crystals, and suggested that discontinuous microplastic deformation was responsible for acoustic emission. James and Carpenter's work [Ref 20] on sodium chloride, lithium fluoride and zinc single crystals indicated that the acoustic emission rate was proportional to the change in the mobile dislocation density rate. Similarly to Schofield, they subscribed to the theory that dislocation breakaway from pinning sites was responsible for acoustic emission. They proposed a concept of stimulated breakaway of dislocations, whereby the freeing of one or two dislocations would trigger the unpinning of others. This concept was used to explain the discontinuous nature of plastic deformation of the sort noted by Fisher and Lally. The concept could also be used to explain the two basic types of acoustic emission, since a homogeneous spatial distribution of pinned dislocations would result in continuous emission while a segregation of pinned dislocations would result in burst emission behavior. Kiesewetter and Schiller [Ref 37], using aluminum single crystals, found that acoustic emission was proportional to the strain rate, and proposed that the source of the emission was elastic radiation accompanying dislocation acceleration and deceleration. Using this acoustic version of "bremsstrahlung" they showed that the strain rate dependence was due to the reduction in ultimate size of the area of Frank-Read generated dislocation loops. Such a reduction would result in a shorter dislocation line length, hence less dislocation energy, and therefore less acoustic emission energy would be created when the dislocation started or stopped.

Polycrystalline materials allow a restriction to be placed on the movement of dislocations, and therefore should result in acoustic emission being dependent upon grain size. Kiesewetter and Schiller [Ref 37] report such a relationship in 99.99% pure aluminum, with acoustic emission activity increasing with increasing grain size up to an upper limit defined by the emission behavior of a single crystal, as shown in Figure 2.1. They explain this result by pointing out that dislocations in one slip system can be stopped from moving by interactions with dislocations in another slip system. As the grain size is decreased more interactions are to be expected, thus the slip area of the dislocation and hence its associated energy are reduced, resulting in less acoustic emission. Frederick [Ref 38] obtained results in 99.99% pure aluminum which somewhat contradict this. As Figure 2.2 depicts, he

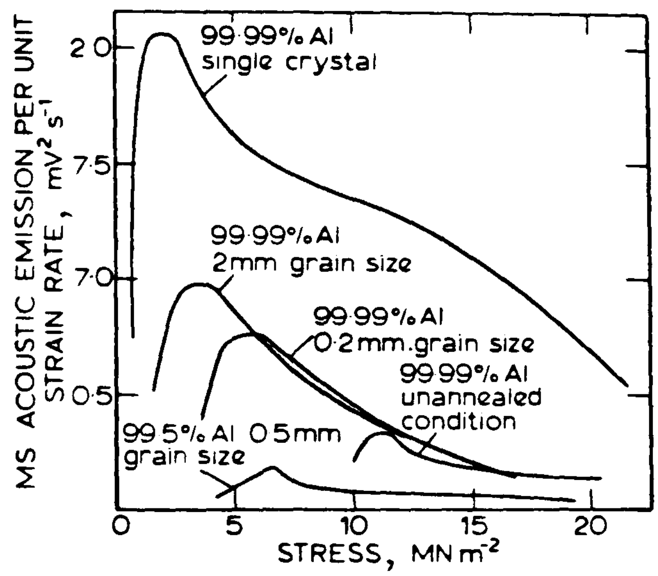

Figure 2.1. Stress dependence of acoustic emission voltage output in 99.99% pure aluminum as a function of grain size [Ref 37].

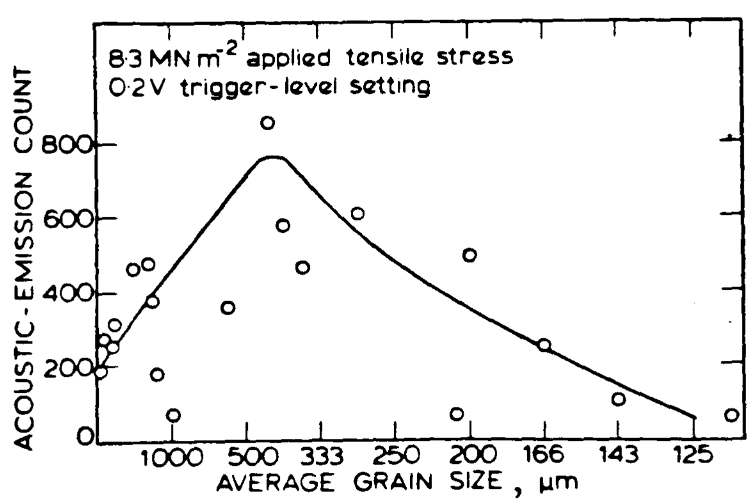

Figure 2.2. Grain size dependence of total acoustic emission up to a specific stress level in 99.99% pure aluminum, note the inverse scale on the abcissa [Ref 38].

found that as the grain size increased to 350 microns the acoustic emission also increased, but when the grain size grew larger than 350 microns the emission output fell. The behavior when the grain size was less than 350 microns was explained by the increasing dislocation slip area with increasing grain size, in agreement with Kiesewetter and Schiller above. However, when the grain size was larger than 350 microns, Frederick attributed the decrease in acoustic emission to a decrease in grain boundary dislocation sources caused by the decreasing grain boundary area. Tandon and Tangri [Ref 39] reported in Fe-3.0 weight percent Si a similar behavior to that found by Frederick in 99.99% pure aluminum, i.e., an increase in acoustic emission with increasing grain size up to a maximum of 400 microns followed by a decrease in acoustic emission as the grain size increased further.

It is reasonable to conclude from the foregoing that dislocation movement is responsible for the acoustic emission generated by the deformation of single crystals and polycrystalline materials. However, the particular aspect of the dislocation movement which is actually responsible for the generation of the acoustic emission under a given circumstance is still in doubt, primarily because of difficulties in interpreting the complex interactions between experimental testing variables and potential changes in deformation behavior. For example, Tandon and Tangri's result above was reversed, i.e., increasing grain size in Fe-3.0 Si caused a decrease in acoustic emission when the test included the acoustic emission output up to 2.5% total plastic strain. This occurred because Luders' band formation above 90% of yield limited the slip area of dislocations, and since larger grain sizes allowed more extensive Luders' band formation the acoustic emission output fell with increasing grain size. Carpenter and Heiple [Ref 40] show that other parameters in addition to grain size, surface condition and strain rate discussed above can affect the acoustic emission output observed during deformation of materials. They cite such things as test temperature, sample purity, crystal structure, stacking fault energy, prior mechanical work, heat treatment, and sample size which have also been found experimentally to have a bearing on acoustic emission behavior. Notwithstanding these complications, it is concluded on the basis of the evidence presented that acoustic emission generated during the plastic deformation of single crystals and polycrystals is governed by the glide distance and length of moving dislocations, by the number of dislocations which move simultaneously, or both.

To this point the discussion has been limited to the deformation of relatively pure materials. However, since alloys are of more engineering interest, it is useful to consider how the addition of impurities affects acoustic emission behavior. The work of Wadley and Scruby, et. al. [Ref 41 to 43] is instructive for its systematic approach in explaining the sources of acoustic emission in aluminum alloys as a function of alloying elements. They first assumed that the source of the acoustic emission was an expanding dislocation loop inclined at 45 degrees to the surface normal, which they modeled through the use of two orthogonal force dipoles. Following a procedure described by Burridge and Knoppoff [Ref 44], they showed that the vertical displacement at the epicenter of such a dislocation loop due to the first arrival longitudinal pulse was given by:

$$\delta = \frac{b\, a\, v\, c_s^2}{D\, c_l^3} \tag{2.1}$$

where c_l is the longitudinal wavespeed, c_s is the shear wave speed, b is the dislocation Burgers' vector, D is the depth of the dislocation loop below the surface, a is the radius which the loop expands by, and v is the velocity at which the loop expands. Using values typical of their material and transducer, they calculated that only dislocation motions for which the product of a and v was above 0.036 meters^2 per second could be detected during their experiments.

The results obtained by Wadley and Scruby in 99.999% pure single crystal and polycrystalline aluminum are shown in Figure 2.3, along with a schematic showing how the product of a and v was expected to vary with applied strain and thus control the acoustic emission activity. For the single crystal material, dislocation motion was restricted by forest interactions after yield and for the polycrystalline aluminum dislocation movement was restricted by the grain boundaries and interactions between multiple slip systems, as postulated by Kiesewetter and Schiller. The expanding dislocation loop model required that for a given strain rate the total acoustic emission energy released during a test should increase with increasing grain size, and that the emission power should vary linearly with strain rate for a given grain size. Significantly, both of these requirements were experimentally observed. However, when 1.3 weight percent of magnesium was added to otherwise pure aluminum to form a precipitation and segregation free solid

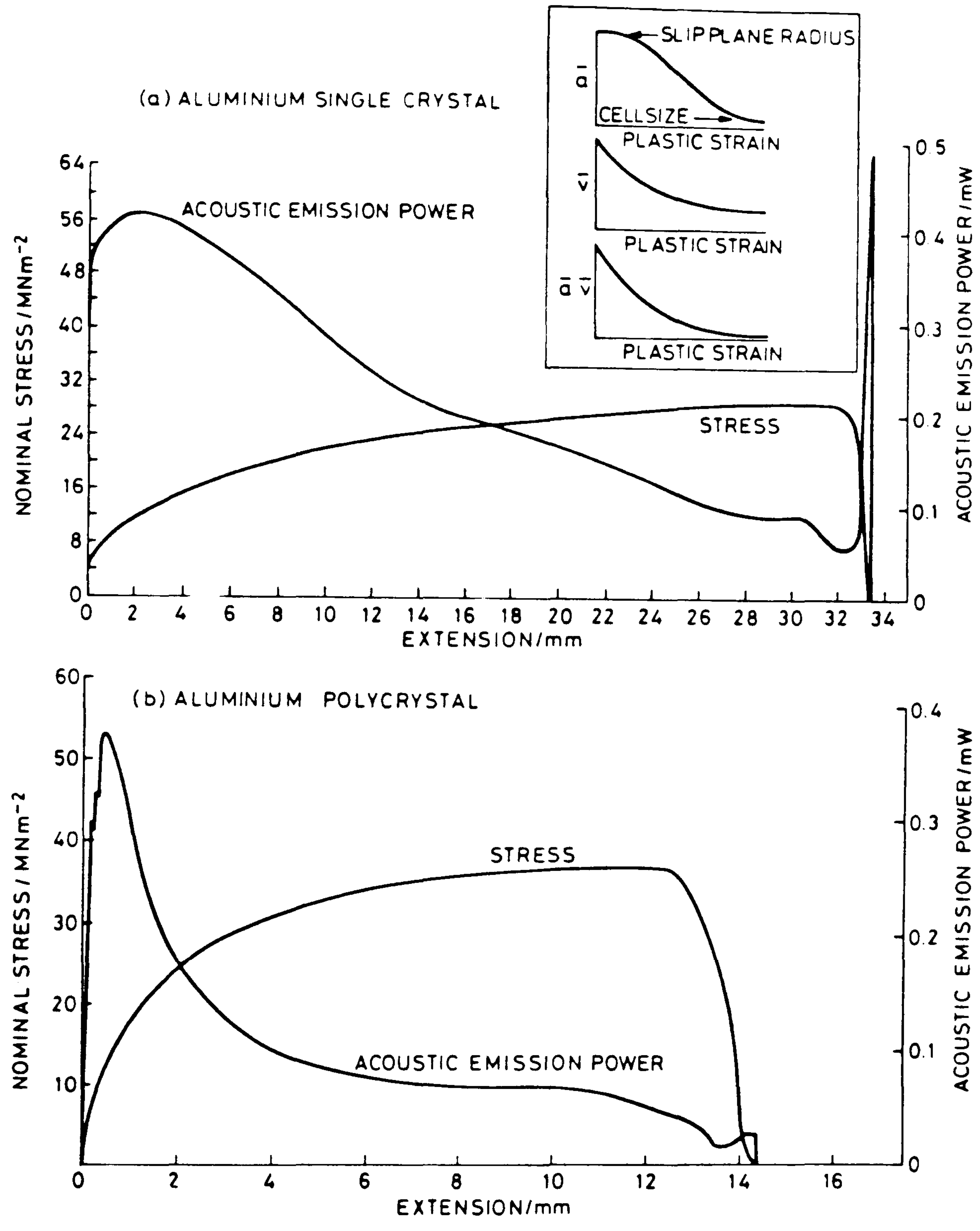

Figure 2.3. Extension dependence of acoustic emission and stress in (a) aluminum single crystal and (b) an aluminum polycrystal of 660 micron grain size. Dislocation mean free path a and velocity v dependence is shown in inset, product av determines the acoustic emission amplitude [Ref 42].

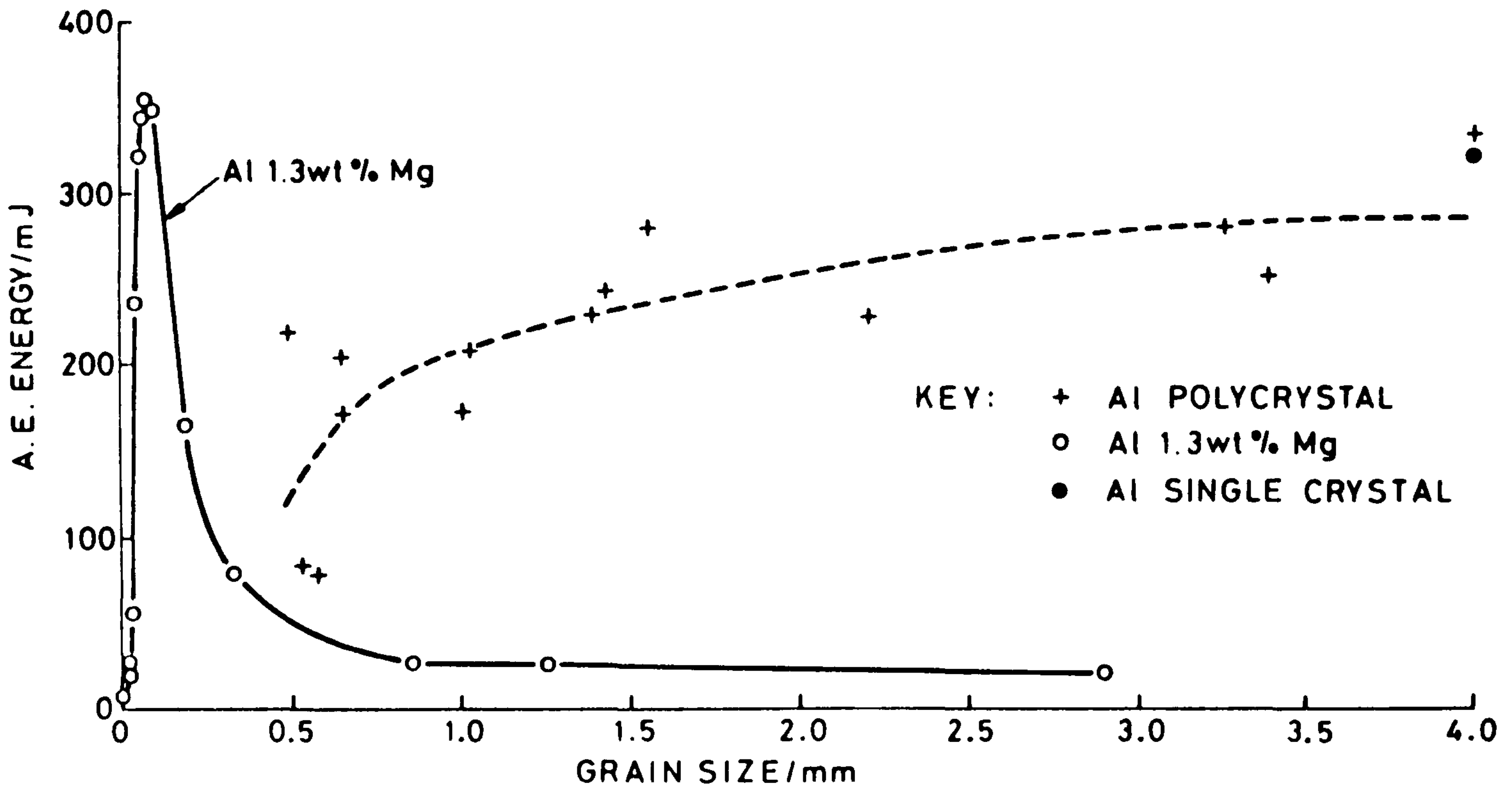

Figure 2.4. Grain size dependence of acoustic emission from 99.99% pure aluminum and Al-1.3 weight percent Mg [Ref 42].

solution, these relationships were profoundly affected, as shown in Figure 2.4. This behavior was explained through increased dislocation slip area as the grain size was increased to 80 microns, followed by a reduced number of dislocations which could move due to the increasing flow stress as the grain size increased from 80 microns. One other important effect which the solid solution had on acoustic emission activity was the replacement of continuous emission by burst emission. This was presumed to be due to the pinning of dislocations caused by solute atom diffusion, with a discontinuous escape of the dislocations as the applied stress exceeded the drag stress.

The effect of precipitation on acoustic emission activity was investigated by Wadley and Scruby by adding 4 weight percent of copper to pure aluminum and studying the effect of isothermal aging. Figure 2.5 shows their results. Acoustic emission in the quenched material is low because the copper is in solid solution. With 1.5 hour 170 °C aging, fine precipitates form which initially impede dislocation movement, but which soften as they are sheared by dislocations at higher applied stresses. This results in an avalanche of dislocations as a slip band is formed, resulting in high energy burst emissions. With increasing aging time the precipitates grow larger and stronger. Dislocations are no longer able to shear the precipitates, thus no discontinuous deformation occurs and the acoustic emission activity reduces. Further study of the effect of precipitates by Wadley and Scruby using Al-5.5 Zn-2.5 Mg and Al-5.5 Zn-2.5 Mg-1.6 Cu (weight percentages) revealed somewhat different results. In the quenched condition acoustic emission was governed by dislocation breakaway from

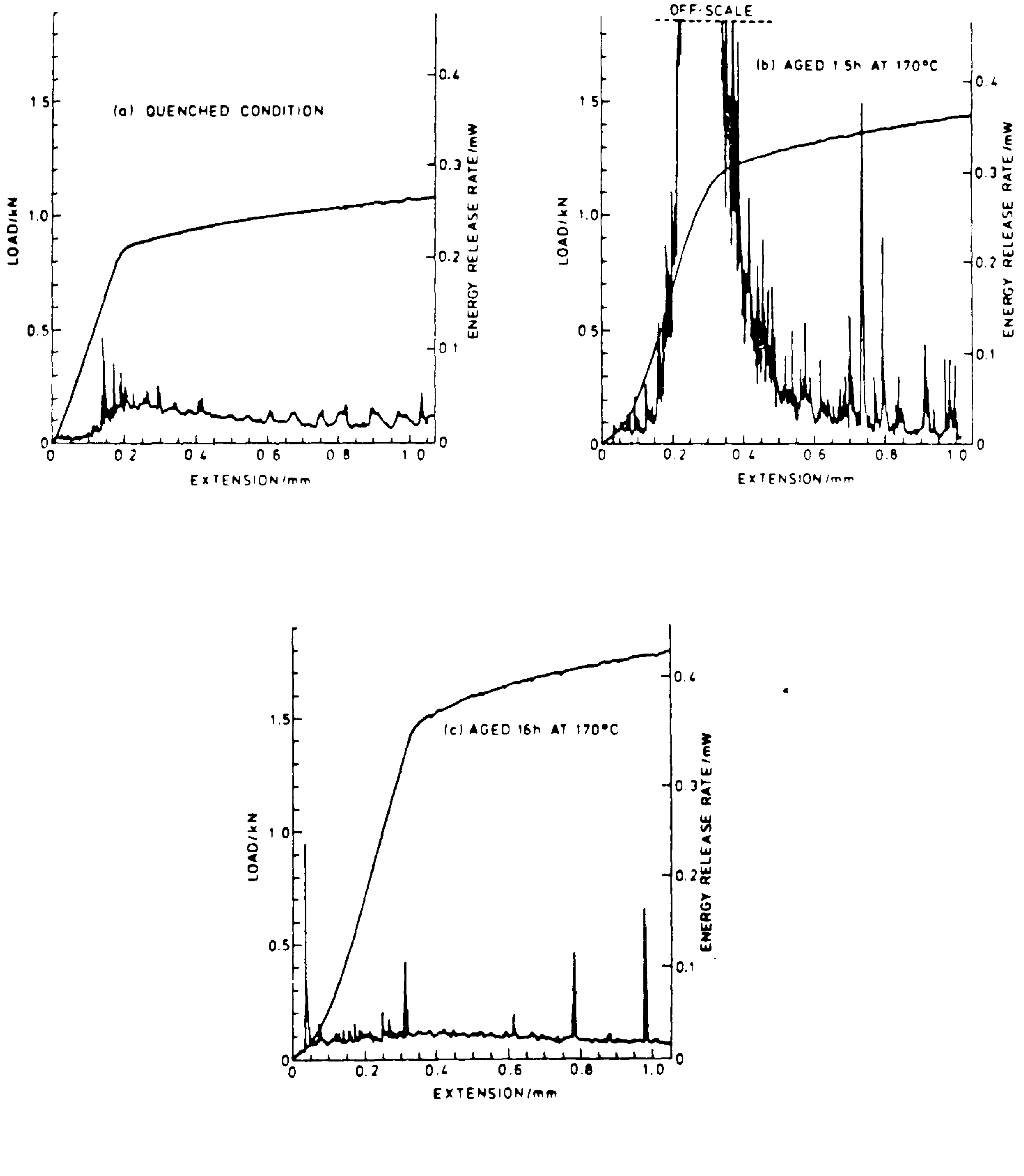

Figure 2.5. Extension dependence of acoustic emission and load for Al-4.0 weight percent Cu as a function of aging [Ref 42].

the pinning solute. Short aging times created small precipitates which limited dislocation velocity and thus reduced the emission output from the quenched condition. Longer aging times were characterized by vigorous burst emission of much higher amplitude than in the quenched material, which was believed to be due to cooperative dislocation movement caused by softening of the precipitate structure on a glide plane, but which could also have been caused by intergranular fracture.

The effect of precipitates on the acoustic emission behavior of aluminum alloys has also been investigated by Cousland and Scala [Ref 45]. They studied 7075 aluminum (Al-6.2 Zn-2.2 Mg-2.3 Cu-0.1 Cr, weight percent) and 7050 aluminum (Al-6.2 Zn-2.2 Mg-2.3 Cu-0.1 Zr, weight percent), both in the T7351 condition. The essential difference between these alloys and those used by Wadley and Scruby is the addition of the zirconium or chromium and the fact that the material received a 2% strain before final aging. They performed both tension and compression tests, and obtained little or no acoustic emission during compression but copious emission during tension, with the "dirtier" 7075 emitting more than the "cleaner" 7050. They argued that since the deformation processes would be similar in tension or compression while particle fracture would be expected only during tensile testing that the source of acoustic emission had to be due to the fracture of brittle precipitates. Support for this hypothesis came from the fact that no slip band formation (which would be associated with dislocation avalanches and burst acoustic emission) was observed despite careful examination of both tension and compression specimens, that the amount of acoustic emission received from a tensile specimen correlated with the amount of large inclusions in that specimen, and that the amount of acoustic emission was dependent upon the cross-sectional area of particles normal to the applied load. One potential problem with their claim that particle fracture is the sole source of acoustic emission in these alloys is that the distribution of burst emission is relatively uniform from just prior to yield until failure. Because of normal particle size variations in metals it would be expected that particle fracture acoustic emission would follow a Gaussian distribution instead of remaining constant as their data shows.

If particle fracture acts as a source of acoustic emission, it is reasonable to assume that the fracture of the metal itself generates acoustic emission, and indeed this is the case as will now be shown. Fracture is a complicated process whose details depend upon the specific material, its structure, impurity content, temperature, heat treatment, environment, geometry, stress state, and loading history. However, a relatively simple process underlies acoustic emission generation during fracture, namely, the motion of the crack tip. Byerlee and Peselnick [Ref 46] demonstrated this in their study of acoustic emission in glass. Glass is brittle, thus no deformation would be expected during the short testing period, and this was proven by subjecting unslotted specimens to compressive loads greater than those used during fracture testing of slotted specimens without generating acoustic emission. Compressive testing of slotted specimens produced acoustic emission only upon the appearance of a crack. Significantly, no acoustic emission was produced during stable, i.e., constant velocity, crack growth. The parallel with acoustic emission generation via dislocation movement during deformation is exact, in that only the starting and stopping of the crack tip during fracture will create acoustic emission, just as does the starting and stopping of a dislocation during deformation.

In metals, where fracture does not occur in such a brittle fashion as in glass, the generation of acoustic emission via crack acceleration and deceleration still occurs, but much more subtly. For example, McBride, MacLachlan and Paradis [Ref 47] performed a study on 7075 aluminum containing different inclusion sizes using O (annealed) and T6 (aged) heat treat conditions to determine the source of acoustic emission during slow crack growth caused by fatiguing. Their results show a direct dependence of the emission upon the size of the inclusions which fractured in the material, and it was shown that crack growth and not manufacture was responsible for the presence of the fractured inclusions. Furthermore, acoustic emission was not detected if the strength of the material surrounding the inclusions was too low. From these results, McBride, MacLachlan and Paradis concluded that the acoustic emission response from 7075-T6 aluminum could be predicted from the distribution of the cross-sectional area of the inclusions. It is clear that the movement of the main crack tip in the aluminum itself is not directly responsible for the acoustic emission, but the result of such movement causes discontinuous crack growth in the inclusions along the main crack front if the metal/particle interface is suitable. It is the discontinuous movement of these small cracks which is directly responsible for the observed acoustic emission.

Nozue and Kishi's work [Ref 48] provides further support for the discontinuous movement of cracks being responsible for generating acoustic emission during fracture. They studied the tensile failure of 4340 steel (Fe-0.4 C-1.8 Ni-0.81 Cr-0.78 Mn-0.3 Si-0.19 Mo, weight percentages) tempered at various temperatures. Stable crack growth in the specimen with the highest tempering temperature produced no acoustic emission, and microscopic examination showed that the fracture surface consisted entirely of dimpled ductile fracture. Specimens tempered at lower temperatures produced acoustic emission during stable crack growth which was inversely related to the tempering temperature. The fracture surfaces showed varying amounts of intergranular brittle fracture. Nozue and Kishi were able to obtain a linear relationship between the cumulative squared emission voltage and the cumulative area of intergranular cracking on the fracture surface. Since discontinuous crack movement is associated with brittle cracking while continuous crack velocity is associated with ductile cracking, it has once again been shown that acoustic emission during fracture is generated by changes in the velocity of cracking.

2.2 Source Models

It was shown in the previous section that the ultimate source of acoustic emission is the acceleration and deceleration of either dislocations or cracks. The purpose of this section will be to show how these phenomena can be modeled to predict how the surface of the material will react.

The movement of a dislocation during deformation or the lengthening of a crack during fracture can both be considered relaxation processes since their operation tends to lower the stored energy of the material. This relaxation will be accompanied by a spherical acoustic wave whose energy density is given by Stone and Dingwall [Ref 49] as:

$$E = \frac{P_o^2}{2\, \varrho_o\, c^2} \left[1 + \frac{c^2}{2\, \omega^2\, r^2} \right] \tag{2.2}$$

where P_o is the acoustic pressure, ϱ_o is the density of the material, c is the wave speed, ω is the angular frequency, and r is the distance from the source. Beyond one wavelength the second term may be neglected, and since:

$$P_o = \frac{\varrho_o\, c^2\, \delta\, \sigma}{E} \tag{2.3}$$

where $\delta\, \sigma$ is a stress drop and E is Young's modulus, the energy density in the acoustic wave is approximated by:

$$E_d \sim \frac{\varrho_o\, c^2\, (\delta\, \sigma)^2}{2\, E^2} \tag{2.4}$$

Now, the elastic energy density in a material is given by:

$$U = \frac{\sigma^2}{2\, E} \tag{2.5}$$

where σ is the stress. If it is assumed that the stress drops slightly by $\delta\sigma$ which is much less than σ, then:

$$\delta U = \frac{\delta\sigma}{2E}(2\sigma - \delta\sigma) \tag{2.6}$$

The second term of (2.6) may be neglected for a first approximation. Dividing (2.4) by (2.6) will relate the energy carried by the acoustic wave to the energy release caused by the stress change:

$$\frac{E_d}{\delta U} \sim \frac{\varrho_o c^2 \delta\sigma}{2E\sigma} = K\frac{\delta\sigma}{\sigma} \tag{2.7}$$

The meaning of (2.7) is that the energy carried by an acoustic emission waveform is not a constant proportion of the released stored energy, but is dependent upon the magnitude of the stress drop and the stress at which the drop occurs. Pollock [Ref 50] in a separate analysis has confirmed the stress dependence of the acoustic emission waveform as given by (2.7) and, as shown in Figure 2.6, experimental verification for (2.7) is obtainable as well.

It is instructive to consider the shape of the stress wave near the source so that estimations of the frequencies contained in the stress wave may be made. Stephens and Pollock [Ref 51] argued intuitively that the basic shape of the stress wave was a pulse, because such a waveform would decay to change the static stress level within a specimen, and it has (according to their analysis) associated with it a step displacement waveform which would alter the length of the specimen after it decayed. An oscillatory stress waveform, on the other hand, has a mean value of zero and thus would not change the static stress in a specimen, nor

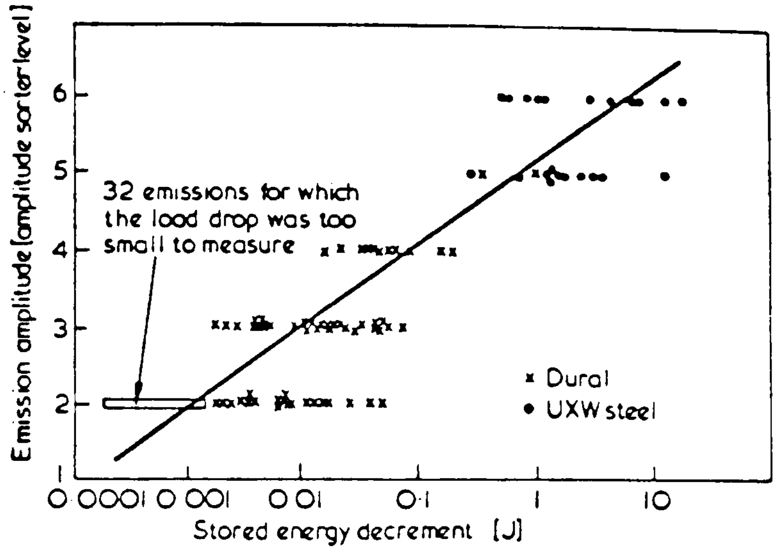

Figure 2.6. Dependence of acoustic emission amplitude on stress drop [Ref 50].

would the associated (according to their analysis) pulse displacement waveform be able to change the specimen length because a sign change upon reflection from a surface would imply a mean value of zero. Using as a hypothetical stress pulse a Gaussian waveform given by:

$$\sigma = \sigma_o \exp\left(\frac{-t}{T^2}\right) \tag{2.8}$$

as shown in Figure 2.7, Stephens and Pollock calculated an energy spectral distribution of:

$$A(f) = \frac{y_o^2 E}{c} \exp\left[-\frac{(2\pi f T)^2}{2}\right] \tag{2.9}$$

where y_0 is the height of the displacement step on the surface. Equation (2.9) is plotted in Figure 2.8. It can be seen that it is a Gaussian waveform and that roughly two-thirds of its energy is below a frequency given by $1/\sqrt{2}\pi T$. Carlyle [Ref 3] has shown from energy considerations that the minimum lower limit for the duration of an acoustic source when the source waveform is a Gaussian is given by:

$$T = \frac{d}{c\sqrt{2\pi}} \tag{2.10}$$

where d is the diameter of the source. For steel, with c = 5900 meters per second and assuming a source diameter of 130 microns, (2.10) and (2.9) imply that two-thirds of the acoustic emission energy will occur between DC and 26 MHz.

Ono [Ref 52], following an approach suggested by Malen and Bolin

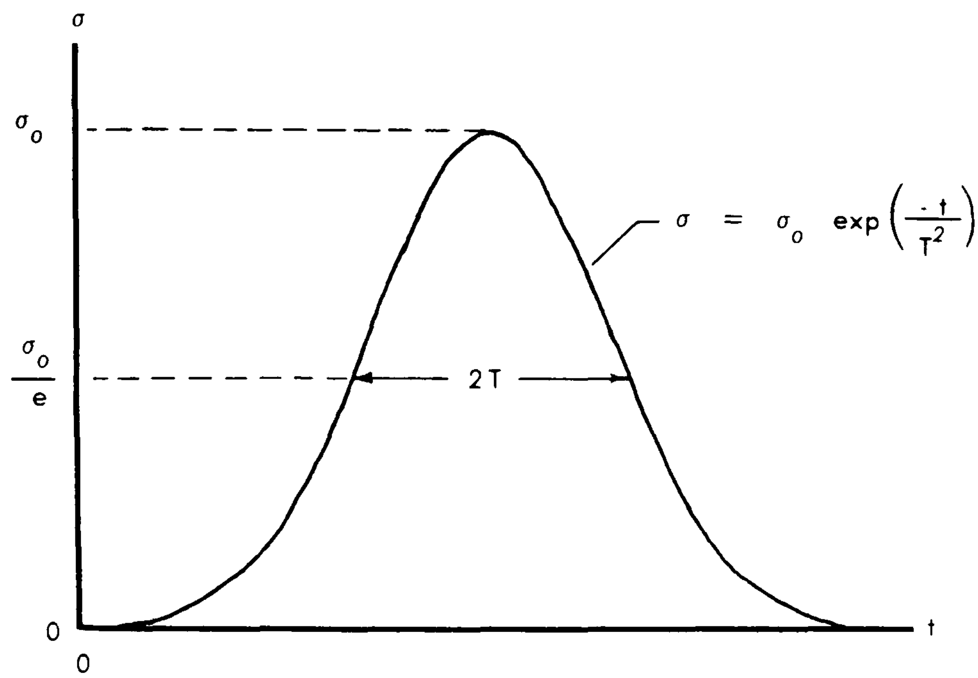

Figure 2.7. Gaussian stress pulse [Ref 51].

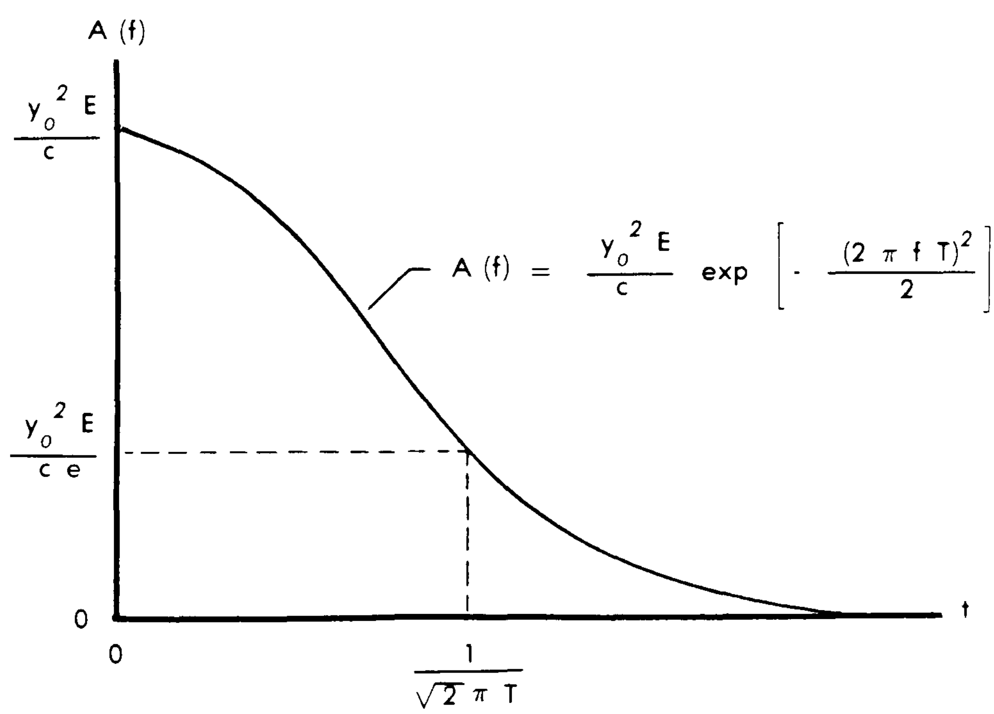

Figure 2.8. Energy spectral distribution resulting from the pulse of Figure 2.7 [Ref 51].

[Ref 53], derived a different expression for the stress waveform. Malen and Bolin had shown that the stress at a distance r from the source had an angular frequency given by:

$$\sigma(r, \omega) = \left\{ \frac{\omega^2}{4 \pi r c^2} \exp\left(\frac{j \omega r}{c}\right) \right\} S_m \left(\pi \delta(\omega) - \frac{1}{j \omega}\right) \tag{2.11}$$

where j is $\sqrt{-1}$, S_m is the magnitude of the source function, and $\delta(\omega)$ is Dirac's delta function. The quantity in brackets is the response function of the medium in which the wave propagates, while the remainder of the right-hand side of (2.11) represents a step source function. Through Fourier transformation and the replacement of the Dirac delta function with the Gauss error function in order to examine rise-time effects, Ono expressed the stress at a distance r as a function of t as:

$$\sigma(r, t) = \frac{-S_m}{8 \sqrt[3]{\pi}\, r c^2 \tau^2} \left[\frac{\frac{r}{c} - t}{2 \tau} \exp\left(- \frac{\left(\frac{r}{c} - t\right)^2}{4 \tau^2} \right) \right] \tag{2.12}$$

where τ is one-quarter of the time it takes the Gauss error function to increase from 0.1 to 0.9 of its final value. The terms in the brackets of (2.12) determine the shape of the stress pulse, which is plotted in Figure 2.9. Ono expressed the magnitude spectrum as:

$$\left| F(\omega) \right| = \frac{S_m \omega_o}{4 \pi r c^2} \left(\frac{\omega}{\omega_o}\right) \exp\left(- \frac{\omega^2}{\omega_o^2} \right) \tag{2.13}$$

where ω_o is the reciprocal of τ. This is plotted in Figure 2.10.

It can be seen that Figure 2.9 and Figure 2.7 do not agree with one another in spite of the fact that similar displacement waveforms were

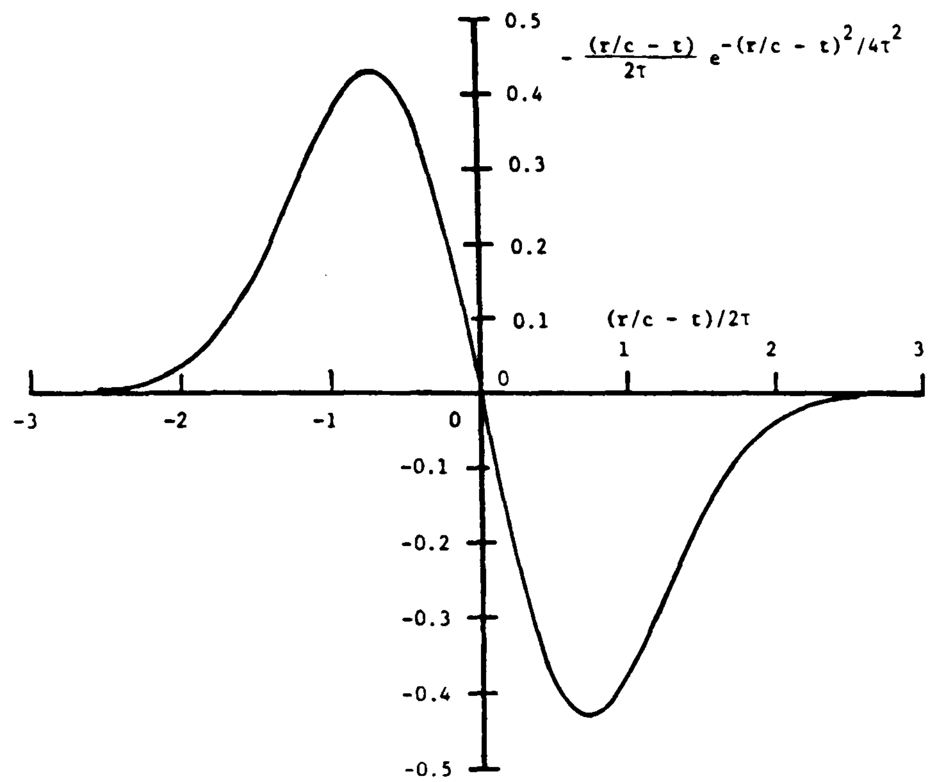

Figure 2.9. Bipolar stress pulse [Ref 52].

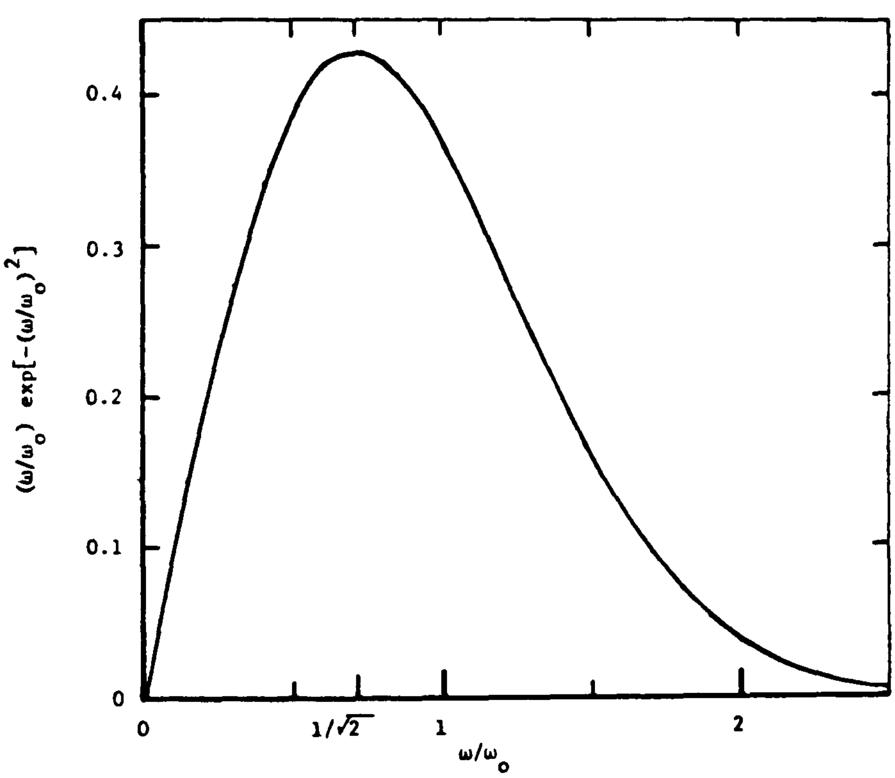

Figure 2.10. Energy spectral distribution resulting from the pulse of Figure 2.9 [Ref 52].

used to obtain them. The reason for this seeming contradiction is that the problem posed by Stephens and Pollock is incomplete because they do not specify the forces acting at the source, nor do they specify where they measure the stress pulse. Ono's derivation, while more complete than Stephens and Pollock's treatment, is also lacking since his theory is based on propagation in an infinite medium and does not treat the effect of surfaces. Pao, Gajewski, and Ceranoglu [Ref 54] have done theoretical work to show the effect of different forces measured at various points in a plate. Figure 2.11a shows their results for a buried vertical monopole force with a step-function time dependency producing a displacement (which must be integrated to obtain stress) at the epicenter of the plate, with Figure 2.11b showing the result when the displacement due to this force is measured six plate thicknesses away from epicenter. Figure 2.12a shows the epicentral response of a buried dipole force with a step-function time dependency, while Figure 2.12b shows the same epicentral response of the same buried dipole force, but this time with a parabolic ramp-function time dependency. Figure 2.12c shows the result when this last force is measured six plate thicknesses away from epicenter. These figures make clear that the results of Stephens and Pollock and of Ono are specific cases of the complete problem and highlight the necessity for being rigorous when attempting to analyze elastic waves emitted by a source in a material.

The propagation of waves in elastic bodies has been studied extensively by seismologists since the problem was first addressed by Lamb in the early part of the twentieth century [Ref 55]. Breckenridge, Tschiegg, and Greenspan [Ref 56] were the first to utilize the formalism

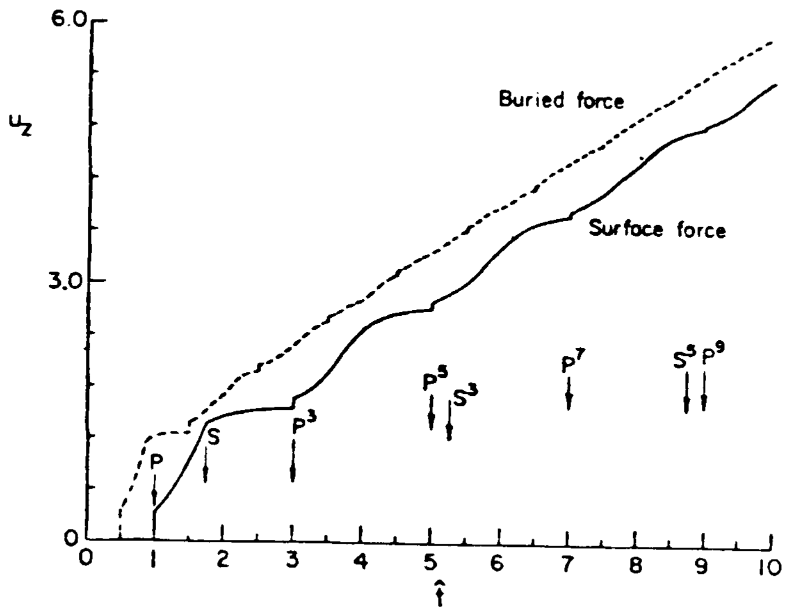

Figure 2.11a. Vertical displacement of a plate at epicenter due to a buried monopole force [Ref 54].

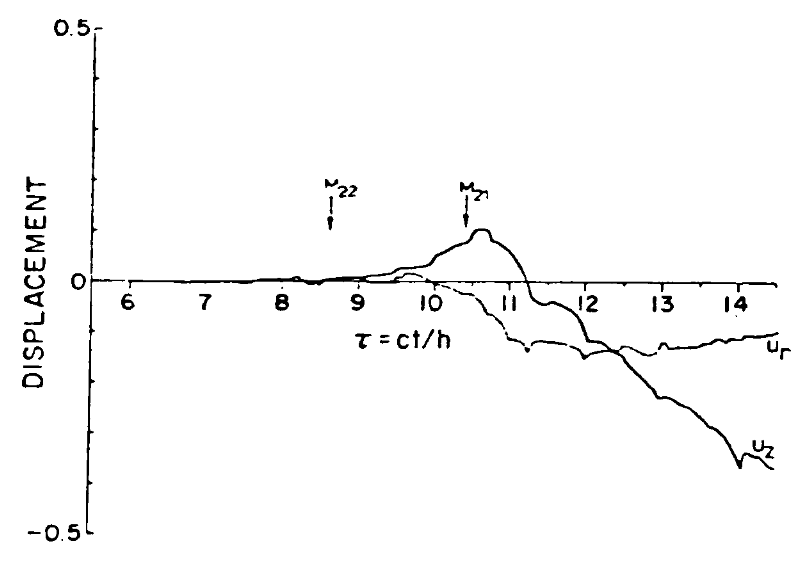

Figure 2.11b. Vertical displacement of a plate six plate thicknesses away from epicenter due to a buried monopole force [Ref 54].

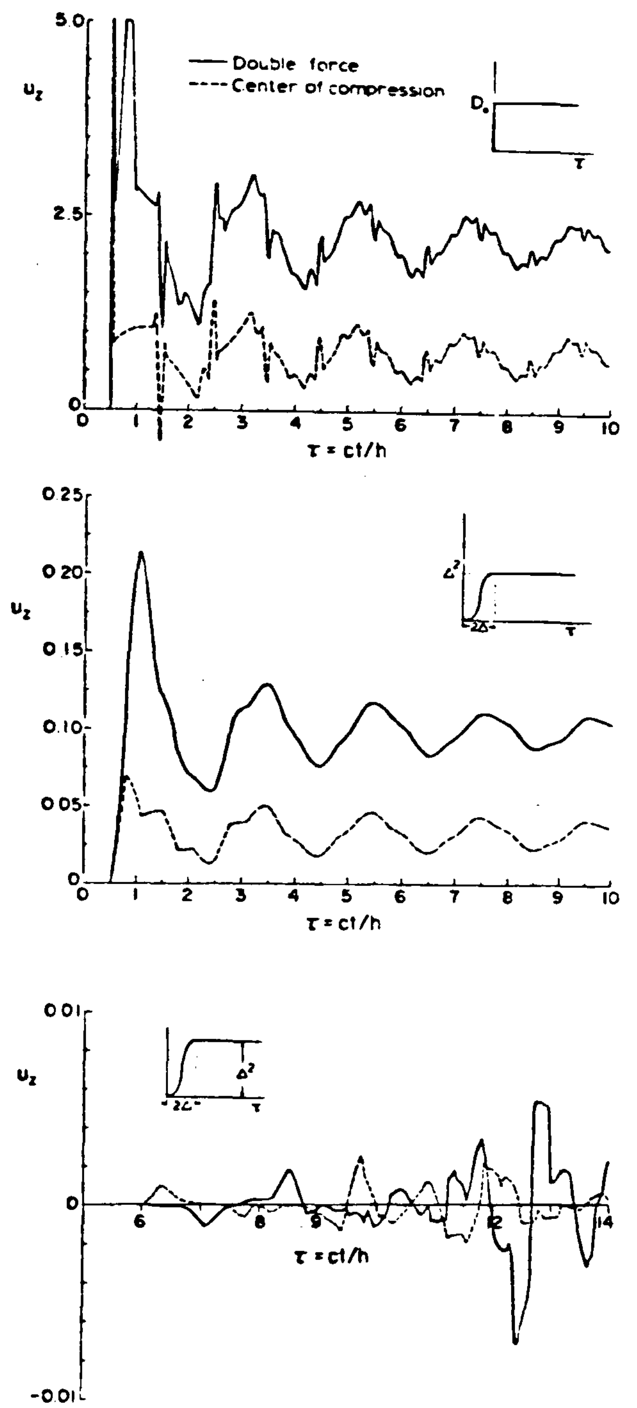

Figure 2.12. Vertical displacement of a plate due to buried dipole forces. (a) Epicenter response when force has a step function time dependence. (b) Epicenter response when force has a ramp function time dependence. (c) Response at six plate thicknesses from epicenter when force has a ramp function time dependence [Ref 54].

of seismology and apply it to acoustic emission. Their interest was in calibrating transducers and, as will be shown in Section 3.1, they were quite successful. Their idea of using seismological concepts to study acoustic emission was furthered by Hsu and Hardy [Ref 57], who, as shown in Figure 2.13, were able to obtain excellent agreement between experimental results and numerical results calculated using the theory of the generalized ray (the same seismological theory used by Pao, Gajewski and Ceranoglu to produce Figures 2.11 and 2.12).

The essence of the generalized ray theory is that the displacement response u in a specific direction i at a position x and time t is given by the convolution with respect to τ of the material response function G with a source function S operating in direction j at position y:

$$u_i(x, t) = \int_{-\infty}^{\infty} \int_{V} G_{ij}(x, t-\tau; y)\, S_j(y, \tau)\, d^3y\, d\tau \qquad (2.14)$$

The material response function $G_{ij}(x,t;y)$ is known as the dynamic elastic Green's function (or transfer function) and has been calculated for an infinite space, an infinite half-space and an infinite plate. Although these are all physically unrealizable objects, the results of the calculation will also be valid in a finite plate from time zero to a time immediately prior to the arrival of any waves reflected from the edges of the plate. Another problem is that (2.14) is not capable of analytic solution, but needs to be evaluated numerically through an algorithm. Although the algorithm is capable of being solved for an arbitrary number of reflections from the plate surfaces, round-off errors and computer run-time costs will place an upper limit on the

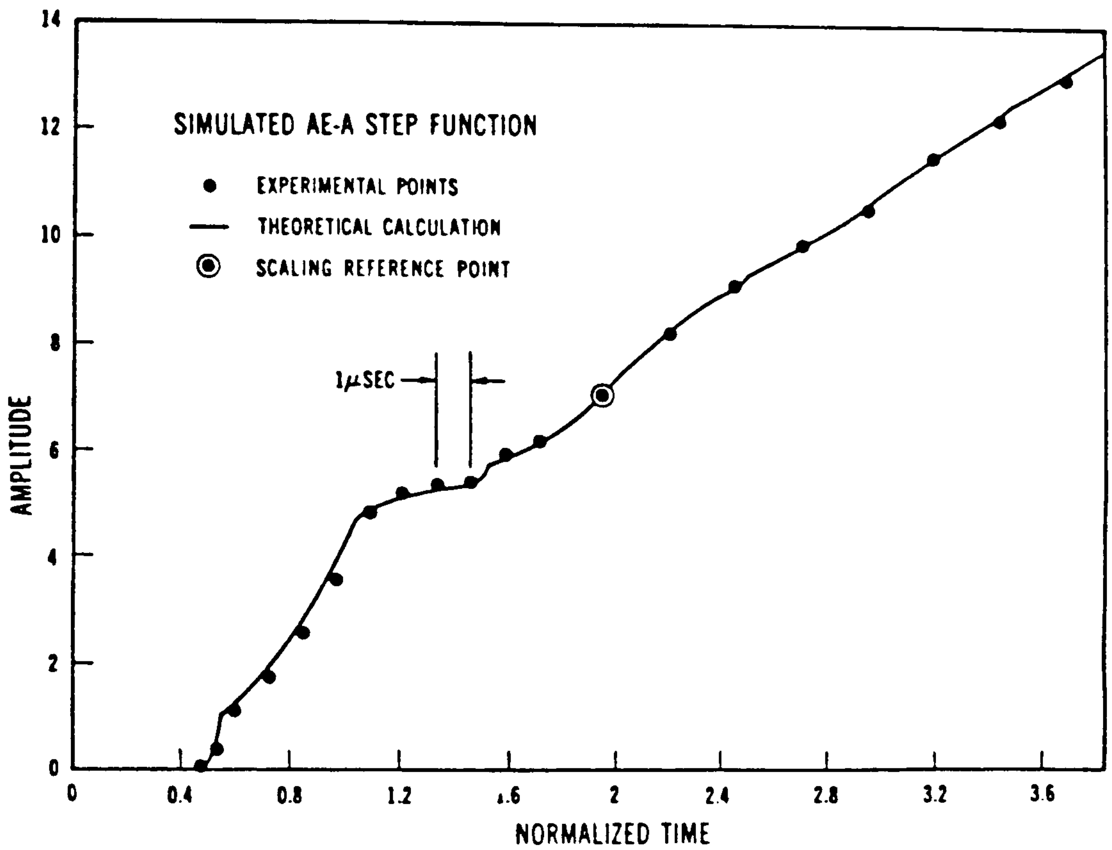

Figure 2.13. Comparison between prediction of generalized ray theory and experimental results for the vertical displacement of a plate at epicenter due to a surface monopole [Ref 57].

number of surface reflections which can actually be used. Thus the generalized ray theory is constrained by specimen size and computer limitations to the first few (typically 10) microseconds of displacement at a location typically within six plate thicknesses from the epicenter of the source.

In spite of the limitations of the generalized ray theory just mentioned, it provides a very useful tool for performing basic studies for source characterization of acoustic emission. To prove this contention, Hsu and Hardy obtained the comparison in Figure 2.13 by breaking a glass capillary on a plate. The excellent agreement between theory and experiment convinced them that the breaking capillary was acting like a step displacement (since that was what had been assumed in the theory) and also that the Green's function was correct for their experimental conditions. They could therefore deconvolve (2.14) to obtain the source force-time function for the glass capillary, and thereby produced Figure 2.14. Another experiment in which a 1.5 mm steel ball was dropped 5 cm produced the deconvolved source force-time function shown in Figure 2.15. Both of these force-time functions are precisely what such mechanisms should produce. The important point is that they were deduced from a displacement measurement made remotely from the point of application of the force, said displacement being caused by the propagation of a stress wave through the material.

Building on these simulated source results, Wadley and Scruby [Ref 58] investigated actual acoustic emission sources caused by cracking in iron and steel. In order to accomplish this task, they modeled the

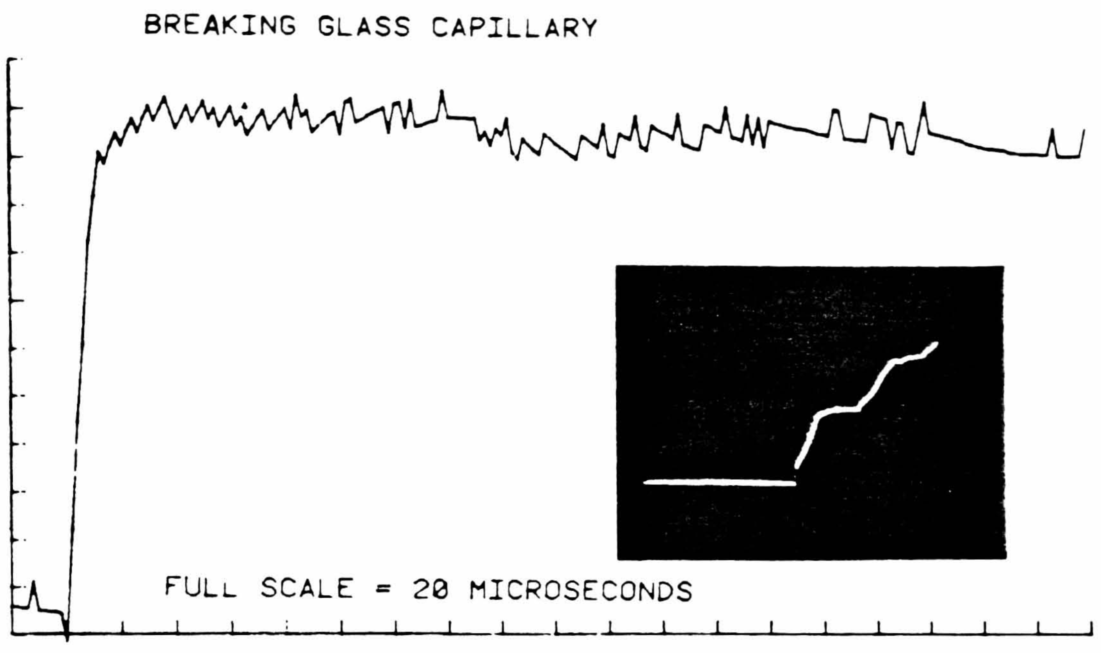

Figure 2.14. Deconvolved source force-time function of a breaking glass capillary calculated from epicentral displacement shown in inset [Ref 57].

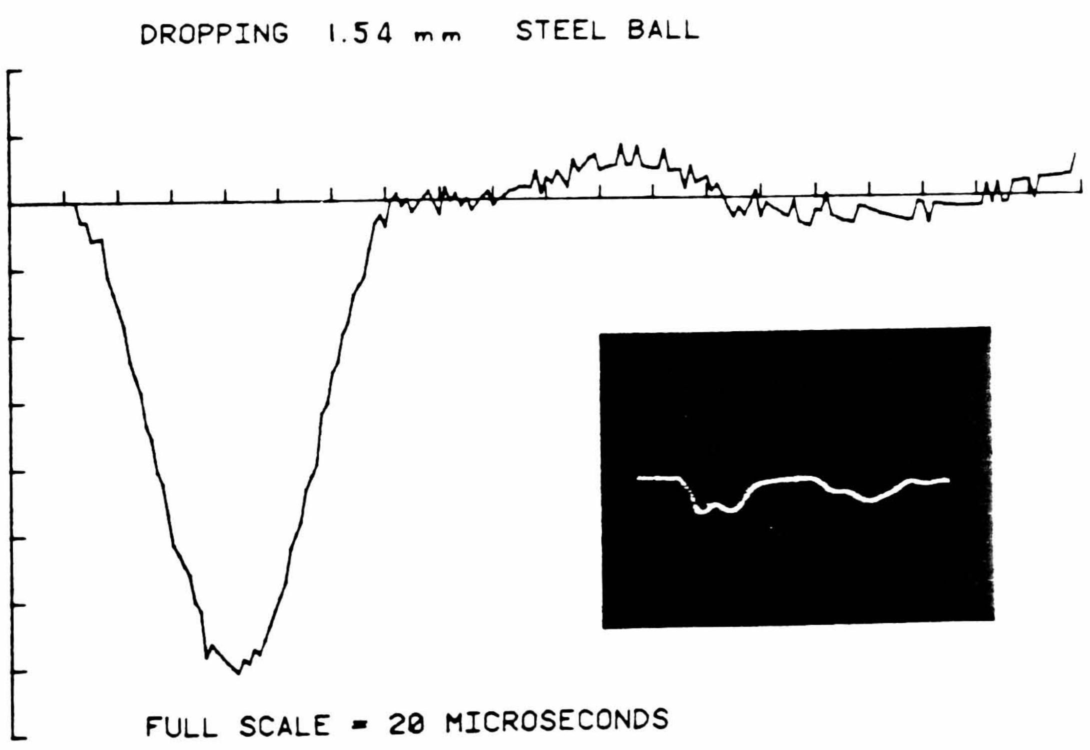

Figure 2.15. Deconvolved source force-time function of a dropped steel ball calculated from epicentral displacement shown in inset [Ref 57].

crack as a combination of three orthogonal force dipoles as suggested by Burridge and Knopoff [Ref 44]:

$$\underset{\sim}{D}_{ij} = \begin{bmatrix} \lambda & o & o \\ o & \lambda & o \\ o & o & \lambda + 2\mu \end{bmatrix} b\,\delta A \tag{2.15}$$

where λ and μ are Lame's constants, b is the Burgers vector of an equivalent edge dislocation loop and δA is the area of the equivalent edge dislocation loop (see Figure 2.16). Using the formalism of equation (2.14) and assuming a step function crack opening, Wadley and Scruby calculated the displacement-time function at epicenter. This function is also shown in Figure 2.16, and can be seen to consist of a singularity when the longitudinal wave arrives followed by an increasing ramp whose maximum corresponds to the arrival of the shear wave. The area of this singularity is proportional to the source strength, and is given by:

$$\Delta = \frac{b\,\delta A}{2\,\pi\,x_3\,c_l} \tag{2.16}$$

where x_3 is the depth of the source below the surface and c_l is the longitudinal wavespeed. Of considerable importance is the fact that real cracks will open in a finite time. This will have the effect of widening the singularity and thus giving a means of measuring the time over which the source operates.

It is possible to use (2.16) to arrive at an expression which will allow an estimate of a minimum detectable crack size and velocity to be

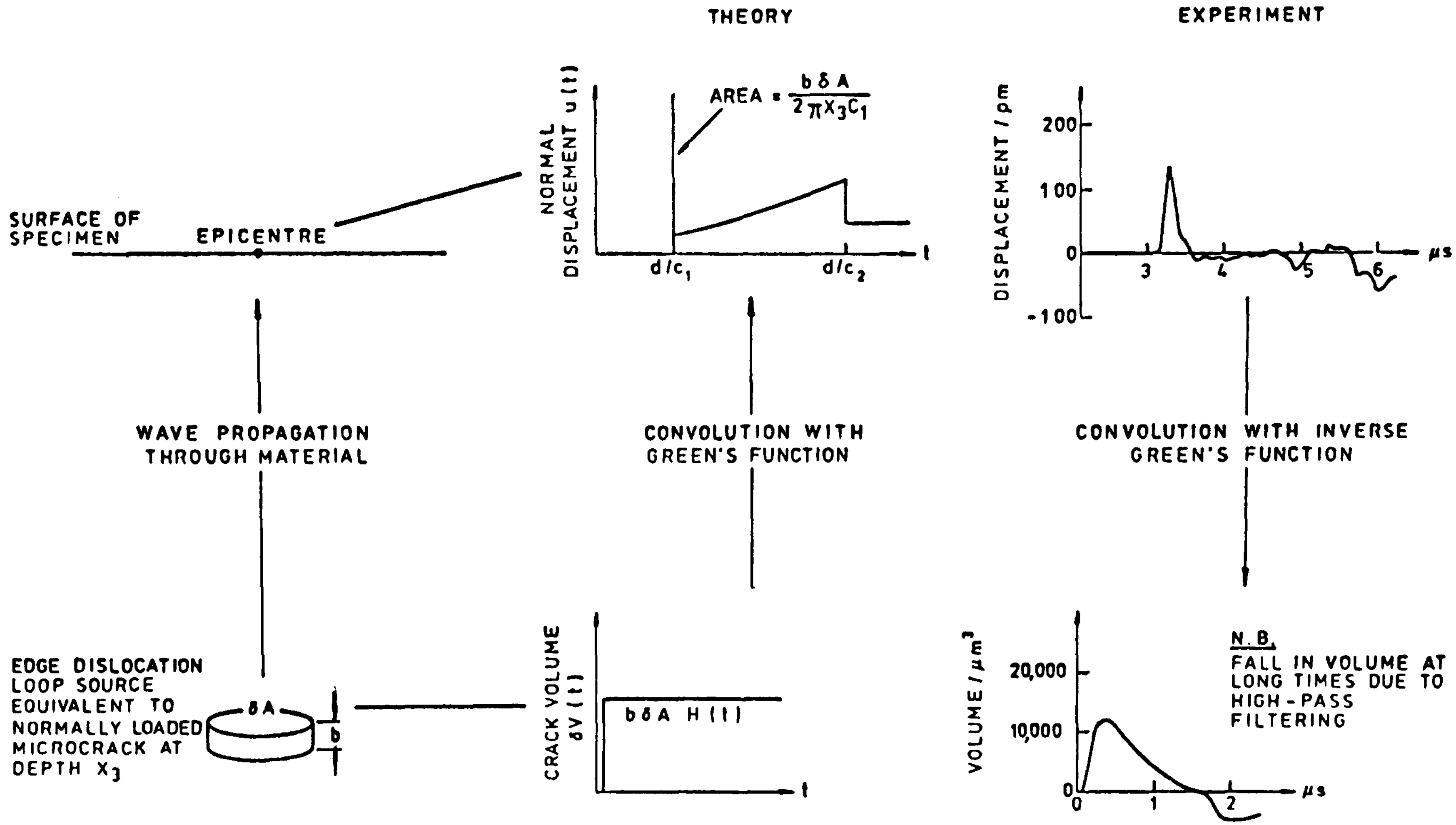

Figure 2.16. Comparison of theoretical and experimental results for the operation of an edge dislocation loop. Contrast the theoretical displacement with that of Figure 2.13; the difference is due to the choice of source functions [Ref 58].

made. Assume that the area of the crack, δA, is πa^2 where a is the crack radius. Further assume that the crack grows to radius a in a time τ equal to a/v, where v is the crack velocity. Differentiating (2.16) once with respect to τ, it can be shown that the maximum displacement for the singularity is given by:

$$U_{max} = \frac{b \, \delta A \, v}{\pi \, c_l \, x_3 \, a} \tag{2.17}$$

Wadley and Scruby show that the relationship between the crack volume and crack radius due to an applied stress is:

$$b \, \delta A = \frac{8 \, \pi \, (1 - \nu^2) \, \sigma \, a^3}{3 \, E} \tag{2.18}$$

where ν is Poisson's ratio, E is Young's modulus, and σ is the applied stress. Substituting (2.18) for $b\delta A$ in (2.17) yields:

$$U_{max} = \frac{8 \, (1 - \nu^2) \, \sigma \, a^2 \, v}{3 \, E \, c_l \, x_3} \tag{2.19}$$

which is the desired expression. By inserting typical values for the specimen and knowing the minimum detectable displacement for the transducer, an estimate of the minimum detectable a^2v product can be obtained.

Wadley and Scruby performed their experiments in electrolytic iron and mild steel, and obtained numerous acoustic emission displacement waveforms from microcracking sources. They then deconvolved these displacement waveforms using equation (2.14), and obtained results which showed how the crack volume varied as a function of time (see Figure 2.16). It is clear that the agreement with theory is not exact, but this is explainable because their detection system was band-pass filtered between 35 kHz and 25 MHz. Loss of DC coupling caused the displacement curve to not produce the expected ramp before the shear wave arrival, with the resulting "droop" in the calculated source volume.

2.3 Propagation Effects

The source models discussed in the previous section presuppose a lossless media in which the stress wave propagates. Real materials are not lossless, however, and it is necessary to understand the various mechanisms by which the wave energy is lost in order to predict how acoustic emission signals might be affected during actual experiments.

The first component of attenuation which is important to acoustic emission signals is geometrical spreading. Because acoustic emission comes from a point source rather than a line or an area, the stress wave will propagate as a diverging spherical wave. Kinsler and Frey [Ref 59] give the spherical wave equation as:

$$\frac{\partial^2 (r\,p)}{\partial t^2} = c^2 \frac{\partial^2 (r\,p)}{\partial r^2} \tag{2.20}$$

where r is the radius, p is the pressure, c is the wave speed, and t is the time. For a diverging spherical wave having harmonic vibrations, the solution to (2.20) is:

$$p = \frac{A}{r} \exp\left(j(\omega t - k r)\right) \tag{2.21}$$

where A is the amplitude, j is $\sqrt{-1}$, ω is the angular frequency, and k is ω/c, the wavelength constant. Thus, a given diameter transducer sensitive to force would have an electrical output inversely proportional to its distance r from the source simply due to the spreading of the wavefront.

In general, the amplitude of the wave will not be constant as indicated in (2.21), but will instead decrease:

$$A = A_o \exp(-\alpha r) \tag{2.22}$$

where α is the attenuation coefficient. The attenuation is due to two general processes, namely absorption, wherein the acoustic wave performs work as it propagates and thus loses energy, and scattering, whereby part of the energy in the wave is reflected out of the path of propagation. The value of the attenuation coefficient is a function of the material, its homogeneity, its temperature, and the frequency content of the acoustic wave.

Absorption in metals at room temperature for frequencies around 1 MHz can be divided into losses due to hysteresis and losses due to relaxational processes. Hysteresis refers to the lag between the applied stress and the resulting strain when a material is cycled from a positive stress to the negative of that stress and back again. One mechanism for hysteresis loss occurs when an ultrasonic wave interacts with the stress field of a pinned dislocation [Ref 60]. At low strain amplitudes (about 1 microstrain) the attenuation resulting from this mechanism is proportional to frequency, while at higher strain amplitudes the attenuation is frequency independent. Relaxational losses can occur when there is anisotropy in the structure causing strain variations, and thus heat flow from highly strained regions to lesser strained areas. Relaxation losses can also occur when the acoustic pressure forces atoms into vacant lattice positions against resisting interatomic forces; this is called structural relaxation. Both of these processes are frequency dependent because of the finite relaxation time needed for energy to flow from one position to another. If it is assumed that the acoustic frequency is less than the reciprocal of the relaxation time, then it can be shown according to Blitz [Ref 61] that the attenuation will be proportional to the square of the frequency. The total attenuation due to absorption will be the sum of the attenuations produced by the three absorption mechanisms discussed above:

$$\alpha_a = c_1 + c_2 f + c_3 f^2 \qquad (2.23)$$

where the c's represent constants.

Scattering results when the sound wave encounters inhomogeneities such as inclusions, pores and flaws. Since, in general, the scatterer will have a different acoustic impedance than the main material, reflection and refraction will occur and energy will be directed out of the path of propagation of the acoustic wave. The amount of scattering which will occur in a given situation depends upon the frequency of the sound, the cross-sectional area of the scatterer which is normal to the sound propagation direction and the shape of the scatterer. Figure 2.17 shows the kind of behavior obtained from a spherical scatterer by Hochschild [Ref 62]. For a given cross-section of scatterer, the Rayleigh region occurs at low frequencies, where the scattering power is low and varies as the fourth power of the frequency. As the frequency increases the Mie or resonance region occurs, where oscillations in the scattering power occur. At high frequencies the optical region occurs, where the scattering power is constant. The attenuation coefficient due to scattering, as depicted in Figure 2.17, has been expressed by Filipczynski, Pawlowski and Wehr [Ref 63] as:

$$\begin{aligned} \alpha_s &= c_4\, d^3\, f^4 \qquad (d << \lambda) \\ \alpha_s &= c_5/d \qquad (d >> \lambda) \end{aligned} \tag{2.24}$$

where d is the diameter of the scatterer and λ is the wavelength of the sound.

In addition to the straight forward energy loss caused by wave spreading and attenuation discussed above, an apparent energy loss can occur if energy is channeled into propagation modes which the transducer cannot detect. Such a phenomenon is called mode conversion. It occurs at boundaries where there is an acoustic impedance mismatch. The physics behind mode conversion has been discussed by Carlyle [Ref 3], and is shown in Figure 2.18a, where a longitudinal wave exerts a force F on a boundary between a solid and air. Resolving F into components F_x

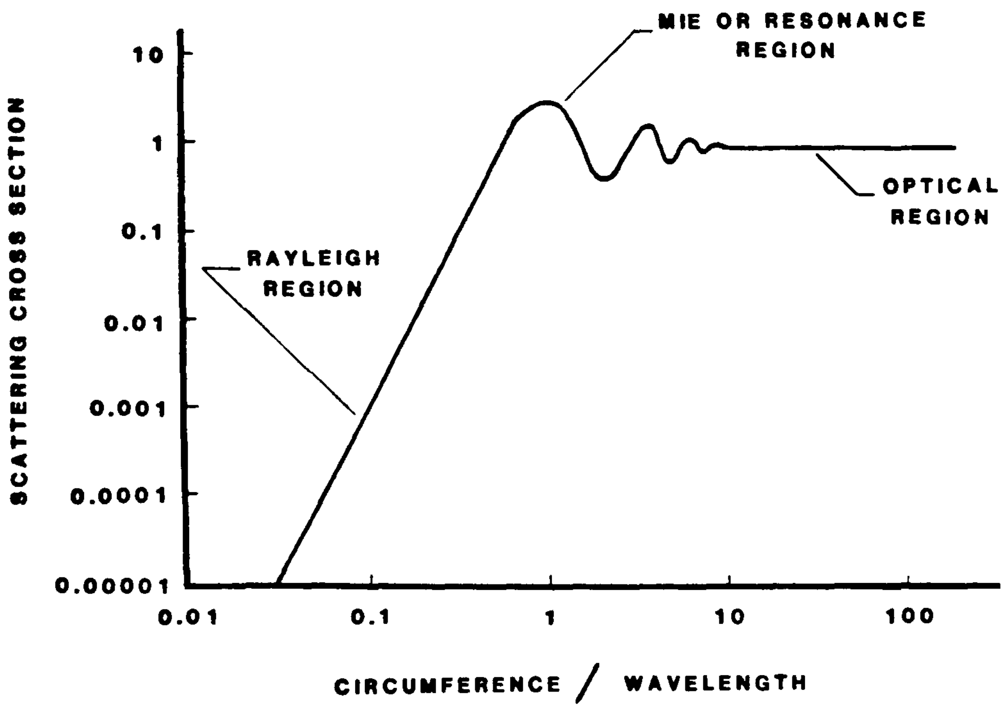

Figure 2.17. Variation in effective size of a spherical flaw with frequency [Ref 62].

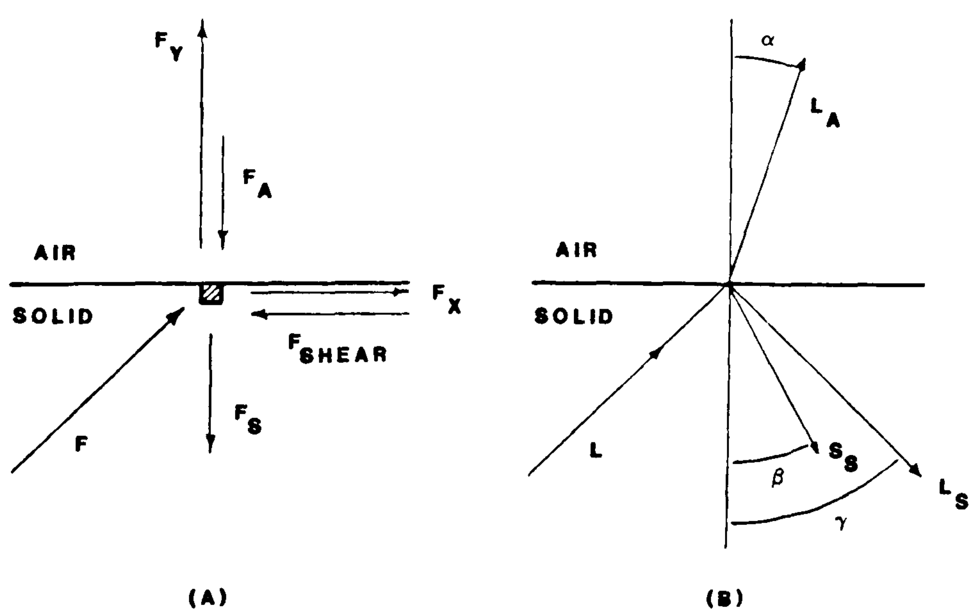

Figure 2.18. Mode conversion. (a) Physical origin of phenomenon. (b) Reflection and refraction of a longitudinal wave at a boundary [Ref 64].

and F_y, it can be seen that F_y must be balanced partly by a compressional force F_a in air and partly by the elastic reaction F_s of the solid, while F_x must be entirely balanced by a shear force in the solid since air cannot support a shear stress. Assuming for the moment that a small isolated element is located at the boundary, it will be subjected to both shear and compressional forces and will therefore become a Huygen's source of both shear and compressional waves. The angles that these waves make with a normal to the surface can be found using Snell's law:

$$\frac{\sin \alpha}{c_{la}} = \frac{\sin \beta}{c_{ss}} = \frac{\sin \gamma}{c_{ls}} \tag{2.25}$$

where α, β and γ are defined in Figure 2.18b, c_{la} and c_{ls} are the speeds of longitudinal waves in air and in the solid, respectively, and c_{ss} is the speed of shear waves in the solid. In addition to the types of waves mentioned, surface waves may also be produced in the solid.

To this point only propagation energy loss mechanisms have been discussed. However, there is at least one other propagation effect of importance to acoustic emission work, namely, dispersion. Dispersion will cause a spreading or broadening of a pulse in the time domain through frequency dependent velocities of various components of the wave. The effect is caused by interference of the wave with itself due to geometry, and is most apparent in Lamb waves in plates. Figure 2.19, due to Krautkramer [Ref 65], shows the complex relationship between plate thickness, sound frequency and velocity. Restricting attention for the moment to the fundamental, or zero order waves, it can be seen

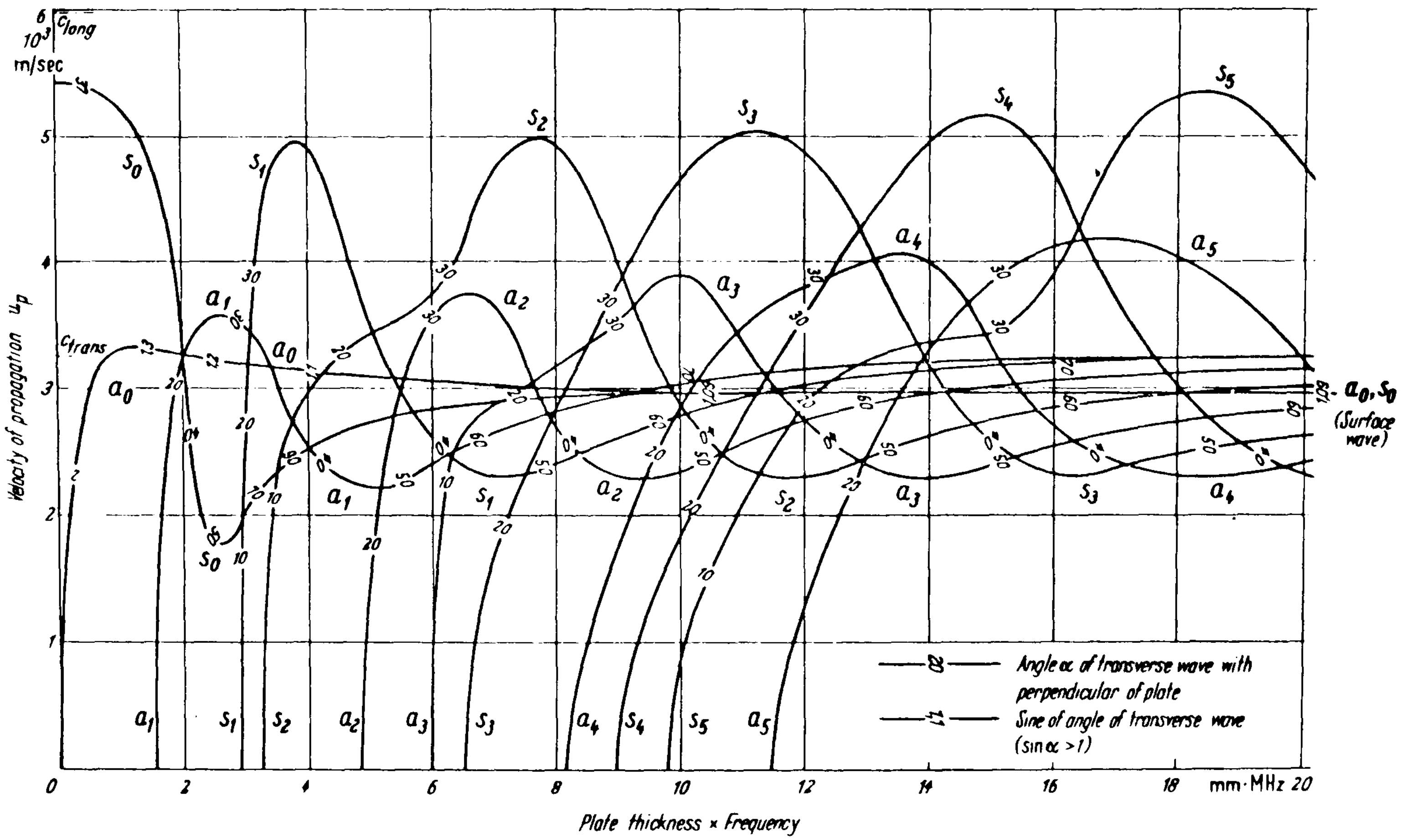

Figure 2.19. Dispersion of Lamb waves in steel where c_l = 5.96 km/s and c_s = 3.26 km/s [Ref 65].

that the antisymmetric wave propagates slower than the symmetric wave at low values of the plate thickness-sound frequency product, but the situation reverses as this product gets bigger. At any given frequency several orders of both types of Lamb waves can propagate, all at different velocities.

The practical implications of Figure 2.19 have been demonstrated by Elsley and Graham [Ref 66]. The physical arrangement and velocities of propagation, along with the velocity versus frequency curves for the specimen used are shown in Figure 2.20. Also appearing in Figure 2.20 is an equation that they used to calculate the ray path lengths, the first six values of which are 103, 123, 168, 210, 244, and 291 mm. Through appropriate computer programs, they obtained the plots of Figure 2.21, which show a pulse dispersing as it propagates as an antisymmetrical Lamb wave and as a symmetric Lamb wave. It is easy to see in the symmetric Lamb wave plots how the high frequency components arrive later than the low frequency components, with the effect becoming more pronounced as the path length increases. Dispersion in the antisymmetric Lamb wave plots is not so easily seen because a 100 kHz high pass digital filter was used. Of more importance than the graphical illustration of the effects of dispersion is the result obtained when all of the plots in Figure 2.21 are added together to construct a theoretical multipath dispersed waveform. This is shown at the bottom of Figure 2.22, along with a real acoustic emission signal at the top of the graph. The real signal had as its source a crack growing at (x_0,y_0) in Figure 2.20, and it was recorded at (x_1,y_1), precisely the same spot where the theoretical waveform was constructed. Considering

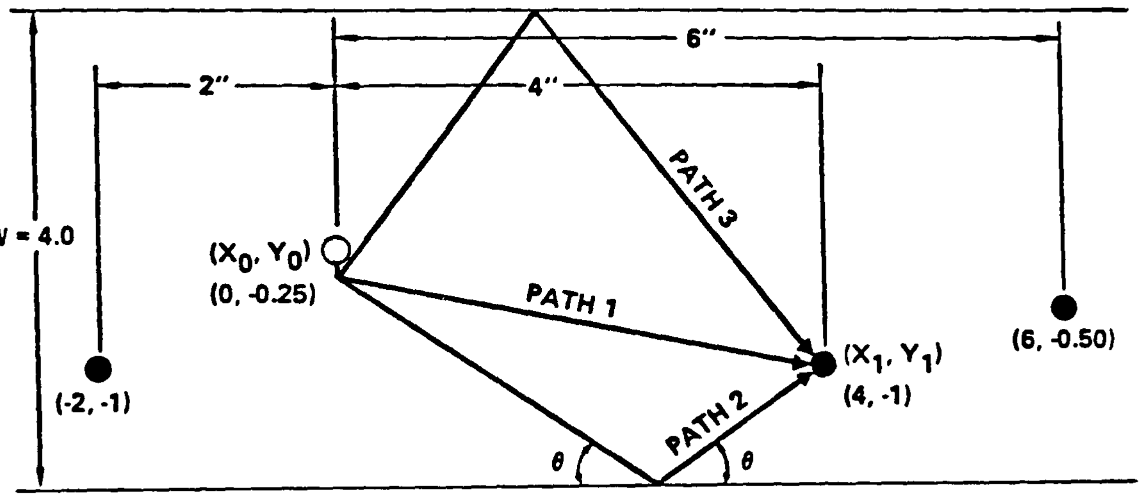

$$P_n = \frac{Z_n}{\sin\left(\tan^{-1}\frac{Z_n}{|x_1 - x_0|}\right)} \; ; \; Z_n = \mathrm{MOD}\left(\frac{n}{2}\right)W + (-1)^{\mathrm{MOD}\left(\frac{n+3}{2}\right)}\left[y_1 + (-1)^{\mathrm{MOD}\left(\frac{n+2}{2}\right)} y_0\right]$$

$V_L = 6374$ m/s
$V_S = 5440$ m/s
$V_A = 3170$ m/s
$V_R = 2897$ m/s
$V_M = 1600$ m/s

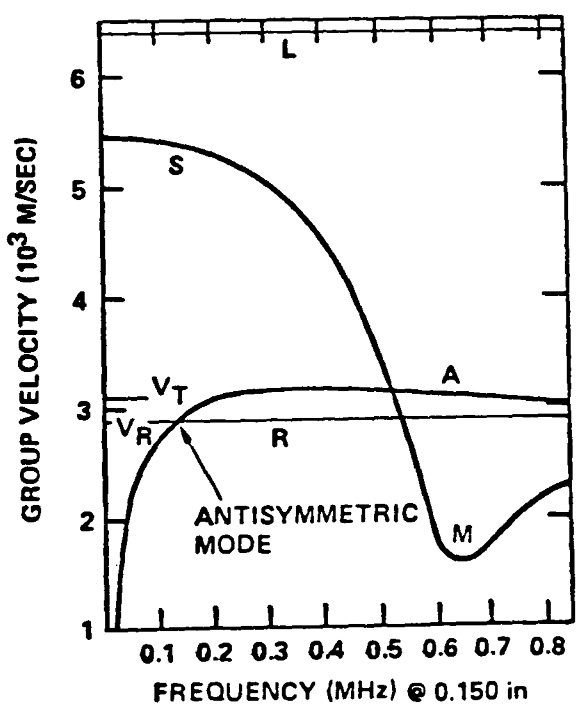

Figure 2.20. Geometry, path length equation and simplified dispersion curves used for theoretical modeling of acoustic emission propagation [Ref 66].

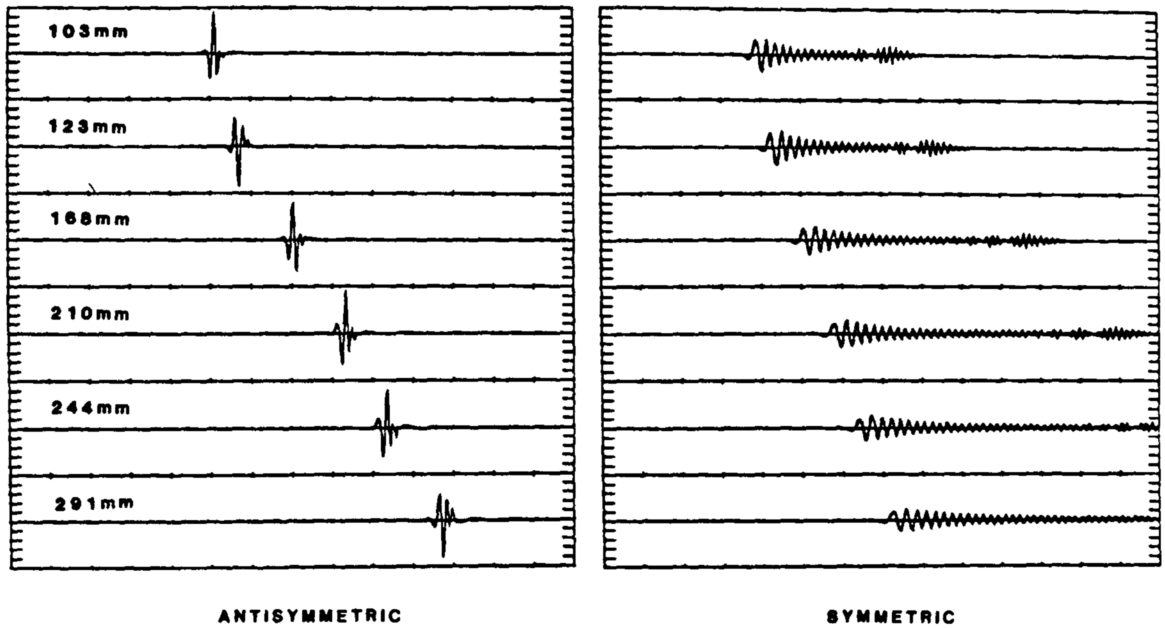

Figure 2.21. Dispersion of a pulse propagating as a symmetric and as an antisymmetric Lamb wave over six path lengths [Ref 66].

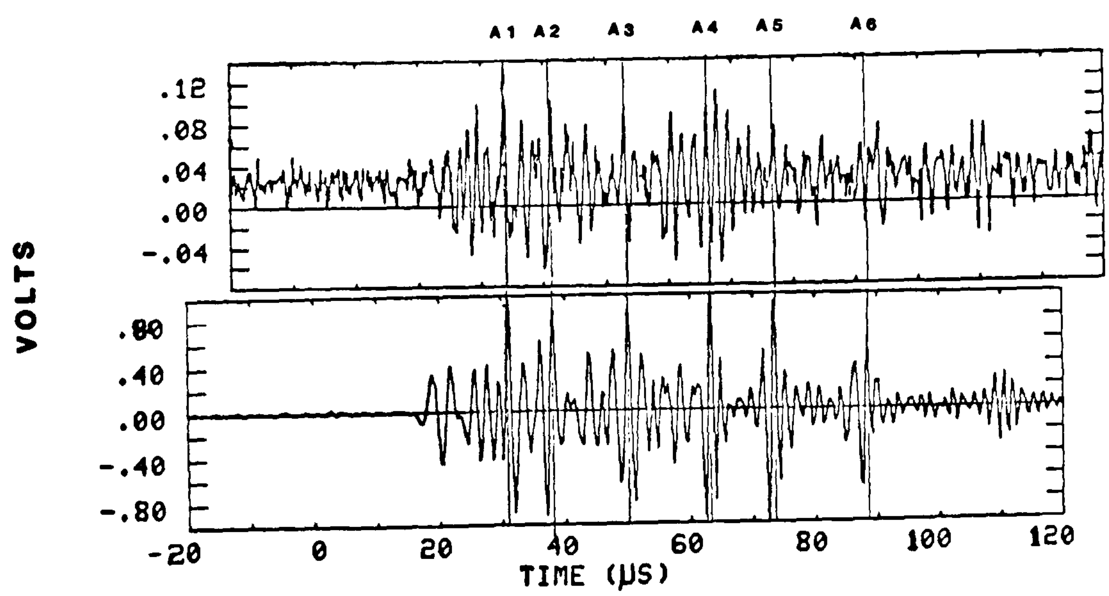

Figure 2.22. Comparison of an actual acoustic emission signal due to crack growth (top) with a theoretical waveform formed by adding together all of the signals in Figure 2.21 [Ref 66].

that there are probably many more paths and higher orders of Lamb waves contributing to the real signal, that the shape of the crack stress wave is probably different from the pulse assumed for the theoretical calculations, and that the transducer averaged the response over an area instead of producing an output from a point as the computer did, the agreement is remarkable.

2.4 Signal Detection

Once an elastic wave from an acoustic emission has propagated to the surface of the specimen it must be detected if any use is to be made of its information content. Detection is commonly accomplished with a transducer, which performs its function by converting a particular component of the mechanical elastic wave into an electrical signal which can be conveniently amplified, recorded and processed. Many design requirements must be considered in the selection of a suitable transducer for acoustic emission work, including broad bandwidth, high sensitivity, high response fidelity, small element size, low acoustic impedance, omni-directional reception, and wide dynamic range. These requirements are in some cases mutually exclusive, as for example a broad bandwidth with a high sensitivity, so most often a compromise is necessary.

Three of the design criteria can be treated without consideration for the specific type of transducer to be used; these are omni-directional reception capability, element size, and acoustic impedance. With regard to omni-directional reception, the only option available is to design the transducer to respond to the particle displacement normal to the surface of the specimen and to give the element a circular shape when viewed along the specimen normal. Since the response of most transducers is the average value of the displacement over their area, it can be shown according to Kino [Ref 67] that the response of the transducer to the normal displacement caused by a surface wave is given by:

$$V_s = \frac{2 J_1 (k_s a)}{k_s a} \tag{2.26}$$

where k_s is $2\pi/\lambda_s$, a is the radius of the transducer, and $J_1(x)$ is a Bessel function of the first kind. The 3 dB points of (2.26) occur when:

$$a/\lambda_s = 0.24 \tag{2.27}$$

For a longitudinal wave the response can be calculated from:

$$V_l = 2 \cos\theta \left[\frac{J_1 (k_l a \sin\theta)}{k_l a \sin\theta} \right] \tag{2.28}$$

where k_l is the wave number for longitudinal waves and θ is measured from the surface normal. Using (2.27) and assuming that $k_l = 0.5\ k_s$, (2.28) can be solved to show that the 3 dB points for longitudinal waves are $\theta = \pm 45$ degrees. For a transducer which must respond to frequencies up to 2 MHz mounted on aluminum where $c_s = 3$ km/s, (2.27) requires that the transducer diameter be 0.75 mm. This dependence of the transducer response upon the ratio of the transducer diameter to sound wavelength is termed the aperture effect.

Acoustic impedance is defined as the product of the density of the media, ϱ, and the speed of sound in the media, c. Using the acoustic impedances of the transducer and the solid in which the acoustic emission propagates, it has been shown by Frederick [Ref 68] that the power transmission coefficient of a longitudinal wave arriving at a boundary at normal incidence is given by:

$$T = \frac{4 \varrho_2 c_2 \varrho_1 c_1}{(\varrho_2 c_2 + \varrho_1 c_1)^2} \tag{2.29}$$

Assuming that media 1 is aluminum with $\varrho_1 c_1 = 17.3 \times 10^6$ kg/m²s, and media 2 is a PZT-5 transducer with $\varrho_2 c_2 = 28 \times 10^6$ kg/m²s, then only 94% of the incident sound power in the area under the transducer is transmitted into the transducer. Note that this is the maximum amount of power which can be transmitted; at angles other than normal mode conversion occurs and less power gets into the transducer.

One of the most popular types of transducer is the piezoelectric. Piezoelectricity was discovered by the Curie brothers in 1880, and refers to the production of electric charges on the surface of crystals that do not possess a center of symmetry which have been deformed by mechanical pressure. A schematic representation of the effect as described by Hueter and Bolt [Ref 69] is shown in Figure 2.23. Four different constants are used to characterize piezoelectricity; these are d, the strain developed in an unloaded crystal for a given electric field; e, the stress developed by a given electric field when the

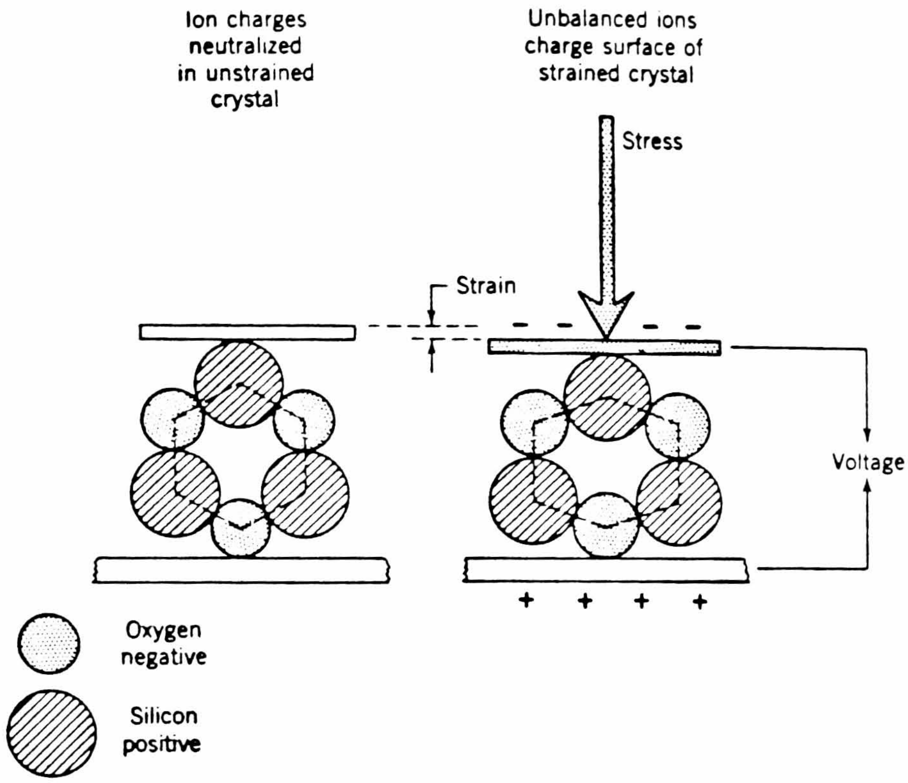

Figure 2.23. Schematic representation of the origin of piezoelectricity [Ref 69].

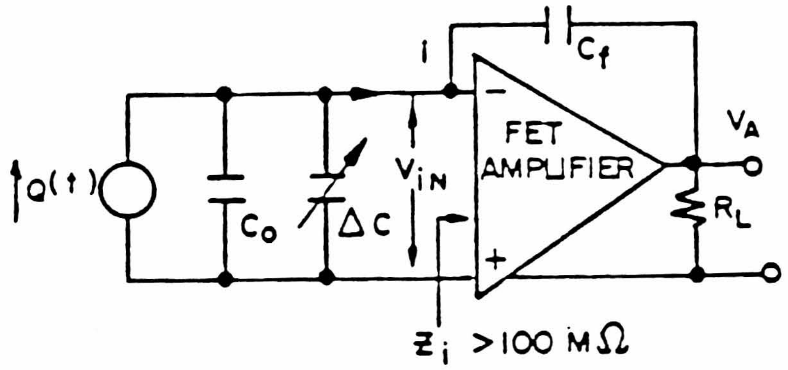

Figure 2.24. Equivalent circuit used to derive Equation 2.35 [Ref 71].

crystal is clamped; g, the open circuit electric field developed for a given stress; and h, the open circuit electric field developed for a given strain. These constants are not independent, and according to Mason [Ref 70] are related in tensor notation as follows:

$$d_{nj} = \frac{\epsilon^T_{mn}\; g_{mj}}{4\pi} = e_{ni}\; s^E_{ij}$$

$$e_{nj} = \frac{\epsilon^S_{mn}\; h_{mj}}{4\pi} = d_{ni}\; c^E_{ij} \qquad m, n = 1 \text{ to } 3$$

$$g_{nj} = 4\pi\,\beta^T_{mn}\, d_{mj} = h_{ni}\; s^D_{ij} \qquad i, j = 1 \text{ to } 3 \tag{2.30}$$

$$h_{nj} = 4\pi\,\beta^S_{mn}\, e_{mj} = g_{ni}\; c^D_{ij}$$

where the superscripts T, S, E, and D mean constant stress, strain, electric field and electric displacement, respectively, ϵ is the permittivity, s is the elastic compliance, c is the elastic stiffness, and β is the dielectric impermeability.

The piezoelectric g constant has the useful property of predicting the minimum detectable displacement a crystal can sense. By definition:

$$E_m = g_{mn}\, T_n = \frac{v_m}{l_m} = g_{mn}\, c_{mn}\; S_m = g_{mn}\, c_{mn}\, \frac{\xi_m}{l_m} \tag{2.31}$$

where ξ is the displacement and l is the thickness of the crystal. Solving Equation (2.31) for displacement:

$$\xi_m = \frac{v_m}{g_{mn}\; c_{mn}} \tag{2.32}$$

According to Frederick [Ref 68], PZT-5 has g_{33} = 0.0248 mV/N and

c_{33} = 67.5 GN/m². Assuming a high impedance amplifier (so as not to disturb the open circuit condition) with an input noise voltage of 10 μV, PZT-5 can theoretically detect a minimum displacement of 5.97 femtometers!

To obtain a complete description for the behavior of a piezoelectric crystal, it is necessary to consider the internal energy stored in various forms such as mechanical, electrical, and thermal. Mason shows that it is possible to use the elastic enthalpy function to define the relationship between independent variables such as T (stress), D (electric displacement), and σ (entropy):

$$dH = -S_i \, dT_i + \frac{E_m \, dD_m}{4\pi} + \theta \, d\sigma \qquad (2.33)$$

where θ is the temperature, and derive the constitutive equation for a piezoelectric crystal in terms of the dependent variables S and E (θ is not shown because isothermal adiabatic conditions are assumed in Mason's derivation):

$$\begin{aligned} T_i &= c^E_{ij} S_i - e_{mj} E_m \qquad & n, m = 1 \text{ to } 3 \\ D_n &= 4\pi e_{ni} S_i + \epsilon^S_{mn} E_m \qquad & i, j = 1 \text{ to } 6 \end{aligned} \qquad (2.34)$$

Equation (2.34) can be solved subject to Newton's second law ($\frac{\partial T_{kl}}{\partial x_k} = \varrho \frac{\partial^2 \xi_k}{\partial t^2}$ where ϱ is the density) and one of Maxwell's equations ($\frac{\partial D_i}{\partial x_i} = 0$) along with suitable boundary conditions to obtain a complete solution for the behavior of the piezoelectric crystal in a particular situation.

The approach just outlined is seldom attempted. Instead, it has been found easier to develop equivalent circuit models for the piezoelectric transducer and solve the resulting circuit equations to predict the behavior of the transducer. Vahaviolos [Ref 71] used the equivalent circuit of Figure 2.24 to derive an expression for the voltage output of an air-backed piezoelectric crystal operating at its resonant frequency. In Figure 2.24, C_0 represents the static capacitance of the transducer, which is equal to the product of the electroded area, A, the dielectric constant of the crystal, and the permittivity of free space, divided by the thickness of the crystal, l. (For a 1 cm diameter crystal of PZT-5 three mm thick C_0 is 400 pf). ΔC is a variable capacitor used to control the gain of the FET amplifier in conjuction with C_F, and R_L is the output resistance of the circuit. The output voltage of the circuit in Figure 2.24 is given by:

$$V_A = \frac{d_{33} A v_t}{l C_F} \int_0^T (\sigma_1(t) - \sigma_2(t))\, dt \tag{2.35}$$

where σ_1 is the stress induced by the media in the crystal, σ_2 is the stress induced by the air backing on the crystal, v_t is the velocity of the wave in the crystal, and T is the duration of the acoustic pulse.

The assumptions of air backing and resonant operation were used by Vahaviolos because he was interested in obtaining maximum sensitivity. The shape of the waveform was not important to him as his work was concerned with estimating the energy content of an acoustic emission waveform, which he proved could be done using a narrow band transducer. Identification of the mechanisms which cause an acoustic emission, however, requires a broad bandwidth since information content is proportional to bandwidth. Further, flatness of response over the operating bandwidth is desirable, which cannot be obtained using an air backed transducer. This fact may be appreciated from Figure 2.25, which compares the response of an air backed transducer and a terminated transducer to identical inputs. It is obvious from the oscillations that the air backed transducer must have a peak in its frequency response. The penalty for wide bandwidth is also clear in Figure 2.25, in that the terminated transducer's response is about 3 dB less than the air backed transducer. Kino [Ref 67] has investigated the more general problem of a terminated transducer using the equivalent circuit shown in Figure 2.26. For a transducer backed with a substance that perfectly matches the acoustic impedance of the transducer, the output voltage is given by:

$$V_3 = \frac{h}{j\,\omega} \left(1 - \exp\left\{- j\omega \left(\frac{\varrho}{E}\right)^{1/2} l\right\}\right) \frac{2\,Z_1}{Z_1 + Z_o}\, v_1 \tag{2.36}$$

where ω is the angular frequency, h is the piezoelectric open circuit strain constant, Z_1 is the acoustic impedance of the solid in which the acoustic emission propagates, and v_1 is the particle velocity of the acoustic emission waveform. At resonance the output is:

$$V_3 = \frac{2\,h}{\pi} \left(\frac{\varrho}{E}\right)^{1/2} \frac{2\,Z_1}{Z_1 + Z_o}\, v_1 \tag{2.37}$$

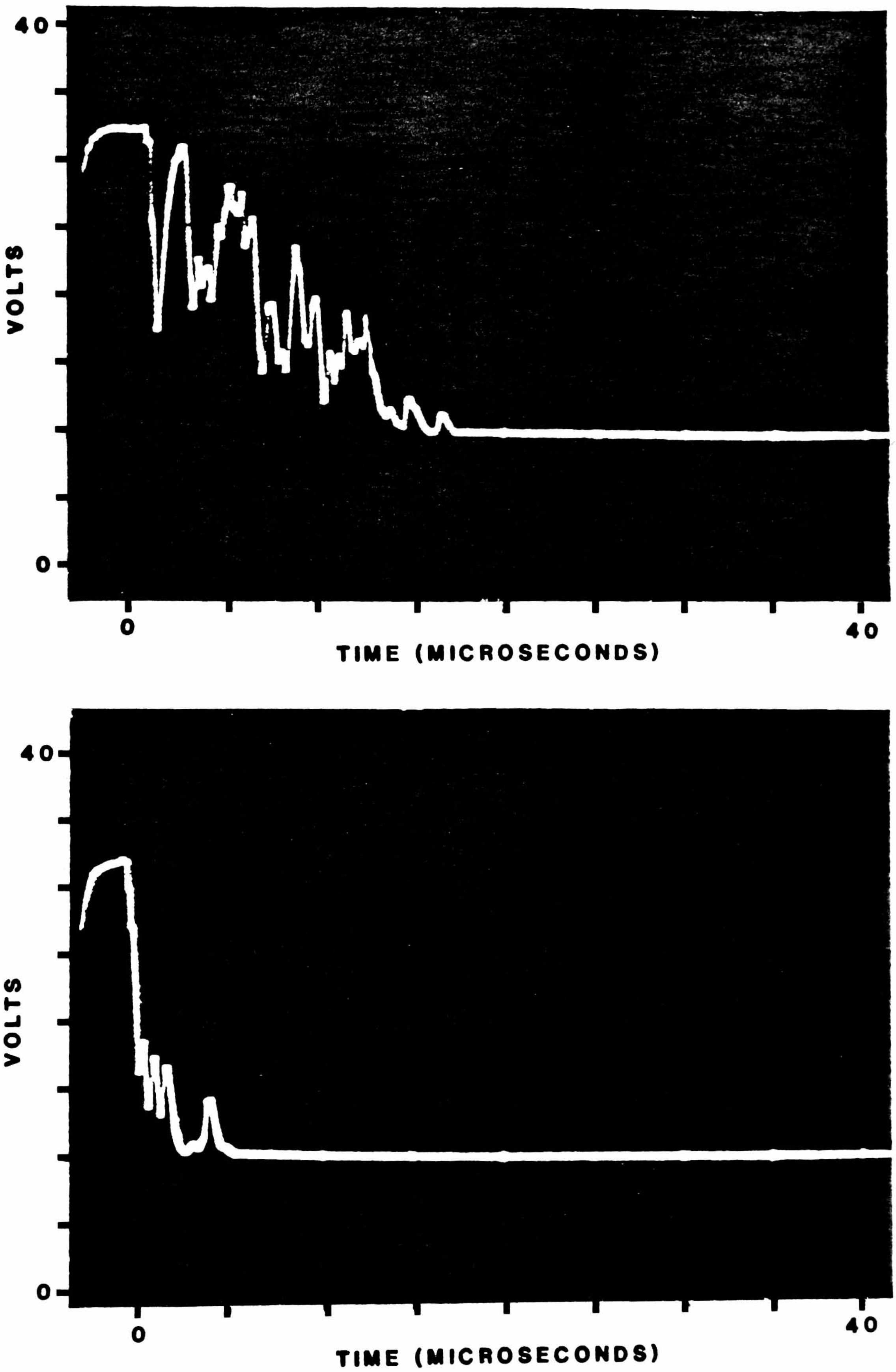

Figure 2.25. Time domain response of an air-backed transducer (top) compared with that of an acoustically terminated transducer (bottom) [Ref 72].

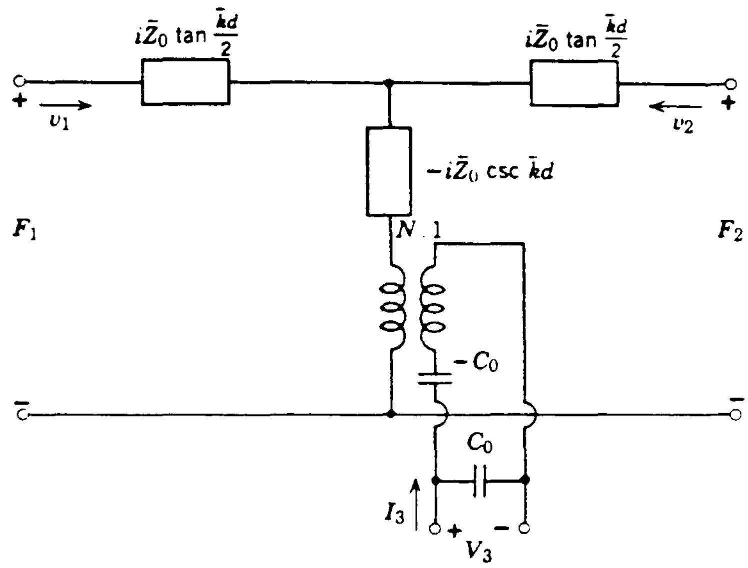

$$\bar{Z}_0 = A(\rho \bar{c}_{44})^{1/2}, \quad \bar{k} = \omega(\rho/\bar{c}_{44})^{1/2}, \quad C_0 = \frac{\epsilon^S_{xx} A}{d}, \quad N = C_0 h_{x5}.$$

Figure 2.26. Equivalent circuit for a thin disc piezoelectric transducer used to derive Equation 2.36 [Ref 67].

and as the frequency goes to zero the output approaches:

$$V_3 - j\,h\,l \left(\frac{\varrho}{E}\right)^{1/2} \frac{2\,Z_1}{Z_1 + Z_o}\, v_1 \tag{2.38}$$

For a transducer backed with air the output as given by Kino is:

$$V_3 = \frac{-h}{j\,\omega} \frac{2\,Z_1\,v_1}{\left(Z_1 + j\,Z_o \tan \omega\, l \left(\frac{\varrho}{E}\right)^{1/2}\right) \cos \omega\, l \left(\frac{\varrho}{E}\right)^{1/2}} \tag{2.39}$$

At resonance the air backed transducer produces a voltage:

$$V_3 = \frac{4\,h\,l}{j\pi} \left(\frac{\varrho}{E}\right)^{1/2} v_1 \tag{2.40}$$

and as the frequency goes to zero the output approaches:

$$V_3 - \frac{j\,h\,l^2\,\varrho}{E}\,\omega\, v_1 \tag{2.41}$$

It can be seen from (2.41) that the response of an air backed transducer falls off at low frequencies. This occurs because the back is free to move with the front surface, so at low frequencies there is no net applied strain. Thus, an air backed transducer is an inferior choice when broad band response is desired. It should also be noted that equations 2.36 through 2.41 show that the output of a piezoelectric transducer is proportional to the particle velocity of the acoustic wave rather that the particle displacement. Since particle velocity is equal to $j\omega u$ where u is the particle displacement, it follows that a piezoelectric transducer's response to displacement will vary linearly with frequency.

Another type of transducer used for acoustic emission work is the capacitive transducer. In its simplest form, it is a polished disc of area A suspended over the specimen at a distance l. The capacitance of such a transducer is:

$$C = \frac{Q}{V} = \frac{A\epsilon_0}{l} \tag{2.42}$$

where Q is the charge, V is the operating voltage and ϵ_0 is the permittivity of free space. Differentiating (2.42) with respect to distance yields the charge sensitivity:

$$dQ = \frac{-A\epsilon_0 V}{l^2}\, dl \tag{2.43}$$

and it is easy to derive the voltage change for a given displacement as:

$$dV = \frac{dQ}{C} = \frac{-V dl}{l} = -E dl \tag{2.44}$$

where E is the electric field in the transducer. Using a potential of 50 volts and a separation of 2 microns, a 10 µV output would be produced for a 0.4 picometer displacement. This is two orders of magnitude less sensitive than a piezoelectric transducer. However, the capacitive transducer has the advantage that its output is directly proportional to displacement, and is independent of frequency. A further advantage of the capacitive transducer is that it is non-contacting and thus does not acoustically load the specimen. All of these qualities make the capacitive transducer ideally suited for calibration work.

CHAPTER 3

CALIBRATION TECHNIQUES

This chapter discusses the two most common techniques used to calibrate acoustic emission transducers. Three different system calibration methods which eliminate response variations due to sample geometry are also presented.

3.1 Transducer Calibration

Although acoustic emission experiments can be performed using uncalibrated transducers, it is wise to attempt to obtain a calibration because of the benefits to be obtained by doing so. These include the potential ability to quantitatively compare results with either theoretical predictions or the work of other experimenters, the ability to match an appropriate sensor for a task based on experimental conditions and desired response characteristics and the ability to replace an accidentally damaged transducer in the middle of a test series while maintaining overall data integrity. Useful as it may be, though, calibration is not an easy undertaking, and a complete absolute calibration is an ideal. Any practical calibration procedure utilizes certain assumptions, the nature of which affect not only the results themselves but also limit the conditions under which the calibration can be used.

Sachse and Hsu [Ref 73] have described some of the assumptions commonly made to obtain a practical calibration of a sensor placed on a solid. The first assumption is that the pressure of the sensor does not significantly affect the distributed mechanical field vector quantities (which are traction, or force per unit area, and particle velocity) in the solid near the transducer. The second assumption is that the transducer detects stress waves of a single mode, i.e., only longitudinal or shear waves, which is equivalent to writing the mechanical field vectors as scalars. The third assumption is that the traction and velocity fields are uniform over the region next to the transducer, which means that the traction and velocity fields depend only upon time. The fourth assumption is that the transduction process itself is linear. The fifth assumption is that the calibration medium and the excitation are fixed, i.e., the mechanical loading is constant.

All of the above assumptions taken together result in the transduction relation becoming a transfer function equation which is given by a real convolution integral in the time domain or by a complex multiplication in the frequency domain:

$$V(\omega) = T(\omega)\, U(\omega) \tag{3.1}$$

where V is the output voltage, U is the displacement, and T is the transfer function. Equation (3.1) is valid for all frequencies, but recording devices work over a fixed time interval. Thus, practical calibration procedures will result in a bandwidth limited transfer function, which is usually represented as an amplitude spectrum and a phase spectrum over the frequencies of interest. It should be noted that because of the assumptions outlined above questions such as the effect of different media on the transducer response, or the effect of a velocity input on the response as opposed to a displacement input, or the detection capability of a transducer to surface waves as opposed to longitudinal waves are unanswerable using the transfer function from one calibration procedure. The transfer function, then, represents only a partial calibration for a transducer.

With the limitations of calibration clearly defined the two general methods of calibration, namely reciprocity and comparison, can be described. Reciprocity is a technique which requires that a transducer be reciprocal, i.e., that it be linear and capable of transmitting and receiving and that the ratio of its receiving sensitivity to its transmitting response be constant. This constant is termed the reciprocity parameter. It depends on the acoustic media, the frequency, and the boundary conditions, but is independent of transducer design. As pointed out by Bobber [Ref 74], not all transducers are reciprocal, and no absolute method exists for determining if a transducer is reciprocal. The best that can be done is to infer reciprocity from additional measurements, or by comparing a reciprocity calibration with a comparison calibration. If the results agree, it is evidence that all of the assumptions made doing both calibrations were correct and that the transducer is reciprocal. However, evidence is not proof, and it is possible both methods were wrong and that the errors were coincidentally equal.

The reciprocity method of calibration can be demonstrated using a procedure outlined by Bobber for hydrophones. Figure 3.1 shows the three necessary arrangements and measurements, along with a fourth used for checking the reciprocity of the reversible transducer, T, which is used as both a projector of sound and as a receiver. Sensor P in Figure 3.1 is only used as a projector of sound for the reciprocity calibration, and H is the receiving transducer under calibration. The distance d_1 between the projector and the hydrophone in Figure 3.1 is such that only direct spherical waves impinge on the hydrophone (free-field far-field conditions). Derivation of the free-field voltage sensitivity of the hydrophone, M_H, proceeds by driving the projector with a current i_P. During the first measurement, the output voltage e_{PH} of the hydrophone is given by:

$$e_{PH} = M_H \, P_P = \frac{M_H \, i_P \, S_P \, d_o}{d_1} \tag{3.2}$$

where P_P is the free-field pressure of the projector, S_P is the transmitting current response of the projector, and d_o is the reference distance specified for S_P. During the second measurement the output voltage e_{PT} of the reciprocal transducer is given by:

$$e_{PT} = M_T \, P_P = \frac{M_T \, i_P \, S_P \, d_o}{d_1} \tag{3.3}$$

where M_T is the free-field voltage sensitivity of the reciprocal transducer. From the definition of reciprocity ($M_T/S_T = J$) and the

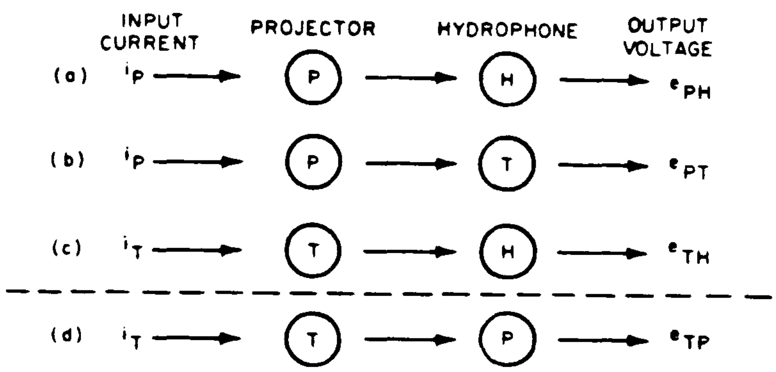

Figure 3.1. Physical arrangement and measurements needed for a reciprocity calibration, (d) can be omitted since it is only used as a check of the reversibility of transducer T [Ref 74].

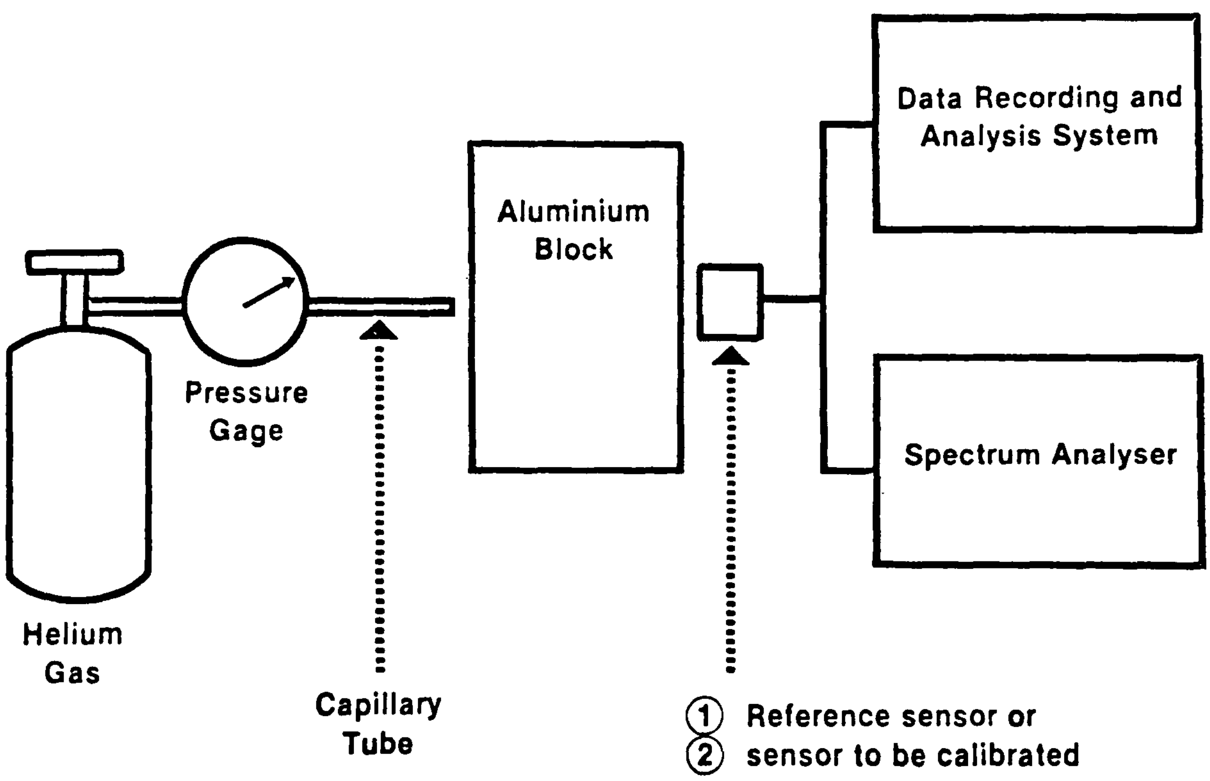

Figure 3.2. Physical arrangement used for comparison calibration using the helium gas jet [Ref 77].

relations shown in (3.2) and (3.3), the following can be derived:

$$M_H = \frac{J\, S_T\, e_{PH}}{e_{PT}} \qquad (3.4)$$

In the third measurement, the reciprocal transducer is driven with a current i_T to produce an output voltage e_{TH} from the hydrophone according to the relationship:

$$e_{TH} = M_H\, P_T = \frac{M_H\, i_T\, S_T\, d_o}{d_1} \qquad (3.5)$$

where S_T is the transmitting current response of the reciprocal transducer. Solving (3.5) for M_H and multiplying this result by (3.4) yields:

$$M_H = \left(\frac{e_{TH}\, e_{PH}}{e_{PT}\, i_T} \; \frac{d_1}{d_o} \; J \right)^{1/2} \qquad (3.6)$$

For the free-field far-field condition assumed, J is given by:

$$J = \frac{2d_o}{\varrho f} \qquad (3.7)$$

where ϱ is the density of the media and f is the frequency. Thus the free-field far-field voltage sensitivity of the hydrophone is given by:

$$M_H = \left(\frac{2d_1}{\varrho f} \; \frac{e_{TH}\, e_{PH}}{e_{PT}\, i_T} \right)^{1/2} \qquad (3.8)$$

which is the reciprocity calibration. As a check for reciprocity the fourth measurement in Figure 3.1 can be made, it can then be shown that:

$$M_H = \left(\frac{2d_1}{\varrho f} \frac{e_{TH} \, e_{PH}}{e_{TP} \, i_P} \right)^{1/2} \tag{3.9}$$

Equation (3.9) provides additional confidence in the value for M_H. It can be seen that only electrical quantities need to be measured during a reciprocity calibration, which are easier to conduct than mechanical measurements.

The derivation of reciprocity calibration just given is for a transducer sensitive to longitudinal waves operating in free-field far-field conditions. Leschek [Ref 75] used equation (3.8) to calibrate a primary sensor which was then used as a reference standard for obtaining calibrations of general acoustic emission sensors when they were mounted on a steel block in which a random frequency ultrasonic generator produced a diffuse acoustic field. He recognized the limitations of his approach and suggested that research be done to derive a diffuse field reciprocity parameter which would be valid for compressional and shear waves in a bounded media. About a year later, Hatano and Mori [Ref 76] developed a reciprocity calibration procedure using Rayleigh wave excitation in a steel block. To do so, they first defined the free-field voltage sensitivity as the ratio of the open circuit receiving voltage to the vertical component of the Rayleigh wave particle velocity at the receiver. They then derived the reciprocity parameter H as the product of a constant (computable from the elastic constants and the density of the media) and the frequency to the three-halves power divided by the square root of the separation distance. Finally, they assumed that all three of the transducers to be used were reciprocal and obtained the free-field voltage sensitivity for the sensor of interest:

$$M_l = \left(\frac{1}{H} \frac{Z_f(1)\, Z_f(3)}{Z_f(2)} \frac{1}{E_T} \frac{E_1\, E_3}{E_2} \right)^{1/2} \tag{3.10}$$

where $Z_f(n)$ is the free impedance of transducer n, E_T is the constant transmission voltage, and E_n is the received output voltage of transducer n.

As was pointed out before, the reciprocity technique depends on the fact that at least one transducer must be reciprocal, a condition which cannot be absolutely proven but only inferred. To avoid this difficulty, calibration by comparison with a standard transducer is preferred. One of the earliest experiments in which this was done was reported by Mcbride and Hutchison [Ref 77], Figure 3.2 shows the test arrangement they employed. The calibration itself is performed by first recording the frequency spectrum of the helium gas jet as detected by a 5 MHz quartz crystal over the range of 0.2 to 1.0 MHz. Next the quartz crystal is replaced by the transducer to be calibrated and a similar spectrum is obtained. The calibration of the transducer is then defined as the ratio between the transducer output and the quartz crystal at each frequency. Although the technique is quite easy to perform, it has several drawbacks. First, it is impossible to obtain the phase response of the transducer being calibrated since there is no way to obtain a reference signal from the gas jet. Second, it is not clear what the excitation mode is at the sensor and therefore it is impossible to predict the calibrated transducer's response to a specific mechanical input. Finally, the calibration is relative to a quartz crystal whose absolute response is unknown, although evidence is presented to show that it is frequency independent.

Another technique for calibration by comparison has been described by Hsu and Breckenridge [Ref 78]; they have termed it the step-force calibration. The unique feature of their method is the fact that the conditions of the calibration procedure have been chosen so that theoretical results can be used to validate the results of the calibration. The theory is due to Pekeris [Ref 79], and predicts the value of vertical displacement on the surface of a semi-infinite isotropic solid at a distance from a step-force function which has been applied to the same surface of the solid in a direction normal to the solid surface. The theory assumes no loading of the block where the displacement is to be measured, which can be accomplished by using a capacitive transducer of the type described in Section 2.4. A contacting transducer will load the specimen and any calibration of it will include this loading effect as part of the calibration.

The step-force calibration is performed using the arrangement shown in Figure 3.3. A glass capillary of 0.2 mm diameter, B, is placed on the test block, A, and is broken by tightening screw C. The step-force released (with a rise time of approximately 0.1 µS) is measured by load cell D, and displayed on the storage oscilloscope F after passing through the charge amplifier E. The surface displacement caused by the step-force is measured at symmetrical points by two transducers, with

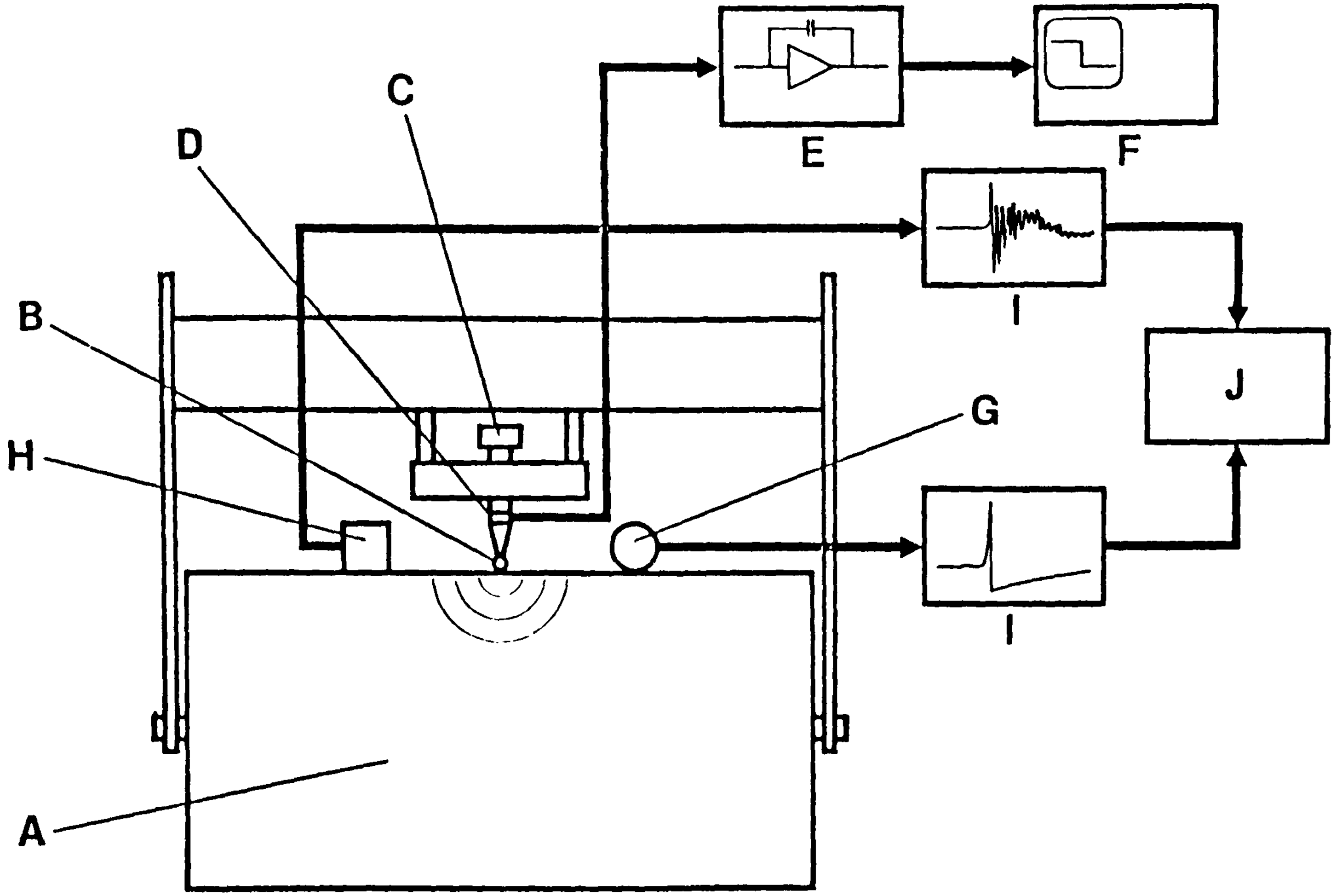

Figure 3.3. Physical arrangement used for comparison calibration using the step-force method [Ref 78].

the true displacement detected by capacitive sensor G and the transducer-loaded displacement detected by the sensor under calibration, H. The transducer voltage outputs are digitized by recorders, I, and stored in the computer, J.

Using the equipment in Figure 3.3, remarkably good agreement can be obtained between the theory of Pekeris and the output of the capacitive transducer, as can be seen in Figure 3.4. The two areas of disagreement, namely the finite displacement and fall time of the drop associated with the arrival of the Rayleigh wave in the experiment, as well as the jog near the end of the experimental trace, are due to experimental constraints. Specifically, the finite area of the capacitive transducer creates most of the disagreement prior to the Rayleigh wave arrival and the finite dimensions of the block itself lead to reflections, the first of which causes the jog near the end of the oscillogram.

Since the agreement between theory and experiment is so good, the response of the capacitive transducer can be used as a standard traceable to basic physical quantities. Figure 3.5 shows the amplitude spectrum and the phase spectrum of the capacitive transducer caused by the step-force function. When similar spectra obtained from the transducer under calibration are divided by the information in Figure 3.5 on a frequency by frequency basis, the amplitude and phase response spectra of the transducer relative to the capacitive sensor are obtained. These latter spectra are the transfer function $T(\omega)$ in equation (3.1). Amplitude and phase spectra relative to the standard

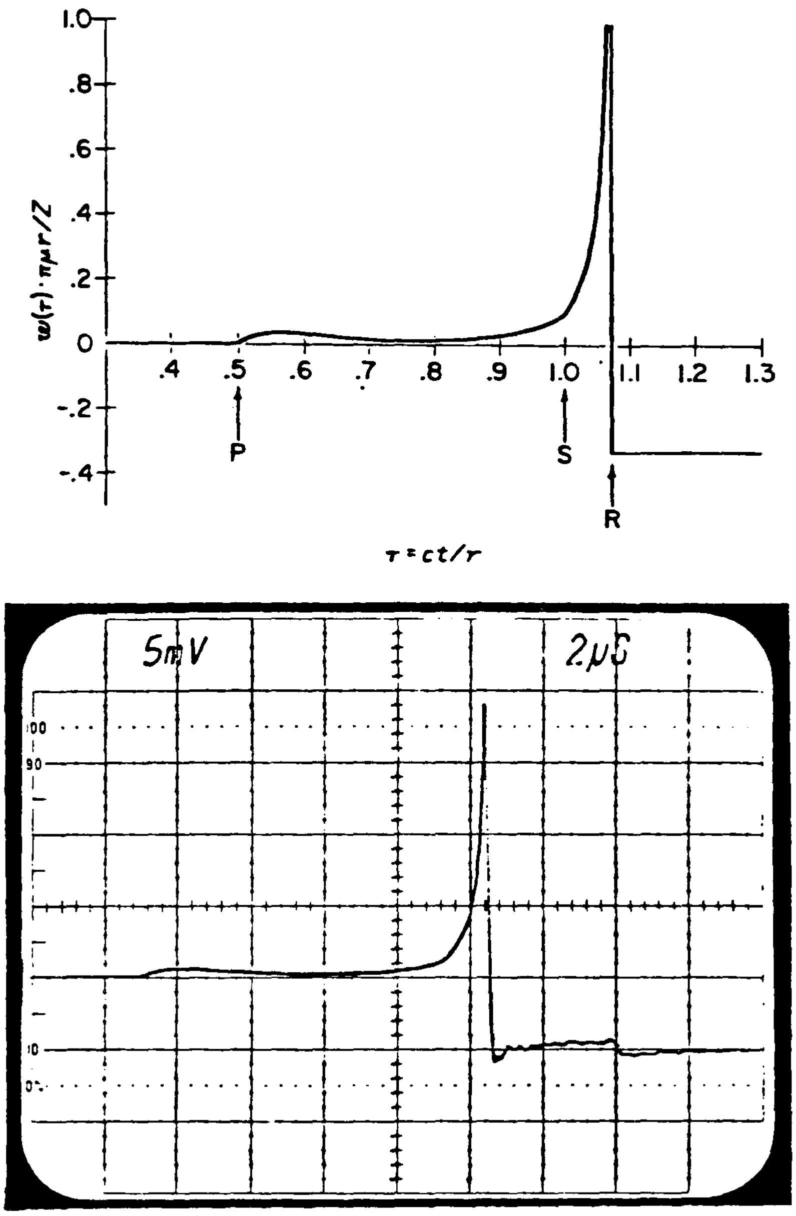

Figure 3.4. Comparison between theoretical vertical displacement (top) and experimental vertical displacement (bottom) achieved in the step-force calibration method [Ref 78].

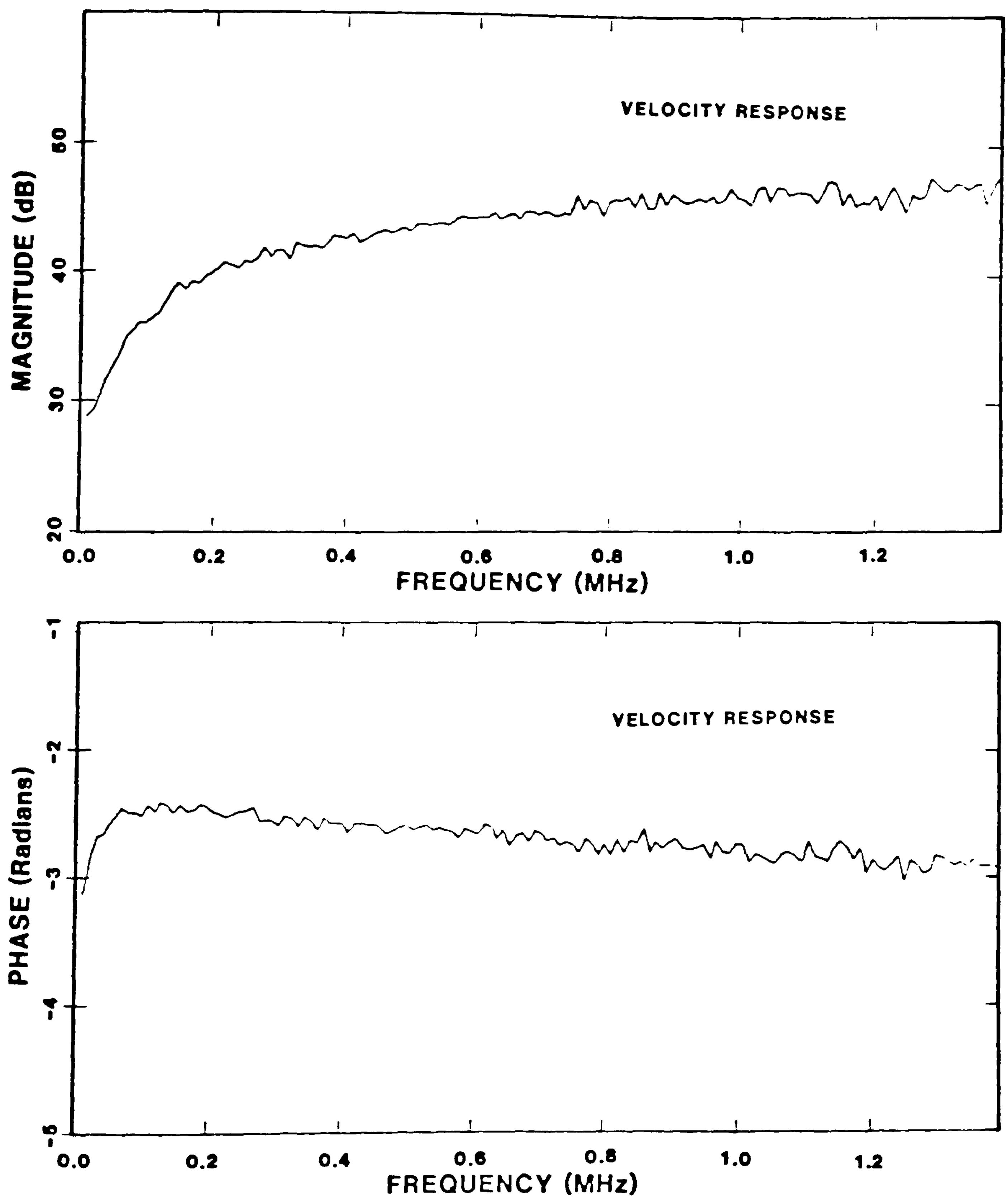

Figure 3.5. Amplitude spectrum (top) and phase spectrum (bottom) of NBS standard capacitive transducer to step-force function [Ref 80].

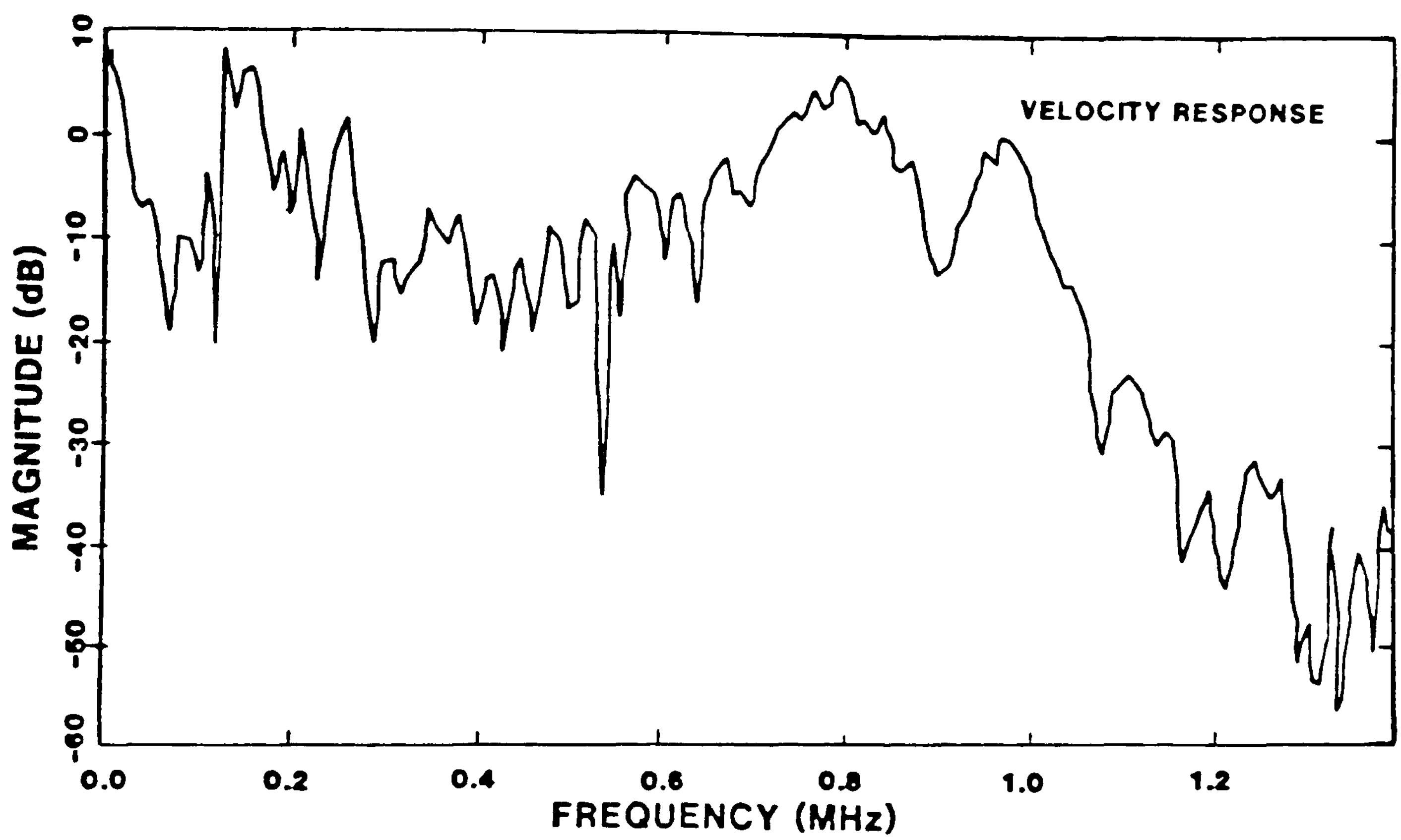

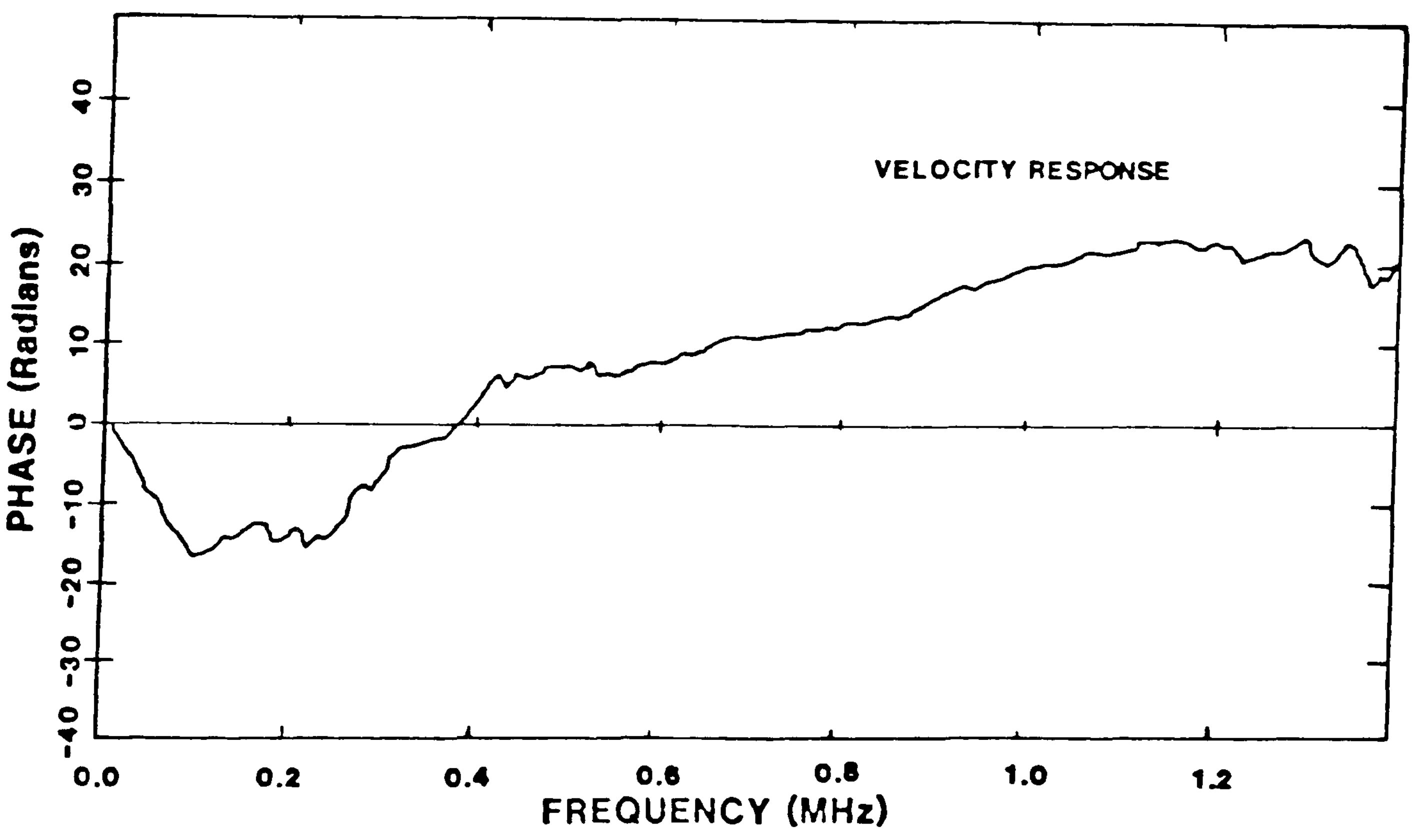

Figure 3.6. Amplitude spectrum (top) and phase spectrum (bottom) of a modified S9201 transducer to step-force function [Ref 80].

capacitive transducer for the type of transducer used in the experiments reported upon in Chapter 6 are shown in Figure 3.6.

The particular transducer for which the response is shown in Figure 3.6 is owned by the National Bureau of Standards, and is a Dunegan/Endevco model S9201, serial number AD52. According to Breckenridge [Ref 80] it has been modified by machining off the plastic surrounding the wear face, and the wear face itself has been optically ground and polished to be flat within a few light fringes. It was held down during the calibration on the NBS block with a force of one kilogram using clock oil as a couplant, and a 100 pF cable (which is part of the calibration) connected the transducer to the electronics. Note that the spectra are velocity responses; they were obtained by multiplying the displacement spectra by $j\omega$. This operation is equivalent to differentiating the time displacement signal, as can be easily shown using equation 4.7. The zero dB level represents 44.2 dB above 1 VS/m.

It must be reiterated that the calibration curves of Figure 3.6 constitute a partial calibration because of the assumptions used in deriving them. For example, the transducer was assumed to respond to a single mode, it was assumed to be a linear device, it was assumed that the mechanical fields were uniform over the transducer face, and it was assumed that the transducer was to be used on a medium which mechanically loaded it like the calibration block. It is important to keep these points in mind when interpreting test results, otherwise gross misunderstandings can result.

3.2 System Calibration

The use of a calibrated transducer by itself does not mean that the results of an acoustic emission experiment will be reproducible by other experimenters. All transducer calibration guarantees is that a known output will be produced when any transducer so calibrated is mounted in a specific location on a specific specimen in which a known force operates at a specific location. To obtain more flexibility it is necessary to devise procedures whereby a variation in specimen geometry, transducer location or source location can be corrected for in the output data set. The easiest way to accomplish this task is to adopt a similar approach to that outlined by Sachse and Hsu [Ref 73] in Section 3.1 for calibrating transducers and apply it to the whole system of specimen, couplant and transducer. The output of the system will then be given by:

$$Y(\omega) = H(\omega)\, X(\omega) \tag{3.11}$$

where $X(\omega)$ is the input to the system and $H(\omega)$ is the transfer function of the system.

There are several implications to equation (3.11). First, if the transducer is calibrated and the input is known and reproducible, the system transfer function can be obtained. This approach must be performed with caution, however, since as was shown in Section 3.1 many assumptions are made in calibrating a transducer which will clearly bear on any experimentally derived transfer function. Perhaps significantly, there has been no research reported in the literature regarding this approach to date. Second, if a known and reproducible signal is used to obtain a spectrum at a specific location and that spectrum is divided into the spectrum caused by a real acoustic emission at the same location, the result will be the source spectrum of the real acoustic emission referred to the constant source spectrum of the standard signal. This approach to system calibration has received attention from several experimenters, and there are several candidates for a standard input.

The simplest technique for creating a standard input is the breaking of a modified mechanical pencil lead as patented by Hsu [Ref 81]. The modification consists of mounting the pencil on a stand as shown in Figure 3.7 to allow the generation of both vertical and horizontal components in the stress pulse. By restricting the selection of lead to a single manufacturing lot, Hsu has shown that the generated signal displacement is reproducible, as shown in Figure 3.8. Advantages claimed for the pencil acoustic emission simulator are realistic stress wave generation via a sudden release of a slowly built-up static stress field which can easily be oriented to create particular wave modes, simplicity, ruggedness, portability, convenience of use and inexpensiveness. Hsu further claims that the slight variation in signal displacement shown in Figure 3.8 can be compensated for by measuring the exact breaking load with a force gauge, thus allowing the possibility of absolute calibration. Two disadvantages which Hsu does not address are the monopolar nature of the stress pulse, and the fact that the displacement amplitude is some five orders of magnitude (100 dB) above the minimum detectable displacement of a PZT-5 transducer.

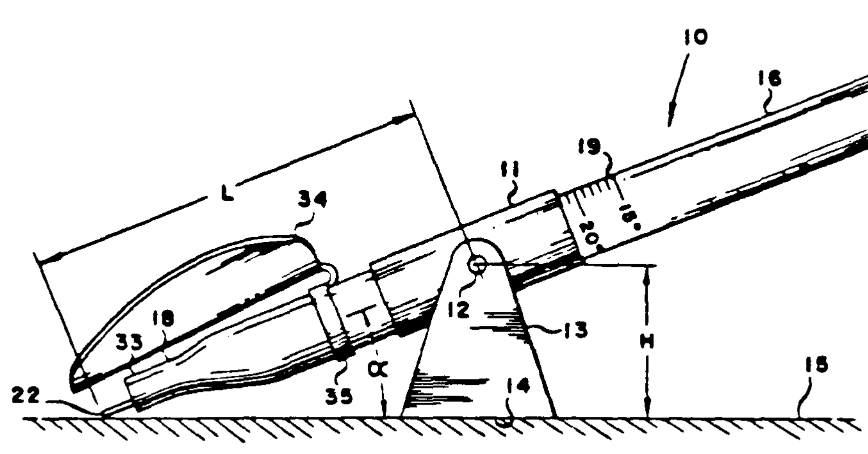

Figure 3.7. Modified mechanical pencil used for generating a standard acoustic emission source [Ref 81].

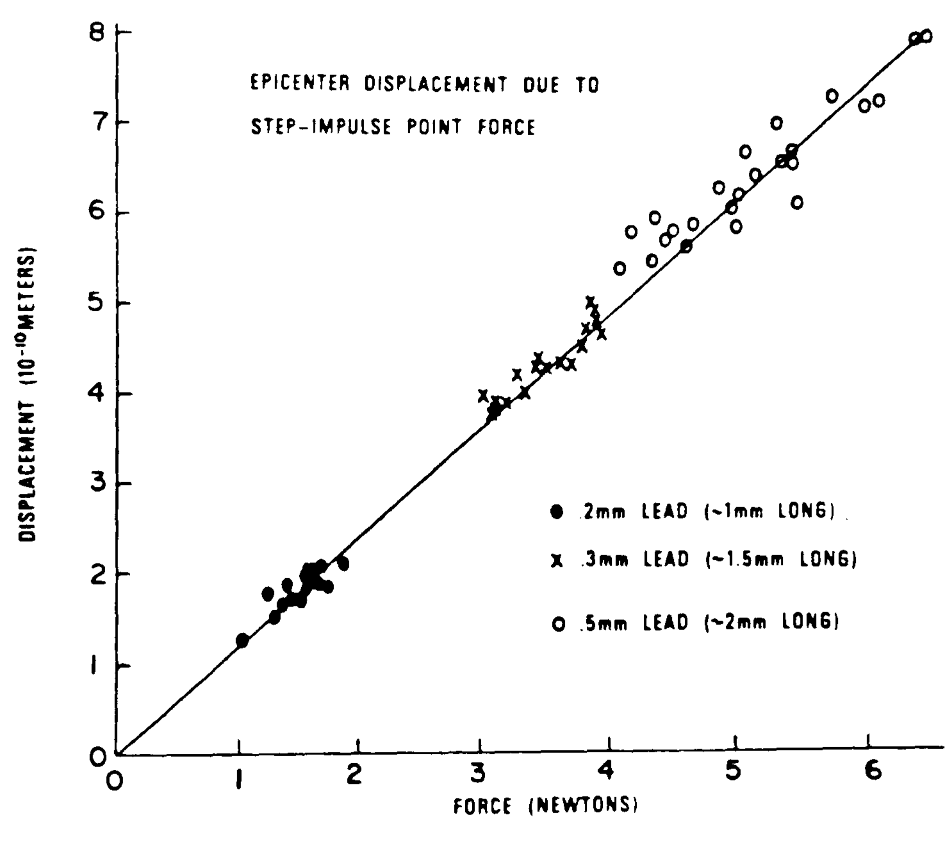

Figure 3.8. Force dependence of vertical epicentral displacement as a function of pencil lead diameter [Ref 57].

A second technique that is being used for generating a standard signal is transient localized heating caused by a pulsed laser beam. Scruby, Wadley, Dewhurst, Hutchins and Palmer [Ref 82] have reported on the use of a Q-switched Nd-YAG laser for such a purpose, their experimental arrangement is shown in Figure 3.9. In operation, a 24 nS duration optical pulse of 1.06 microns wavelength generated by the laser was applied to the surface of a test specimen through a 3 mm aperture, resulting in an energy of 41 mJ at the surface. Figure 3.10 shows the waveforms detected using a capacitance transducer at the epicenter of the optical pulse, it is clear that there is good agreement between theoretical prediction and experimental results and that the pulse to pulse variation is small. The stress wave generated by the action of the laser is explained as resulting from thermal gradients set up within 3 microns of the specimen surface during the laser pulse period. The resulting thermal transient causes expansion and thus stresses which are primarily parallel to the surface since the surface is unconstrained. Unlike the breaking pencil lead simulator just described, the laser generated stress wave can be considered to be the result of dipole forces, which are similar to the stresses around a crack or dislocation loop. In addition to realistic simulation of real acoustic emission sources, the laser pulse stress wave has the advantage that it is non-contacting and can be focussed on an area of interest that may be out of reach or in a hostile environment. Further, the energy imparted to the specimen can be readily reduced in a quantitative manner through the use of neutral density filters in the laser beam to be consistent with the energy released from a real acoustic emission source. Two

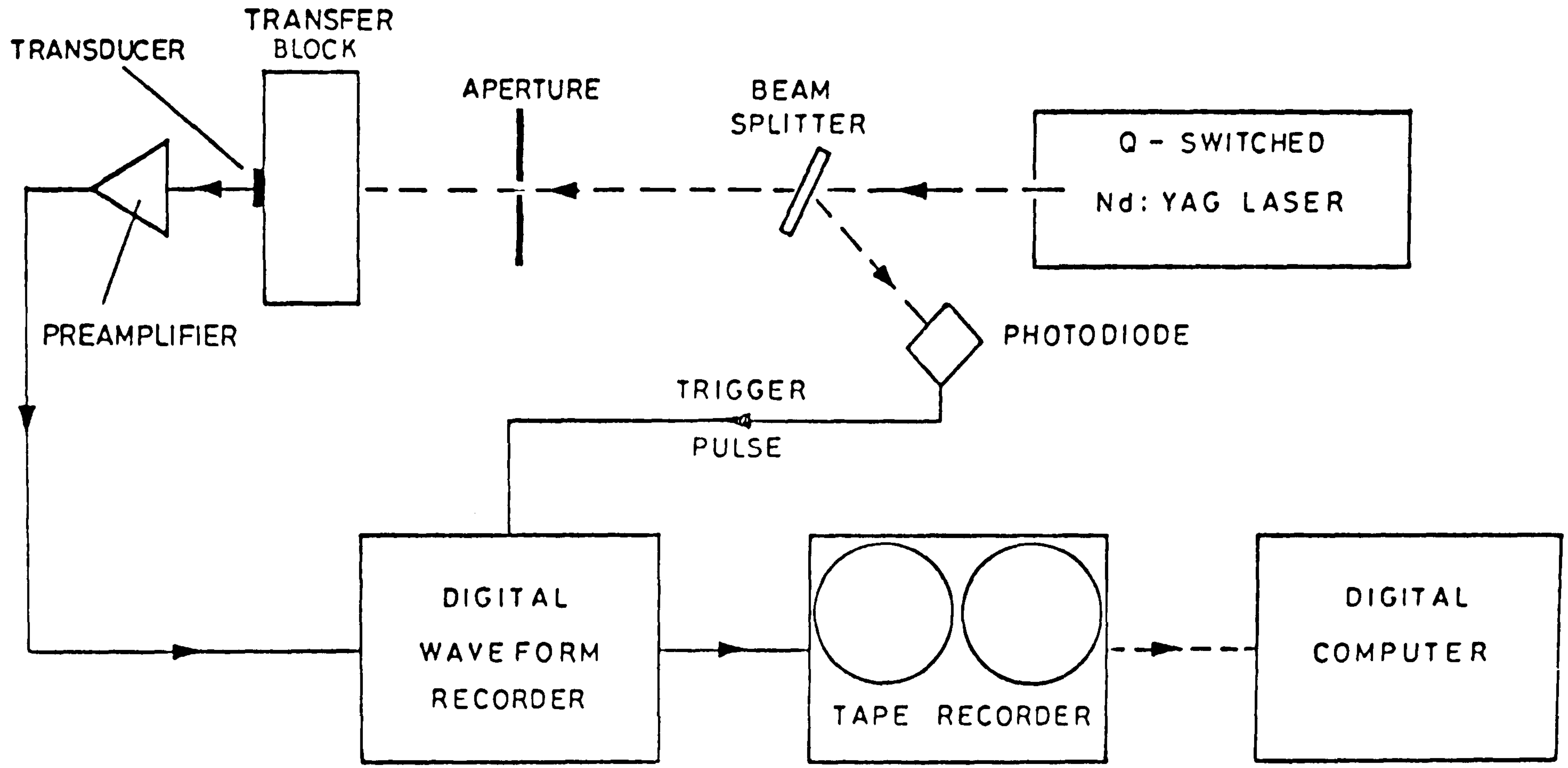

Figure 3.9. Schematic diagram of pulsed laser apparatus used for generating a standard acoustic emission source [Ref 82].

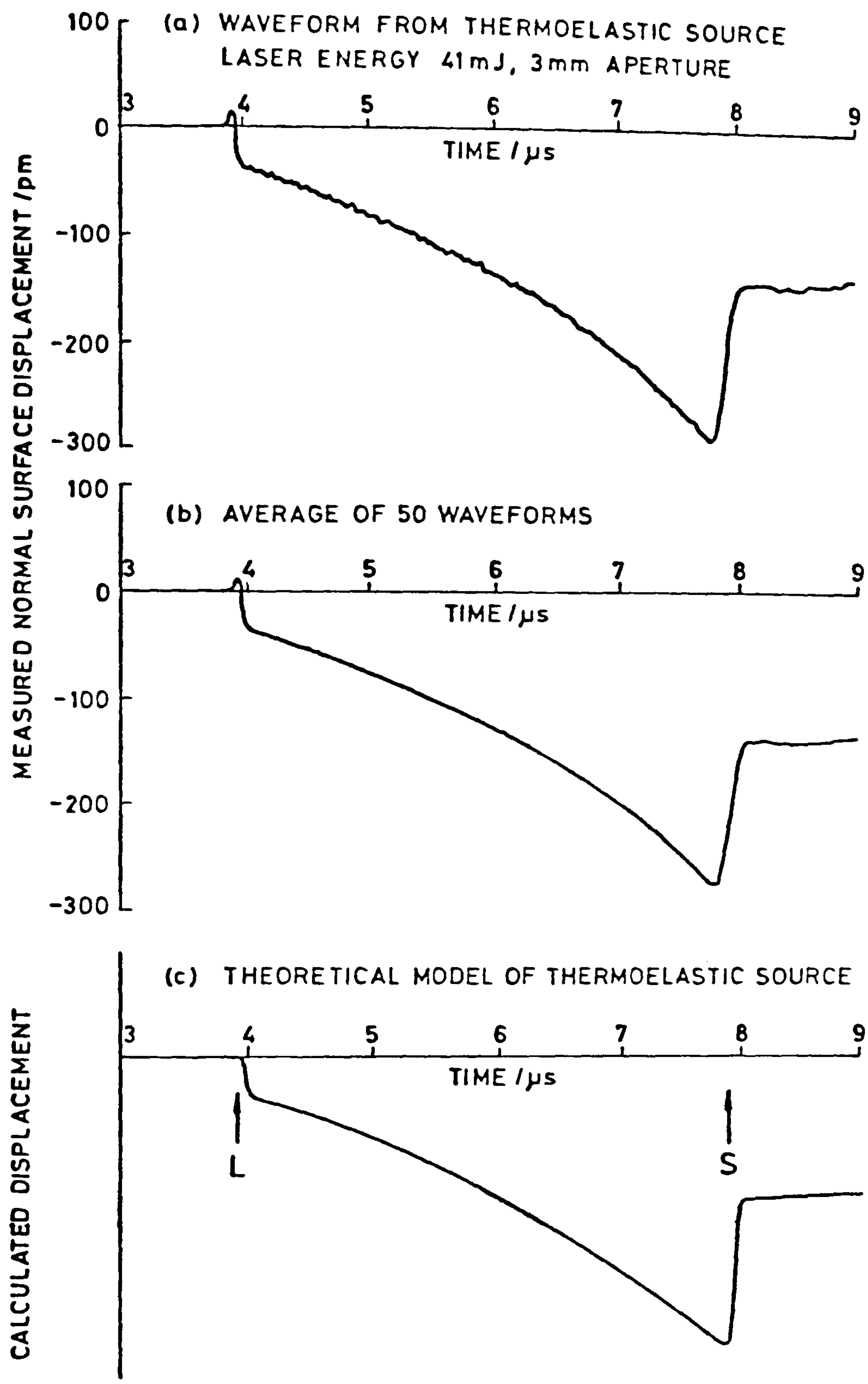

Figure 3.10. Comparison of theoretical and experimental vertical epicentral displacements produced with apparatus of Figure 3.9 [Ref 82].

disadvantages to the technique are the expense of the equipment necessary to generate and control the pulses and the safety precautions required to protect personnel from eye damage.

The third technique of system calibration uses the helium gas jet technique described by McBride and Hutchison [Ref 77] as a standard input. As described in Section 3.1, this technique consists of causing helium gas emerging from a capillary tube to impinge on the surface of a specimen to produce a continuous acoustic signal. Bentley and Green [Ref 83] found that it was necessary to restrict certain operating variables to specific values in order to obtain a reproducible output, Table 6.1 (on page 161) summarizes their conclusions. Green and Dingwall [Ref 84] later showed that it was possible to use the helium gas jet technique to correct for the effect of grossly dissimilar transducer characteristics on a received signal. Figure 3.11a shows the responses of a wide-band sensor and a narrow-band sensor to a repetitive 4 μS pulse. The familiar sin x/x shape of a square pulse is evident in the wide-band response, but is not so noticeable in the narrow-band plot. When these responses are respectively divided by the spectrum recorded for the gas jet input to each transducer, Figure 3.11b results. The discrepancy at 780 kHz is explained as being due to a response difference between the transducers to the particular mode of excitation produced by the pulse at that frequency. To prove this contention, Green and Dingwall used two dissimilar wide-band transducers in a similar experiment and produced Figure 3.12, which does not contain such a discrepancy.

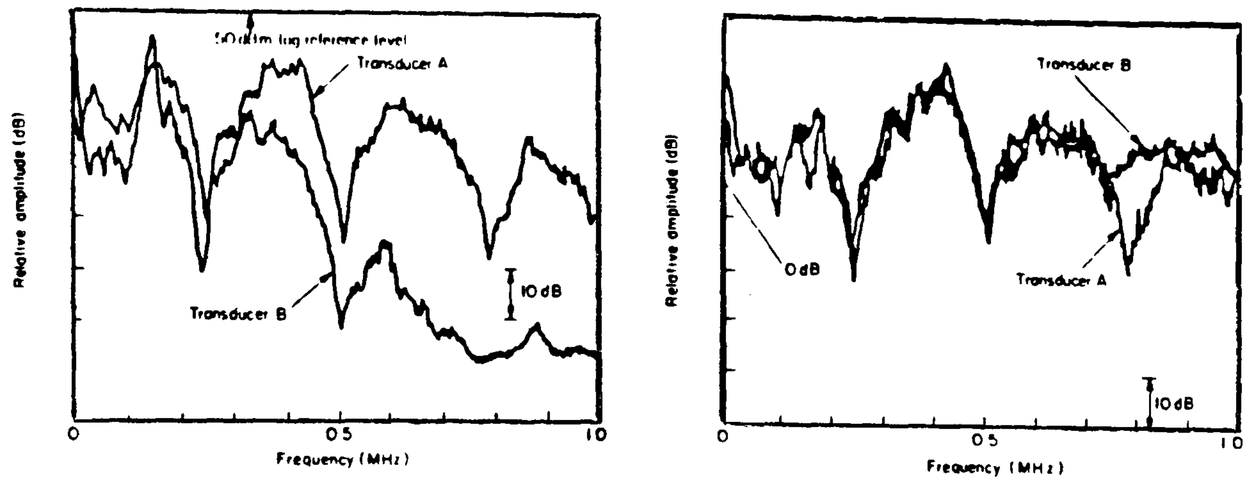

Figure 3.11. Response of a wide-band and a narrow-band transducer to a square pulse (left) and the normalized response obtainable using the helium gas jet (right) [Ref 84].

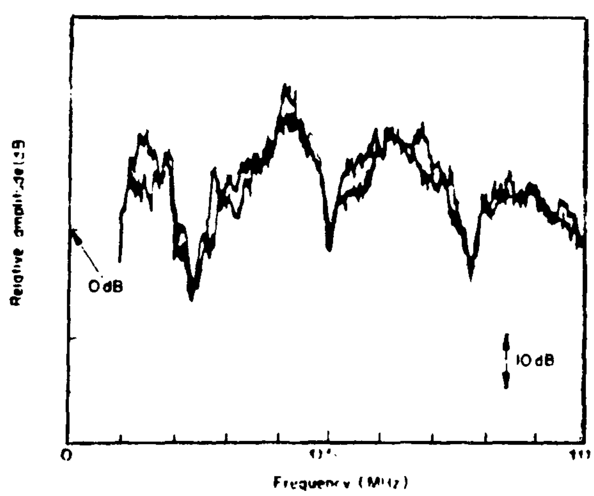

Figure 3.12. Normalized response of two dissimilar wide-band transducers sensing a square pulse obtainable using the helium gas jet [Ref 84].

The advantages of the helium gas jet technique are simplicity, portability, inexpensiveness and ease of use. Counteracting these attributes are the facts that it does not produce a transient pulse like a real acoustic emission, that phase information cannot be obtained and that the mode of excitation at the transducer cannot be predicted. Nevertheless, the helium gas jet technique is the only system calibration method which has been reported in the literature as allowing the quantitative comparison of acoustic emission spectra recorded by various experimenters (including the author) [Ref 85]. In this article, ten different laboratories in different countries recorded acoustic emissions from two dissimilar specimen geometries in which two different failure modes were operating using different transducers and recording systems. Raw acoustic emission data obtained in two laboratories is shown in Figure 3.13a, while Figure 3.13b shows the same data after normalization with the appropriate helium gas jet data. Figure 3.13b should be contrasted with Figure 3.14, which shows normalized data obtained by the author at a third laboratory under similar test conditions to those used in producing Figure 3.13b. The fact that Figure 3.13b and Figure 3.14 quantitatively agree to within 5 dB is evidence of the fact that the transducer, couplant, recording system and experimental technique differences can effectively be eliminated with the helium gas jet system calibration technique.

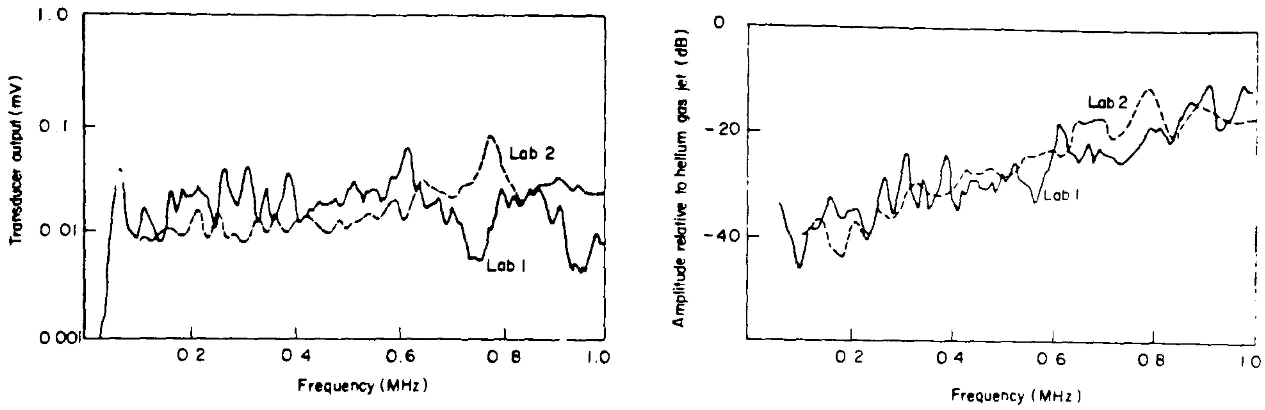

Figure 3.13. Quantitative comparison between acoustic emission obtained in two laboratories (left) after normalization with helium gas jet to remove system variables (right) [Ref 85].

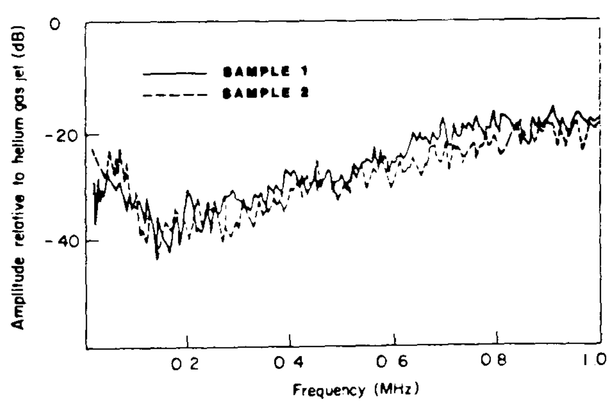

Figure 3.14. Normalized response obtained by the author under similar conditions to result shown in Figure 3.13. Note consistency between these graphs showing that system variables were removed [Ref 85].

CHAPTER 4

SIGNAL PROCESSING CONCEPTS

This chapter describes common pitfalls caused by the improper application of digital signal processing techniques. Practical methods are presented for digitally calculating the Fourier transform.

4.1 Data Acquisition

Once an acoustic emission source has been detected by a calibrated sensor the experimenter must have ready a suitable instrument to both record the output of the transducer and to process the signal so as to extract the information of interest. Carlyle [Ref 3] has summarized some of the equipment used in the past for acoustic emission work, Figure 4.1 shows the kinds of information which have been obtained using such equipment. For the experimental work described in this thesis more intricate hardware was required. Therefore, a substantial effort was expended in constructing an advanced acoustic emission system, details of which are given in Section 5.1. It is sufficient for the present to describe the equipment by stating that the transducer output was amplified, converted to a digital signal through the use of an analog to digital converter, and recorded on digital magnetic tape. This tape was

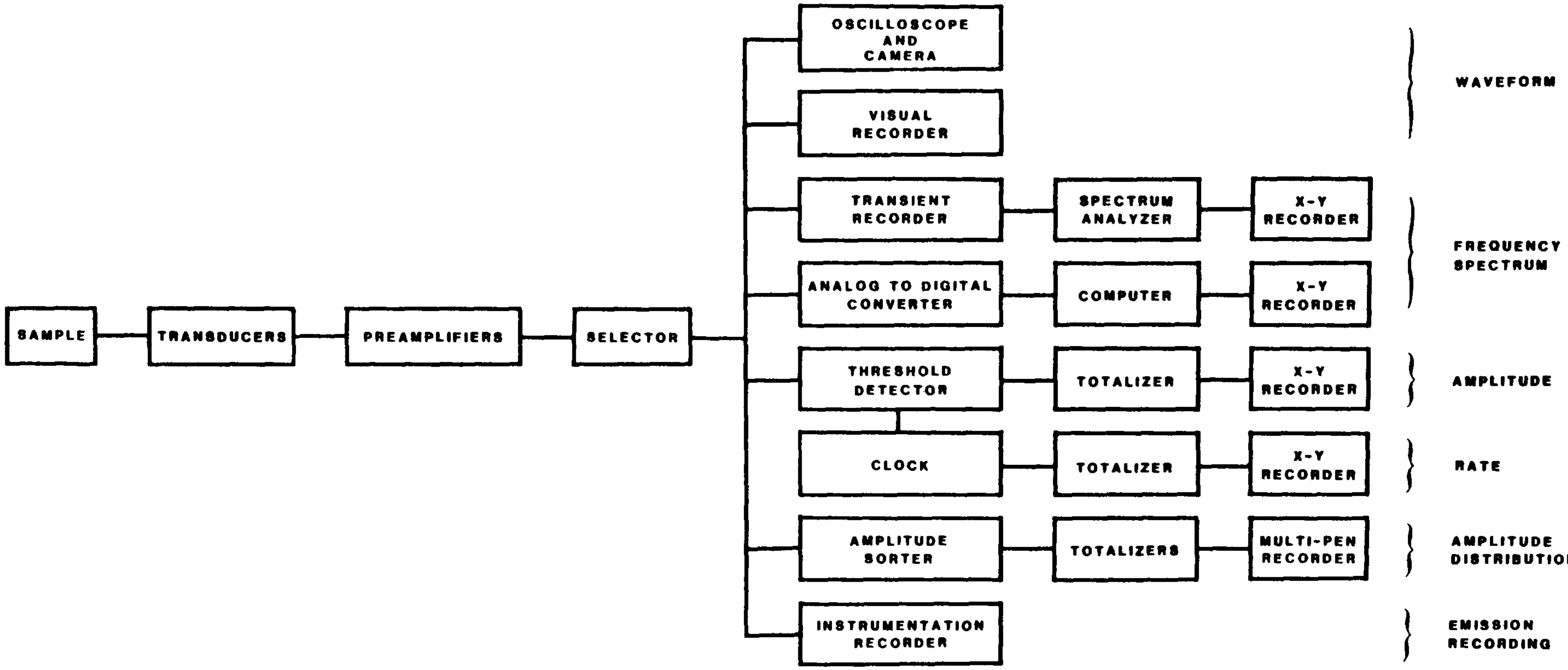

Figure 4.1. Various types of equipment utilized for acoustic emission experiments and the information obtainable from them [Ref 3].

then read by a digital computer and processed using a number of computer programs written by the author, which are described completely in Section 5.2. Of particular interest in this section is the analog to digital conversion process itself - the kinds of errors which it causes and anomalies which might be expected in the data.

A typical analog to digital converter is shown in Figure 4.2. The analog signal which is to be converted is input to the sample and hold, and upon the reception of a pulse from the external sampling control circuit a voltage measurement of the analog input signal is made. Simultaneously, the digital counter is reset to zero. The counter then commences to accumulate the pulses coming from the internal clock through the AND gate. The digital output of the counter is converted back into an analog signal by the D/A converter, whose output is compared to the voltage being held by the sample and hold. When the voltage produced by the D/A converter just exceeds the output voltage of the sample and hold, the AND gate blocks further clock pulses from incrementing the counter and signals that the conversion is complete. The external circuit then stores the digital representation of the sampled analog waveform and produces another sample control pulse, causing the cycle to repeat.

According to Otnes and Enochson [Ref 86], several types of errors may occur during the analog to digital conversion process just described. The first type, called aperture error, arises from the fact that the sample and hold works over a finite time interval termed an aperture. If it is possible for the analog signal to vary in the

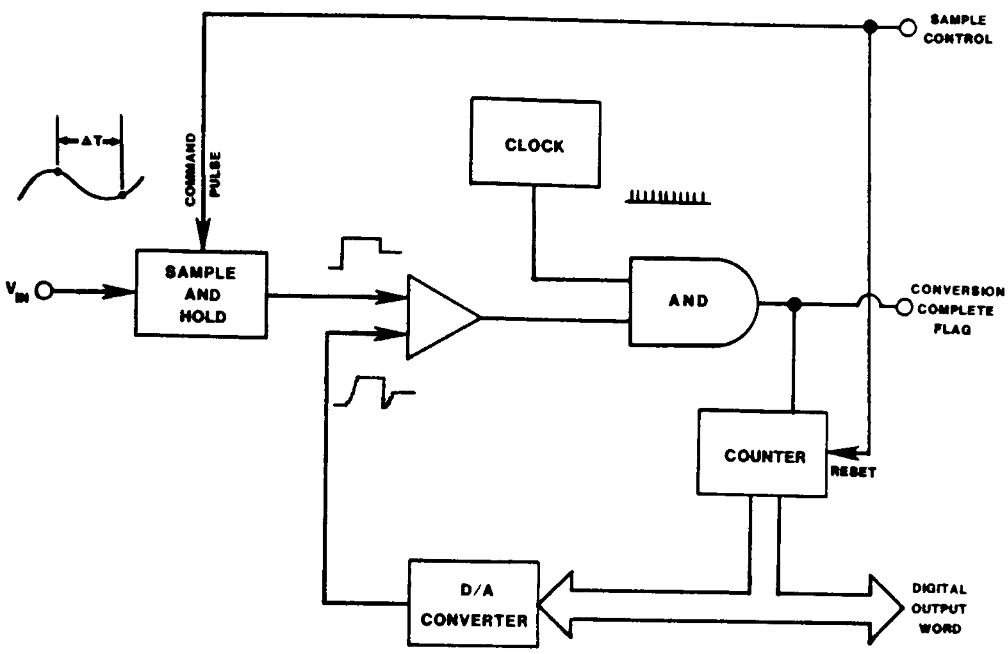

Figure 4.2. Schematic diagram of an analog to digital converter.

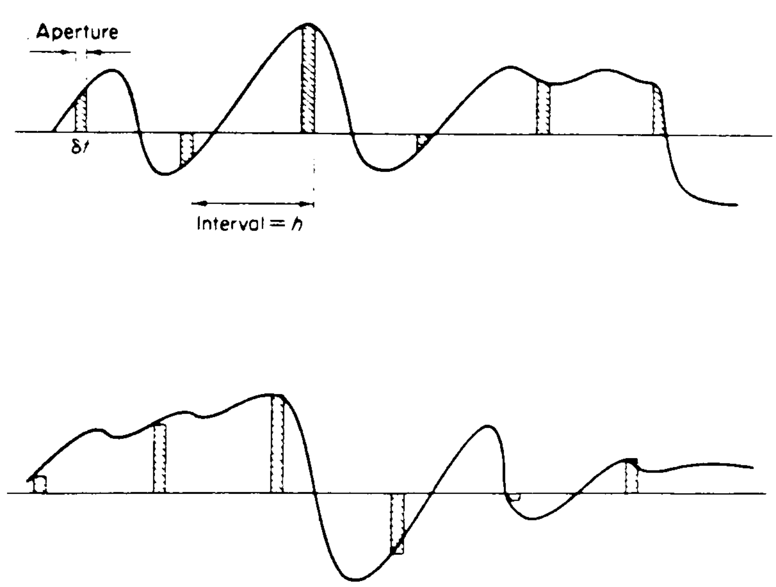

Figure 4.3. Aperture error arising from the signal changing during the sampling period [Ref 87].

aperture, then what is measured is not the magnitude of the signal at the start of the aperture (the ideal situation) but rather the average of the signal's magnitude during the aperture, as illustrated in Figure 4.3. Clearly, the way to reduce this error is to make the aperture small compared to the reciprocal of the highest frequency in the analog signal.

The second type of error in an analog to digital conversion, called jitter, is caused by random variations in the length of time between samples. The effect of jitter is twofold - it introduces spurious frequencies into the sampled data which will manifest themselves in spectral plots and it introduces errors in the phase information of high frequency signals which can cause problems with deconvolution. Jitter can be reduced by using a stable crystal controlled pulse generator to produce the sampling commands.

Another type of error associated with analog to digital conversion is non-linearity. This has several causes, most of which are traceable to the analog to digital converter being out of adjustment or to some portion of it being inoperative. An example of an adjustment non-linearity is non-uniform spacing of the quantization levels. In Figure 4.2, such an error would be traceable to the D/A converter, the comparator, or the sample and hold. An example of a non-linearity caused by circuit malfunction is bit dropout. This can occur when one of the digital output data lines "sticks" on an intermittent or regular basis; in Figure 4.2 such a malfunction could occur only in the counter.

The process of quantization has been shown by Beauchamp [Ref 87] to introduce noise into a signal. This arises from the fact that the signal is continuous, while the quantized representation has discrete steps of size q. The relationship between the input signal x(t) and the quantized output $x_q(t)$ can be expressed as:

$$x_q(t) \;=\; x(t) + \epsilon \tag{4.1}$$

where ϵ is an error term whose magnitude lies between -q/2 and +q/2. Assuming for the moment that q = 1, the probability density function for the error, p(x), is uniform for the range $-0.5 \leq x \leq +0.5$ and zero otherwise, and the mean value of the error is zero. Thus, the variance of the error is given by:

$$\sigma^2 \;=\; \int_{-\infty}^{\infty} (x-\overline{x})^2 \, p(x)\, dx \;=\; \int_{-0.5}^{0.5} x^2\, dx \;=\; \frac{1}{12} \tag{4.2}$$

which yields the standard deviation for one unit of quantization as $1/\sqrt{12} = 0.29$. For a signal quantized using 8 bits (256 levels), the signal to noise ratio introduced by the process of quantization will be:

$$Q_{s/n} \;=\; \frac{2^q}{0.29} \;=\; \frac{256}{0.29} \;\sim\; 60\text{dB} \tag{4.3}$$

Several points need to be emphasized regarding quantization signal to noise ratios calculated using (4.3). The first point is that if care is not taken to amplify the analog signal properly so as to utilize all of the bits available in the analog to digital converter, the signal to noise ratio calculated using the maximum number of bits in (4.3) will be too high. The true value of the signal to noise ratio will be given by (4.3) only when q is equal to the exact number of levels used for digitizing the analog signal. The second point concerns the determination of the proper number of quantization levels needed for a particular application. In this decision the experimenter needs to be guided by the analog signal to noise ratio at the input to the quantizer. Use of a quantizer with a vastly better signal to noise ratio than the analog signal possesses will merely produce a better representation of the noise in the analog signal, while reducing the maximum sampling speed because of the increased time necessary to digitize with greater precision.

Sampling speed is a very important quantity in digital processing because of an effect known as aliasing, caused by sampling a signal at too slow a rate to resolve its highest frequency. Figure 4.4 shows a dramatic example, where improper sampling causes a high frequency sine wave to be represented (aliased) as a low frequency signal in the computer. It is clear from Figure 4.4 that the high frequency sine wave could be correctly reconstructed if it had been sampled at least twice per period. This observation has been formalized as the Nyquist criterion (or sampling theorem):

$$f_N = \frac{1}{2\Delta t} \tag{4.4}$$

where f_N is the Nyquist or folding frequency, and Δt is the sampling interval.

A familiar example of aliasing is the reversal in rotation direction of a stage coach wheel in a cowboy film as the coach

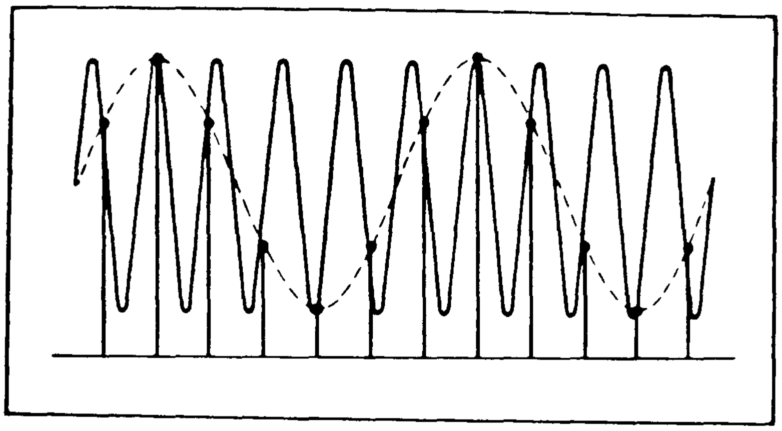

Figure 4.4. Aliasing of a high frequency signal by a low frequency signal caused by insufficient sampling rate [Ref 88].

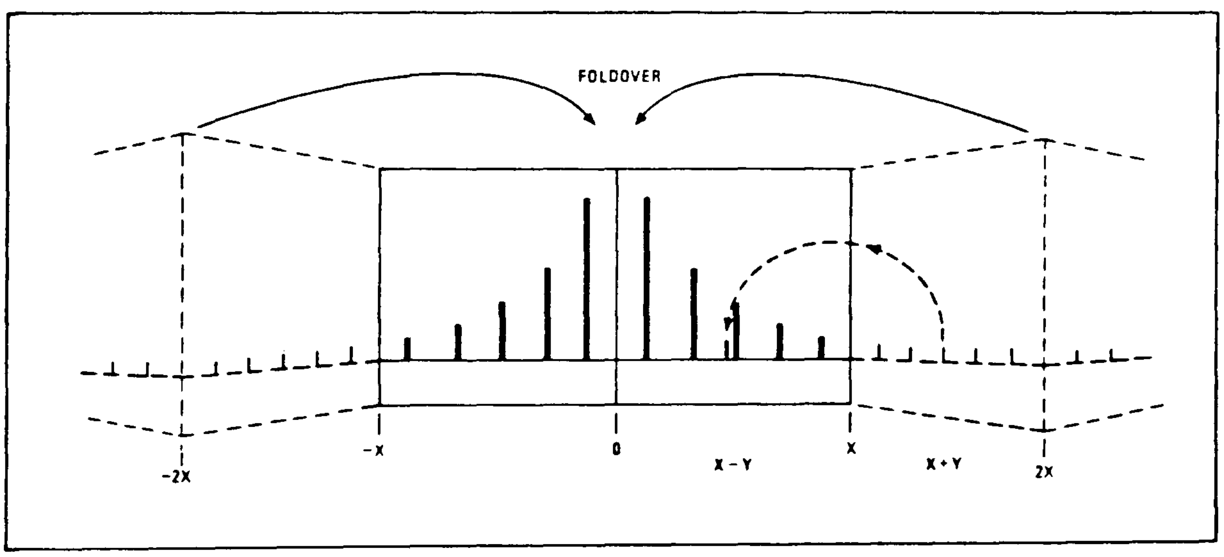

Figure 4.5. Alias signals fold over about the Nyquist frequency, i.e., a signal of frequency x+y will have an alias at frequency x-y [Ref 88].

accelerates through a certain speed. At this speed the wheel has reached an angular frequency which is an integral multiple of the Nyquist frequency defined by the reciprocal of twice the sampling interval of the camera. The rotation reversal occurs because as the angular frequency increases beyond the Nyquist frequency an alias appears at a frequency as far below the Nyquist frequency as the real frequency is above the Nyquist frequency, as shown in Figure 4.5. To illustrate this more completely, assume that the high frequency sine wave in Figure 4.4 has a 100 Hz frequency. The sampling rate in Figure 4.4 is 120 Hz, which corresponds to a Nyquist frequency of 60 Hz. Subtracting the Nyquist frequency from 100 Hz yields 40 Hz, and subtracting 40 Hz from the Nyquist frequency results in an alias frequency of 20 Hz, which is exactly the frequency of the dotted sine wave in Figure 4.4.

Aliasing can be prevented in one of two ways - either the sampling rate can be increased so that the Nyquist frequency is above the highest frequency in the signal, or the analog signal can be low pass filtered to remove all frequencies above the Nyquist frequency. If the first method is used, it must be remembered that high frequency noise components will be aliased within the Nyquist bandwidth, thus decreasing the signal to noise ratio. For this reason the second method is preferred. However, practical anti-aliasing filters do not abruptly attenuate signals to zero at their cut-off frequency, but rather have a finite attenuation per octave characteristic. In general, this trait of filters will require that the sampling rate be higher than necessary to insure that no aliasing occurs.

The fact that a digital representation of a signal has a finite length can create some problems if a periodic signal is being digitized, as illustrated in Figure 4.6. In Figure 4.6a a cosine wave with a 4 second period is shown in both the time and frequency domains. Note particularly that the only lines which appear in the frequency domain are at 0.25 Hz, which is the frequency of the cosine wave. Suppose that the experimenter elects to record 10 seconds worth of data by multiplying the cosine wave by the rectangular window shown in Figure 4.6b. In the time domain this yields 2.5 cycles of the cosine wave, as shown in Figure 4.6c. The result of the data recording in the frequency domain is very complicated, but can be explained by saying that it results from convolving the frequency spectrum of the cosine wave in Figure 4.6a with the spectrum of the rectangular pulse in Figure 4.6b. Digitization consists of sampling the waveform of Figure 4.6c using the N impulses shown in Figure 4.6d, this results in the windowed and sampled cosine wave shown in Figure 4.6e. In the frequency domain, digitization consists of convolving the spectrum of Figure 4.6c with the spectrum of Figure 4.6d, which results in the spectrum depicted by the dashed line in Figure 4.6e. Because the digitization occurs during a finite period, however, the continuous dashed line of Figure 4.6e cannot be resolved. Instead, points in the frequency domain spread $1/N\Delta t$ Hz apart result, as actually shown in Figure 4.6e. Note that no line appears at 0.25 Hz as it should, but that instead power has "leaked" into the closest available lines to 0.25 Hz.

The leakage effect just described results entirely from choosing to digitize a non-integral number of periods of the original cosine wave.

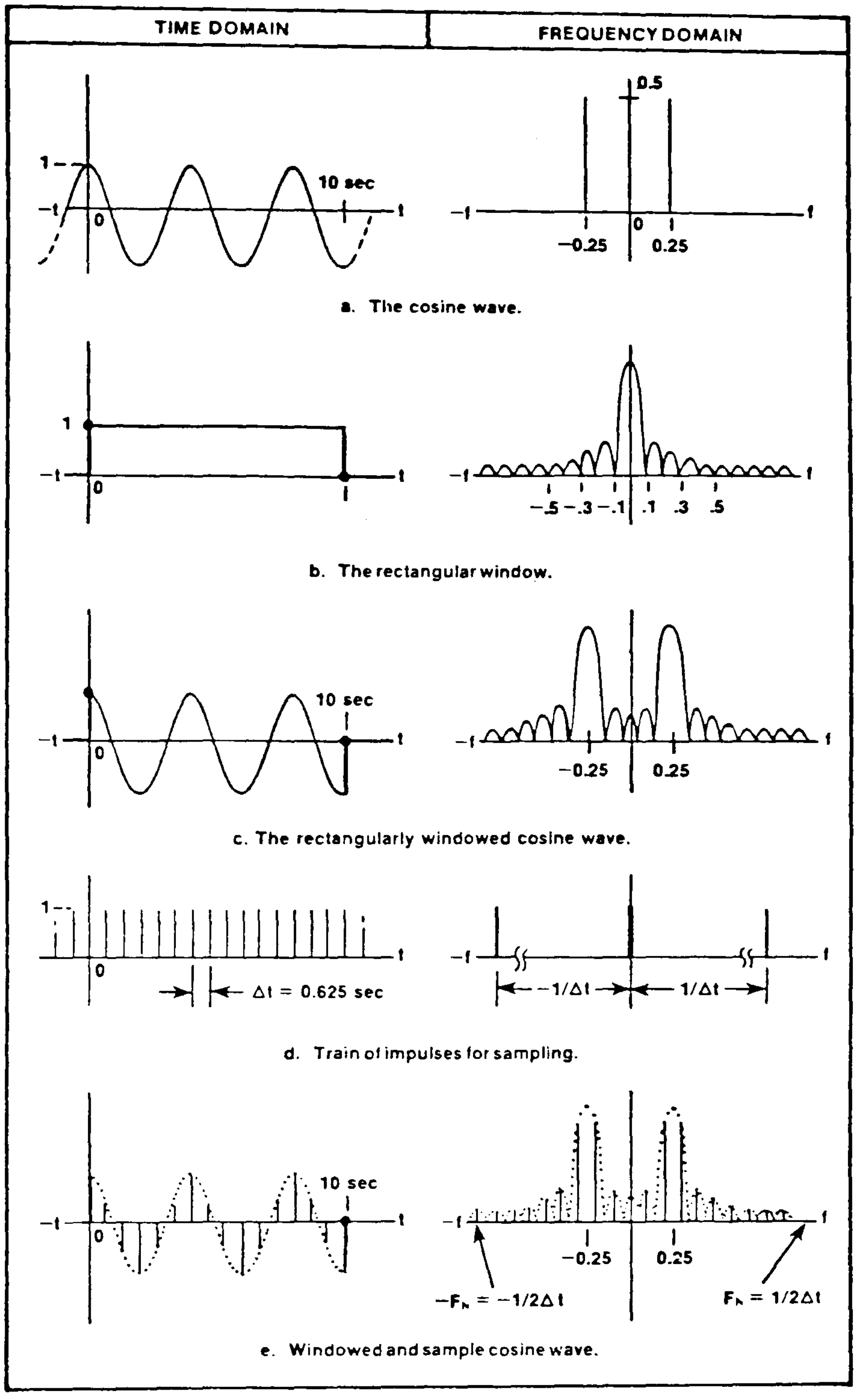

Figure 4.6. Origin of leakage caused by not sampling an integral number of cycles of a periodic waveform [Ref 88].

Although not shown explicitly in Figure 4.6, the digitization of a signal over a finite time period results in an implied periodicity. Reproduction of the time domain waveform in Figure 4.6e on both sides of the one shown would clearly result in a discontinuity at 0 and 10 seconds. The effect of this discontinuity in the frequency domain is to produce unwanted high frequency components. Elimination of these unwanted frequencies can be accomplished by digitizing an integral number of periods to eliminate the discontinuity. However, non-periodic waveforms can be affected by leakage, too. For example, acoustic emission waveforms are not periodic, but if the whole transient waveform is not digitized the implied periodicity caused by the digital recording will result in a similar discontinuity to that just described for the cosine wave. In this event it may be useful to try a technique called windowing.

The windowing technique seeks to eliminate discontinuities by forcing the beginning and the end of the data to have the same value. This is accomplished by replacing the rectangular recording window shown in Figure 4.6b with a more favorably shaped window such as the ones shown in Figure 4.7. As can be seen in Figure 4.7, the essence of the windowing technique is to reduce the sidelobes of the window in the frequency domain, thus directly affecting unwanted high frequencies of the sort shown in Figure 4.6e. The price that is paid for the sidelobe reduction, however, is that the main lobe is broadened. Thus, although frequencies far from the major true frequency will contain less power as a result of windowing, more frequencies adjacent to the true frequency component will contain power and the spectrum will be smeared. Clearly,

Unity Amplitude Window	Shape Equation	Frequency Domain Magnitude	Major Lobe Height	Highest Side Lobe (dB)	Band-width (3 dB)	Theoretical Roll-Off (dB/Octave)
Rectangle 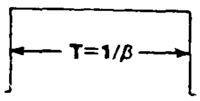	A=1 for t=0 to T	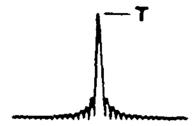	T	−13.2	0.86β	6
Extended Cosine Bell 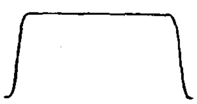	A=0.5 (1−cos 2π5t/T) for t=0 to T/10 and t=9T/10 to T A=1 for t=T/10 to 9T/10	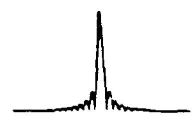	0.9 T	−13.5	0.95β	18 (beyond 5β)
Half Cycle Sine 	A=sin 2π0.5t/T for t=0 to T	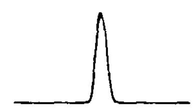	0.64 T	−22.4	1.15β	12
Triangle 	A=2t/T for t=0 to T/2 A= −2t/T + 2 for t=T/2 to T	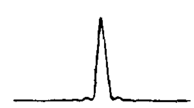	0.5 T	−26.7	1.27β	12
Cosine (Hanning) 	A=0.5(1−cos 2πt/T) for t=0 to T	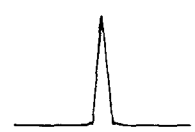	0.5 T	−31.6	1.39β	18
Half Cycle Sine^3 	A=sin^3 2π0.5t/T for t=0 to T	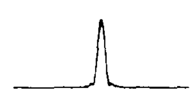	0.42 T	−39.5	1.61β	24
Hamming 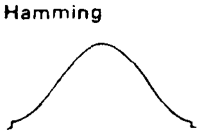	A=0.08 − 0.46 (1−cos 2πt/T) for t=0 to T	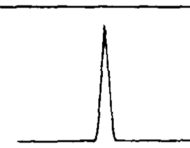	0.54 T	−41.9	1.26β	6 (Beyond 5β)
Cosine^2 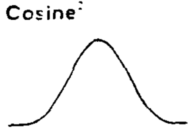	A=(0.5(1−cos 2πt/T))^2 for t=0 to T	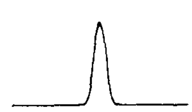	0.36 T	−46.9	1.79β	30
Parzen 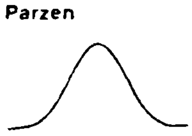	A=1−6(2t/T−1)^2+6|2t/T−1|^3 for t=T/4 to 3T/4 A=2(1−|2t/T − 1|)^3 for t=0 to T/4 and t=3T/4 to T	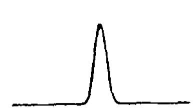	0.37 T	−53.2	1.81β	24

Figure 4.7. Window functions used to control leakage [Ref 88].

if at all possible it is best to avoid the need for windowing by digitizing the entire acoustic emission transient.

4.2 Spectral Analysis

The discussion of data acquisition in Section 4.1 touched on the concept of spectral analysis when aliasing and windowing were explained by hinting that the knowledge of the frequency content of a signal was important. This importance arises because the manner in which the frequency spectrum displays information will often reveal details of a signal that are too subtle to observe in the time domain, in spite of the fact that the frequency spectrum of a signal has no more information in it than the time domain signal. For example, Figure 4.8 shows what appears to be a sine wave in the time domain, but the frequency spectrum clearly reveals that the signal is composed of one large sine wave and several smaller sinusoidal components. This analytical power of spectral analysis makes it an attractive technique for characterizing acoustic emission signals because each source mechanism should have a characteristic frequency spectrum based upon its size and speed of operation.

Spectral analysis grew out of heat conduction studies performed by Jean-Baptiste Fourier in the early nineteenth century. Fourier was able to obtain a solution for his heat flow problem in the form of a trigonometric series which now bears his name. Of importance to this thesis is the fact that the Fourier series can be used to obtain the frequency components of a periodic waveform that meets three conditions.

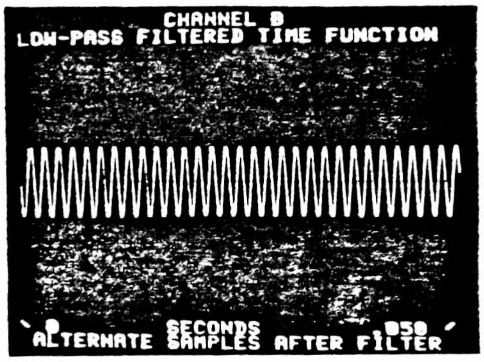

a) Time Domain
Small signal not visible

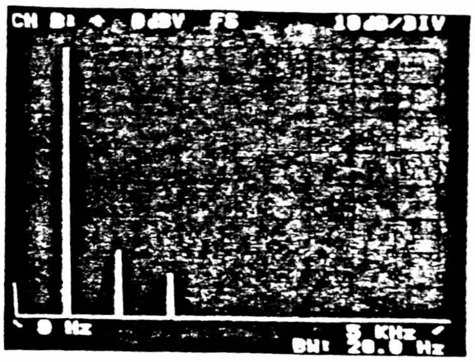

b) Frequency Domain
Small signal easily resolved

Figure 4.8. Analysis power of frequency spectrum for revealing the presence of small signals in the presence of large ones [Ref 89].

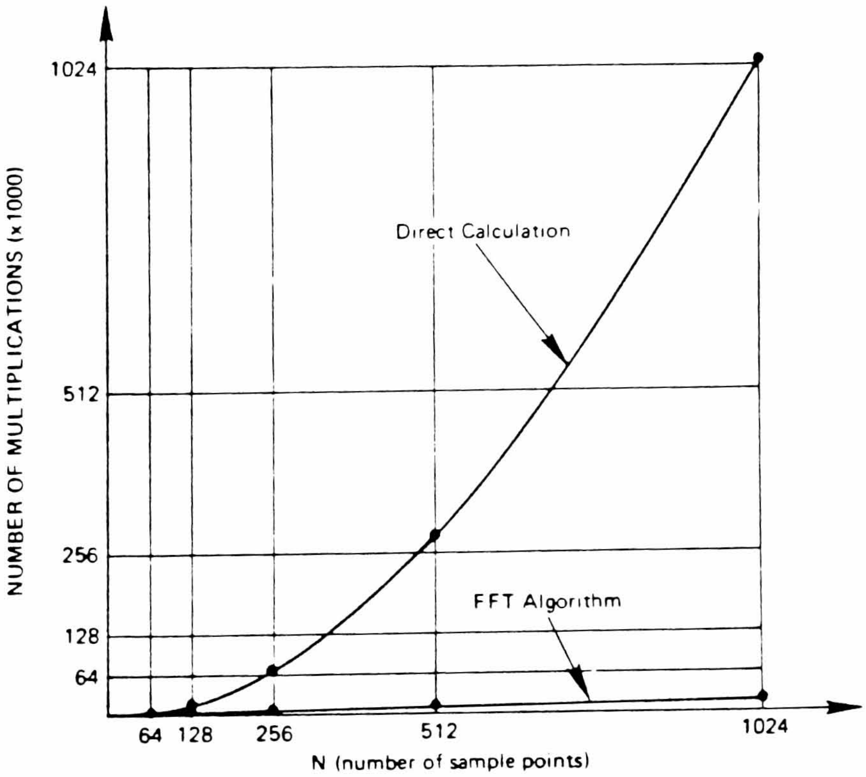

Figure 4.9. Comparison of multiplications needed for spectral calculation via direct method and fast Fourier transform [Ref 90].

First, the waveform must have a finite number of discontinuities in any period. Second, the waveform must have a finite number of maxima and minima in any period. Third, the integral of the function with respect to time over one period must be finite. If these conditions (known as the Dirichlet conditions) are met, then the Fourier series exists for the periodic waveform and is given by:

$$x(t) = \frac{a_o}{2} + \sum_{n=1}^{\infty} (a_n \cos 2\pi n f_o t + b_n \sin 2\pi n f_o t) \tag{4.5}$$

where f_o is the reciprocal of the period, T, and:

$$\begin{aligned} a_o &= \frac{2}{T} \int_o^T x(t)\, dt \\ a_n &= \frac{2}{T} \int_o^T x(t) \cos 2\pi n f_o t\, dt \qquad n = 1,2,3\ldots \\ b_n &= \frac{2}{T} \int_o^T x(t) \sin 2\pi n f_o t\, dt \end{aligned} \tag{4.6}$$

The a_o coefficient is the average value of the waveform and thus is the DC term in the frequency domain. The a_n and b_n terms are the frequency coefficients, implying that the frequency spectrum of a periodic waveform consists of discrete lines in the frequency domain.

Often it is desirable to obtain the frequency spectrum of a transient waveform. This can be done using the Fourier integral, which can be derived from the Fourier series by assuming that the period of the transient waveform is infinite [Ref 88]. Once again the Dirichlet conditions must be satisfied in order for the Fourier integral to exist, but assuming that this is the case then the following is true:

$$x(t) = \int_{-\infty}^{\infty} X(f)\, e^{j2\pi ft}\, df \tag{4.7}$$

where:

$$X(f) = \int_{-\infty}^{\infty} x(t)\, e^{-j2\pi ft}\, dt \tag{4.8}$$

Equations (4.7) and (4.8) are known as the Fourier transform pair, with (4.7) generally called the inverse transform and (4.8) the direct or forward transform. Note that in contrast to the situation discussed above for periodic waveforms the frequency spectrum of a transient waveform is a continuous function.

The Fourier series and Fourier integral just explained are extremely useful mathematical tools and as such can be used to obtain the frequency spectra of periodic and transient time functions that are mathematically describable. From a practical standpoint, however, signals encountered in the laboratory are rarely analytic functions of time. Another problem is that no real waveform can be considered to be periodic from a mathematical standpoint over the time span of negative infinity to positive infinity, and thus strictly speaking the Fourier series is never usable on practical signals. To handle these problems, an approximation of the Fourier transform which uses a digitized approximation of the time waveform has been developed. This approximation to the Fourier transform is known as the discrete Fourier transform, and is given by:

$$X(n) = \sum_{k=o}^{N-1} x(k) \exp\left(\frac{-j2\pi kn}{N}\right) \tag{4.9}$$

where N is the number of samples in the digitized waveform, n is the frequency domain index and k is the time domain index. The inverse discrete Fourier transform is:

$$x(k) = \frac{1}{N} \sum_{n=o}^{N-1} X(n) \exp\left(\frac{j2\pi kn}{N}\right) \tag{4.10}$$

where the scaling factor of 1/N should be noted. Together, Equations (4.9) and (4.10) form a Fourier transform pair for digitized waveforms.

Although Equation (4.9) represents a practical means of approximating the frequency spectrum of real signals, it requires a substantial amount of calculation to accomplish this goal. Specifically, N^2 multiplications are required to obtain the frequency components of a time domain signal which has been digitized into N samples. Fortunately, there is a means whereby the number of multiplications can be dramatically reduced to a number given by $N \log_2 N$ instead of N^2. This feat is accomplished by exploiting certain periodicities and symmetries in the discrete Fourier transform, resulting in algorithms which are known generically as fast Fourier transforms. The relative calculation advantage of fast Fourier transforms over the discrete Fourier transform may be appreciated in Figure 4.9, which shows that for a time waveform with 1024 samples the discrete Fourier transform will take approximately 200 times longer than the fast Fourier transform.

The details of how one fast Fourier transform algorithm accomplishes its calculation speed increase over direct computation are discussed in Appendix A. The algorithm is complicated, and perhaps because of this has been subject to modification by various authors. The modified algorithms have in turn been implemented in various forms by programmers to take advantage of the peculiarities of a particular computer architecture or programming language. Thus an experimenter wishing to perform digital spectral analysis will discover that he needs to choose a particular fast Fourier transform program from among a dozen or so possibilities.

The crucial step in making an informed choice of a particular fast Fourier transform program is to rank the relative importance of the final result precision, execution speed and memory requirements for the task at hand. This ranking will of course depend upon the computer on which the program is to run, and a program which may be an excellent choice for use on one machine may not provide optimal results in another. In the present case a 16 bit machine was to be used and fast Fourier transform programs were available which used integer numbers or floating point numbers for the input and output data. It was decided that a floating point routine was required since the integer routines limited the dynamic range of the data to 90 dB with the 16 bit word size. This choice meant that additional memory would be required since a floating point number requires twice the storage space of an integer number, but this was acceptable because sufficient memory space was available. However, this choice also meant that the execution time would be longer since floating point arithmetic takes more time than integer arithmetic. This, too, was deemed acceptable since real-time results were not required and longer program execution times could therefore be tolerated.

The considerations just described lead to the selection of a fast Fourier transform program named FOUR2, whose source code appears in Appendix B. The main advantage which FOUR2 provided was a dynamic range of about 640 dB, which meant that sharp anti-resonances in the frequency spectra would be preserved. This was important to the experimental program since it was known that deconvolution by means of power spectral division would be necessary during gas jet normalization, and any loss of anti-resonances would lead to sharp spikes in the final spectrum. Another advantage which FOUR2 possessed was that it used a radix 4 + 2 factoring scheme instead of the more common radix 2 factoring described in Appendix A. This meant that the input data set was factored by 4 with any remainder being factored by 2. This procedure made the calculation of the Fourier transform of the input data execute approximately 25% faster than normal. Actual use of FOUR2 in the programs written for this thesis (described in Section 5.2) revealed that it required 6358 words of program memory (including 4096 words used for the 2048 floating point data array) and executed a 2048 point transform in 1.19 seconds.

CHAPTER 5

INSTRUMENTATION CONSTRUCTION

This chapter discusses the design and operation of a unique acoustic emission system built for signal identification research. Computer programs developed to provide an acoustic emission source discrimination capability using data from this system are described.

5.1 Hardware

Although acoustic emission has been recognized as a distinct nondestructive testing technique since the mid 1960's when the first commercial acoustic emission equipment became available, laboratory quality instrumentation is not readily obtainable. The experimenter must therefore assemble his own system to meet his particular requirements. In the present case the requirement to make broadband waveform recordings of acoustic emission signals for source identification purposes meant that a unique instrument would have to be built. This was done by making substantial modifications to a multiple channel source location system (manufactured by the Trodyne Corporation) which was known as the MSCD system.

In its original state the MSCD system had twelve channels whose band-limited outputs were processed by a non-programmable logic circuit to obtain a planar or a linear source location as well as conventional acoustic emission parameters such as oscillation count and peak voltage. The modifications consisted of adding a programmable microprocessor, a twelve channel broadband switch, an analog to digital converter, a digital magnetic tape recorder, a converter-recorder interface and modems. This resulted in a system with separated data acquisition and data processing sections which could make broadband digital acoustic emission waveform recordings in environments hostile to computer operation while simultaneously performing source location. A block diagram of the system after modification is shown in Figure 5.1.

Numerous problems were encountered during the construction of the system. One of the most troublesome was an intermittent corruption of the waveform recorded by the analog to digital converter when the waveform was stored on magnetic tape at the command of the microprocessor. The solution to this problem came about when it was finally noticed that it was data dependent, thus providing a means of getting a regular failure. Subsequent trouble shooting of the data path from the analog to digital converter to the magnetic tape recorder revealed that an improper choice of biasing resistors in the interface data lines had created an impedance mismatch which caused oscillations when the data had a particular value. A simple change of resistors was sufficient to eliminate the problem. This is a particularly significant problem because it is one which can easily occur in any digital system assembled using equipment built by different manufacturers, and is most

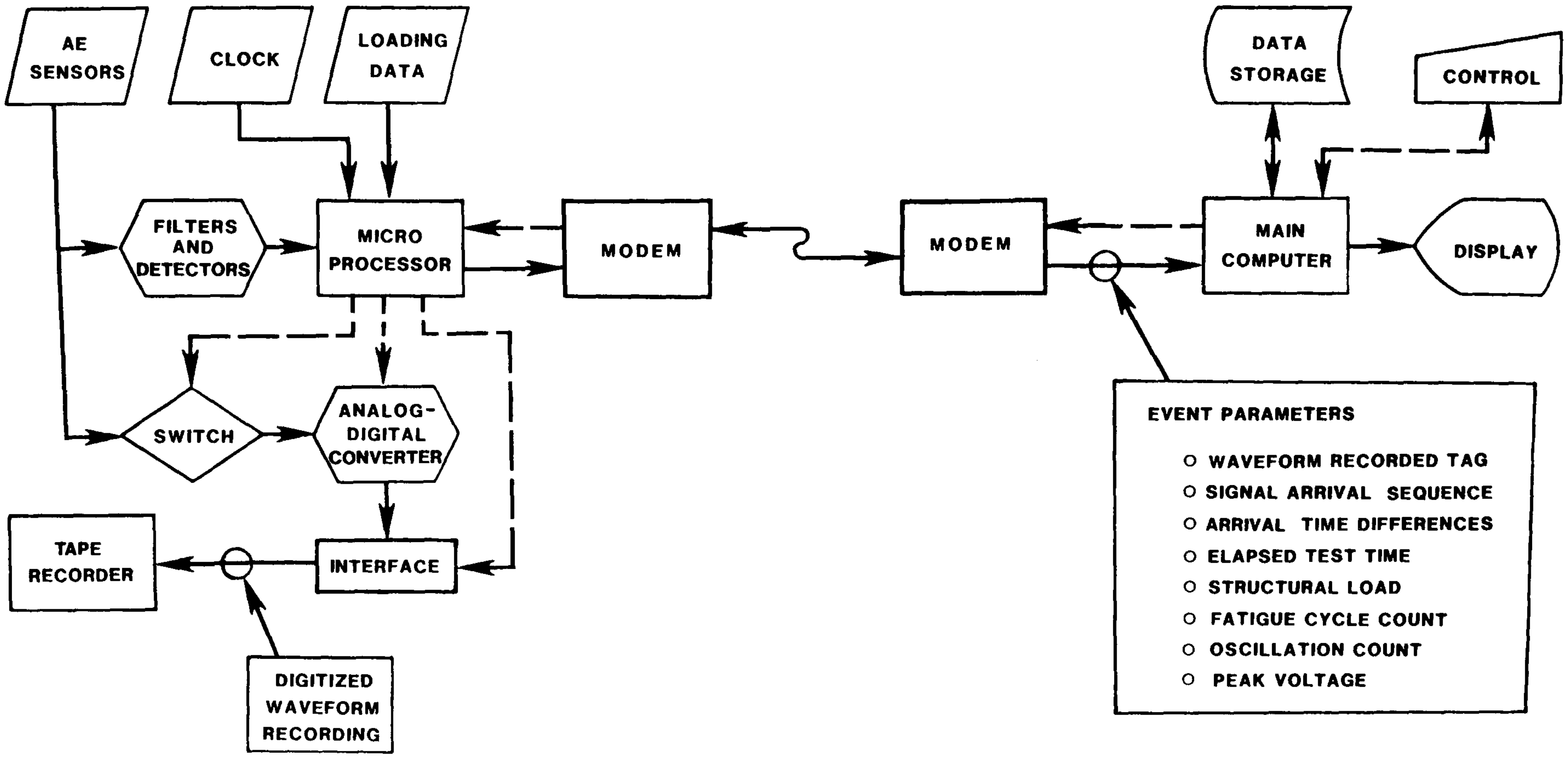

Figure 5.1. Block diagram of experimental broadband acoustic emission system assembled for thesis research program.

difficult to solve because of the intermittent occurence of the data corruption.

The capabilities of the modified system can best be understood by explaining the way it handles an individual acoustic emission signal propagating through a specimen. Although the acoustic emission signals must first enter the sensors, which could therefore form a legitimate part of the system, sensors will not be discussed as if they were part of the system design because they can readily be changed to meet different needs. Thus for the purposes of this discussion the first system component the signals must enter is the preamplifier.

The preamplifiers which are employed in the system are notable for their bandwidth, which extends from 10 kHz to 15 MHz at the 3 dB points. This is not common practice, as it is usually desirable to reduce thermal noise to a minimum. Thermal noise in RMS volts is given by Skolnik [Ref 91] as:

$$V_N = \sqrt{4 R k T B} \tag{5.1}$$

where R is resistance, T is temperature in degrees Kelvin, k is Boltzmann's constant, and B is the bandwidth over which the noise is measured. Thus the preamplifiers used in this acoustic emission system generate about 4 times more noise that the typically employed 1 MHz bandwidth acoustic emission preamplifiers. The increased noise was felt to be an acceptable penalty, however, since the increased bandwidth provided more information which signal processing routines could utilize for source characterization. One problem with the preamplifiers was their 10 kilohm input impedance which loaded the sensors and reduced the output. As described in Section 6.2 this loading was eliminated by building a FET impedance converter to effectively make the preamplifier impedance 1 megohm.

The preamplified acoustic emission signals are input simultaneously into two separate sections of the system, where different parameters are derived. In the main path, the signals from all channels are filtered between adjustable limits (typically 100 - 300 kHz) before an event detector produces a pulse for each event. In the other path, all of the signals in their unfiltered state are passed through a switch which when activated will allow only one channel to be input to the analog to digital converter. This switch, which was built as part of the modifications to the MSCD system, attenuates the 11 inactive channels by 60 dB when it is activated by the microprocessor. This occurs after the microprocessor determines that the signal being detected is the first arrival of a new acoustic emission event. The two path concept is used in an attempt to avoid problems in locating with dispersive waves. As described in Section 2.3, various modes of plate waves travel at different speeds as a function of frequency and plate thickness. Judicious selection of the filter bandwidth for a particular application allows the event pulse to be derived from a particular constant velocity component of the acoustic emission signal.

After the event pulses are generated from the narrowband data a programmable microprocessor controls the acquisition of the wideband data and the transmission of the entire data set to the data processing section. This microprocessor is another modification of the MSCD system and is crucial to the operation of the system because it controls the acoustic emission data collection. The microprocessor does this by means of a program named MSCD, whose source code appears in Appendix B. The writing and debugging of MSCD accounted for most of the time spent in modifying the original acoustic emission system, because MSCD had to be written in ASSEMBLY language and installed in an EPROM chip to be tested. Provisions were made to accomodate numerous error conditions and timing difficulties in MSCD. A complete diagram of the logic it incorporates is shown in flow chart form in Figure 5.2. Starting with the system in a quiescent state the first event pulse starts two arrival time clocks running, values corresponding to the channel number, the time of day, the load on the structure and the number of fatigue cycles are saved, and the wide band switch is activated to allow only the presently active channel to be recorded by the analog to digital converter. The arrival of the second event causes the first arrival time clock to be stopped and the channel number of the second event to be saved with similar action taking place when the third event is detected.

The MSCD program now must determine if the acoustic emission signal which has just been processed has propagated out of the monitored area (or has been attenuated sufficiently) so that the next detected event pulse will correspond to the first arrival signal of a new acoustic emission source. This is done by combining all of the event pulses onto one signal bus and measuring the time separation between the pulses. When this value is greater than the maximum time of propagation between

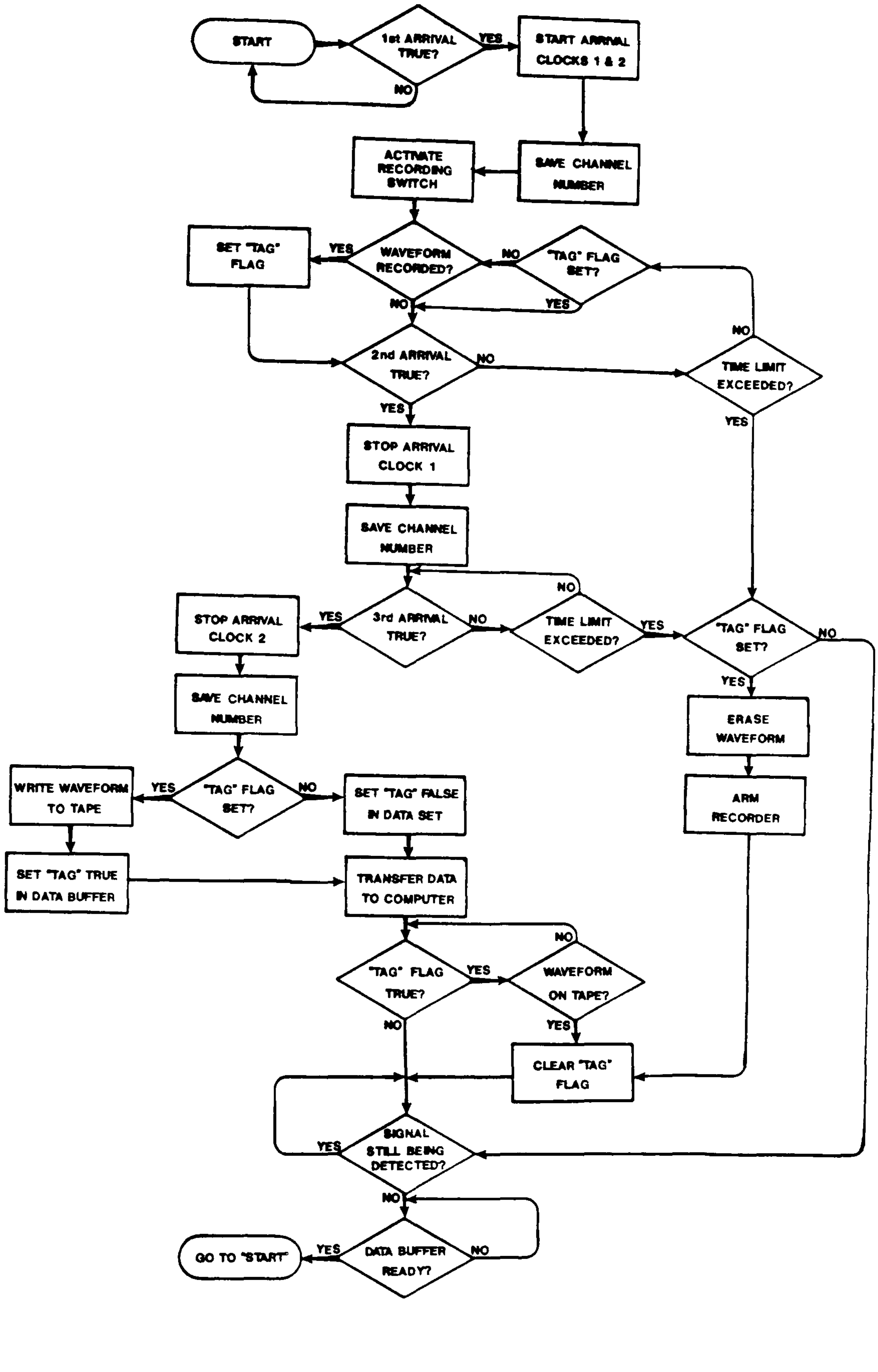

Figure 5.2. Flow chart of logic employed by microprocessor used in experimental acoustic emission system.

adjacent sensors on the structure, it is physically impossible for the old signal to be present (at least at an amplitude that matters) and so the system can get ready to reset and begin the cycle again. (It should be pointed out that this procedure can result in missed data if the acoustic emission bursts occur at different locations but happen to overlap one another in time. If this is the case, the experimenter must either move the sensors closer together or modify the loading on the structure to cause emission at a lower rate.)

Prior to the occurrence of the reset the data which has been collected is examined for errors. For example, if either arrival time clock has exceeded a preset value which corresponds to the maximum time of propagation over the entire monitored area, or if the arrival sequence of the events was such that the participating channels were not adjacent to one another (as determined by programming variables prior to the experiment), the data set is considered invalid. If this is the case the reset will occur immediately and new data will be recorded directly over the invalid data. Another error which could occur is if the analog to digital converter did not complete a recording after the arrival of the first event pulse but prior to the arrival of the second event pulse. If this occurred the waveform recording would be erased, but the rest of the data would be treated normally.

Assuming that no error conditions existed, the MSCD program would initiate a transfer of all of the data. Because of transmission line speed restrictions the waveform data is stored locally on 9 track digital magnetic tape while the rest of the data is transmitted via a modem link over telephone lines to the minicomputer data processing section. The transmitted data set contains such items as an indicator showing that a broadband waveform recording was made, the sensor arrival sequence of the acoustic emission signal, two arrival time differences, the elapsed test time, the structural load, the fatigue cycle count, the narrowband signal oscillation count, and the narrowband signal peak voltage. When the transmission has been initiated, the MSCD program checks to see if one of a pair of local data buffers is available to receive new data. If a buffer is available an immediate reset occurs and data collection can start, otherwise the program waits. This double buffering concept helps to smooth out the process of data acquisition since one buffer is usually available to receive data.

The crucial factors limiting the performance of the acoustic emission data collection system are the times required to transmit the data set from the microprocessor to the minicomputer and to transfer the waveform data from the analog to digital converter to the 9 track digital magnetic tape recorder. In the current implementation of the system these times are 0.2 S and 0.15 S, respectively. The reset concept employed in this system requires that the wave propagate a minimum of 1.5 times the sensor spacing before the next event can be recorded, which would require a time of 1 mS if the sensor spacing were 2 m and the propagation velocity were 3 km/S. Although it is clear that substantial room for improvement is available, it was not done with this version of the system since a virtual boost in performance can be realized by slowing the loading rate, and because the necessary electronics to transfer the data faster would have been prohibitively expensive.

After the data set reaches the data processing section many different options can be selected which will determine exactly what happens. Typically, the data will be coming from a test in which it is desired to anticipate failure and perhaps save the specimen. In this case, the data set will first be checked for a proper sensor arrival sequence and the arrival time differences will be checked to insure that they do not exceed the maximum permissible limits. Although this seems redundant, it is not, because the time resolution in the data collection section is rather coarse and the arrival sequence programming is not too sophisticated. Thus, the MSCD program could validate a data set which upon further inspection with finer time resolution and more intricate adjacent sensor definitions would not be legitimate.

Assuming that the data passes these first two checks, though, the arrival time differences and the sensor arrival sequence would be used by the minicomputer to calculate a source location. The locus of a constant difference between two points forms a pair of curves called hyperbolae, thus the two arrival time differences result in four curves. Each intersection point represents a possible source location, the correct one is chosen using the information in the sensor arrival sequence. This concept is illustrated in Figure 5.3. Although it is possible to have an intersection point lying outside of the area bounded by the sensors, the present acoustic emission system does not handle this situation. Instead, adjacent triangles must be built using additional sensors and at least one or two of the sensors pictured in

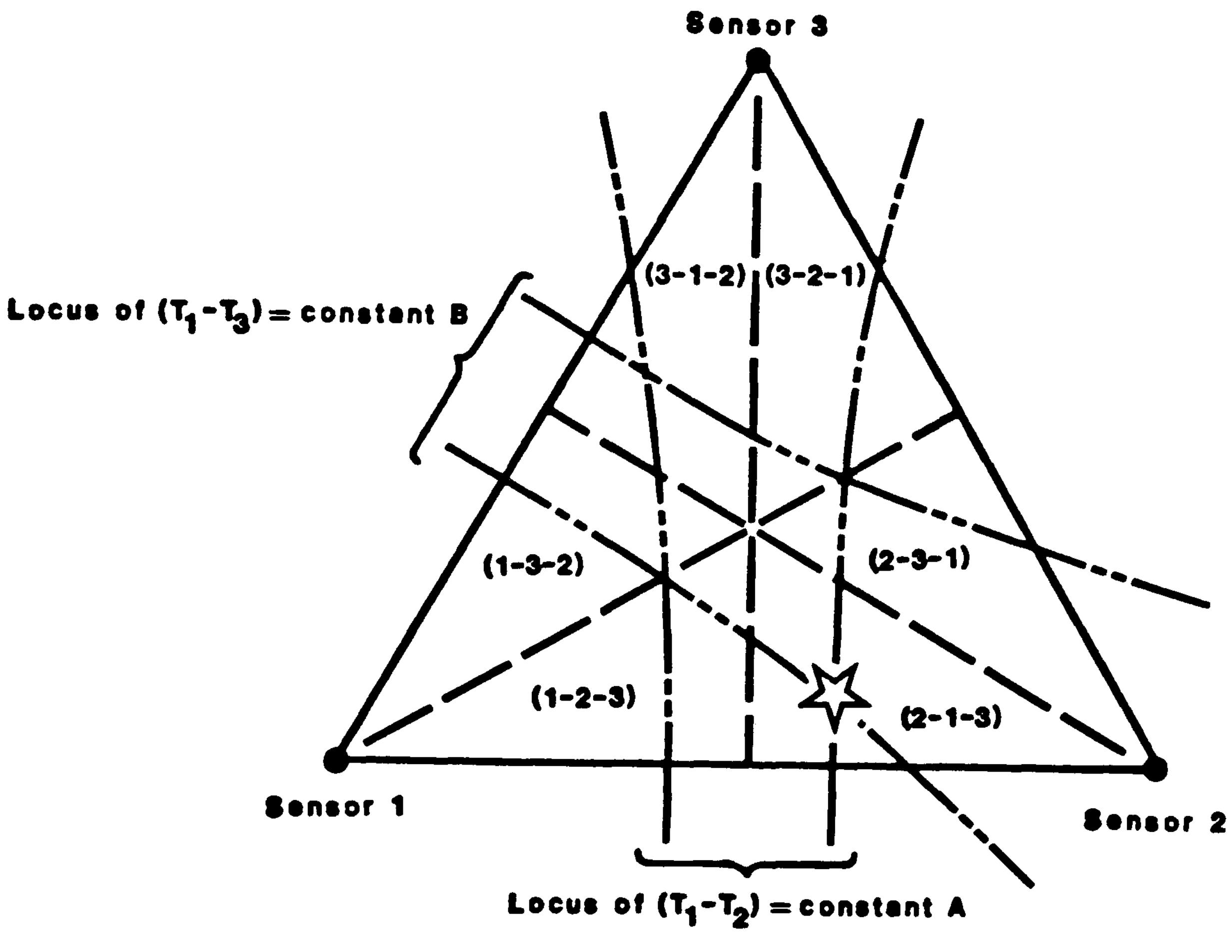

Figure 5.3. Schematic demonstrating how to locate an acoustic emission source. Arrival time differences yield four possible sites, the correct one is selected using the sensor arrival sequence data.

Figure 5.3. Any physical situation in which an intersection point could be constructed outside of the largest triangular area in Figure 5.3 would now result in the sensors of the adjacent triangle containing this intersection point detecting the signal first, and similar logic to that used in Figure 5.3 would be sufficient to resolve the true source location.

Two error conditions can result from the calculation of the source location. First, a mathematical error might occur due to truncation. To check for this condition the inferred source location is used to calculate arrival time differences. If these differences do not agree with the measured arrival time differences to within 10%, an error is declared. Secondly, a physical source might lie entirely outside any areas bounded by three adjacent sensors. As mentioned previously this situation is not legal under the present location logic and thus an error would be declared.

Once a data set is validated and a source location is calculated the data processing section records the entire data set along with its associated calculated values on a disc drive and then displays certain subsets of the data. It is possible to obtain any one of three tabulated displays of sequential data sets or any one of three graphical schematics of the specimen with source locations superimposed as the data is acquired.

One of the tabulated displays is shown in Figure 5.4. This version, termed the raw data display since it shows the values which are being received from the remote acoustic emission data acquisition

```
INPUT DATA BUFFER

000012
051000
000022
000006
000010
001001
000003
007227
001017
003142
000000
000004

OUTPUT DATA BUFFER

EVENT NUMBER       =     328
DELTA T1           =       6    US
DELTA T2           =       8    US
FIRST SENSOR       =       1
SECOND SENSOR      =       2
THIRD SENSOR       =       3
DISTANCE  (X)      =      14.5  CM
DISTANCE  (Y)      =      12.0  CM
OSCIL. COUNT       =    3735
PARAMETRIC VAL     =       0.2
PEAK VOLTAGE       =       5.0
ELAPSED TIME       =     408.0
PARA. CYCLE CNT    =       1
ERROR CODE         =       0
REJECTION COUNT    =       5
```

```
INPUT DATA BUFFER

000012
051100
000022
000011
000011
001001
000003
003062
001014
003142
000000
000004

OUTPUT DATA BUFFER

EVENT NUMBER       =     329
DELTA T1           =       9    US
DELTA T2           =       9    US
FIRST SENSOR       =       1
SECOND SENSOR      =       2
THIRD SENSOR       =       3
DISTANCE  (X)      =      13.0  CM
DISTANCE  (Y)      =      13.5  CM
OSCIL. COUNT       =    1586
PARAMETRIC VAL     =       0.2
PEAK VOLTAGE       =       4.0
ELAPSED TIME       =     408.0
PARA. CYCLE CNT    =       1
ERROR CODE         =       0
REJECTION COUNT    =       5
```

Figure 5.4. Example of a raw data display obtained during a test. Typically used for operational check of equipment prior to a test.

section, is useful mainly in the initial setting up of experiments. It is convenient to use this display to check the physical limits of the monitored area (through the use of the error code), to equilize overall amplifier gains in each channel (through the use of oscillation counts and peak voltages in response to a calibrated input), to check for the proper calculation of the parametric value (coefficients for a second order equation are entered to obtain an engineering response from a voltage input that is generated by a load cell, pressure transducer, strain gauge, etc.), to insure that the cycle counter is advancing properly (with changes in load, pressure, strain, etc.), and to help diagnose transmission line problems.

The remaining two tabulated displays are used to obtain information on individual acoustic emissions while the test is in progress. An example of one of these displays is shown in Figure 5.5, the other is identical except that it shows the parametric cycle count instead of the parametric value. The primary intelligence to be gleaned from these displays is the amount of energy carried by individual emissions as a function of either specimen load or fatigue cycles. Energy is proportional to the product of the oscillation count and the peak voltage. In general, the energy is indicative of the amount of damage that is occurring in the specimen, so it is instructive to look for rapid increases in acoustic emission energy at specific locations or groups of locations.

The graphical displays are used to help the experimenter quickly locate areas on the specimen where damage is occurring, as evidenced by

EVENT	S1	S2	S3	X LOC	Y LOC	OSC CNT	PAR VAL	PK VOLT	ELP TIME	EC
331	1	2	3	14.5	12.0	929	10.0	5.0	4123.0	
332	3	4	5	55.8	16.7	503	10.0	4.8	4124.0	
333	1	2	3	15.1	16.0	953	10.0	5.0	4127.0	
334	2	3	4	38.1	27.4	783	10.0	3.6	4131.0	
335	2	1	3	21.2	17.5	696	12.0	4.4	4132.0	
336	2	1	3	21.2	17.5	710	12.0	4.8	4133.0	
337	2	3	1	25.0	18.2	827	12.0	1.9	4135.0	
338	2	3	1	24.3	17.8	983	12.0	2.0	4135.0	
339	2	3	1	24.4	17.7	926	12.0	2.1	4136.0	
340	2	3	1	24.5	17.9	979	12.0	1.7	4137.0	
341	1	2	3	13.7	14.3	708	13.0	5.0	4140.0	
342	2	5	3	6.0	7.0	567	13.0	0.0	4141.0	1
343	2	3	4	38.3	28.1	787	13.0	4.4	4142.0	
344	2	3	4	39.3	27.5	888	15.0	5.0	4143.0	
345	2	3	1	24.7	17.6	980	15.0	4.8	4152.0	
346	2	3	1	24.5	17.5	1087	15.0	5.0	4153.0	
347	2	3	1	24.5	17.5	989	15.0	4.9	4153.0	
348	2	3	5	0.0	0.0	0	15.0	0.0	0.0	2
349	2	3	1	24.3	18.0	1121	16.0	4.4	4166.0	
350	2	3	4	38.3	27.8	772	16.0	1.2	4168.0	
351	2	3	1	24.1	17.9	771	16.0	4.9	4169.0	
352	2	3	1	26.0	17.0	1001	16.0	5.0	4171.0	
353	3	2	1	31.9	17.0	202	16.0	4.2	4174.0	
354	1	2	3	15.0	11.9	903	17.0	4.9	4182.0	
355	3	4	5	54.4	16.3	442	17.0	3.8	4184.0	
356	3	4	5	55.0	16.8	509	17.0	4.5	4185.0	
357	2	3	4	38.0	27.3	663	18.0	3.3	4193.0	
358	2	3	1	25.8	18.9	707	18.0	4.1	4195.0	
359	2	3	4	39.0	28.2	602	18.0	5.0	4197.0	
360	3	2	1	30.1	17.3	412	18.0	3.3	4201.0	

Figure 5.5. Example of a tabulated data display obtained during a test. Typically used for monitoring energy carried by individual emissions.

either large numbers of events or large amounts of energy release. The two dimensional planar version is shown in Figure 5.6. The crosses correspond to the transducer locations, the upper number in each box represents the number of valid events which have occurred within the box, the lower number in each box is the cumulative magnitude of the valid events which have occurred within the box, the letter E is the total number of events in the monitored area, the letter R is the number of events which have been rejected due to errors and the letter P is the current parametric value. The one dimensional linear graphs are similar except that only the valid events or only the cumulative magnitudes of the valid events are displayed at any one time.

So far the discussion of the data processing section operation has been limited to situations in which a test is being monitored and it is necessary to have information immediately available so as to predict failure. However, it is also possible to process the acoustic emission data sets recorded during a test after the test is history. This can be accomplished in several ways. The most straightforward is to use the same program described above for real time data set processing except that input is specified from the disc instead of from the remote acoustic emission data acquisition section. The program will convert the recorded data back into raw data exactly like it was originally received and then process it using new information and re-record it on the disc. In this manner one can investigate the effects of changing the acoustic emission propagation velocity and the coefficients of the second order parametric voltage conversion equation.

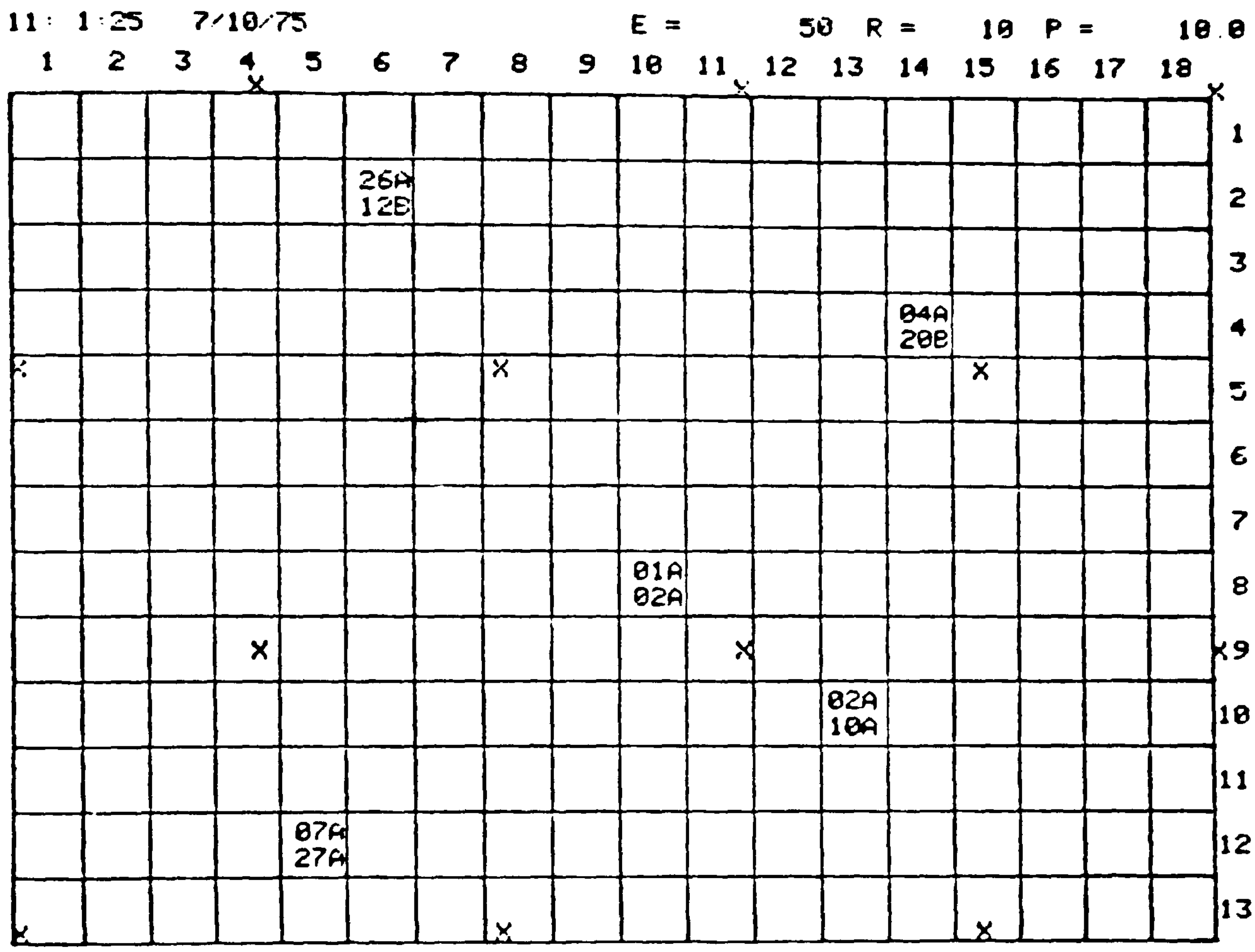

Figure 5.6. Two dimensional graphical display obtained during a test. Typically used to locate areas where damage is occurring. Top number in boxes is the number of events at the location, bottom number is the cumulative magnitude of those events. Letters are multipliers with A = 1 and B = 10.

Another method of post test processing can be utilized which will produce graphical displays and tabulated data very similar to that obtainable during test monitoring except that upper and lower acceptance limits can be specified for the parametric value, the peak voltage, the location, the event number, the parametric cycle count and the elapsed time. Each data set is compared to these limits and only those sets which meet the criteria are plotted or tabulated. This capability has two important uses. First, it allows the experimenter to analyze a completed test in segments. For example, if acoustic emission activity occurred at several locations at different times the experimenter could specify location limits and time limits which would enable him to plot each source's activity during the entire test. Or, he could produce plots showing each source's behavior during a portion of the test when the parametric value reached a critical limit. The second use is to produce statistics for each acoustic emission source which are used as inputs to yet another post test processing program.

The final post test processing program has as its purpose the production of functional relationships between various parameters. It can produce graphs of the parametric value versus elapsed time, occurrence versus elapsed time, occurrence rate versus elapsed time, magnitude versus elapsed time, magnitude rate versus elapsed time, occurrence versus magnitude, occurrence versus parametric value, magnitude versus parametric value, occurrence versus parametric cycle count, magnitude versus parametric cycle count and occurrence versus first arrival sensor. All of these graphs are subject to the same limits mentioned previously.

The technology of acoustic emission instrumentation was advanced by the building of this system for several reasons. First, it made possible the broadband digital recording of acoustic emission waveforms. Second, it permitted the broadband waveform recordings to be associated with a planar or a linear source location even in dispersive structures. And third, it allowed acoustic emission data to be gathered from specimens in environments that had previously precluded such monitoring because the delicate data processing minicomputer was physically separated from the data acquisition section.

5.2 Software

The experimental acoustic emission instrument described in detail in Section 5.1 produces digital magnetic tapes containing acoustic emission waveforms. To obtain the desired source identification information from these tapes it was necessary to write computer programs to process them. It was decided that the most useful information contained in the acoustic emission signals would be found in the time and frequency domains so major emphasis was placed on writing plotting programs that would produce graphs of these domains. It was also necessary because of the large amount of data to write the programs to run with a minimum of operator guidance. Additionally, methods were needed to deconvolve the data using gas jet information and also to calibrate the output using engineering units so that results would be directly comparable to the work of other experimenters.

Before describing all of the programs in detail, mention must be made of the computer system that was utilized for the experiments. As can be seen on the system block diagram in Figure 5.7 the main processor was a Hewlett Packard 2117F. It had 192 kilowords of random access 16 bit semiconductor main memory, two channels of direct memory access, a floating point processor for enhancing floating point arithmetic operations, dynamic memory mapping to allow direct addressing of up to 1 megaword of memory and 268 recognized instructions including some designed to enhance trigonometric and logarithmic calculations, FORTRAN operations and matrix manipulations. The main mass storage unit consisted of a HP 7906 disc drive capable of storing 20 megabytes, complemented by a HP 7970B magnetic tape unit utilizing a 9 track 800 bpi IBM compatible NRZI format. Acoustic emission data was input through a Vadic 3415A modem operating at 1200 baud, while plotting was done on a Tektronix 4010-1 graphics terminal. A Lear Seigler ADM-31 terminal served as the main system console and a Houston Instrument 8210 line printer provided the program listings. All of these devices (plus several others which appear on Figure 5.7) operated under the control of a Hewlett Packard program named RTE-IVB. This is a multi-programming, multi-tasking operating system which allows program scheduling by interrupt, time of day, operator request, or program request. Program execution is dependent both upon the state of the system resources and the priority of the program relative to other programs already executing or scheduled. It is possible that two equal priority programs can execute concurrently via a central processing unit time-slicing feature.

RTE-IVB supports several high level languages including BASIC, PASCAL, ASSEMBLY and FORTRAN. It was decided that the acoustic emission

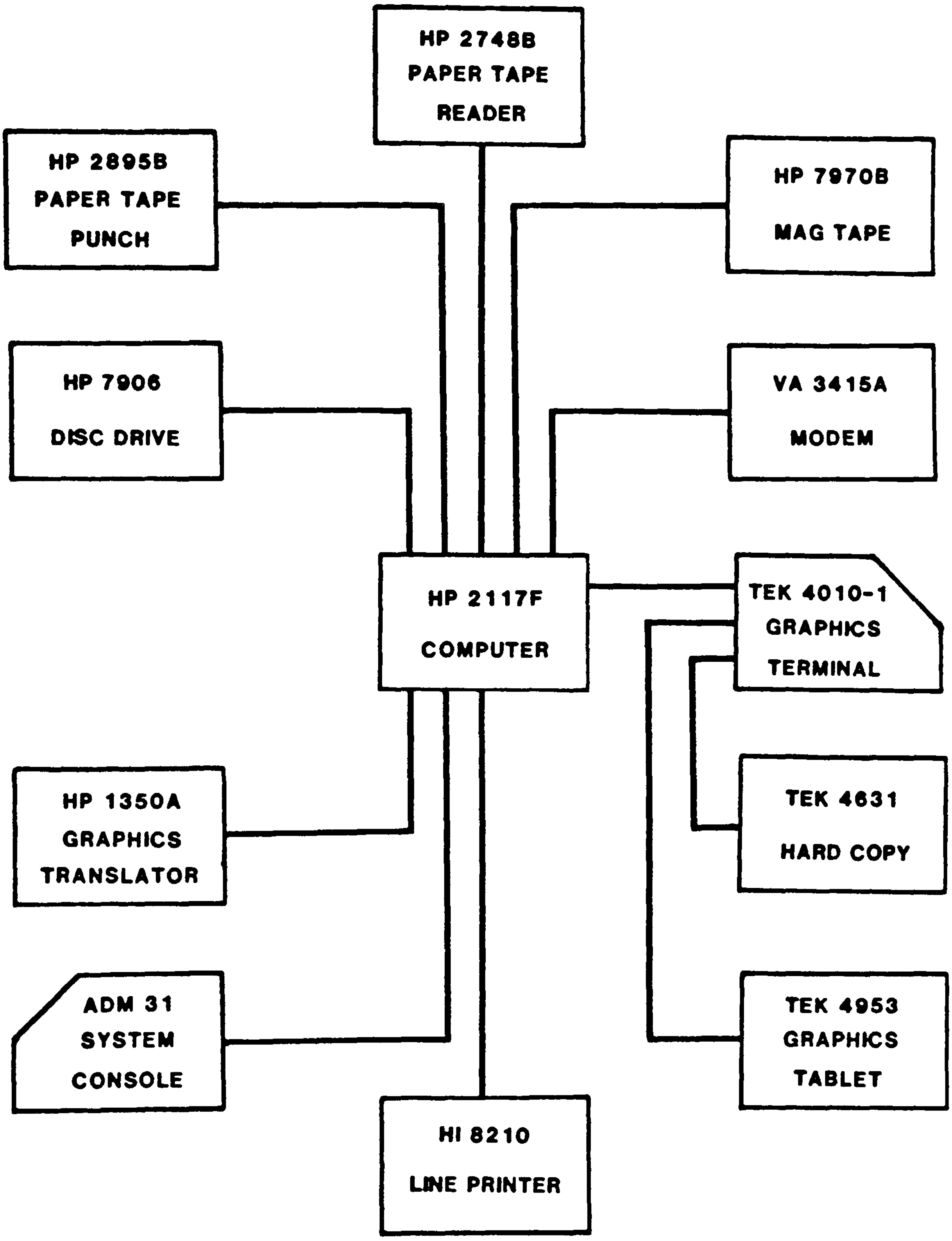

Figure 5.7. Block diagram of computer system and peripheral equipment used for signal processing in this thesis.

signal processing programs would be written in FORTRAN primarily because of programmer familiarity, available callable subroutine libraries and execution speed, but also because the readability of FORTRAN provided an easy means for debugging, modifying and maintaining the programs. Input/output operations and disc file read/write requirements were handled using HP supplied routines, both because of the detailed device control offered by this method and because of the efficiency of execution. Thus, extensive use of subroutines such as EXEC, CREAT, READF, WRITF, PURGE and CLOSE were made in the writing of the acoustic emission signal processing programs. Tables 5.1 and 5.2 provide a summary of the use and function of these HP peculiar utilities; more detailed information is contained in the RTE-IVB system manuals [Ref 92 through 95].

Computer systems are oriented towards the production of listings, which do not provide the most useful form of information for signal processing work. Graphs are much more desirable because of the manner in which they can compress information into a relatively small area, because they allow easy comparison between different experimental results, and because they help define data trends as a function of several variables. To produce graphs using the system in Figure 5.7, however, it was necessary to write some software because equipment from two different manufacturers was involved. The routines were written in HP ASSEMBLY language [Ref 96] because the table accesses and memory location manipulations that were required proved difficult to perform under FORTRAN. Two subroutines were written, named PLOT and SYMB. (See Appendix B for their source code.) Together they allow the programmer

Table 5.1
INDEX TO EXEC CALLS

Format

CALL EXEC (ICODE, ICNWD, IBUFR, IBUFL)

Parameters

ICODE - Type of operation desired (1 - Read, 2 - Write, 3 - I/O Control)

ICNWD - Operation subdefinition (FF00B + LUB)

LUB - Octal device logical unit

FF00B - Octal subfunction code, depends on ICODE

ICODE - 1 or 2	FF00B -	100B	(Binary mode select)
	-	400B	(Keyboard input printed)
ICODE - 3	FF00B -	100B	(Write EOF)
	-	200B	(Backspace record)
	-	300B	(Forward space record)
	-	400B	(Rewind)
	-	600B	(Dynamic status)
	-	1300B	(Forward space file)
	-	1400B	(Backspace file)

IBUFR - Buffer which contains or will receive data (ICODE - 1 or2)

IBUFL - Length of IBUFR (n = words, -2n = bytes)

Table 5.2

INDEX TO FMP CALLS

NAME	FORTRAN CALL	FUNCTION
CLOSE	CALL CLOSE(IDCB,IERR,ITRUN)	Close file NAME to further access by caller.
CREAT	CALL CREAT(IDCB,IERR,NAME,ISIZE,ITYPE,ISECU,ICR,IDCBS)	Create file NAME of size ISIZE, type ITYPE.
LOCF	CALL LOCF(IDCB,IERR,IREC,IRB,IOFF, JSEC, JLU,JTY,JREC)	Returns information on open file; next record in IREC, next block (IRB), next word (IOFF), etc.
OPEN	CALL OPEN(IDCB,IERR,NAME,IOPTN,ISECU,ICR,IDCBS)	Open file NAME for access by calling program.
PURGE	CALL PURGE(IDCB,IERR,NAME,ISECU,ICR)	Purge file NAME and its extents from disc.
READF	CALL READF(IDCB,IERR,IBUF,IL,LEN,NUM)	Read record from open file to buffer (IBUF).
RWNDF	CALL RWNDF(IDCB,IERR)	Rewind or position to first record in file.
WRITF	CALL WRITF(IDCB,IERR,IBUF,IL,NUM)	Write record from buffer (IBUF) to file.

COMMON PARAMETERS	
IBUF	user-defined integer array used as read/write buffer for READF and WRITF calls.
ICR	one-word integer variable set to cartridge reference number of cartridge containing file: positive integer = cartridge label negative integer = logical unit number
IDCB	user-defined integer array (Data Control Block) containing file control information on open file (16 words) plus packing buffer for data transfer (minimum 128 words), IDCB assumed to be 144 words unless IDCBS is specified.
IDCBS	one-word integer variable containing exact number of words in IDCB when IDCB greater than 144.
IERR	one-word variable where negative error code is returned, or for successful OPEN, file type, for successful CREAT, number of 64-word sectors.
NAME	3-word integer array containing legal 6-character file name, must not begin with blank or number; no embedded blanks; use any printable ASCII character.
ISECU	one-word security code; integer or two ASCII characters: positive = write protected negative = read/write protected zero = not protected

OPTIONAL PARAMETERS IN FORTRAN CALLS ARE UNDERLINED.

to draw line segments, input cross-hair cursor intersection coordinates to interactively designate and quantify points of interest, draw alphanumeric symbols of any size and orientation to label the plot, erase the plot and produce hard copies of the plot.

With the basic tools developed work began on the actual acoustic emission signal processing routines. The first program, designed to be used after the generation of the acoustic emission signal magnetic tape, is named PLTME for "plot time domain". (See Appendix B for its source code.) It can be used in one of two modes, one of which allows viewing any particular acoustic emission signal recorded during an experiment and contained within one file on the tape. The other mode views all acoustic emission signals recorded during any experiment in sequence until the end of file is reached, allows the operator to select waveforms worthy of further processing, and writes the waveform number of the selected signals into a disc data file. Additional features of PLTME are its automatic vertical scaling which works in a 1, 2, 5 multiplication sequence to show as much detail on the plot as possible, its vertical and horizontal labelling sections which produce automatically labelled plots over a full scale range of 0.01 to 500 volts and 20.4 to 409 microseconds, respectively, and its automatic association of the plot with the particular acoustic emission waveform number that produced it.

The disc data file produced by PLTME has a specific flexible format that permits the experimental conditions to be retained as the signals are processed. An example of such a file appears in Figure 5.8. The

```
"7039 SCC EXPERIMENT (K=31)"
"EMISSIONS GATHERED OVER A 55 MINUTE PERIOD"
"TOTAL OF 60 AE SIGNALS RECORDED"
"GOOD SIGNALS WERE DETERMINED FROM VISUAL APPEARANCE"
"PREAMP GAIN = 36 DB, BIOMATION ATTENUATOR = 0.05 VOLTS"
"TRIGGER SETTING = +0.06, PRETRIGGER, 1.80 TRIGGER DELAY"
"GAIN CORRECTION FACTOR ="0.05,"SAMPLING RATE ="0.1
"RAW DATA TAPE FILE NUMBER ="3
"GOOD TAPE RECORDS FOLLOW:"
1,2,3,4,5,6,7,8,9,10,11,12,13,14,15,16,17,18,19,20
21,22,23,25,26,27,28,29,30,31,32,33,34,35,36,37,38
39,40,41,42,43,44,45,46,47,48,49,50,51,52,54,55,56
57,58,59
```

Figure 5.8. Disc data file produced by program PLTME.

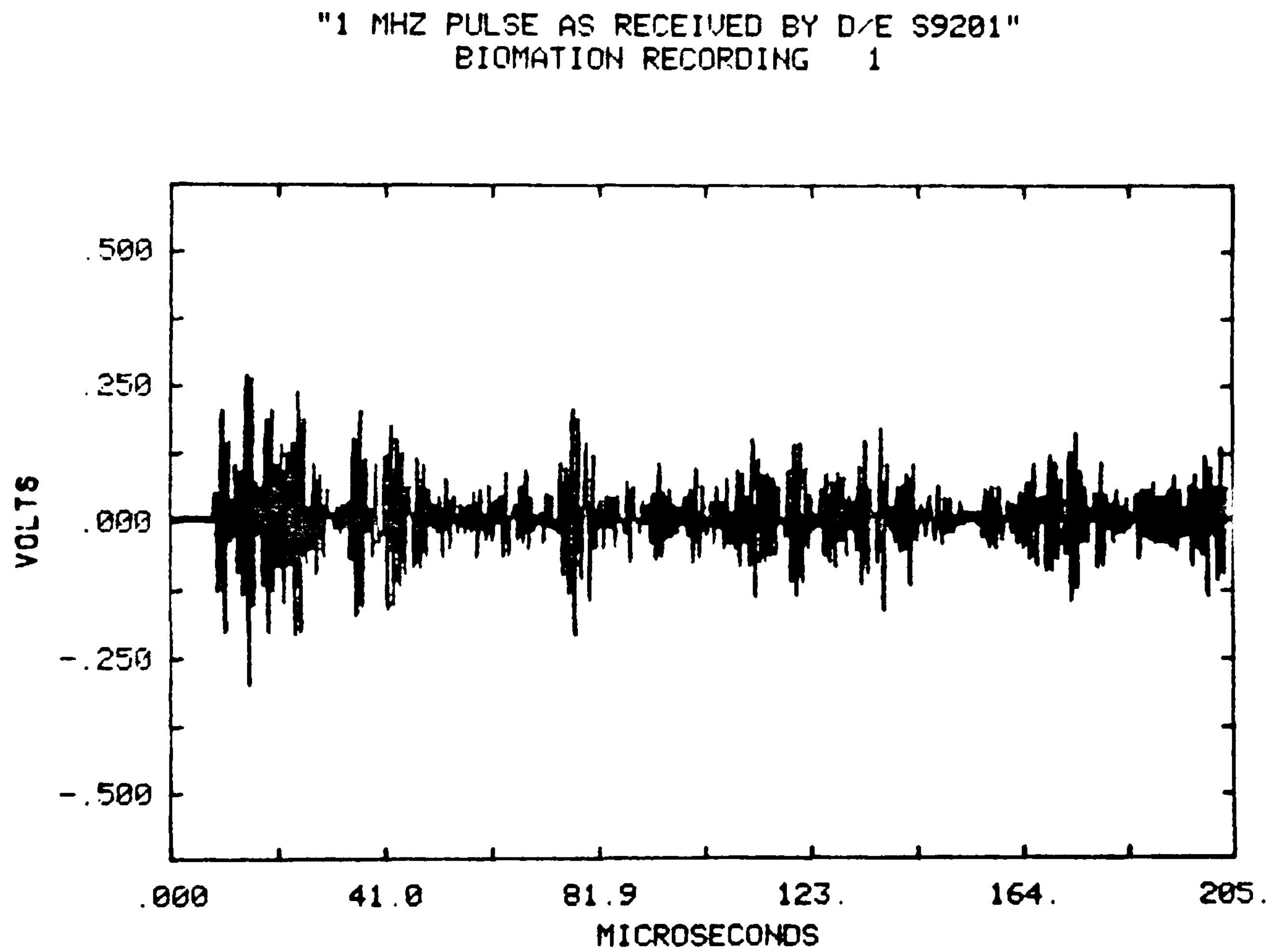

Figure 5.9. Time domain plot produced by program PLTME.

first line becomes the title that PLTME and other programs will place on graphs. It can contain any ASCII character with the exception of double quotes, which are used as delimiters to start and end the string. Subsequent lines have the same content restriction, the difference is that they will not be processed by PLTME or other programs unless they contain a non-zero number outside of the double quotes. When this happens, as in line 7 of Figure 5.8, PLTME interprets the left most number outside of the double quotes as a scaling factor for the ordinate. If there is a second number separated by a blank space, a comma or a delimited string it will be used as a scaling factor for the abscissa, otherwise a value of zero will be used as the abscissa scaler. The next line must then contain a non-zero integer outside of a delimited string to be used as the tape file number. Any other descriptive lines that the experimenter wishes to record can now be entered provided that they begin and end with double quotes, for once another non-zero integer outside of a delimited string is encountered by programs subsequent to PLTME it will be interpreted as a valid acoustic emission record number.

With the entry of the data file header information completed, PLTME produces time domain plots of acoustic emission signals similar to the example shown in Figure 5.9. If the operator judges the signal to be worthy of further processing he presses the G key (for "good") when the cross-hairs appear and the record number of the signal is written to the disc data file. Any other key simply causes the next signal to be plotted. The sequence continues until the end of file on the magnetic tape is reached, signifying the end of the acoustic emission experiment and causing PLTME to terminate. As mentioned previously, Figure 5.8 is an example of the data file output produced by PLTME. Such a file does not have to be produced. Should the operator chose to simply view acoustic emission waveforms he merely enters the appropriate scaling factors, tape file number and waveform number when prompted by PLTME to do so. When the cross-hairs appear after the time domain plot is drawn, typing a Q (for "quit") will cause program termination while any other response causes PLTME to ask for another waveform number.

Having run PLTME, the operator now possesses time domain plots of all of the acoustic emission signals he wishes to analyze and also has a file containing the waveform numbers of those signals along with relevant experimental documentation. Program AENOR, which stands for "acoustic emission normalization", is now scheduled to produce a data file containing frequency domain information. (See Appendix B for its source code.) AENOR will first request the name of the waveform data file produced by PLTME and then will request a name for a file in which to write the frequency domain data. The header information in the PLTME output file will be transferred verbatim to the frequency domain file, thus insuring that experimental conditions are kept with experimental results. Next, the magnetic tape containing the acoustic emission signals will be read using the tape file number and the signal numbers in the PLTME output file for positional information. A power spectrum will be calculated for each signal number in the PLTME output file and the resulting spectrum will be written to disc along with a normalization factor and the appropriate signal number. The normalization factor is defined as the ratio of the total energy in the first signal encountered by AENOR to the total energy in the signal presently being processed. This factor provides a convenient way for subsequent programs to produce "constant energy" spectral plots of acoustic emission waveforms in a particular experiment to simplify spectral shape comparisons. AENOR terminates when all of the signal numbers in the PLTME output file have been processed.

One of the prime concerns in writing AENOR was that it produce a power spectrum calibrated in engineering units. This requirement was met through careful attention to detail in lines 166 through 180 of AENOR (see page 272), which are responsible for the calculation of the power spectra. The process starts with obtaining the real and imaginary parts of the frequency spectrum from the time domain data, this is done using subroutine FOUR2 in line 166. This particular subroutine performs a base 4 + 2 FFT which results in approximately 25% faster execution than a straight base 2 FFT. (See Section 4.2 and Appendix A for more discussion on the FFT.) Lines 170 and 171 correct for the fact that FOUR2 scales the spectral data by the dimension of the transform. Line 172 calculates the power spectrum from the complex frequency spectrum by multiplying each complex frequency component by its complex conjugate. Line 173 reflects the fact that the most commonly used 0 dB reference level is 1 milliwatt into a 50 ohm impedance, while the power spectrum calculated in line 172 uses as a 0 dB level 1 watt into a 1 ohm impedance. The final correction, made in line 174 of AENOR, is made because the mathematical definition of a Fourier transform requires integration over time from negative infinity to positive infinity which results in frequencies from negative infinity to positive infinity.

Negative frequencies have no physical meaning, but the power carried in these frequencies must be accounted for. Because of the symmetry of the power spectrum about 0 Hz when analyzing real (as opposed to complex) time domain signals, it is only necessary to double the power in the positive frequency band to produce a plot of total power versus the absolute value of frequency.

Verification of the output of AENOR was accomplished by creating an artificial pulse with an amplitude of 0.5 volts, a duration of 12.8 microseconds and a repetition rate of 204.8 microseconds on magnetic tape. A header file was created as if PLTME had been run and AENOR was called to process the magnetic tape. The output file of AENOR was plotted using a program which will be described shortly and Figure 5.10 resulted. The amplitude of each Fourier component of a square pulse is given by Seely [Ref 97] as:

$$C(n) = \frac{Ea}{T} \quad \frac{\sin \pi na/T}{\pi na/T} \tag{5.2}$$

where E is the amplitude of the pulse, a is the duration of the pulse, T is the pulse repetition rate and n equals 0, 1, 2, etc. The power in each Fourier component is found by squaring c(n) for each n and dividing by the impedance. For a 50 ohm impedance it is easy to prove that the DC level (n = 0) of the pulse should be -17.09 dBm, the first sidelobe (n = 23) should be -30.36 dBm, the second sidelobe (n = 39) should be -34.94 dBm and the third sidelobe (n = 56) should be -37.92 dBm. Since Figure 5.10 agrees with these values it can be concluded that AENOR is indeed calibrated.

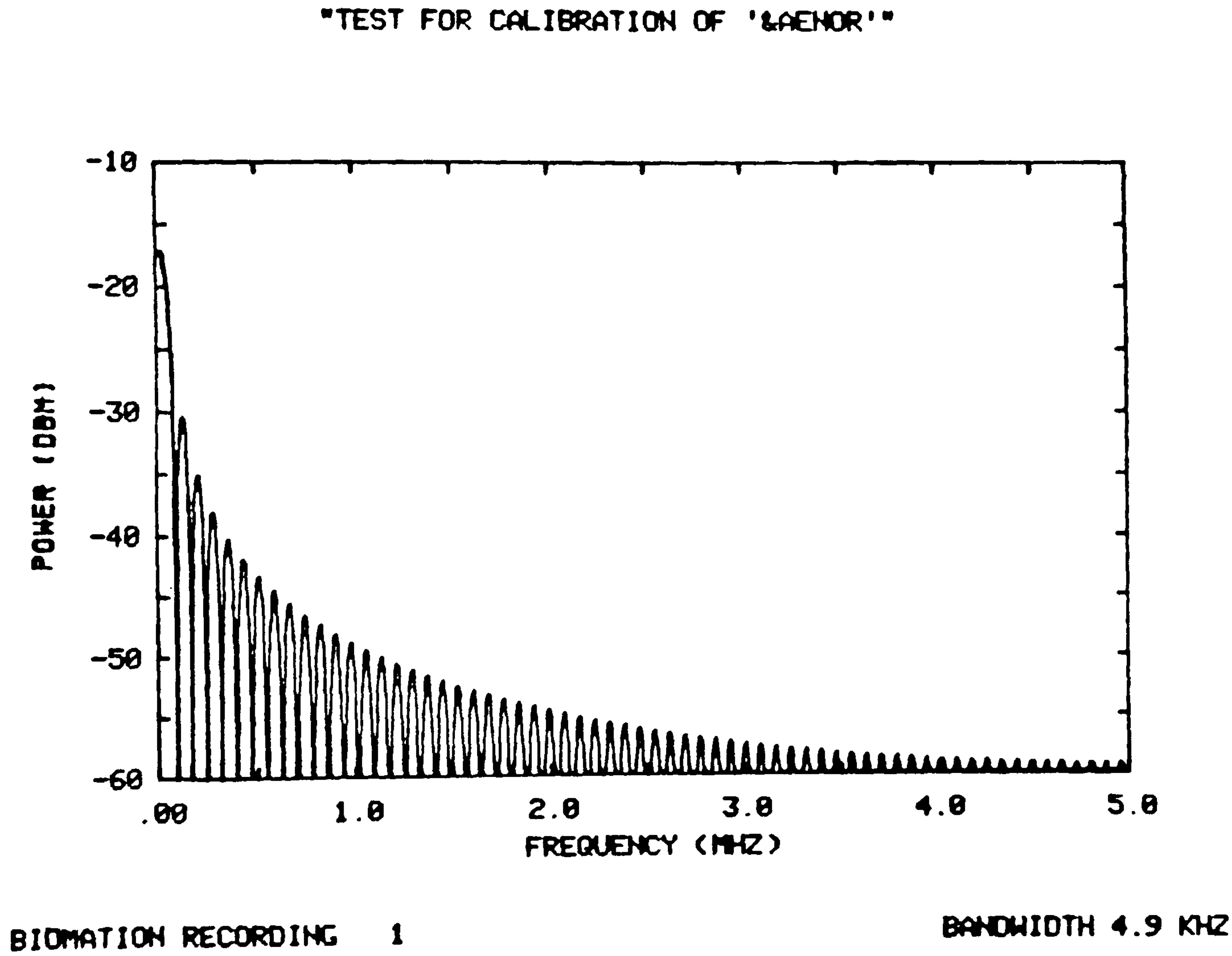

Figure 5.10. Power spectrum produced by program PLFFT for an artificial square pulse of 0.5 V amplitude 12.8 μS wide having a repetition rate of 204.8 μS.

As was explained in Section 3.2 a helium gas jet can be used to remove the effects of system variables on experiments. The process of doing so, however, requires that a power spectrum be developed which describes the long term frequency content of the gas jet signal. For this purpose program GASJT was written. (See Appendix B for its source code.) In operation this program will creat a header file exactly as does PLTME so that the experimental conditions will be recorded. Once the tape file number is entered, however, GASJT proceeds immediately to process every time domain signal in that file on the magnetic tape. For each signal it will calculate a calibrated power spectrum in a manner similar to that described for AENOR and add each succeeding power spectrum on a frequency by frequency basis to the sum of all previous power spectra. When the end of file of the magnetic tape is reached the totalized power spectrum is divided by the total number of signals processed to form an averaged power spectrum for the experiment.

The information contained in the data files produced by AENOR and GASJT is most useful in graphical form. To produce the graphs program PLFFT, for "plot FFT", is used. (See Appendix B for its source code.) The operator is prompted to enter the name of the file containing the acoustic emission signal FFT information. If he so chooses the name of the gas jet power spectrum file can be entered next in order to produce normalized plots. PLFFT then prompts the operator to enter the waveform number he desires to plot and also asks if "constant energy" plots are desired. If this feature is selected all of the plots will contain the same energy as the first plot of the file, otherwise every plot will be calibrated with a log reference level of 0 dB equal to 1 milliwatt into a 50 ohm impedance. The program then proceeds to produce a graph similar to the example shown in Figure 5.10. When the cross-hairs appear typing in a Q (for "quit") will cause program termination. Typing in a # causes PLFFT to request another waveform number, while typing in a M (for "magnify") causes the program to magnify the plot by a factor of 1, 2 or 5 depending on the operator's choice. PLFFT employs automatic vertical scale ranging to insure that the maximum amount of detail is shown over its 60 dB viewing area from a full scale maximum of -940 dBm to 9990 dBm. A clipping algorithm is used to keep the lower limits of the graph from exceeding the plot area and automatic abscissa labelling is employed to produce rational labels over a full scale range of 0.05 MHz to 50 MHz. Additional features include the automatic association of the plot with the acoustic emission waveform number which produced it and the automatic calculation and labelling of the plot with the minimum frequency resolution, or bandwidth.

When experience was gained using the programs just described it was realized that it would also be desirable to be able to calculate an average acoustic emission power spectrum for an entire test, complete with confidence limits. The reason for this was that the variability from spectrum to spectrum between acoustic emission signals within one test was great enough to hinder the search for differences in spectral shape between tests conducted using different failure processes. For this reason, program AECNF (for "AE confidence limits") was written. (See Appendix B for its source code.) This program allows the operator to process any output file produced by AENOR and to normalize the acoustic emission signal power spectrum using helium gas jet data produced by GASJT if such is desired. AECNF will prompt the operator to enter a "t" value and the corresponding confidence limits for the calculated number of degrees of freedom and will then produce a plot similar to that shown in Figure 5.11. When the cross-hairs appear the operator can magnify the plot by typing in a M, or he can enter another "t" value and the appropriate confidence limits by typing a T, or he can terminate AECNF by typing in anything else. AECNF has the same automatic vertical scale ranging, clipping, abscissa labelling and bandwidth calculation features that PLFFT employs. In addition it labels the plot with the confidence limits which were utilized and also the number of spectra that were averaged.

One last program was discovered to be needed when it was found that the extended record length data files produced by AENOR and GASJT could not be saved on magnetic tape or even moved from disc cartridge to disc cartridge through the use of RTE-IVB file manager commands. A program named DBSVR (for "data base save and restore") was therefore written to create a processed acoustic emission data base on magnetic tape. (See Appendix B for its source code.) DBSVR asks the operator if he wishes to save or restore data. If the answer is "save" the program asks if there is already data on the tape so that it can skip over it, then requests the name of the file to save and proceeds to store that file on magnetic tape. If the operator requests to restore data he is asked for the file number on the tape that contains the data he wants to restore. The program then prints out the first line of the header information and asks if this is the data that is desired. If not, DBSVR requests another file number and the process repeats. Otherwise, DBSVR requests

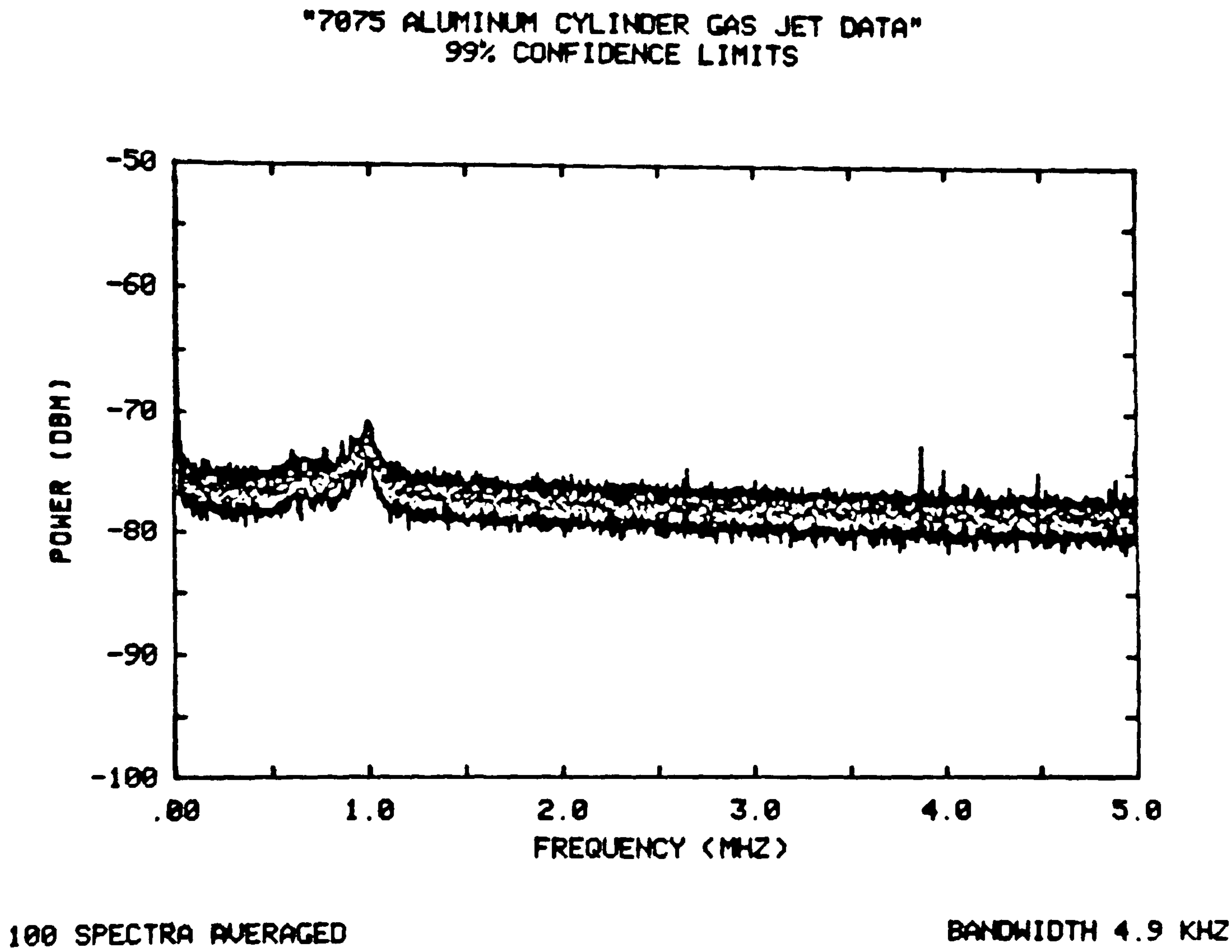

Figure 5.11. Averaged power spectrum with confidence limits produced by program AECNF.

the name of a file in which to store the data and proceeds to restore the data to disc. In both the save and restore modes the data that has been newly created is verified against the original data so that no errors occur.

As was mentioned before care was taken to insure that properly calibrated spectra were created by AENOR and GASJT and it was shown that it was possible to produce frequency spectra which agreed with theoretical calculations. However, due to the fact that other experimenters were producing acoustic emission power spectra using analog techniques through the use of the HP 8553B/8552B/141T swept frequency analysis system it was deemed important to determine if AENOR and GASJT produced comparable spectra. To accomplish this identical signals were input to both the analog and the digital systems and the results were compared.

The test time domain waveform that was chosen for input to both AENOR/GASJT and the HP8553B was not strictly a waveform but rather random noise. The selection of noise as a test input rather than an actual acoustic emission waveform arose partially because of the necessity to repeatedly input the signal to the analog instrument. This is because the HP 8553B electronically sweeps a filter over the desired frequency range, thus the spectral components are sampled sequentially in time. AENOR and GASJT, on the other hand, are real-time analysis systems that calculate all of the spectral components simultaneously from a single input. To get a fair comparison of the two systems using an actual acoustic emission waveform, then, it would be necessary to have a recording system that would accurately reproduce the signal at a constant repetition rate. Although this requirement could conceivably be met it is also important to realize that the HP 8553B instrument suffers from a phenomenon know as "pulse desensitization", which is caused by the fact that the swept filter employed in the instrument responds differently to a pulse than it would to a continuous signal [Ref 98]. The amplitude of the pulse desensitization in dB is given by:

$$\alpha_p \quad = \quad 20 \log \tau_e B_i \tag{5.3}$$

where τ_e is the effective pulse width and B_i is the effective impulse bandwidth of the swept filter. The decay of an acoustic emission signal makes it extremely difficult to assign a value to τ_e, thus the amount of correction required for an acoustic emission signal would at best be a guess. The substitution of random noise for an acoustic emission waveform eliminates all problems since there will be no pulses to desensitize the filter and since the input will be reproducible if a long enough sweep time is used on the HP 8553B to allow the dwell of the filter at a specific frequency to average out short term statistical fluctuations in the noise. AENOR will of course not be usable since it would process a short enough signal that statistical fluctuations would be important. GASJT, however, is ideally suited to this situation since it averages a number of power spectra together to develop an estimate of the long term average power spectrum.

Figure 5.12 shows the output of GASJT when 57 power spectra of background electrical noise signals created by thermal processes in a Dunegan/Endevco S9201 transducer were averaged. Figure 5.12 also shows

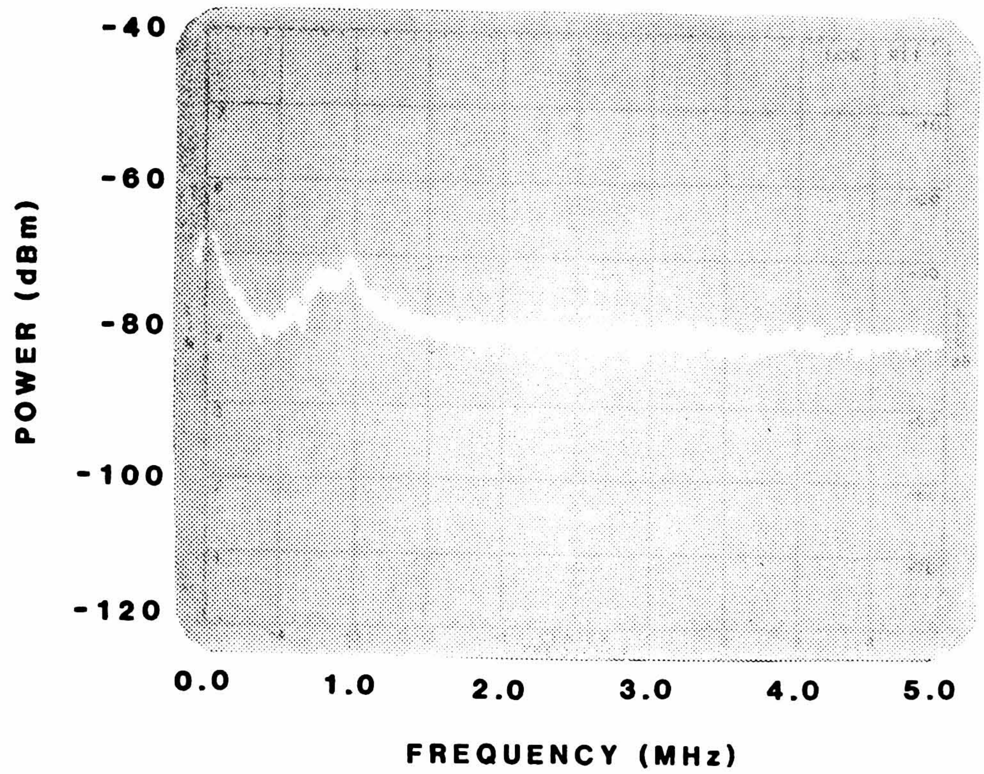

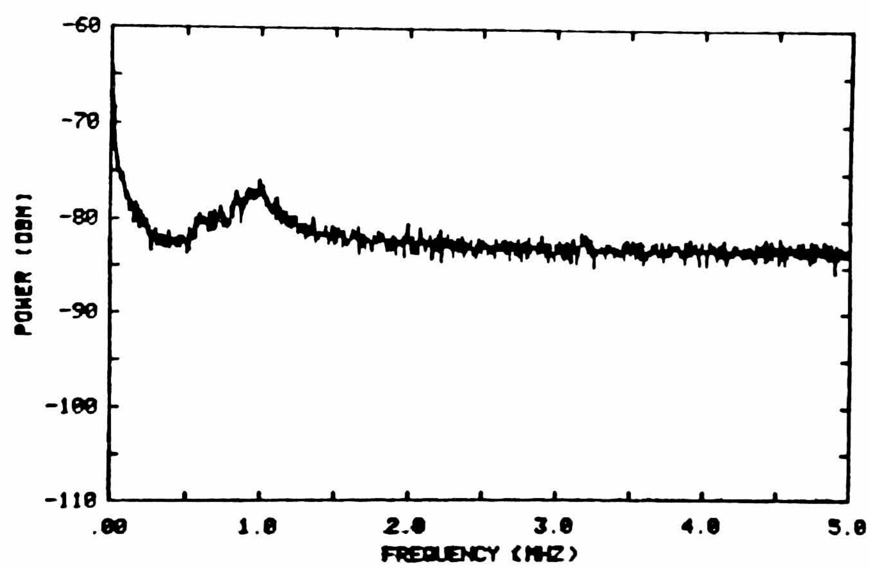

Figure 5.12. Comparison of thermal noise frequency spectral plots produced by analog and digital methods. Comparison is exact if 3 dB bandwidth correction is made.

the scope presentation of the HP 8553B instrument when it was connected to the same noise source. Note that the HP 8553B spectrum is 3 dB higher than the GASJT plot. This is caused by the fact that the bandwidth used on the HP 8553B was 10 kHz as opposed to the 4.9 kHz bandwidth of GASJT. Since random noise is random in both amplitude and phase doubling the measurement bandwidth doubles the measured power [Ref 99]. This requires that a 3 dB correction be made when the bandwidth is doubled and therefore the output of GASJT is precisely comparable to the output of the HP 8553B/8552B/141T swept frequency analysis system. Because the only difference between GASJT and AENOR is that GASJT averages spectra together while AENOR does not it is reasonable to conclude that AENOR would produce a power spectrum for an actual acoustic emission waveform which would be comparable to that produced by the analog system, provided that the problems of producing an accurate, repetitive version of the acoustic emission signal and establishing an accurate pulse desensitization factor for the HP 8553B system could be overcome.

The technology of acoustic emission was advanced by these programs for several reasons. First, they allow the use of digital signal processing for acoustic emission work with the assurance that the results are comparable with earlier analog results. Second, they provide a method for eliminating the effects of geometry changes, couplant variations and transducer aging on the experimental results. And third, they permit confidence limits to be calculated so that for the first time the effects of experimental errors on acoustic emission data may be evaluated.

CHAPTER 6

SIGNAL ANALYSIS RESEARCH

This chapter describes a series of experiments conducted using 4340 steel and 7039 aluminum to determine if different acoustic emission sources can be identified by their emitted signals. The results indicate that this goal can be achieved using the data acquisition methods and signal processing techniques presented.

6.1 Objective

The goal of this thesis was to extend the technology of acoustic emission by developing methods for discriminating between acoustic emission signals to make possible the identification of the failure processes which generated the acoustic emissions. Chapter 5 documented the construction of a unique acoustic emission instrument which advanced acoustic emission technology since it permitted for the first time the acquisition of broadband digital waveform recordings of acoustic emission signals. Also documented in Chapter 5 was the writing of computer programs which collectively advanced acoustic emission technology by allowing such broadband digital waveform recordings to be processed so as to eliminate the effects of various experiment dependent quantities while permitting a meaningful estimate to be made of the effects of experimental error. The purpose of this portion of the research program was to experimentally test the developed acoustic emission system and computer programs to determine if they did indeed provide the desired acoustic emission source discrimination capability.

Three experiments were performed to test the instrument and the programs. Two different materials, three different specimen configurations and two modes of failure were used during the experiments to completely check the ability of the developed techniques to eliminate the effects of experiment dependent quantities while still performing source discrimination. The conducting of only three experiments is justifiable because the large number of acoustic emission signals that were recorded (1164 in all) required a tremendous amount of processing (628 pairs of useful plots resulted from the experiments). Since these acoustic emission signals were generated by growth of cracks over many interatomic distances (the total crack length increase monitored during the experiments was 16 mm) a valid statistical sampling was made of the population of all possible acoustic emission signals from the specimens and therefore further experiments would be redundant. Also, other workers associated with the author on another project reported that their experiments with similar specimens produced similar acoustic emission waveforms [Ref 85]. Thus, the analysis performed in this thesis utilized acoustic emission signals which were typical of the materials monitored.

It will be shown that the techniques developed in Chapter 5 do permit an experimenter to discriminate between different acoustic emission source mechanisms on the basis of the received signals. This is particularly significant since it will be shown that such source discrimination can be achieved in specimens of engineering interest rather than specimens of strictly laboratory interest. A limitation of the developed techniques is that they do not discriminate on an individual signal by signal basis but rather work on a collection of signals from an entire experiment. However, since the experiments do firmly establish the feasibility of source discrimination in engineering specimens, it is felt that the developed signal processing techniques advance the technology of acoustic emission. More intricate and expensive signal processing methods can now be investigated with the confidence that identifiable source mechanism characteristics exist in acoustic emission signals.

6.2 Experimental Design

The objective of differentiating between different acoustic emission sources imposed numerous constraints on the experiments. First, faithful recording of the signals over the largest possible bandwidth was required in order to obtain the maximum data base from which to extract the signal characteristics. Second, specimens had to be designed to fail through a single mechanism to enable a positive identification of acoustic emission signals. Third, methods had to be developed to calibrate the specimen-couplant-transducer-recording system to insure that data obtained under different conditions would be comparable. And finally, methods of processing the data to characterize individual acoustic emission sources had to be developed.

The data recording instrumentation starts with the transducer since it is there that the electrical representations of the acoustic stress fields are developed. As was pointed out in Section 2.4 there are several types of transducers from which to choose. However, practical considerations such as ruggedness, immunity from noise and high sensitivity effectively limit the choice to piezoelectric transducers. Since reproducibility was also a consideration it was decided to utilize transducers that were built in quantity to obtain the advantages of mass production and hopefully limit response variability. Examination of the transducers of three acoustic emission companies including the Acoustic Emission Technology model FC500 and the Trodyne model 7536A led to the selection of the Dunegan/Endevco model S9201 based on its sensitivity, response bandwidth and availability.

The author's prior acoustic emission experience indicated that a typical acoustic emission signal from aluminum and steel impinging on the S9201 transducer would generate an amplitude ranging from 10 to 100 μV peak to peak into 50 ohms at the transducer output and would have a useful frequency range of 0.1 to 1.0 MHz. To condition such signals a high input impedance broad band preamplifier providing a gain of 100 was built. This consisted of an FET input stage, shown in Figure 6.1, feeding a Trodyne model 7529A preamplifier. This combination provided an input impedance of 1 megohm, a gain of 36 dB and a bandwidth of 10 kHz to 15 MHz at the 3 dB points. The importance of the high input

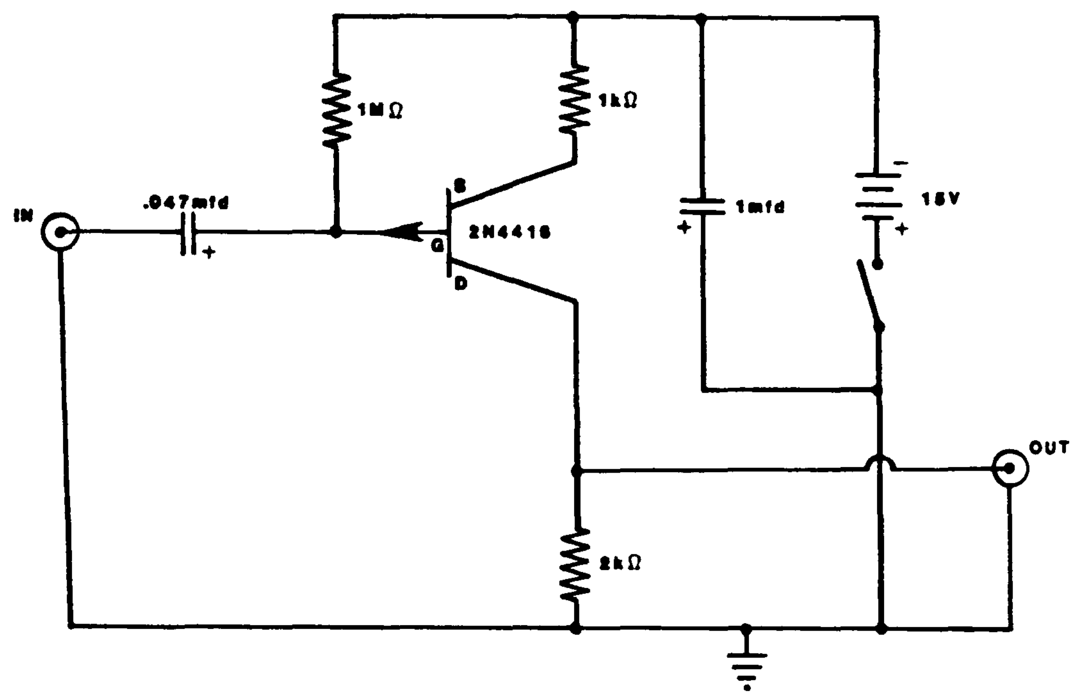

Figure 6.1. Field effect transistor impedance converter built for thesis research program.

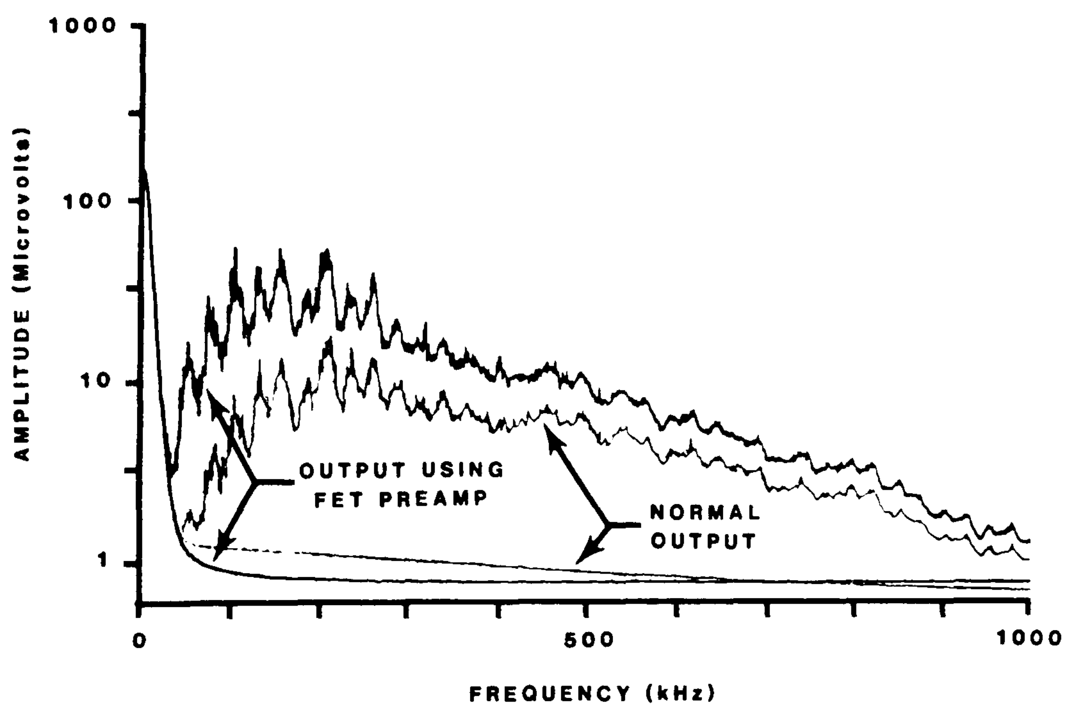

Figure 6.2. Gain increase achieved from use of circuit of Figure 6.1 (top curve) over normal operation (bottom curve).

impedance may be seen in Figure 6.2, where a simultaneous increase in the signal to noise ratio as well as a higher voltage output is realized by going from 10 kilohm to 1 megohm input impedance. Another important aspect of the preamplifier was that it was completely shielded and battery operated. This modification was made to eliminate pickup of extraneous signals such as radio stations, radar, lights, etc.

Recording of the amplified acoustic emissions was performed using the acoustic emission system described in Section 5.1. The equipment directly involved in the recording process consisted of a Biomation Model 8100 analog to digital converter, a specially designed interface unit and a Kennedy Model 9000 digital magnetic tape drive. Digital recording of the signal offered significant advantages over analog recording in that daily calibration was unnecessary, long term signal degradation did not occur after a waveform was recorded on the tape, a better dynamic range was available, triggering was available to record signals during long quiet periods, and most importantly, easy and versatile signal processing could be performed via a digital computer. Another useful feature of digital recording was the pretrigger capability it offered which effectively allowed signal recording to start before the trigger occurred, thus preserving the all important leading edge of the acoustic emission. Some disadvantages were that quantization was introduced into the recordings and continuous recording of the signal was impossible. In the system used, quantization was 8 bits (1 part in 256), sampling rates could vary from 0.01 μS to 10 μS in a 1-2-5 sequence and 2048 consecutive points could be recorded with a fixed dead time of 140 mS. A sampling rate of 0.1 μS was found to be

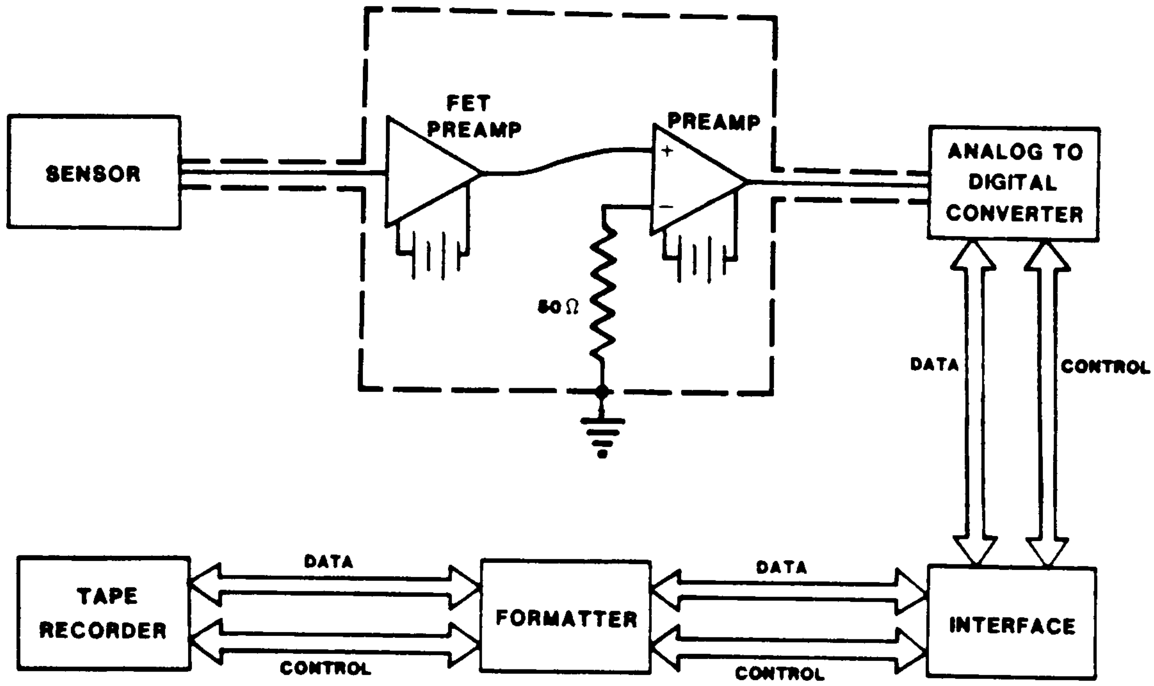

Figure 6.3. Block diagram of the digital recording section of the acoustic emission system built for thesis research program.

TABLE 6.1 GAS JET OPERATING SPECIFICATIONS [Ref 83]

Parameter	Value of Parameter
Type of Gas	Helium
Pressure	144.8 $kN/m^2 \pm 6.9$ kN/m^2
Jet	As supplied by RMC, Canada - glass capillary of approximately 0.8 mm diameter by 60 mm long.
Stand Off	3.5 mm $\pm$ 0.1 mm
Bore Angle	$0° \pm 2°$ with respect to surface normal
Miscellaneous	Install filter in gas delivery line (such as nylon stocking). Clamp jet assembly only on plastic inlet section of capillary. Measure pressure at jet inlet (use of flowmeter recommended to detect perturbations in delivery).

the most useful since it permitted recording most of the envelope of a typical acoustic emission signal emitted from aluminum and steel while providing a Nyquist frequency of 5 MHz, thus 205 μS of acoustic emission data was recorded at least every 140 mS. For clarity Figure 6.3 shows a block diagram of the digital recording section of the acoustic emission system.

The specimens employed in the acoustic emission source identification experiments are depicted in Figure 6.4. The double cantilever beam design was chosen for stress corrosion cracking specimens since it was a simple geometry that featured self loading. These attributes helped to reduce echoes within the sample, and eliminated the possibility that machine noise would contaminate the acoustic emission signals. The compact tension design was chosen for tensile overload specimens because it is well defined from a fracture mechanics point of view, thus insuring a known stress field and hopefully, therefore, a reproducible failure. Two materials, 4340 steel (Fe-0.4 C-1.8 Ni-0.8 Cr-0.7 Mn-0.3 Si-0.2 Mo, weight percentages) and 7039 aluminum (Al-4.0 Zn-2.8 Mg-0.4 Fe-0.3 Si-0.25 Mn-0.2 Cr-0.1 Cu-0.1 Ti, weight percentages) were selected. This was done to provide some insights into the acoustic emission behavior of different materials failing through different mechanisms. Prior to testing, the 4340 steel was quenched and tempered to produce a Rockwell "C" hardness of 49, while the 7039 aluminum was solution treated, quenched and aged to produce a Rockwell "B" hardness of 78.

Calibration of the specimen-couplant-transducer-recording system

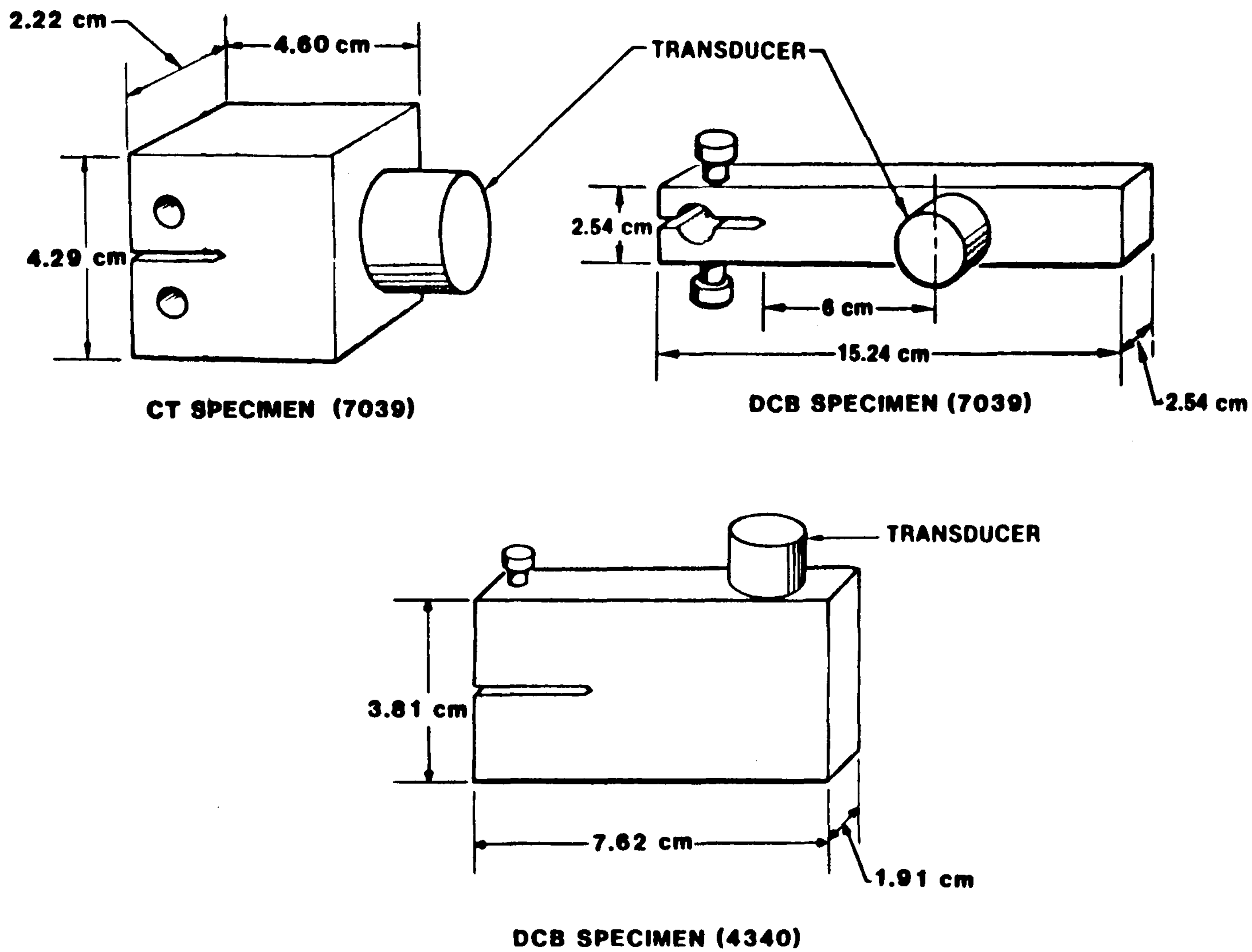

Figure 6.4. Schematic diagram of specimens used in thesis research showing transducer locations employed.

was carried out using the helium gas jet technique. Selection of this calibration procedure over some of the others mentioned in Section 3.2 was made because it was easier to implement in a reproducible manner and because it yielded signal amplitudes which were more typical of acoustic emissions. To insure a reproducible calibration signal the gas jet operating parameter values listed in Table 6.1 were used. These values were reported by Bentley and Green [Ref 83] as being the most optimal for helium gas jet system calibration work. The reference gas jet spectrum was then developed by making a number of recordings of the time domain signals, calculating the power spectral density for each signal and then averaging all of these power spectra. It was found that 100 time domain signals averaged together would be sufficient to yield a reference power spectrum with an error of plus or minus 0.1 dB from 0.1 to 1.0 MHz. It should be reiterated that the purpose of the helium gas jet system calibration is to eliminate the variability between experiments caused by geometry changes, couplant variations and transducer aging. As will be seen, if these variations were not removed from the data they would overwhelm the spectral changes caused by acoustic emission source differences and therefore source discrimination could not be done.

6.3 Results

The goal of these experiments was to determine if differences could be discerned between acoustic emissions emanating from different materials undergoing different failure processes. Thus, it was

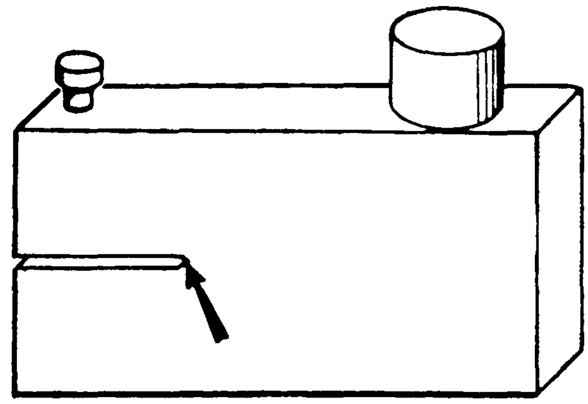

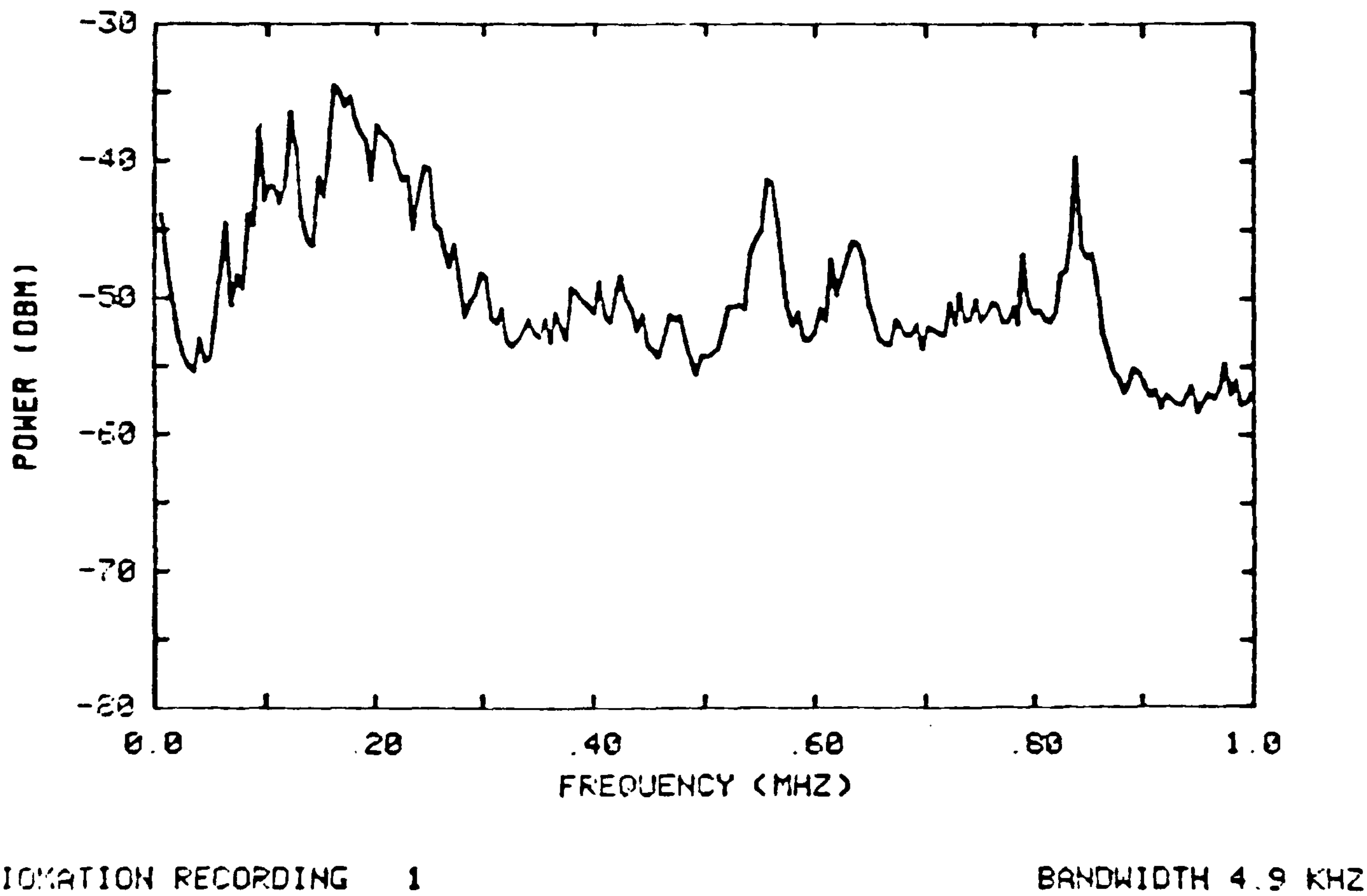

Figure 6.5. Point of application of gas jet and resulting power spectrum for 4340 DCB specimen.

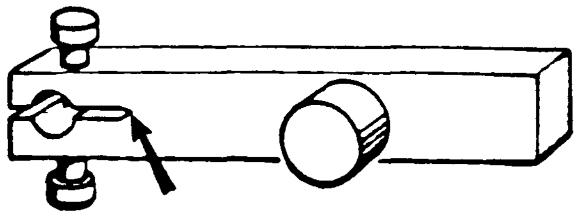

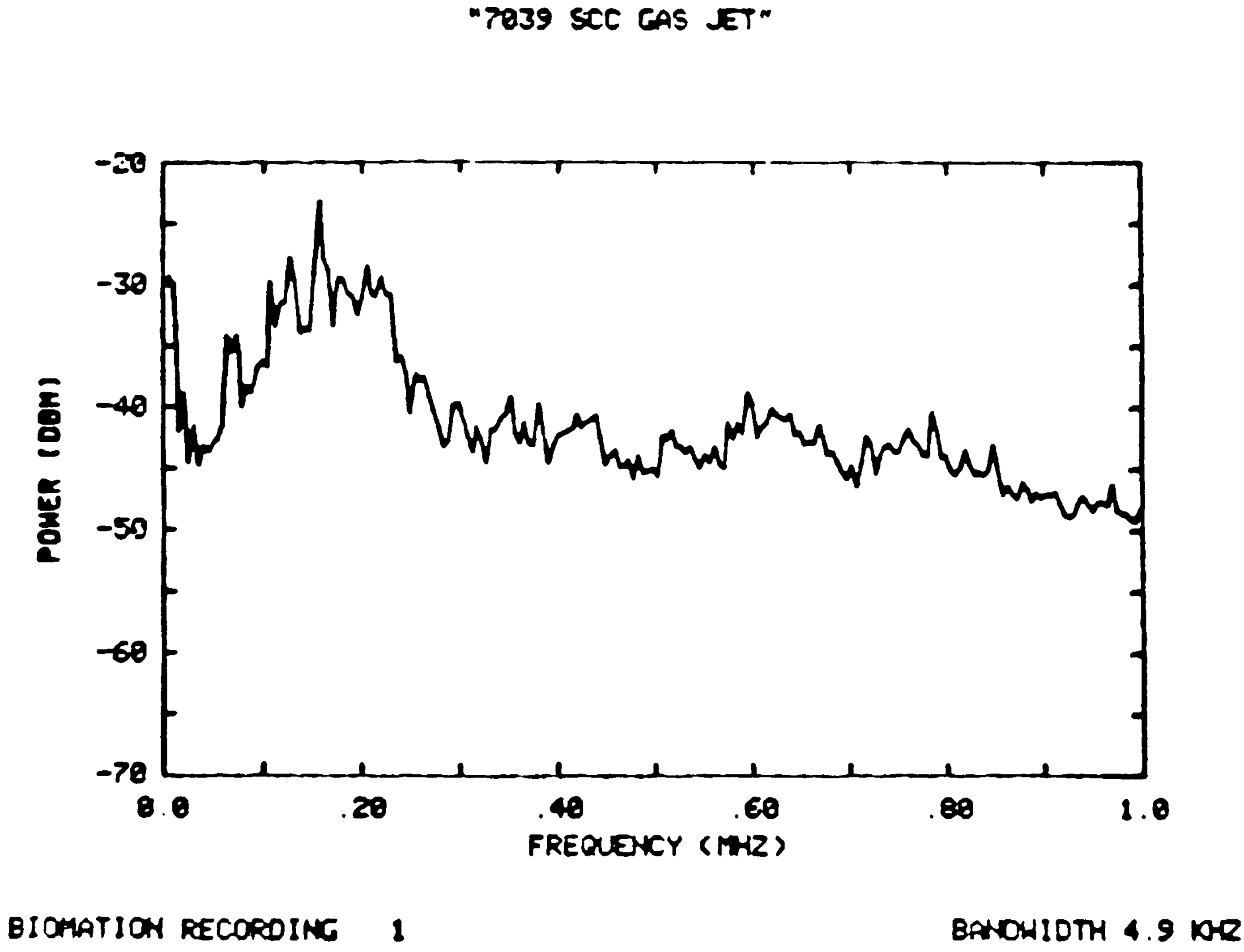

Figure 6.6. Point of application of gas jet and resulting power spectrum for 7039 DCB specimen.

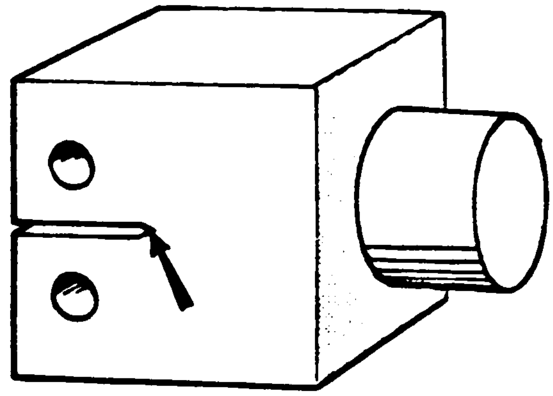

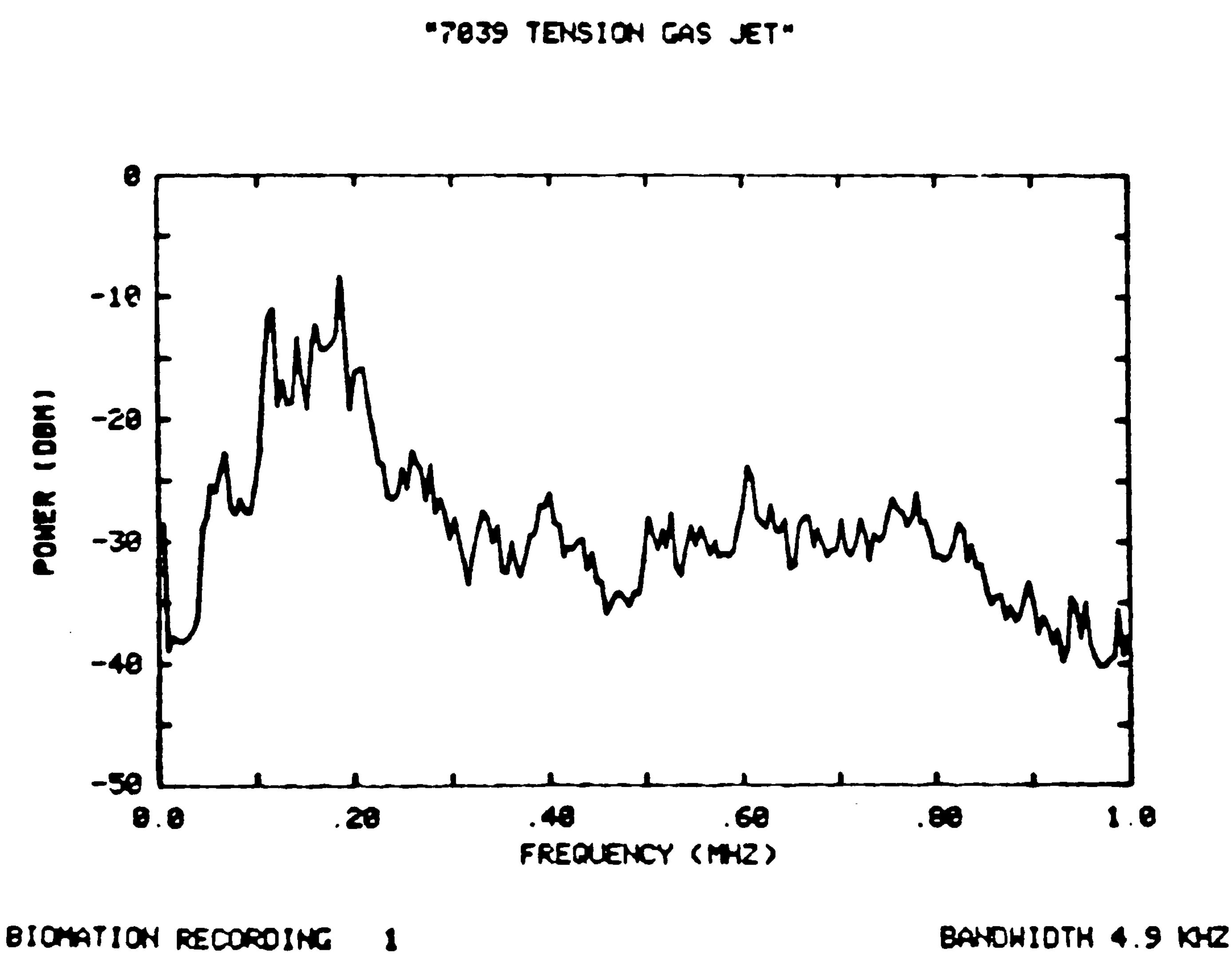

Figure 6.7. Point of application of gas jet and resulting power spectrum for 7039 CT specimen.

imperative before any experiment started to obtain a calibration signal to provide a basis for comparison. This was accomplished as described above, and Figures 6.5, 6.6 and 6.7 show the resultant reference power spectra and the point of stimulation for each experimental situation. The choice of the stimulation point was made to provide a reference signal in the vicinity of the expected acoustic emissions. In such small specimens no significant variation in the reference power spectrum resulted when the stimulation point was moved. This would not generally be the case in a larger specimen. Examination of the spectra in Figures 6.5, 6.6 and 6.7 reveal that all three are different. This is to be expected since three drastically different geometries are involved because it has been found by McBride and Hutchison [Ref 100] that geometry is the major source of changes in the reference spectra.

Having obtained a reference spectrum for each specimen mechanical testing commenced starting with the 4340 steel DCB specimen. A razor blade was used to create a fresh surface at the root of the notch, then the corroding agent (a saturated solution of sodium chloride) was added and finally the loading screw was tightened one quarter of a turn. During the next 70 minutes a crack formed and propagated approximately 8 mm into the steel while a total of 553 acoustic emission signals were recorded. The trigger level for recording an acoustic emission signal from this material was 32 μV referred to the transducer.

Of the 553 signals recorded only 382 were found to be useful. This was determined by visual inspection of the data set. Visual inspection is of course not desirable for routine source identification work. For

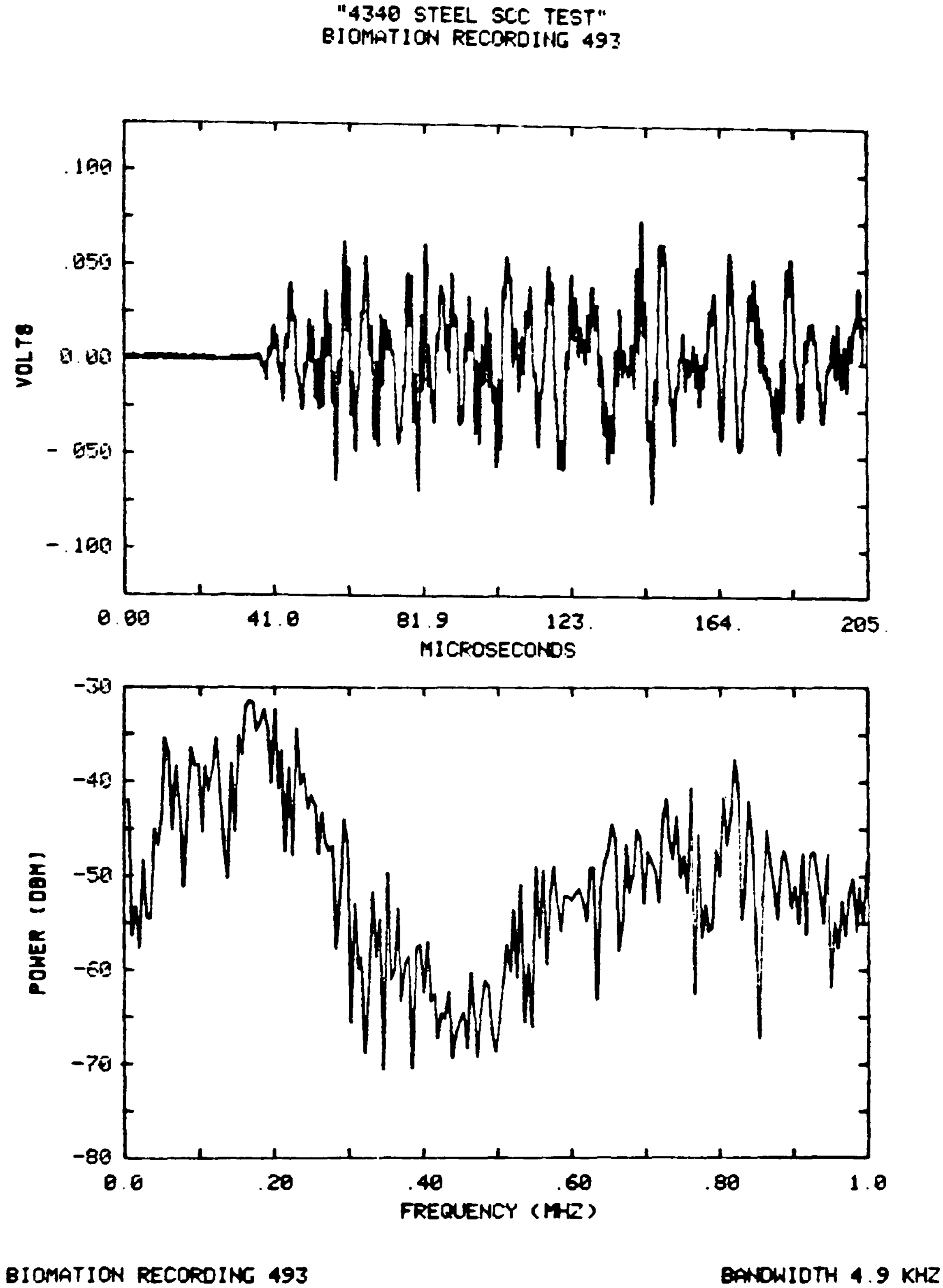

Figure 6.8. Time domain waveform and corresponding power spectrum obtained from 4340 steel stress corrosion cracking.

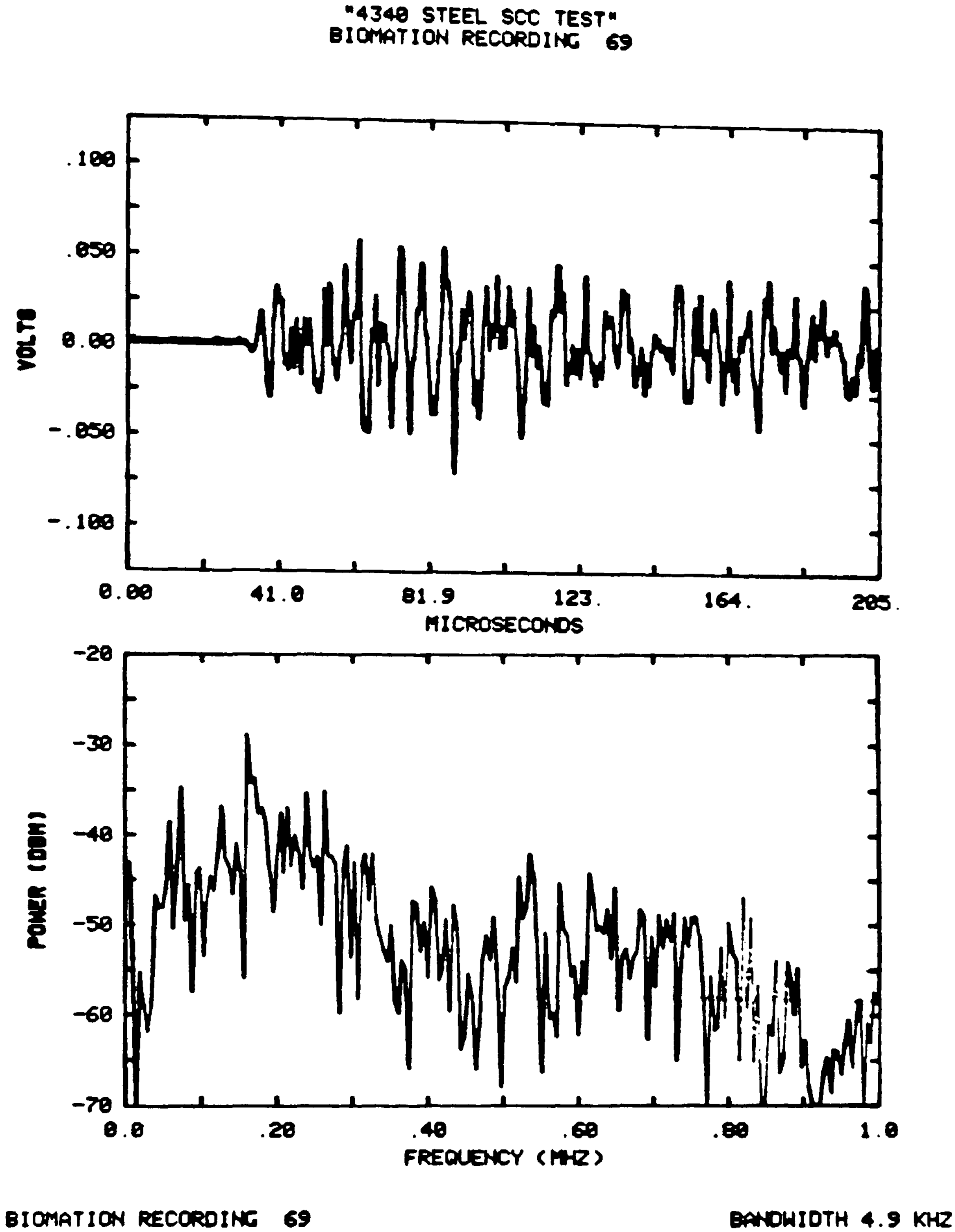

Figure 6.9. Time domain waveform and corresponding power spectrum obtained from 4340 steel stress corrosion cracking.

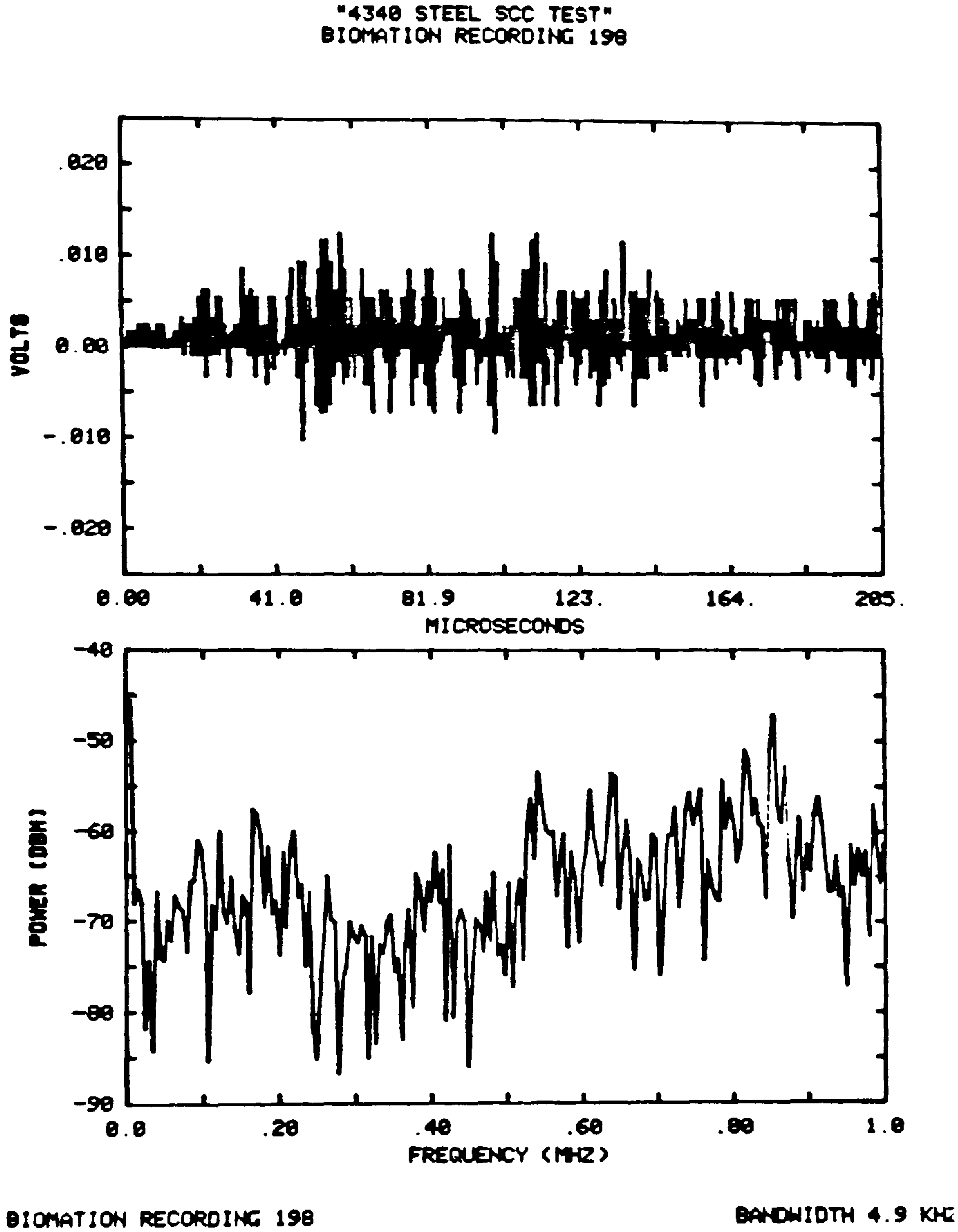

Figure 6.10. Time domain waveform and corresponding power spectrum obtained from 4340 steel stress corrosion cracking.

this reason a computer program was written to automatically select signals for further processing. However, it proved too difficult to make the program selective enough to keep all of the good signals while rejecting all of the bad ones. Thus, only visual selection of good signals was used for the experiments in this thesis. Signals which were clipped or whose envelopes did not conform to the expected appearance of an acoustic emission signal's envelope (ie, initial quiet period followed by a short steep rise to a maximum value and an exponential decay after the peak) were rejected. Examples of good signals are shown in Figure 6.8, 6.9 and 6.10 along with their frequency transforms. It can be seen that these signals are quite distinct from one another.

A similar experiment was conducted on the 7039 aluminum DCB specimen, except steps were taken to calculate the stress intensity factor, K, at the start of the data gathering process. This was accomplished by measuring the unloaded height of the specimen perpendicular to the plane of the crack (2h), obtaining the crack opening displacement (d) after turning the screw to produce pop-in, obtaining the crack length (a) by measuring from the center of the loading screws to the tip of the crack along the plane of the crack and then calculating K using an equation due to Kanninen [Ref 101]:

$$K = \frac{\sqrt{3}}{2} \frac{E h^{3/2} d}{a^2} \left[\frac{1 + 0.64(h/a)}{1 + 1.92(h/a) + 1.22(h/a)^2 + 0.39(h/a)^3}\right] \qquad (6.1)$$

where E is the elastic constant.

Once again a razor blade was used to create a fresh surface at the

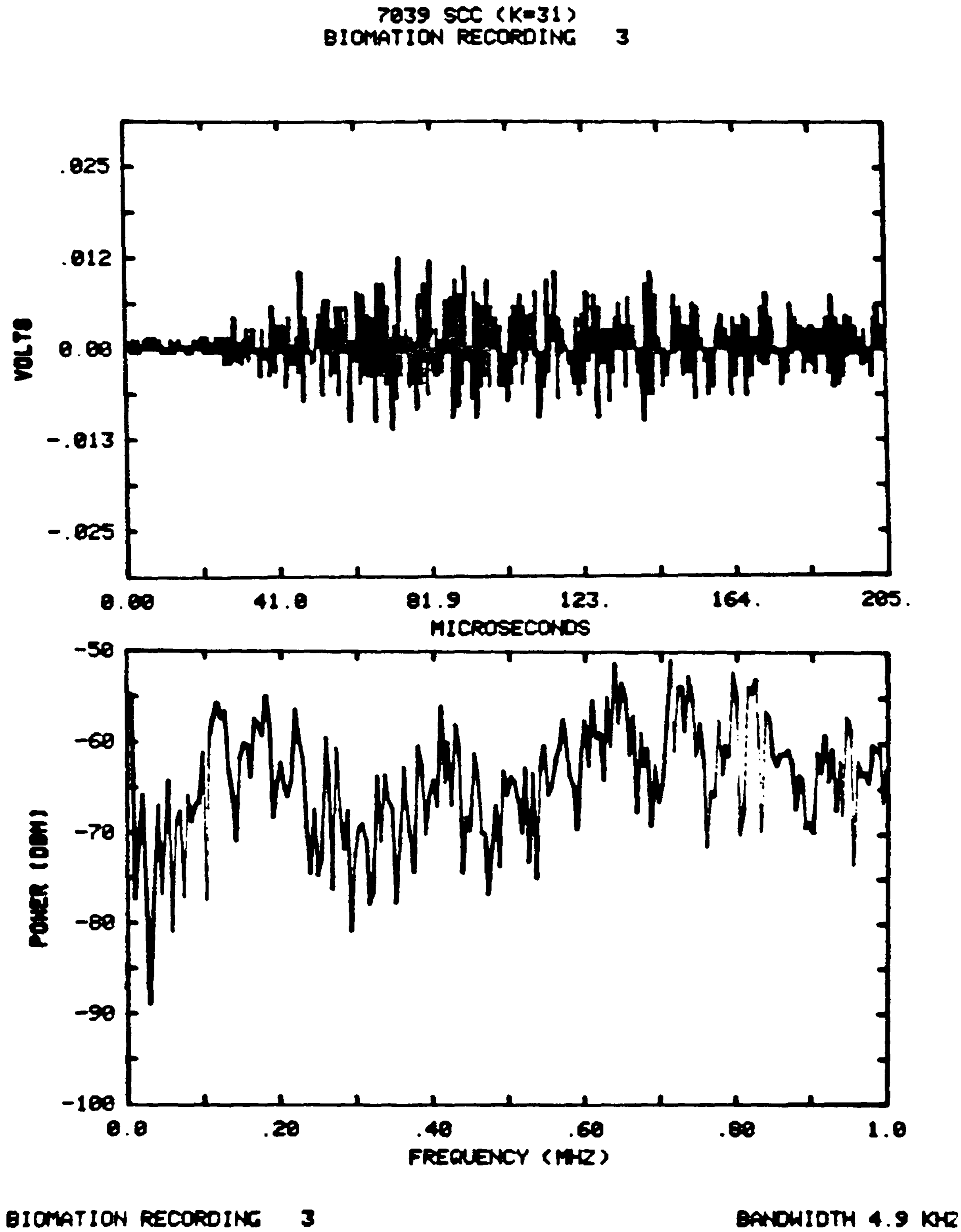

Figure 6.11. Time domain waveform and corresponding power spectrum obtained from 7039 aluminum stress corrosion cracking.

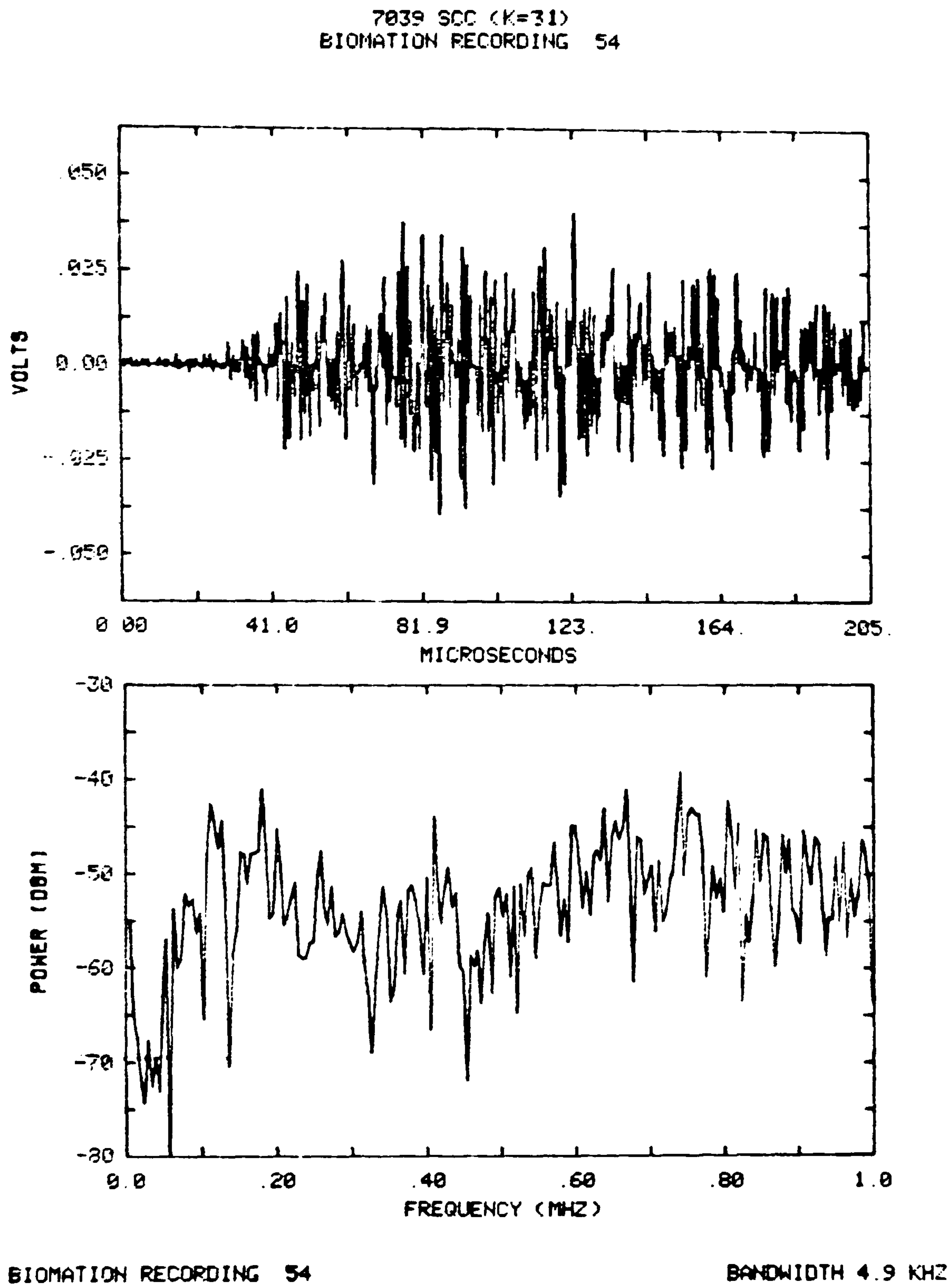

Figure 6.12. Time domain waveform and corresponding power spectrum obtained from 7039 aluminum stress corrosion cracking.

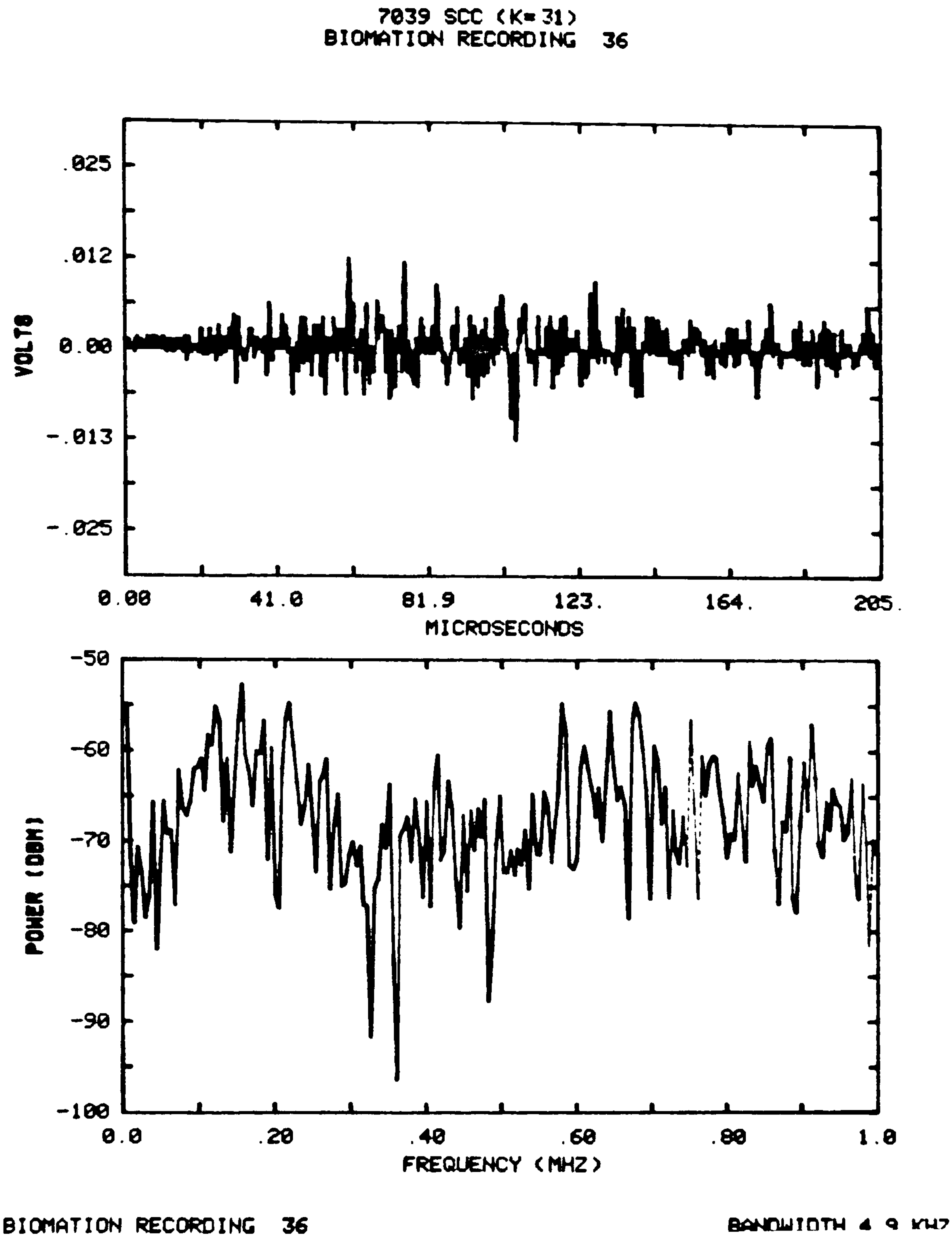

Figure 6.13. Time domain waveform and corresponding power spectrum obtained from 7039 aluminum stress corrosion cracking.

root of the notch and then the saturated solution of sodium chloride was added. With the screw tightened to produce pop-in K was found to be 31 $MPa\sqrt{m}$. Sixty acoustic emission signals were recorded over a 55 minute period while the crack grew approximately 2 mm. The trigger level for recording an acoustic emission signal from this material was 48 μV referred to the transducer. Visual inspection revealed that 57 signals were useful. Examples of these signals in both the time and frequency domains are shown in Figures 6.11, 6.12 and 6.13.

Repetition of this experiment with a K level of 22 $MPa\sqrt{m}$ resulted in a data set of 67 useful acoustic emission signals gathered over a 90 minute period while the crack extended another 2 mm. The trigger level remained the same, 48 μV referred to the transducer. These signals appeared very similar to those shown in in Figures 6.11, 6.12 and 6.13. The only distinguishing difference between the data gathered from the 7039 DCB specimen at a K value of 31 and a K value of 22 was that the amplitudes of the signals taken at a K value of 22 were generally smaller than those taken at a K value of 31.

To obtain data on a different failure mechanism a 7039 aluminum CT specimen having a 3.42 mm long pre-existing fatigue crack specimen was mounted in an Instron machine using specially designed clevises. Grip noise was minimized by using felt washers to separate the interior faces of the clevises from the specimen and the pins were liberally greased to prevent fretting. The cross-head speed was set at 83.8 microns per minute to allow ample time to record each acoustic emission and a clip-on gauge was used to record the crack opening displacement as a

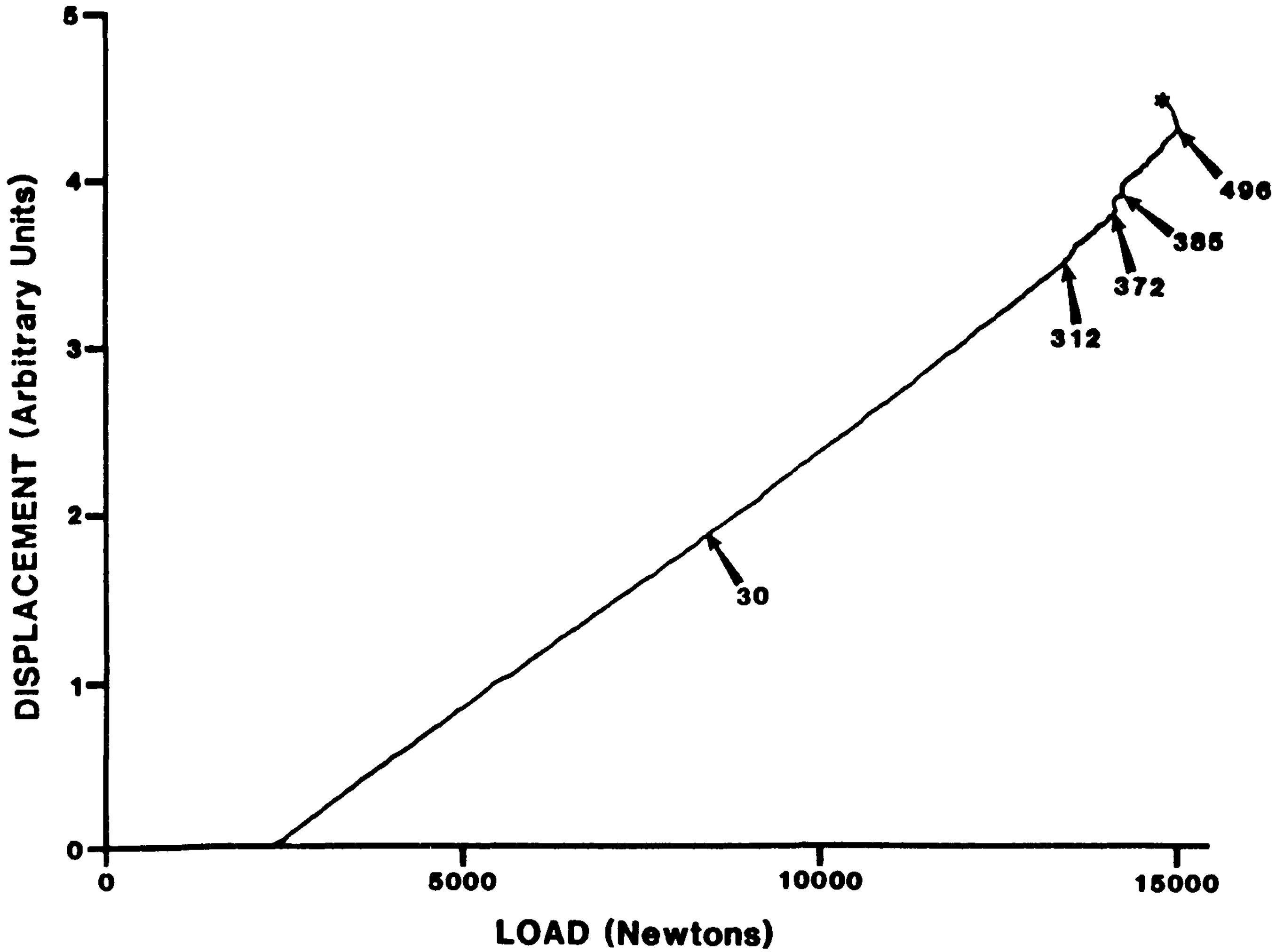

Figure 6.14. Displacement of 7039 CT specimen as a function of load showing waveform numbers of acoustic emissions recorded during the test.

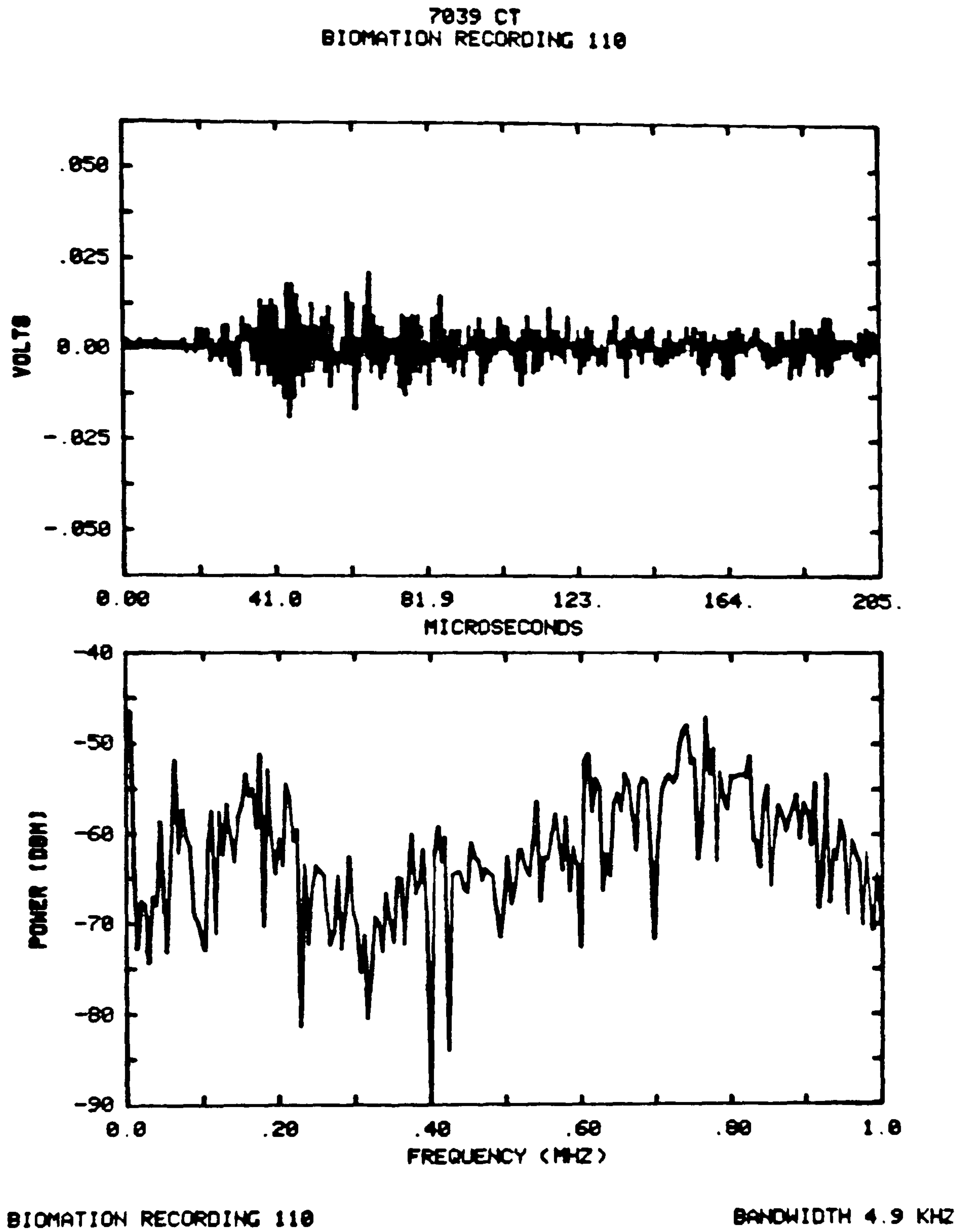

Figure 6.15. Time domain waveform and corresponding power spectrum obtained from 7039 aluminum tensile loading.

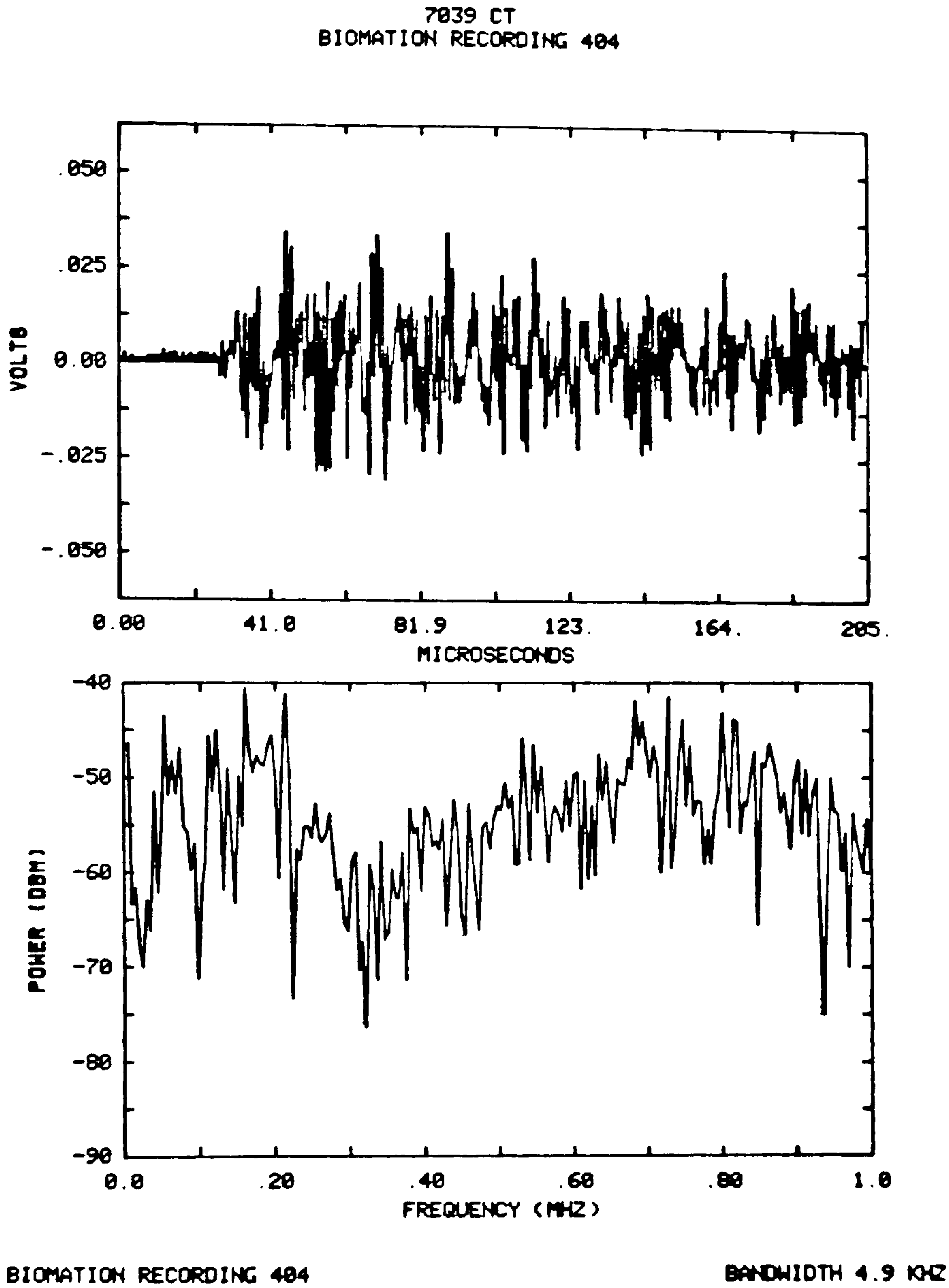

Figure 6.16. Time domain waveform and corresponding power spectrum obtained from 7039 aluminum tensile loading.

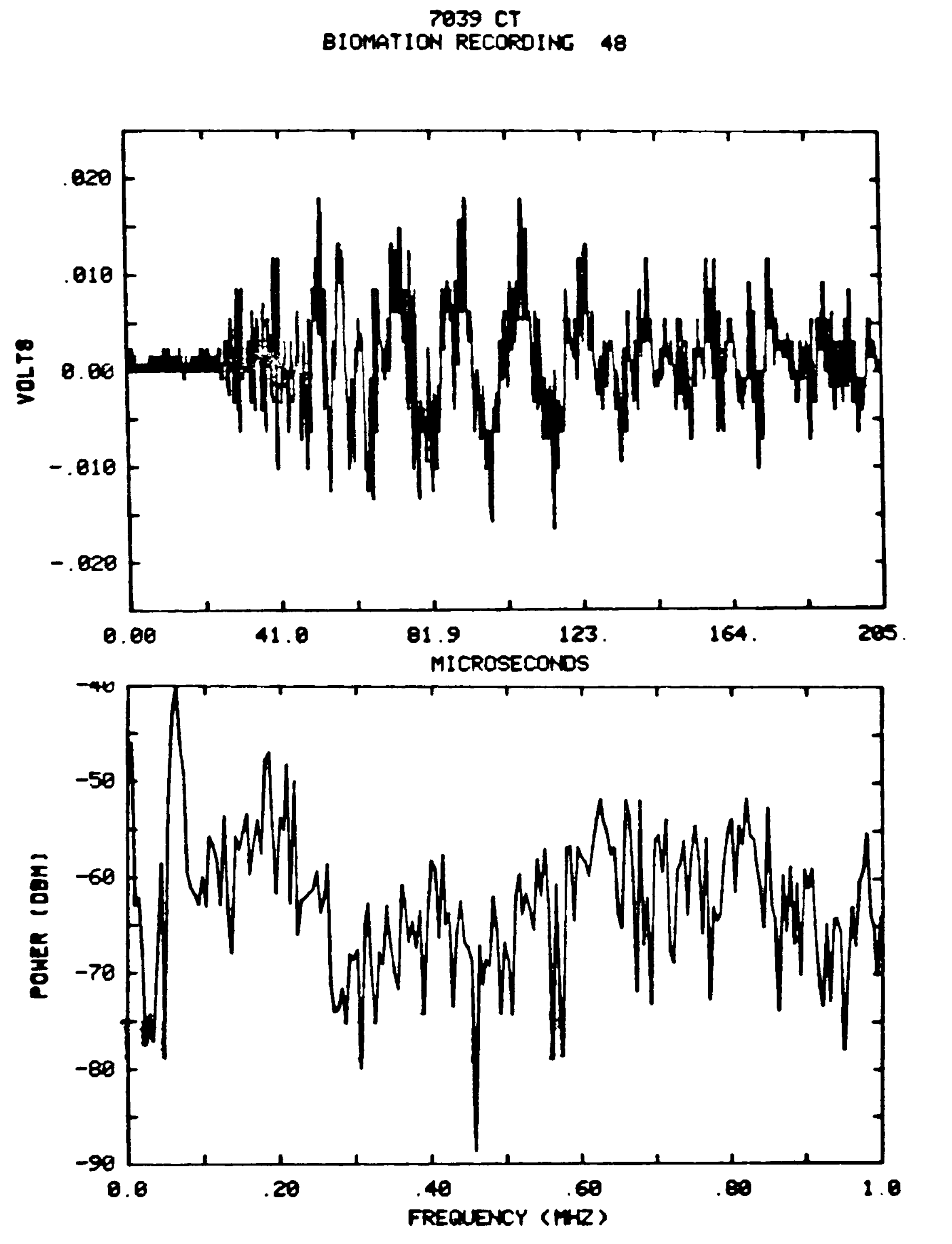

Figure 6.17. Time domain waveform and corresponding power spectrum obtained from 7039 aluminum tensile loading.

function of tensile load. The output of the gauge, shown in Figure 6.14, provides an easy means of detecting pop-in and final failure. Annotation of the graph with the acoustic emission waveform numbers provides evidence that the acoustic emission came from tensile overload failure and not from crack interface rubbing during unloading. A total of 496 acoustic emission signals were recorded during the test, of which only 189 were found via visual inspection to be useful. The trigger level for recording an acoustic emission waveform during the test was 32 μV referred to the transducer. Examples of good signals in both the time and frequency domains are shown in Figures 6.15, 6.16 and 6.17.

6.4 Data Analysis

Analysis of the acoustic emission signals recorded during the three experiments outlined in Section 6.3 was accomplished using the computer programs described in Section 5.2 and commenced with the examination of the time domain representation of each signal using program PLTME. The envelope of each signal was required to be free of clipping and to conform to the general shape of an initial quiet period followed by a short steep rise to a maximum value with an exponential decay after the peak. Acoustic emission signals from a particular experiment which met these two criteria had their waveform numbers saved in a disc file whose name was mnemonically related to the root experiment. Each file was then read by program AENOR, which created a frequency spectral data base for each experiment. Each data base was processed in turn using program PLFFT to produce a permanent record of the power spectrum of each accepted acoustic emission signal.

The operations described in the preceding paragraph produced 628 pairs of plots, 18 of which appear in Section 6.3. To analyze this vast amount of data it was decided to first produce bar charts for each experiment showing the relative occurrence of signals separated according to their raw (not normalized by use of the helium gas jet spectra for the particular test) spectral shape. The distribution classes were based on the relative heights of the two predominant spectral peaks and the presence or absence of either of the two peaks. Thus a continuous distribution of spectral shapes was transformed into the six categories shown in Figure 6.18. Figures 6.18, 6.19 and 6.20 depict the result of this classification. Clearly, each experiment produced a dominant spectral shape (see Figures 6.8, 6.11 and 6.15 for examples of these), a secondary spectral shape (see Figures 6.9, 6.12 and 6.16), as well as miscellaneous other spectral shapes (see Figures 6.10, 6.13 and 6.17). A general observation about all these spectral examples is that they have a bimodal appearance. This is no doubt due to the transducer response characteristics, a statement which is supported by Figure 3.6a which shows the magnitude velocity response spectrum produced by a transducer similar to that used in the present experiments when it was excited by a flat frequency input.

There are several possible reasons for the appearance of multiple spectral shapes during the course of a single experiment where only one basic fracture mechanism was operating. Crack length, since it changes the geometry of the specimen and thereby its normal resonant modes,

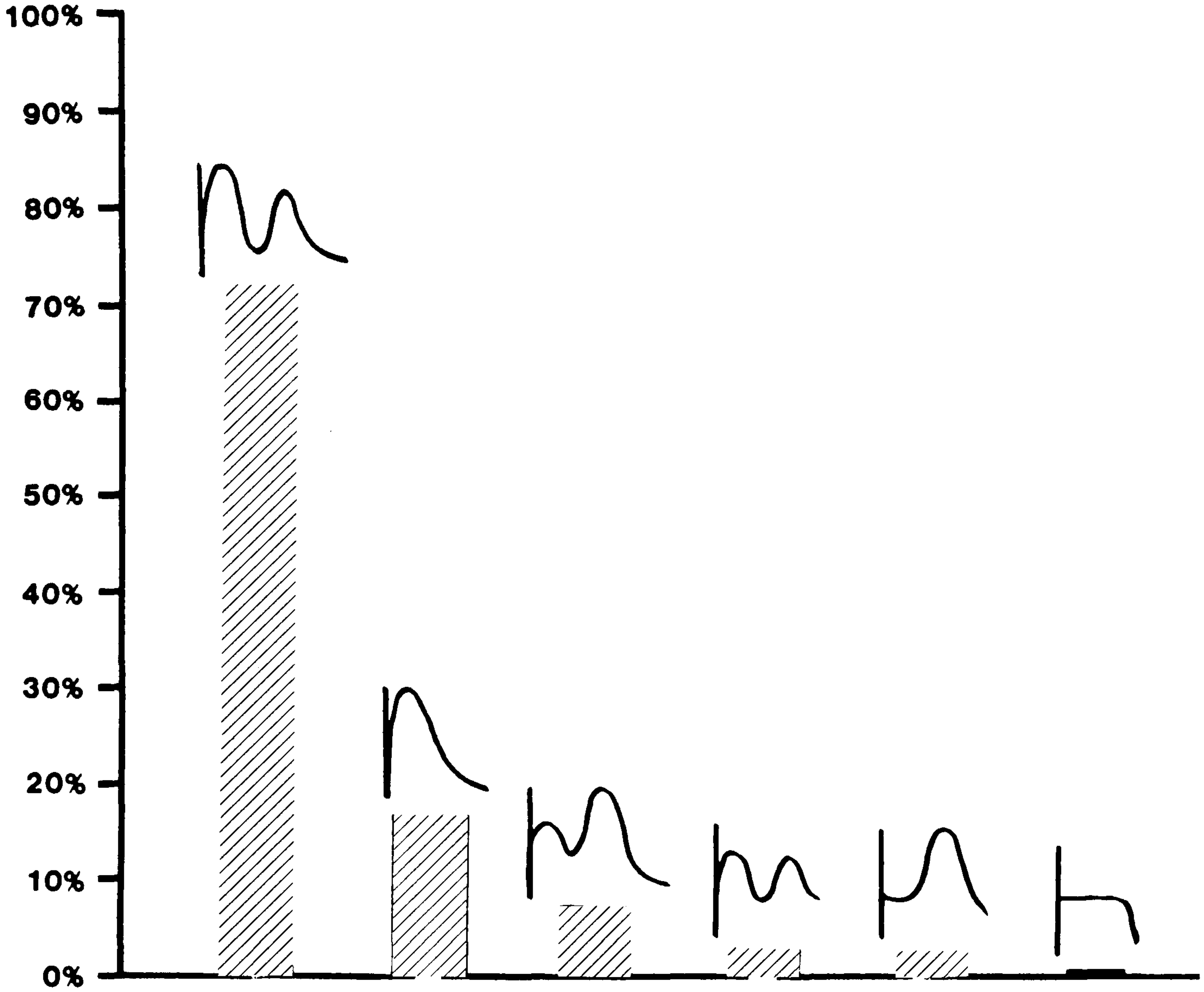

Figure 6.18. Classification of acoustic emission signals from 4340 DCB specimen according to their raw spectral shapes.

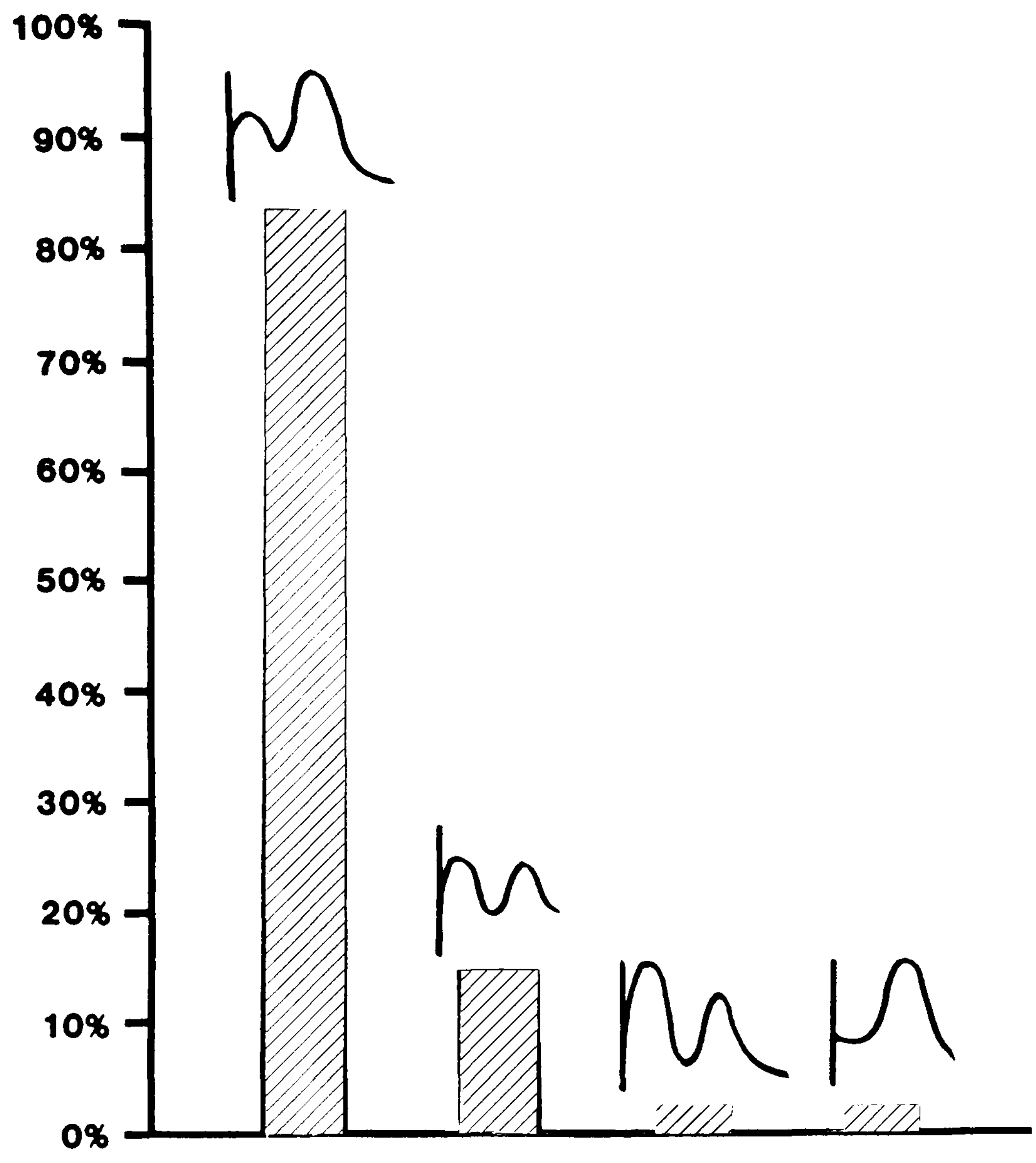

Figure 6.19. Classification of acoustic emission signals from 7039 DCB specimen according to their raw spectral shapes.

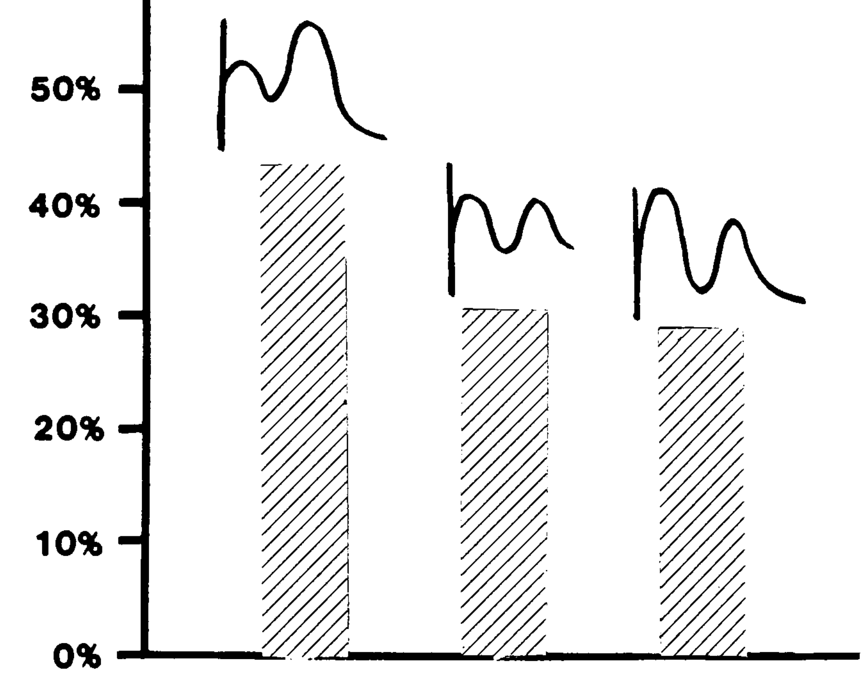

Figure 6.20. Classification of acoustic emission signals from 7039 CT specimen according to their raw spectral shapes.

offers an obvious explanation for the generation of different spectral shapes. However, a careful examination of the distribution of spectral types with test time revealed that no correlation could be made between spectral shape and crack length.

Another possibility for the spectral shape change mechanism is that waveform interference occurred at the transducer location, either because of multiple propagation paths from a single source or because of simultaneously operating sources. Destructive interference of shear waves traveling at 3 kilometers per second would occur at 750 kHz if a path difference which was an integral multiple of 2 mm existed, while at 250 kHz a basic path difference of 6 mm would be required. Constructive interference, on the other hand, would require a 4 mm basic path difference at 750 kHz, and 12 mm at 250 kHz. While these path differences are physically realizable in the specimens used, interference would not be capable of removing broad spectral peaks such as is documented in the changes between Figures 6.8 and 6.9, and Figures 6.8 and 6.10, but would instead create narrow peaks and valleys.

Still another explanation for the appearance of multiple spectral shapes during the course of an experiment where only one fracture mode was operative is that there may have been multiple acoustic emission source generation mechanisms. However, as was shown in Section 2.1 there are only two sources for acoustic emission when cracking occurs, namely, brittle particle fracture and discontinuous crack movement. The 4340 steel tested here contained no brittle second phase particles, only carbides having diameters of less than 0.1 microns. It is known that carbides of this size do not generate detectable acoustic emission [Ref 102]. Since there were six different spectral classes observed during the experiment with this material, the hypothesis of multiple acoustic emission source mechanisms operating during one test must be incorrect.

The most likely explanation for the occurrence of multiple spectral shapes during the course of one experiment is that there was a variation in the speed of crack advancement or there was a variation in the amount of cracked area, or both. For example, if a constant crack advance rate of 100 mm per second were assumed, then a change in the predominant frequency of the acoustic emission waveform from 250 kHz to 750 kHz would occur if the diameter of the cracked area varied from 0.4 mm to 0.1 mm. A similar frequency shift would occur if a constant cracked area of 0.2 mm were assumed and the crack advance rate changed from 50 meters per second to 150 meters per second. The reason that this mechanism is the most plausible explanation for the existence of multiple spectral shapes is because variations in crack area and crack advance rates have been found to exist by Wadley and Scruby [Ref 103] and because the predominant frequency change in the acoustic emission waveform which would result would excite the two broad resonances in the detection transducer to differing degrees, causing an energy loss or gain over a wide frequency range such as actually occurred in Figures 6.8, 6.9 and 6.10

Because the spectral shape variations during the course of each experiment do not result from the operation of different acoustic emission sources but rather arise because of the geometry or the rate of

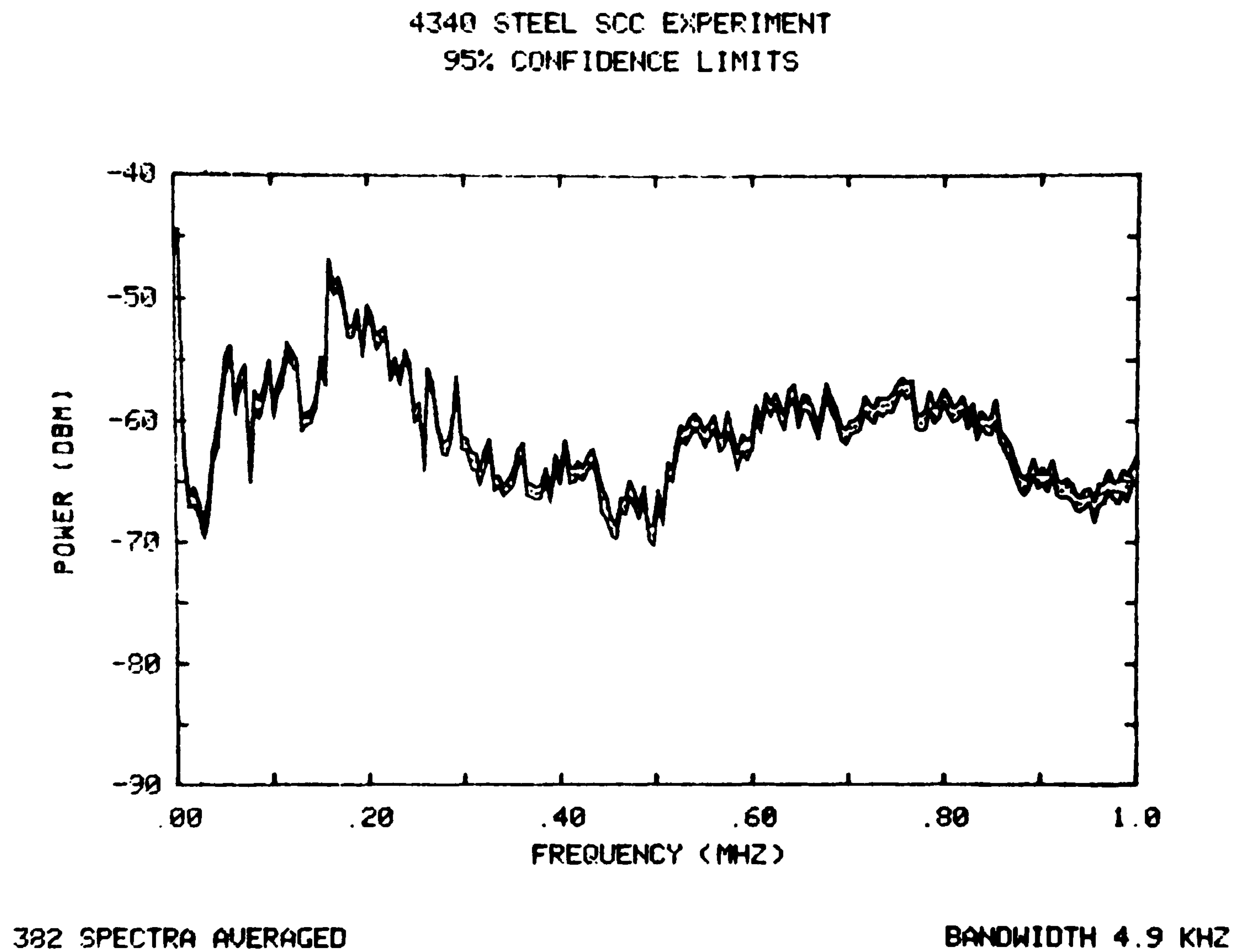

Figure 6.21. Average power spectrum for acoustic emissions emitted from 4340 steel undergoing stress corrosion cracking showing 95% confidence limits. There is no correction for system variables.

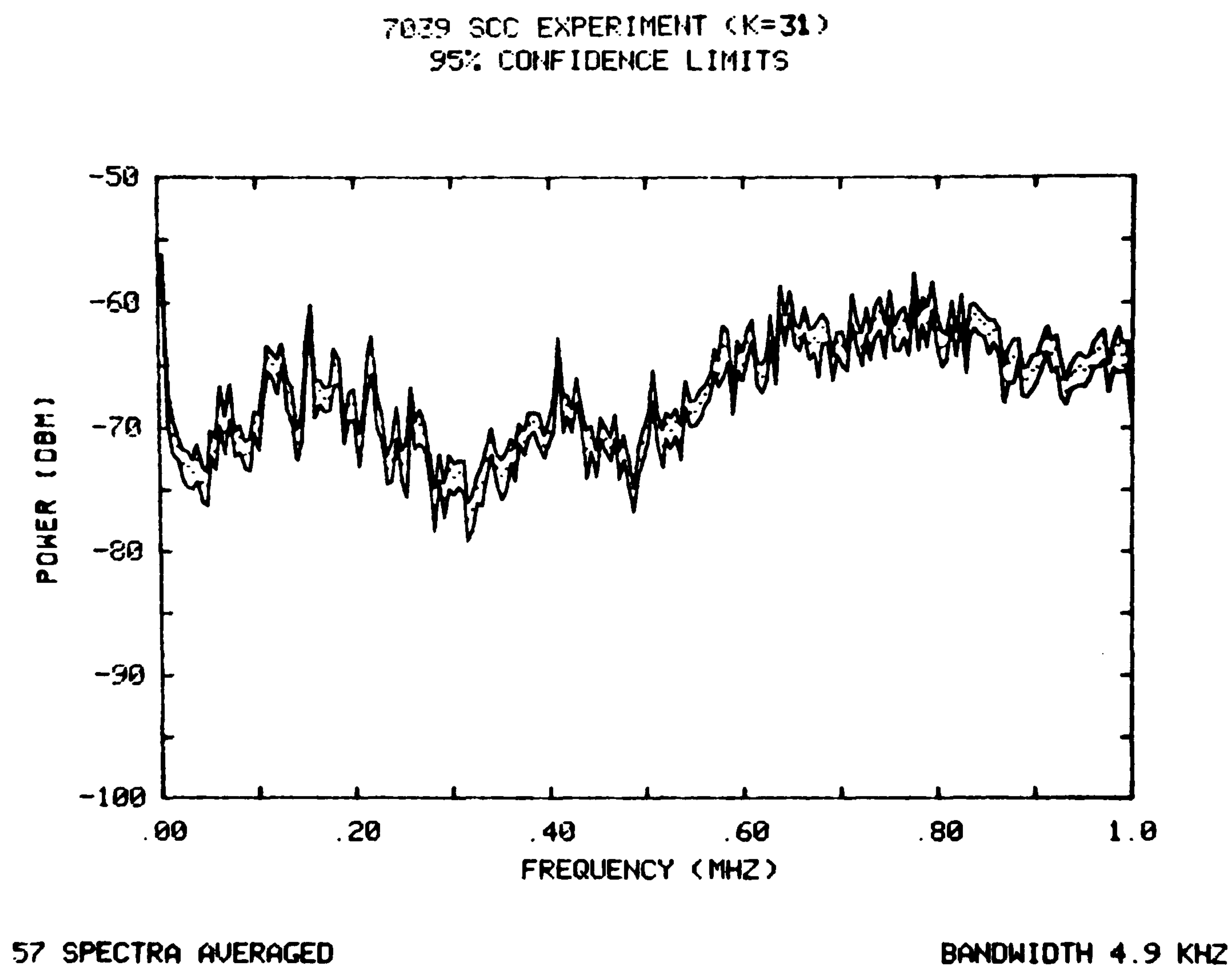

Figure 6.22. Average power spectrum for acoustic emissions emitted from 7039 aluminum undergoing stress corrosion cracking showing 95% confidence limits. There is no correction for system variables.

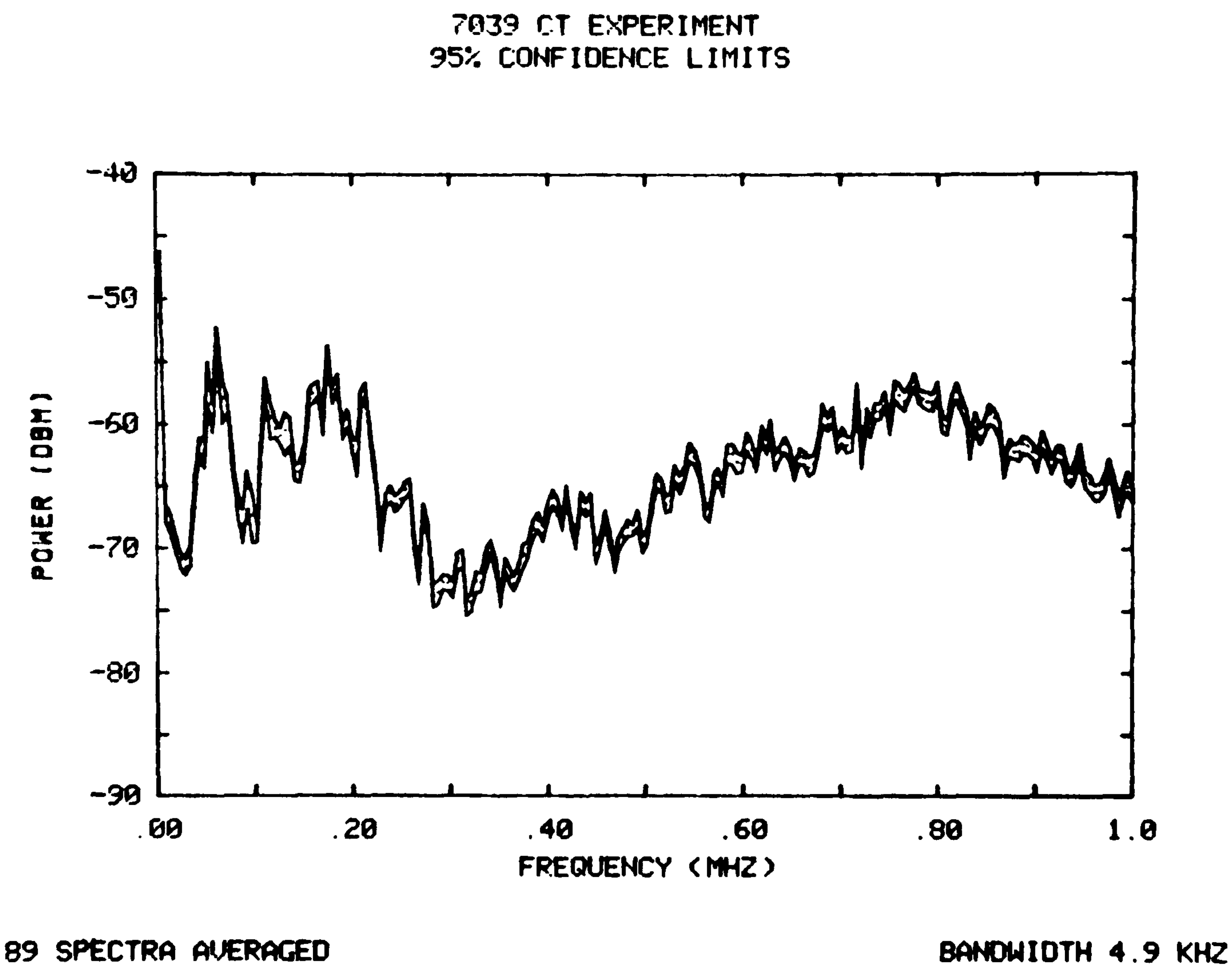

Figure 6.23. Average power spectrum for acoustic emissions emitted from 7039 aluminum undergoing tensile loading showing 95% confidence limits. There is no correction for system variables.

operation of a particular emitter, it was decided that averaging the power spectra would produce a valid spectral description of the failure of each specimen. Program AECNF was used for this purpose; in operation it averaged the power spectra in a particular experiment's data base after first normalizing each spectrum to unity energy. Confidence limits were then calculated for each frequency using the "t" statistic. The results for the three experiments are shown in Figures 6.21, 6.22 and 6.23. Comparison of these averages with the predominant spectral types of each corresponding experiment shown in Figures 6.8, 6.11 and 6.15, respectively, show that the averaging process did indeed produce a faithful summary spectrum for an entire test.

To allow a direct comparison of the information in Figures 6.21, 6.22 and 6.23, it was necessary to deconvolve them with their respective gas jets shown in Figures 6.5, 6.6 and 6.7. The results of these deconvolutions are shown in Figures 6.24, 6.25 and 6.26. Comparison of the deconvolved spectra reveals that a substantial difference exists between the acoustic emission output from steel undergoing stress corrosion cracking and the acoustic emission from aluminum undergoing either stress corrosion cracking or tensile overloading.

The inconsequential differences between the deconvolved spectral shapes for the aluminum samples was surprising, especially in view of the gross overall appearance differences which existed between the fracture surfaces of the 7039 SCC specimen and the 7039 CT specimen (see Figure 6.27). Note that the stress corrosion cracking specimen has the large smooth plates indicative of an intergranular fracture, while the

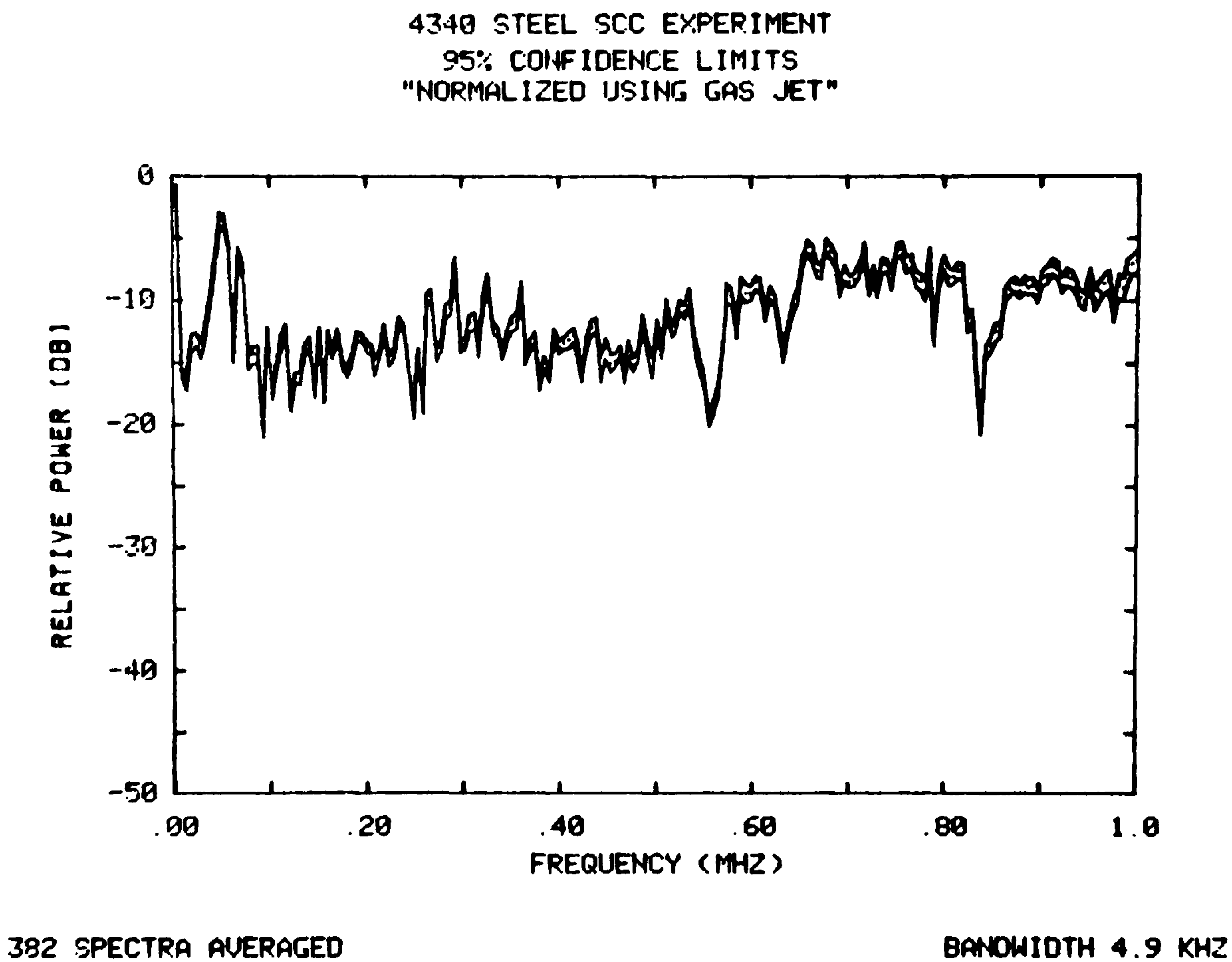

Figure 6.24. Deconvolved average power spectrum for acoustic emissions emitted from 4340 steel undergoing stress corrosion cracking showing 95% confidence limits. System variable correction has been applied.

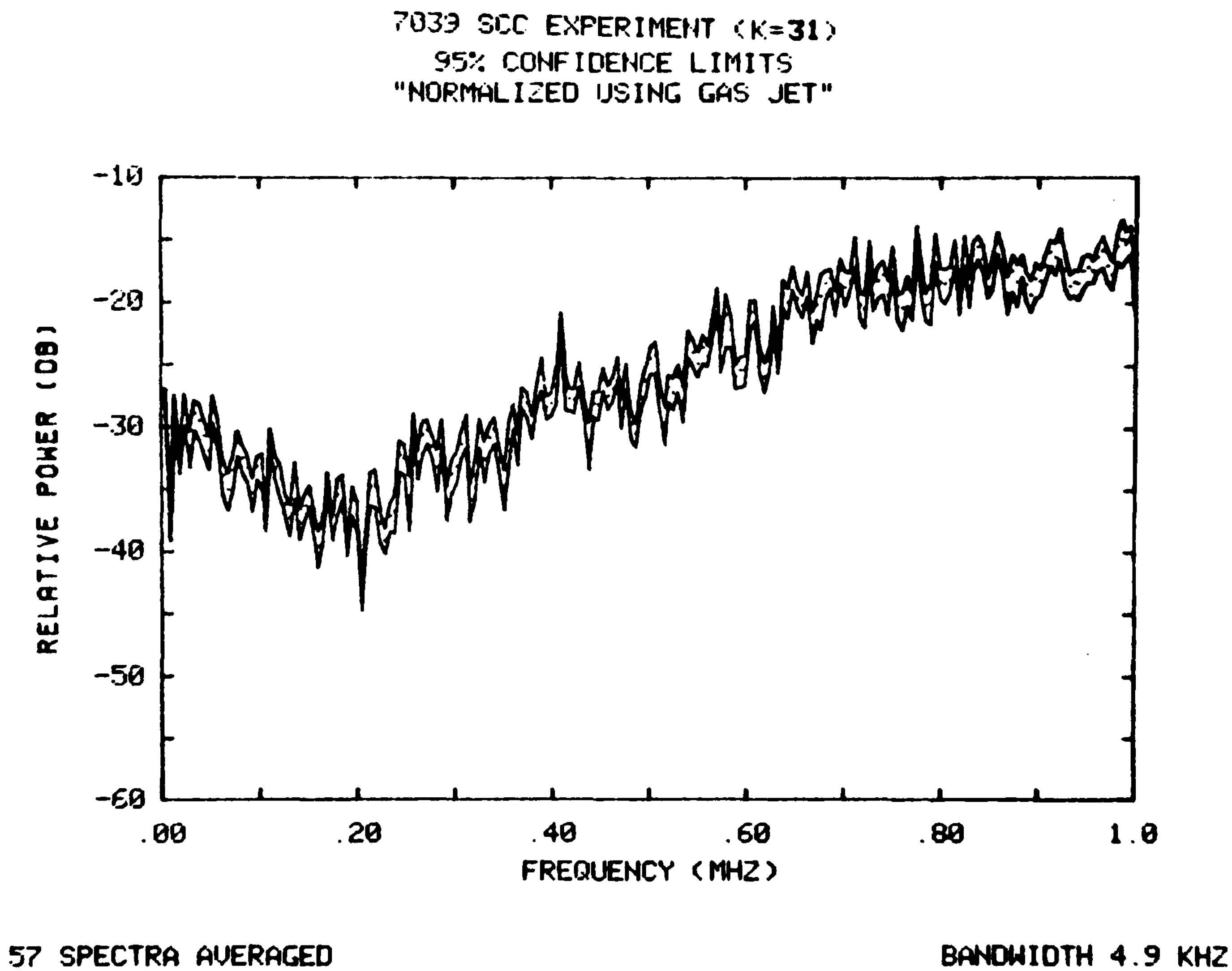

Figure 6.25. Deconvolved average power spectrum for acoustic emissions emitted from 7039 aluminum undergoing stress corrosion cracking showing 95% confidence limits. System variable correction has been applied.

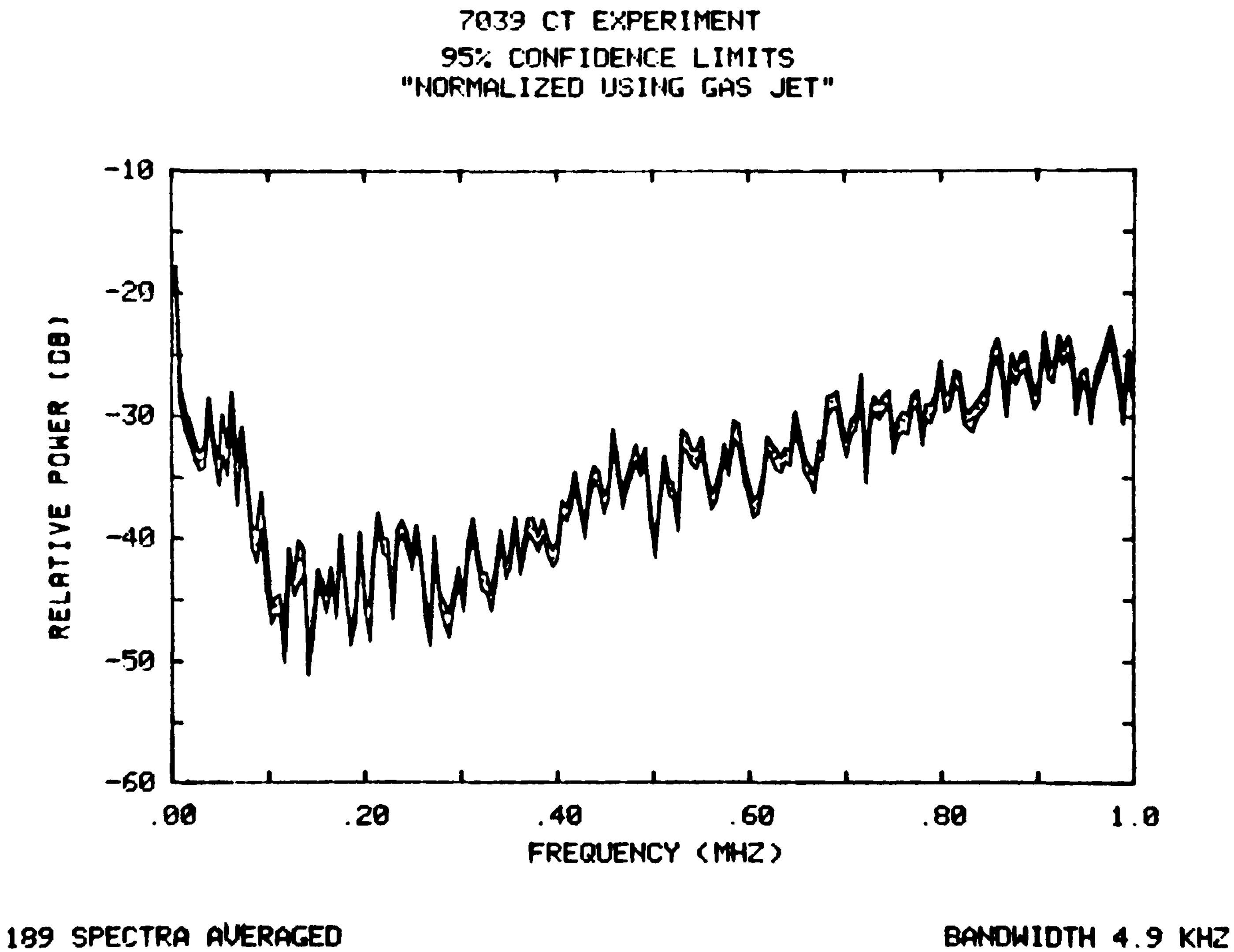

Figure 6.26. Deconvolved average power spectrum for acoustic emissions emitted from 7039 aluminum undergoing tensile loading showing 95% confidence limits. System variable correction has been applied.

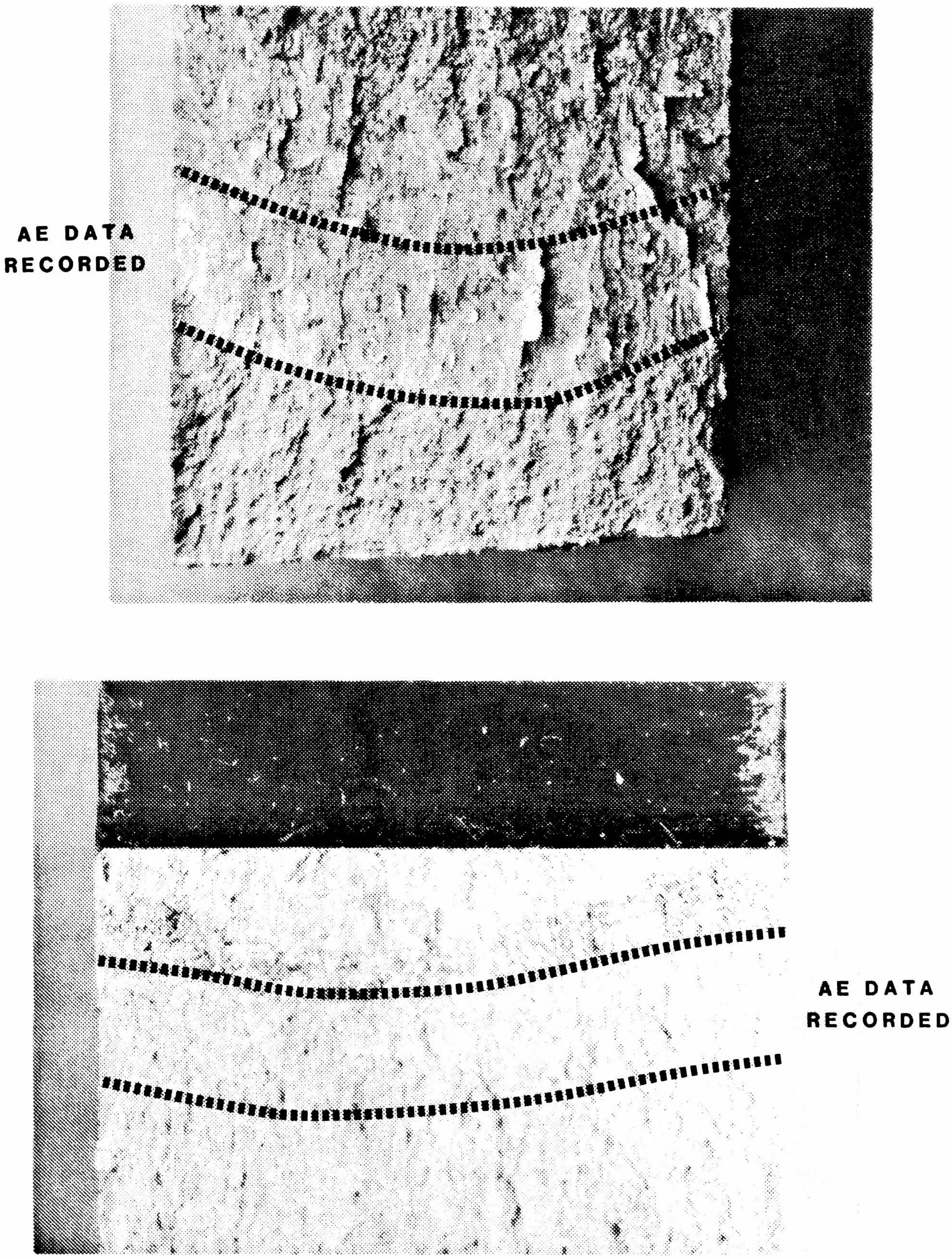

Figure 6.27. Fracture surface of 7039 DCB stress corrosion cracking specimen (top) contrasted with fracture surface of 7039 CT tensile loading specimen (bottom).

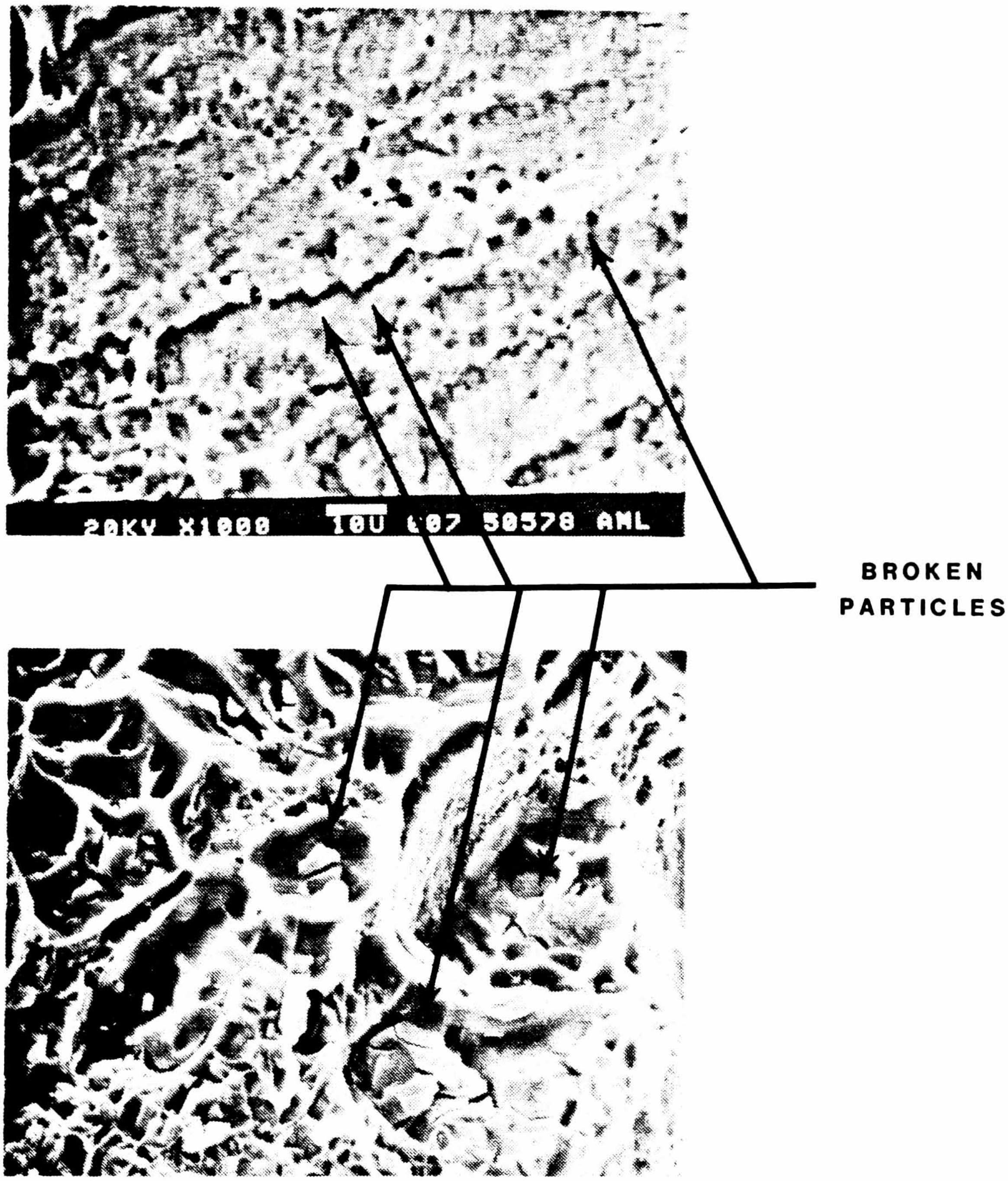

Figure 6.28. Scanning electron micrographs at 1000x magnification showing broken particles in both the 7039 DCB specimen (top) and the 7039 CT specimen (bottom).

tensile overload specimen shows the dimpled appearance characteristic of ductile fracture. It seemed almost inconceivable that two such dissimilar failures could produce the surprisingly similar spectra appearing in Figures 6.25 and 6.26, thus a series of scanning electron microscope photographs were taken of each fracture surface at increasingly higher magnifications. Careful examination of the aluminum sample micrographs made at a magnification of 1000 diameters revealed a common factor - fractured brittle particles (see Figure 6.28). Contrasting with this result, there were no brittle particles found in the micrographs of the 4340 steel (as expected).

It was shown in Section 2.1 that the source of acoustic emissions in metals which are fracturing is the discontinuous movement of cracks. This discontinuous motion arises either from the temporary stopping of a crack by a particle which then breaks as the localized stress increases, or by the slowing of a crack front due to a reduction in stress caused by the misalignment between the grain boundary the crack is following and the principle tensile axis. In the case of the 4340 steel specimen it is clear from the lack of brittle particles that the sole source of acoustic emission was the starting and stopping of the crack front as it followed grain boundaries. In the case of the aluminum alloys, the work of McBride, MacLachlan and Paradis described in Section 2.1 demonstrated that brittle particle fracture was the sole source of acoustic emission in 7075 aluminum. They were able to show that ductile fracture of 7075 aluminum which was not accompanied by particle fracture was completely silent. Combining their results with the data from the present experiments in 7039 aluminum where the ductile fracture of the CT specimen and the brittle fracture of the DCB specimen produced identically shaped spectra, the inescapable conclusion is that particle fracture was solely responsible for the acoustic emission generated by the fracture of 7039 aluminum.

From the data analysis presented in this section it can be concluded that it is possible to distinguish between individual failure processes occurring during the fracture of metals. As Figures 6.24, 6.25 and 6.26 show, the magnitude spectrum of fracture caused by the discontinuous movement of a crack front during the stress corrosion cracking of 4340 steel is radically different from the magnitude spectra of fracture in 7039 aluminum which was caused by brittle particle fracture during both tensile overloading and stress corrosion cracking.

A most significant result of these experiments is that they were achieved in engineering specimens in the presence of multiple reflections, both of which make the application of the generalized ray theory discussed in Section 2.2 impossible. This is not to say that the generalized ray theory is unnecessary for acoustic emission work, since it does offer the only means of quantitatively predicting the waveform at a specific site. However, the restrictions of having to work in simple geometries such as plates and also having to limit the receiver site to being less than six plate thicknesses away from the acoustic emission source limit the generalized ray theory to laboratory conditions. The experiments presented in this thesis show that it is possible to overcome these limitations and still differentiate between various acoustic emission sources by using appropriate signal processing.

The shortcoming of the processing techniques developed in this thesis is that they could not identify the acoustic emission source associated with each individual signal because of the large variability between signals obtained during a single test. However, because the feasibility of discriminating between signals emitted by different source mechanisms has now been firmly established, the task of developing techniques for associating a source with an individual signal can be undertaken with the confidence that there are indentifying characteristics to be found. This is of extreme importance because the magnitude of the data processing required means that such an undertaking will be very expensive.

A suggestion for researchers interested in developing such a technology is to utilize the approach being followed by experimenters in the area of speech analysis. At the present large computer software packages are becoming available which will perform interactive data processing using a variety of pattern recognition techniques. With a simple frequency translation such packages could probably be utilized very effectively in acoustic emission source identification research.

CHAPTER 7

SUMMATION

This chapter summarizes the thesis, which consists of a literature review of the field of acoustic emission, necessary theoretical development relevant to acoustic emission monitoring, acoustic emission calibration techniques, digital signal processing, instrumentation construction, software development and experimental verification of acoustic emission signal identification.

7.1 General

The intent of this thesis was to extend the technology of acoustic emission by developing methods for discriminating between acoustic emission signals to make possible the identification of the material processes which caused the received acoustic emissions. This technology extension is important because it would make economically feasible continuous defect monitoring in important structures to prevent their catastrophic failure. Acoustic emission signal discrimination would accomplish such a goal by permitting commonly occurring inconsequential acoustic emission sources to be differentiated from rarely occurring dangerous acoustic emission sources, thus eliminating costly service interruptions and unnecessary additional inspections using other nondestructive testing techniques.

A historical review of the phenomenon of acoustic emission was given revealing that although many practical nondestructive testing needs in materials research and structural integrity verification were already being satisfied through the use of acoustic emission monitoring, there were still significant limitations to the applicability of the technique because of the lack of a capability for acoustic emission signal source identification.

In the theoretical development, specific sources of acoustic emission in metals were discussed. It was shown that cooperative discontinuous dislocation motion could create detectable acoustic emission, but the fracture of brittle particles and the discontinuous movement of cracks were also found to be important sources of acoustic emission. A seismological concept known as the theory of the generalized ray was presented which enabled stress waveform predictions to be made for various source force functions. Experimental evidence was given to show that the theory could successfully predict acoustic emission waveforms occurring in plates when appropriate source force models were used, as long as the waveform was detected not more than six plate thicknesses away from epicenter. It was therefore concluded that although the theory is important for acoustic emission research, it is too restricted to be generally applied on real structures.

The minimum surface displacement detectable using capacitive and piezoelectric transducers was calculated using theoretical analyses of the operating principles of both types of transducers. This calculation showed that piezoelectric transducers provide maximum displacement sensitivity, while capacitive transducers offer a displacement response which is independent of frequency. The effects which material properties and specimen geometry have on the propagation of acoustic emission were discussed. The concepts of geometrical spreading, absorption, scattering, mode conversion and dispersion were covered and experimental evidence was presented to show that predictions of these effects could be made so as to facilitate the analysis of acoustic emission signals.

Experiments were reviewed which showed that the helium gas jet calibration technique used in the thesis studies provides a geometry independent calibration by characterizing the entire acoustic system of specimen, couplant and transducer. The basic assumptions which are made to obtain a calibration of a transducer were outlined and the procedures used for reciprocity calibration and comparison calibration were explained. For the calibration of acoustic emission transducers it was shown that comparison calibration was preferable to reciprocity calibration because the theory of the generalized ray provides a convenient means of checking the validity of comparison calibration while the reciprocity calibration involves the use of a non-verifiable assumption. Amplitude and phase spectral calibration curves obtained during a comparison calibration on a transducer similar to that used in the experiments in this thesis were shown.

The fast Fourier transform computer program used in this thesis was explained and the theory of Fourier spectral analysis was discussed. A method for approximating a Fourier transform that is usable with non-analytic time-limited signals was described. Special considerations required when signals are digitally processed were explained. The errors and noise introduced by analog to digital conversion were described and the concepts of aliasing and leakage were introduced. Practical methods for preventing or at least minimizing both aliasing and leakage were given.

The acoustic emission data acquisition system assembled for this study was described. Special features include such items as extremely wideband preamplifiers, band limited arrival sequence and timing circuits, wideband first arrival signal digital waveform recording on magnetic tape, comprehensive error detection logic, an optimal valid data reset detector and modem transmission of individual acoustic emission event location, energy and load parameters to a remote computer. The constructed instrument is unique because it makes possible for the first time the acquisition of information necessary for signal source identification while simultaneously permitting real-time source location on dispersive structures and because it allowed such activities to occur in environments hostile to computer operation.

The computer programs written to process the digital acoustic emission waveforms were described. The routines produce time domain digital plots of the recorded acoustic emissions, plot calibrated power spectra for validated signals, calculate a representative power spectral shape for an experiment complete with confidence limits and enable the experimenter to create a processed data base for archival purposes. A unique feature of the programs is that they possess the capability to use helium gas jet system calibration data to correct for the effects of changing specimen geometry, different couplant thickness and transducer aging, thus producing experiment invariant results. Other features of the programs are that the original experimental conditions are preserved in the processed data base and that the power spectra produced are identical to those produced using conventional less versatile analog instrumentation. The technology of acoustic emission was advanced by these programs since for the first time it was possible to analyze acoustic emission source waveforms with sufficient confidence to determine if differences were present between experiments in which different materials processes were operative.

A series of experiments were conducted to determine if different acoustic emission sources could be identified by their emitted signals. The experiments involved two different materials, two different failure processes and three different specimen geometries. Experiment invariant results were obtained via the use of the helium gas jet system calibration data and the programs described above. Two spectral shapes which were dramatically different at the 95% confidence level resulted from this processing and it was concluded that one spectral shape was due to the fracture of brittle particles while the other was due to the discontinuous movement of a crack. The new data acquisition methods and signal processing techniques developed in the thesis were thus proven to be effective for their intended purpose of identifying the material processes which caused the received acoustic emission signals.

7.2 Observations

A review of the literature and an analysis of the data contained therein yielded the following important observations:

1. Discontinuous crack movement and the fracture of brittle particles are important sources of acoustic emission in metals.

2. A general model for the prediction of stress waveforms resulting from the action of various internal force functions inside plates exists and is applicable to a distance of six plate thicknesses from epicenter.

3. The effects of material and geometry on the propagation of acoustic emission signals are well understood.

4. Piezoelectric transducers provide the most displacement sensitivity for acoustic emission work, but their frequency response is complicated and difficult to determine analytically.

5. Capacitive transducers provide a flat displacement response necessary for calibration work, but they are two orders of magnitude less sensitive to displacement than piezoelectric transducers.

6. The most useful form of calibration for acoustic emission transducers is comparison to a capacitive transducer because it results in an independently verifiable calibration traceable to physical quantities.

7.3 Conclusions

The following conclusions can be drawn from the work contained in this thesis:

1. The helium gas jet provides a convenient means of obtaining quantitative acoustic emission spectra independent of system variables such as specimen geometry, couplant thickness and transducer response changes.

2. Digital processing of signals provides analytical flexibility not possible using analog techniques.

3. Digital techniques can be used on non-analytic time-limited signals to quickly and economically produce power spectra which are identical to those produced using less flexible analog instruments.

4. Spectral shapes of acoustic emissions contain sufficient information to allow discrimination between different material failure processes, e.g., brittle particle fracture and discontinuous crack movement.

5. Particle fracture was the sole source of acoustic emission detected from the failure of 7039 aluminum specimens tested in this thesis, extending the observations of others who worked with 7075 aluminum.

6. Discontinuous crack motion was the sole source of acoustic emission detected from the failure of 4340 steel specimens tested in this thesis.

7. Acoustic emission signal source identification can be performed in engineering structures where multiple reflections and complex geometry preclude the use of analytic techniques such as the theory of the generalized ray.

APPENDIX A

FAST FOURIER TRANSFORM THEORY

As was described in Section 4.2, the fast Fourier transform is a name given to a class of algorithms which implement the discrete Fourier transform (see Equations 4.9 and 4.10). By taking advantage of certain periodicities and symmetries in these equations, they obtain an appreciable advantage in calculation speed over direct computation of the discrete Fourier transform (see Figure 4.9). To understand how the speed advantage of the fast Fourier transform is obtained, it is instructive to examine the algorithm made famous by Cooley and Tukey [Ref 104] using an explanation devised by Brigham [Ref 90]. First, the discrete Fourier transform is re-written as:

$$X(n) = \sum_{k=o}^{N-1} x_o(k)W^{kn} \tag{A.1}$$

For the fast Fourier transform procedure to work, N must be chosen to be a power of some number. If the number is 2 the resulting algorithm is known as a radix 2 transform, if it is 4 it becomes a radix 4 transform. For convenience let $N = 2^\gamma$ and choose $\gamma = 2$, then (A.1) can be written as:

$$\begin{bmatrix} X(o) \\ X(1) \\ X(2) \\ X(3) \end{bmatrix} = \begin{bmatrix} W^o & W^o & W^o & W^o \\ W^o & W^1 & W^2 & W^3 \\ W^o & W^2 & W^4 & W^6 \\ W^o & W^3 & W^6 & W^9 \end{bmatrix} \cdot \begin{bmatrix} x_o(o) \\ x_o(1) \\ x_o(2) \\ x_o(3) \end{bmatrix} \qquad (A.2)$$

The first key toward gaining computation speed is to recognize that $W^{nk} = W^{nk \bmod (N)}$, thus (A.2) becomes:

$$\begin{bmatrix} X(o) \\ X(1) \\ X(2) \\ X(3) \end{bmatrix} = \begin{bmatrix} 1 & 1 & 1 & 1 \\ 1 & W^1 & W^2 & W^3 \\ 1 & W^2 & W^o & W^2 \\ 1 & W^3 & W^2 & W^1 \end{bmatrix} \begin{bmatrix} x_o(o) \\ x_o(1) \\ x_o(2) \\ X_o(3) \end{bmatrix} \qquad (A.3)$$

The second key in increasing speed is to factor (A.3) to obtain:

$$\begin{bmatrix} X(o) \\ X(2) \\ X(1) \\ X(3) \end{bmatrix} = \begin{bmatrix} 1 & W^o & 0 & 0 \\ 1 & W^2 & 0 & 0 \\ 0 & 0 & 1 & W^1 \\ 0 & 0 & 1 & W^3 \end{bmatrix} \begin{bmatrix} 1 & 0 & W^o & 0 \\ 0 & 1 & 0 & W^o \\ 1 & 0 & W^2 & 0 \\ 0 & 1 & 0 & W^2 \end{bmatrix} \begin{bmatrix} x_o(0) \\ x_o(1) \\ x_o(2) \\ x_o(3) \end{bmatrix} \qquad (A.4)$$

Note that rows 1 and 2 have been interchanged in deriving (A.4), and notice also the large number of zeros which appear in (A.4). It is the introduction of these zeros and also the fact that $W^0 = -W^2$ and $W^1 = -W^3$ which markedly increase the computation speed, since some operations can be completely eliminated and some multiplications can be replaced with additions, which can be performed much faster than multiplication. The fast Fourier transform is thus based on a procedure which factors a N x N matrix into γ matrices (each N x N) such that each of the factored matrices has the special property of minimizing the number of complex multiplications and additions.

As γ becomes large, factored matrix equations such as (A.4) become unwieldy, thus it is common practice to represent the computations required for calculating the frequency components in a signal flow graph. Figure A.1 shows the signal flow graph for N = 4, and thus represents Equation (A.4). To interpret this graph it is necessary to recognize that each node is entered by two transmission paths (the arrows) from previous nodes. The data at each node is calculated by multiplying the data from each applicable previous node by the factor (if any) appearing at the head of the arrow of the respective transmission path and summing the two results. For example, consider node $x_1(2)$ in Figure A.1. This node has the value of $x_0(0) + W^2 x_0(2)$.

Besides conciseness, the reason for expressing the fast Fourier transform calculations in a signal flow graph is that when the operations can be seen certain symmetries become apparent, which can then be exploited to develop an algorithm. One such symmetry, called a dual node pair, can be seen by examining $x_1(0)$ and $x_1(2)$ in Figure A.1. It is apparent that these two nodes use the same data inputs, $x_0(0)$ and $x_0(2)$, and since the inputs do not get used in any other computations it is possible to simultaneously compute $x_1(0)$ and $x_1(2)$ and return the results to the storage locations used by $x_0(0)$ and $x_0(2)$.

The identification of dual nodes is important not only for optimizing storage during computation, but also because it is only necessary to perform one multiplication in determining the value of a dual node pair. This is because the weighting factors of a dual node pair are related, and in particular, if the weighting factor at one node

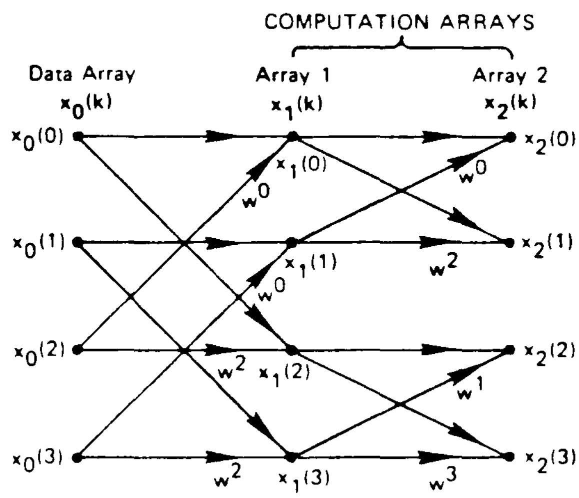

Figure A.1. Representation of Equation A.4 in a signal flow graph [Ref 90].

is W^P then the weighting factor at the dual node will be $W^{P+N/2}$, and $W^P = -W^{P+N/2}$. Since the vertical spacing of a dual node pair is given by $N/2^l$ where l is the index of the computation array, the calculation of any dual node pair is given by:

$$
\begin{aligned}
x_l(k) &= x_{l-1}(k) + W^P x_{l-1}(k+N/2^l) \\
x_l(k+N/2^l) &= x_{l-1}(k) + W^P x_{l-1}(k+N/2^l)
\end{aligned}
\tag{A.5}
$$

Equation (A.5) is the crux of the fast Fourier transform algorithm, since it eliminates the need to multiply in half of any computation array. This is illustrated in Figure A.2, which shows a signal flow graph for N = 16, and the areas in the computation arrays where multiplication can be skipped by using (A.5)

Application of Equation (A.5) in an algorithm requires that a means of calculating W^P be found. Examination of Figure A.2 reveals that p can be calculated by writing the k index in binary using γ bits, shifting this number $\gamma-l$ bits to the right followed by zero filling the $\gamma-l$ high order bits, and then reversing the order of the bits in the result. For example, consider node $x_3(8)$ in Figure A.2. $\gamma = 4$, $k = 8$ and $l = 3$, so k is 1000 in binary. $\gamma-l = 1$, so the shifted and filled number is 0100. Reversing the bit order yields 0010, or 2 in decimal notation, which is exactly the value shown for p in Figure A.2. Equation (A.5) can now be used to calculate all of the values for the dual nodes in Figure A.2, which means that the input time domain data can be transformed into frequency components in an efficient manner. It is necessary to realize that the frequency components will be scrambled, as was shown in Equation (A.4), but they can easily be unscrambled by

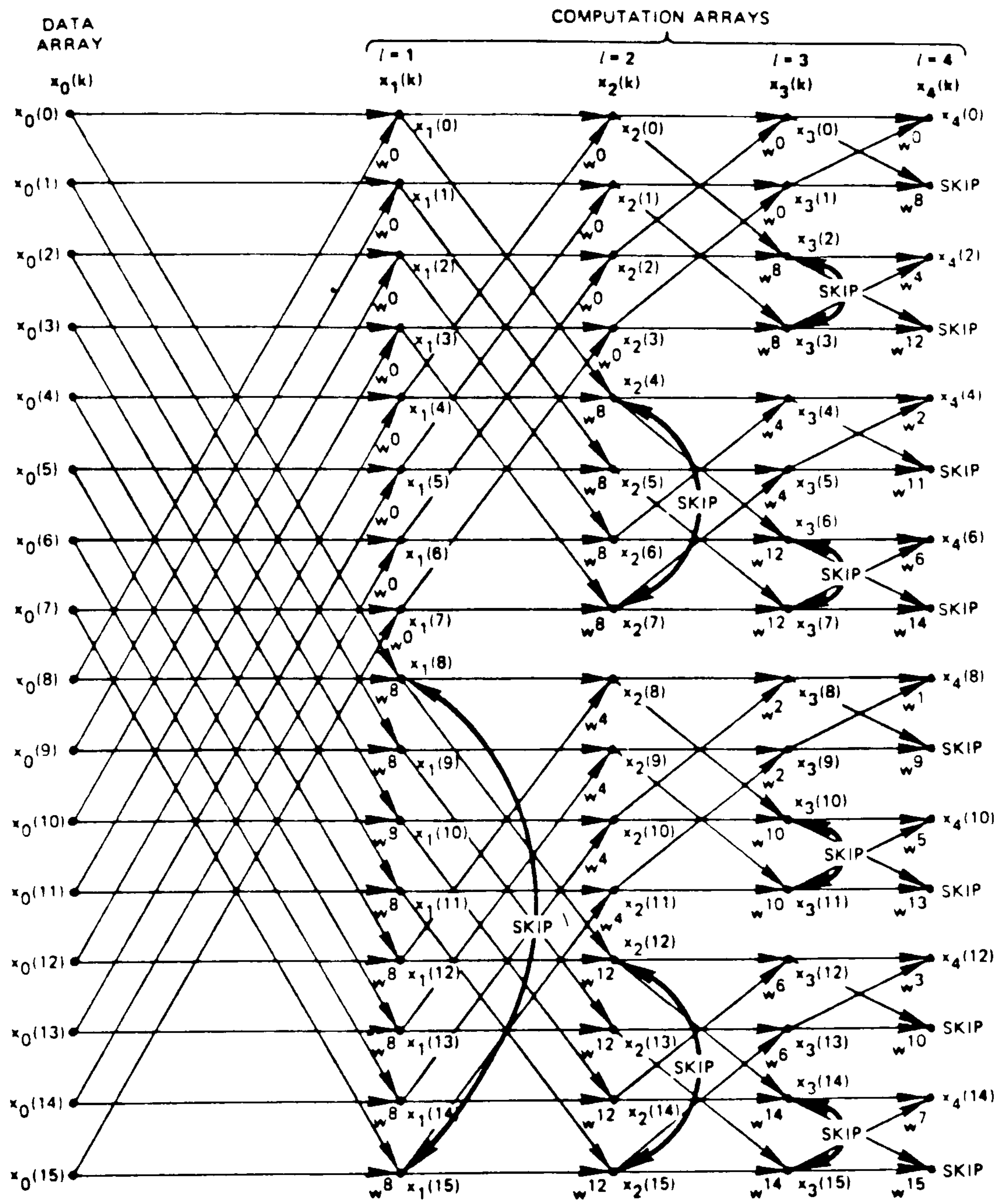

Figure A.2. Computations which may be skipped by means of dual node recognition [Ref 90].

simply reversing the bit order of their k indices.

An algorithm embodying concepts such as in-place calculation, calculation of (A.5), skipping of redundant dual nodes and output unscrambling is shown in Figure A.3 in flow chart form. Box 1 describes the input data required, while Box 2 initializes some variables used during computation. Box 3 checks for completion of the ℓ array calculations, and if calculations remain to be done Box 4 sets a counter which monitors the number of dual nodes that have been encountered. Box 5 calculates the value of p that is needed, which Box 6 uses to perform the computation of Equation (A.5). The index k is incremented by Box 7, and the condition in Box 8 determines if a dual node skip is required. If a skip is not required, Box 9 increments the dual node counter. If a skip is required, Box 10 determines the number of nodes to skip. Box 11 then checks to see if all of the dual nodes in an ℓ array have been calculated, and branches accordingly. If a new value of ℓ is required, Box 12 initializes the variables needed and the process repeats. When all ℓ arrays are computed the results are unscrambled, which starts by bit reversing k in Box 13 using the procedure outlined in Box 18. Boxes 14 and 15 place the unscrambled data in ascending order, and Box 16 determines when the process is complete.

With the flow chart of Figure A.3 developed it is simple to write a computer program to implement the algorithm for the fast Fourier transform. Such a program is shown in Figure A.4, and constitutes what is generally known as a radix 2 Cooley-Tukey fast Fourier transform. It should be noted that Figure A.4 is somewhat inefficient because the

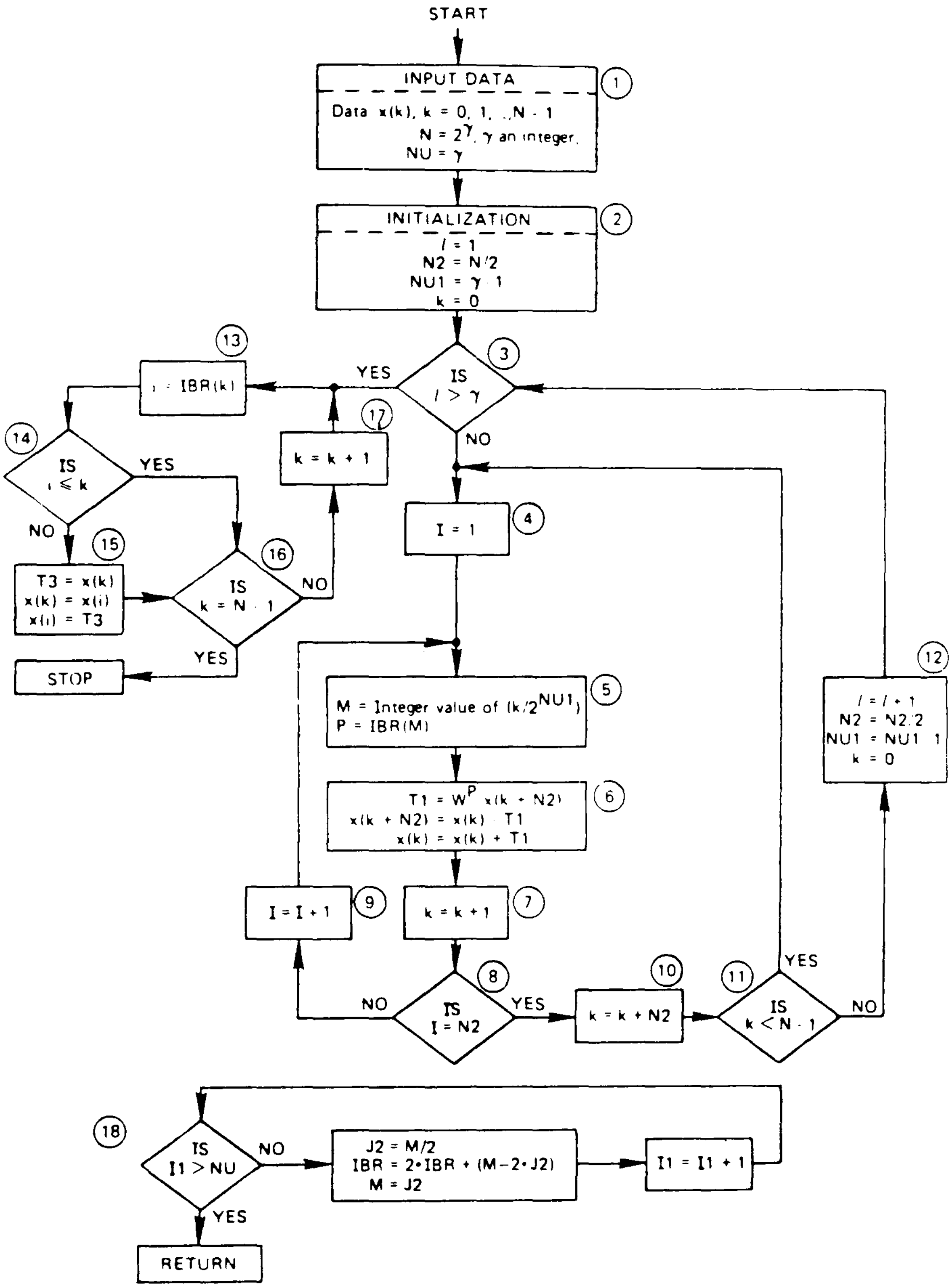

Figure A.3. Fast Fourier transform flow chart [Ref 90].

```
      SUBROUTINE FFT(XREAL.XIMAG.N.NU)
      DIMENSION XREAL(N),XIMAG(N)
      N2=N/2
      NU1=NU-1
      K=Ø
      DO 1ØØ L=1,NU
1Ø2   DO 1Ø1 I=1,N2
      P=IBITR(K/2**NU1.NU)
      ARG=6.283185*P/FLOAT(N)
      C=COS(ARG)
      S=SIN(ARG)
      K1=K+1
      K1N2=K1+N2
      TREAL=XREAL(K1N2)*C+XIMAG(K1N2)*S
      TIMAG=XIMAG(K1N2)*C-XREAL(K1N2)*S
      XREAL(K1N2)=XREAL(K1)-TREAL
      XIMAG(K1N2)=XIMAG(K1)-TIMAG
      XREAL(K1)=XREAL(K1)+TREAL
      XIMAG(K1)=XIMAG(K1)+TIMAG
1Ø1   K=K+1
      K=K+N2
      IF(K.LT.N) GO TO 1Ø2
      K=Ø
      NU1=NU1-1
1ØØ   N2=N2/2
      DO 1Ø3 K=1,N
      I=IBITR(K-1,NU)+1
      IF(I.LE.K) GO TO 1Ø3
      TREAL=XREAL(K)
      TIMAG=XIMAG(K)
      XREAL(K)=XREAL(I)
      XIMAG(K)=XIMAG(I)
      XREAL(I)=TREAL
      XIMAG(I)=TIMAG
1Ø3   CONTINUE
      RETURN
      END
      FUNCTION IBITR(J,NU)
      J1=J
      IBITR=Ø
      DO 2ØØ I=1,NU
      J2=J1/2
      IBITR=IBITR*2+(J1-2*J2)
2ØØ   J1=J2
      RETURN
      END
```

Figure A.4. Computer program in FORTRAN which results from flow chart of Figure A.3 [Ref 90].

array XIMAG must be set to zero when time domain data is placed into XREAL and thus some unnecessary calculations are performed. For this reason and others which are given in Section 4.2, another computer program was used to perform the spectral analysis in this thesis.

APPENDIX B

COMPUTER PROGRAM SOURCE CODE

The source code for the computer programs written for this thesis (whose operations are completely described in Chapter 5) appear on the following pages:

ROUTINE	PAGE
MSCD	219
PLOT	228
SYMB	244
PLTME	261
JSHFT	268
AENOR	269
FOUR2	274
GASJT	282
PLFFT	285
AECNF	291
DBSVR	298

Source Code of Program MSCD

```
      NAM MSCD     LOGIC FOR AE DATA ACQUISITION HARDWARE
*
*  CONTROLS A M6800 MICROPROCESSOR TO COLLECT AND TRANSMIT VALID
*  AE DATA TO A REMOTE COMPUTER.  RECORDS WIDEBAND AE ON TAPE.
*  PERMITS REMOTE RETRIEVAL OF RECORDED WIDEBAND AE FROM TAPE.
*
      SPC 1
*  WRITTEN BY JOHN CARLYLE  (21 SEP 78)
      SPC 1
*  REVISION DATE:  11 MAY 1981
      SPC 1
      ORG $8000
BEGIN SEI          SET INTERRUPT MASK
      LDS #$7F     STACK PNTR TO TOP OF RAM
      SPC 1
*  INITIALIZE PIA #1  (MSCD INPUT)
      SPC 1
      LDA A #$16   GET "CAB2 IN, LO TO HI, NO IRQ" CODE
      STA A CRA1   SET DRA TO INPUT
      STA A CRB1   SET DRB TO INPUT
      SPC 1
*  INITIALIZE PIA #2  (CONTROL PANEL AND MSCD CONTROL)
      SPC 1
      LDA A #$2E   GET "CAB2 OUT, LO TO HI, NO IRQ" CODE
      STA A CRA2   SET DRA TO INPUT
      COM DRB2     SET DATA DIRECTION REG B TO OUTPUT
      STA A CRB2   SET DRB TO OUTPUT
      SPC 1
*  INITIALIZE PIA #3  (KENNEDY INPUT AND DATACAP CONTROL)
      SPC 1
      LDA A #$2C   GET "CAB2 OUT, HI TO LO, IRQ" CODE
      STA A CRA3   SET DRA TO INPUT
      COM DRB3     SET DATA DIRECTION REG B TO OUTPUT
      STA A CRB3   SET DRB TO OUTPUT
      SPC 1
*  INITIALIZE PIA #4  (KENNEDY STATUS AND CONTROL)
      SPC 1
      LDA A #$2E   GET "CAB2 OUT, LO TO HI, NO IRQ" CODE
      STA A CRA4   SET DRA TO INPUT
      COM DRB4     SET DATA DIRECTION REG B TO OUTPUT
      STA A CRB4   SET DRB TO OUTPUT
      SPC 1
*  INITIALIZE ACIA
      SPC 1
      LDA A #$83   GET "MASTER RESET, ENABLE RCVE IRQ" CODE
      STA A CRSAC  SEND TO ACIA
      LDA A #$55   GET "RTS, 8-WDS, NO PAR, 1 STOP, /16" CODE
      STA A CRSAC  SEND TO ACIA
      JSR CLR      INITIALIZE COMMANDS, SYNC BUFFER AND FLAGS
```

```
        JMP CMD       GO CHECK FOR COMMANDS
        SPC 1
*  CONSTANTS FOR PIA'S AND ACIA
        SPC 1
DRA1   EQU 4004H
CRA1   EQU 4005H
DRB1   EQU 4006H
CRB1   EQU 4007H
DRA2   EQU 4008H
CRA2   EQU 4009H
DRB2   EQU 400AH
CRB2   EQU 400BH
DRA3   EQU 4010H
CRA3   EQU 4011H
DRB3   EQU 4012H
CRB3   EQU 4013H
DRA4   EQU 4020H
CRA4   EQU 4021H
DRB4   EQU 4022H
CRB4   EQU 4023H
CRSAC  EQU 4040H
XRAC   EQU 4041H
OUTAC  EQU 003DH
CMDBF  EQU 003EH
DELAY  EQU 003FH
SYNC   EQU 0043H
TAG    EQU 005AH
       SPC 1
*  SYSTEM RESET SUBROUTINE
       SPC 1
       ORG $805B
SYRST  JSR REWR       REWIND AND READ SELECT TRANSPORT
CLR    LDX #$FFFF     GET 1'S FOR MSCD SYNC WORD
       STX SYNC       STORE FOR LATER USE
       CLR DRB4       CLEAR KENNEDY COMMANDS
CLRP   CLR DRB3       CLEAR "NOT XFR AND WRITE DATA" COMMANDS
       CLR DRB2       CLEAR "BIT 0, BIT 1 AND NOT MRST" COMMANDS
       LDA A DRA3     CLEAR "REOR" FLAG
       LDA A DRA2     CLEAR "XFRC" FLAG
       LDA A DRA1     CLEAR MSCD FLAGS
       RTS            RETURN
       SPC 1
*  REWIND AND READ SELECT SUBROUTINE
       SPC 1
REWR   LDA A #$04     GET "REWIND" CODE
       STA A DRB4     SEND TO KENNEDY
       CLR DRB4       CLEAR "REWIND" COMMAND
LDP    LDA A DRA4     CHECK KENNEDY STATUS
       AND A #$01     LOAD POINT REACHED?
```

```
      BEQ LDP        NO, WAIT IN LOOP
      LDA A #$0F     YES, GET "REWIND COMPLETE" CODE
      STA A OUTAC    STORE FOR MODEM OUTPUT
      JSR ACRDY      GO SEND IT
      RTS            RETURN
      SPC 1
*  ACIA OUTPUT SUBROUTINE
      SPC 1
ACRDY LDA A CRSAC    GET ACIA STATUS
      AND A #$02     TRANSMISSION BUFFER EMPTY?
      BEQ ACRDY      NO, WAIT IN LOOP
      LDA A OUTAC    GET CHARACTER
      STA A XRAC     OUTPUT DATA TO MODEM
      RTS            RETURN
      SPC 1
*  COMMAND DETECTION SECTION
      SPC 1
CMD   CLR $0061      CLEAR "PREMATURE RETURN" TRAP
      CLR $0060      CLEAR "SKIP" TRAP
      LDA A DRA2     CHECK CONTROL PANEL INPUTS
      AND A #$3F     ANY INPUTS HIGH?
      BNE MDCDE      YES, GO DECODE COMMAND
      LDA A CRSAC    NO, CHECK ACIA STATUS
      AND A #$01     COMMAND RECEIVED?
      BNE ADCDE      YES, GO DECODE IT
      BRA CMD        NO, WAIT IN LOOP
      SPC 1
*  MANUAL COMMAND DECODING SECTION
      SPC 1
MDCDE STA A CMDBF    SAVE COMMAND
BUTTN LDA A DRA2     GET CONTROL PANEL INPUTS
      AND A #$3F     BUTTON RELEASED?
      BNE BUTTN      NO, WAIT IN LOOP
      LDA A #$80     YES, GET DELAY TIME VALUE
      JSR DLY        GO DELAY
      LDA A CMDBF    GET COMMAND AGAIN
      CMP A #$01     REWIND COMMAND?
      BEQ JRWD       YES, DO IT
      CMP A #$02     NO, SKIP COMMAND?
      BEQ JSKP       YES, DO IT
      CMP A #$04     NO, READ COMMAND?
      BEQ JREAD      YES, DO IT
      CMP A #$08     NO, RE-READ COMMAND?
      BEQ JRRED      YES, DO IT
      CMP A #$10     NO, SET FOR RECORD?
      BEQ JREC       YES, DO IT
      CMP A #$20     NO, WRITE EOF?
      BEQ JEOF       YES, DO IT
      JMP CMD        FALSE INPUT, LOOP
```

```
      SPC 1
*  AUTOMATIC COMMAND DECODING SECTION
      SPC 1
ADCDE LDA A XRAC      GET COMMAND
      CMP A #$96      REWIND COMMAND?
      BEQ JRWD        YES, DO IT
      CMP A #$A6      NO, SKIP COMMAND?
      BEQ JSKP        YES, DO IT
      CMP A #$99      NO, READ COMMAND?
      BEQ JREAD       YES, DO IT
      CMP A #$5A      NO, RE-READ COMMAND?
      BEQ JRRED       YES, DO IT
      CMP A #$A9      NO, SET FOR RECORD?
      BEQ JREC        YES, DO IT
      CMP A #$6A      NO, WRITE EOF?
      BEQ JEOF        YES, DO IT
      JMP CMD         FALSE INPUT, LOOP
      SPC 1
*  COMMAND JUMPS
      SPC 1
JRWD  JSR SYRST       REWIND AND SELECT READ MODE
      JMP CMD         RETURN TO COMMAND DETECTION
JSKP  JMP SKIP        GO SKIP A RECORD
JREAD JMP READ        GO READ A RECORD
JRRED JMP RREAD       GO RE-READ A RECORD
JREC  JMP WRITE       REWIND AND SELECT WRITE MODE
JEOF  JMP EOF         GO WRITE END-OF-FILE
      SPC 1
*  DELAY SUBROUTINE
      SPC 1
DLY   STA A DELAY     SAVE TIME VALUE
LOOP2 LDA A #$FF      INITIALIZE COUNT
LOOP1 DEC A           DECREMENT COUNT
      BNE LOOP1       COUNT DONE?
      DEC DELAY       YES, DECREMENT VALUE
      BNE LOOP2       TIME VALUE GONE?
      RTS             YES, RETURN FROM DELAY
      SPC 1
*  RECORD MSCD AND WAVEFORM DATA SECTION
      SPC 1
WRITE JSR CLRP        CLEAR PIA COMMANDS AND FLAGS
      JSR REWWS       REWIND TAPE AND SELECT WRITE
      LDA A #$04      GET "ENABLE MSCD" CODE
      STA A DRB2      ENABLE MSCD
      LDA A #$02      GET "ENABLE XFRD" CODE
      STA A DRB3      ENABLE XFRD FLIP-FLOP
TAR1  LDA A DRA2      FIRST ARRIVAL RECORDED ON BIO?
      BMI FLG2        YES, GO HANDLE WITH TAG
      LDA A CRA1      NO, COMPLETE DATA SET OBTAINED?
```

```
      BMI CLFG1     YES, GO HANDLE WITHOUT TAG
      LDA A DRA2    NO, GET CONTROL PANEL INPUTS
      AND A #$3F    COMMAND ISSUED?
      BEQ ACCMD     NO
      JMP MDCDE     YES, GO DECODE IT
ACCMD LDA A CRSAC   GET ACIA STATUS
      AND A #$01    COMMAND RECEIVED?
      BEQ TAR1      NO, CHECK FOR FIRST ARRIVAL
      JMP ADCDE     YES, GO DECODE IT
CLFG1 LDA A DRA1    NO TAG, CLEAR "COMPLETE DATA SET" FLAG
      JSR INDTA     GO INPUT DATA
      CLR $5A       CLEAR TAG
      JSR OTDTA     OUTPUT DATA
      BRA TAR1      CHECK FOR FIRST ARRIVAL
FLG2  LDA A CRA1    TAG REQUIRED, COMPLETE DATA SET OBTAINED?
      BMI CLFG2     YES, GO HANDLE NORMALLY
      ASL A         NO, TIME LIMIT EXCEEDED?
      BMI CLOVR     YES, GO RESET FOR NEXT EVENT
      BRA FLG2      NEITHER, WAIT IN LOOP
CLOVR LDA A DRA1    CLEAR "OVERRANGE" FLAG
      CLR DRB3      CLEAR "NOT XFR AND WRITE DATA" COMMANDS
      LDA A #$02    GET "ENABLE XFRD" CODE
      STA A DRB3    ENABLE XFRD FLIP-FLOP
      JMP TAR1      CHECK FOR FIRST ARRIVAL
CLFG2 LDA A DRA1    CLEAR "COMPLETE DATA SET" FLAG
      LDA A #$03    GET "WDS AND NOT XFR" CODE
      STA A DRB3    SEND TO DATACAP
      LDA A #$01    GET "WDS ENABLE" CODE
      STA A DRB3    LOWER "NOT XFR" TO WRITE ON TAPE
      LDA A #$03    GET "WDS AND NOT XFR" CODE
      STA A DRB3    SEND TO DATACAP
      JSR INDTA     GO INPUT DATA
      LDA A #$FF    GET "BIOMATION RECORD" TAG
      STA A TAG     STORE IN PROPER PLACE
      JSR OTDTA     OUTPUT DATA WITH TAG
XFRC  LDA A CRA2    IS DATA TRANSFER COMPLETE?
      BPL XFRC      NO, LOOP
      LDA A #$02    YES, GET "ENABLE XFRD" CODE
      STA A DRB3    ENABLE XFRD FLIP-FLOP
      LDA A DRA2    CLEAR "XFRC" FLAG
      JMP TAR1      CHECK FOR FIRST ARRIVAL
      SPC 1
*  INPUT MSCD DATA SUBROUTINE
      SPC 1
INDTA LDA B #$0B    INITIALIZE # OF WORDS TO INPUT
      LDX #$44      INITIALIZE POINTER TO MSCD BUFFER-1
INCNT INX           INCREMENT POINTER
      LDA A DRA1    GET 1/2 MSCD WORD AND CLEAR FLAG
      STA A $00,X   STORE IN MSCD BUFFER
```

```
             INX              INCREMENT POINTER
             LDA A DRB1       GET 2/2 MSCD WORD
             STA A $00,X      STORE IN MSCD BUFFER
             DEC B            ALL MSCD DATA INPUT?
             BEQ CLFLG        YES, JUMP
             LDA A #$05       NO, GET "BIT 0 AND MSCD ENABLE" CODE
             STA A DRB2       SEND TO MSCD
             LDA A #$04       GET "ENABLE MSCD" CODE
             STA A DRB2       ENABLE MSCD
       FLG   LDA A CRA1       RESPONSE FROM MSCD?
             BPL FLG          NO, WAIT
             BRA INCNT        YES, GO HANDLE NEXT MSCD WORD
       CLFLG LDA A DRA1       CLEAR "COMPLETE DATA SET" FLAG
             LDA A #$06       GET "BIT 1 AND MSCD ENABLE" CODE
             STA A DRB2       SEND TO MSCD
             LDA A #$04       GET "MSCD ENABLE" CODE
             STA A DRB2       ENABLE MSCD
             RTS              RETURN
             SPC 1
       *  OUTPUT MSCD DATA SUBROUTINE
             SPC 1
       OTDTA LDA B #$18       INITIALIZE # OF WORDS TO OUTPUT
             LDX #$43         INITIALIZE POINTER TO "SYNC" WORD
       TDRE  LDA A CRSAC      GET ACIA STATUS
             AND A #$02       TRANSMISSION BUFFER EMPTY?
             BEQ TDRE         NO, WAIT IN LOOP
             LDA A $00,X      YES, GET MSCD DATA WORD
             STA A XRAC       OUTPUT DATA TO MODEM
             DEC B            ALL MSCD DATA SENT?
             BEQ SRTN         YES, DONE
             INX              NO, INCREMENT POINTER
             BRA TDRE         GO SEND NEXT WORD
       SRTN  RTS              RETURN
             SPC 1
       *  REWIND AND WRITE SELECT SUBROUTINE
             SPC 1
       REWWS LDA A #$05       GET "REWIND AND WRITE SELECT" CODE
             STA A DRB4       SEND TO KENNEDY
             LDA A #$01       GET "WRITE SELECT" CODE
             STA A DRB4       SEND TO KENNEDY
       BSY1  LDA A DRA4       GET KENNEDY STATUS
             AND A #$04       HAS KENNEDY BECOME BUSY?
             BEQ BSY1         NO, LOOP
       BSY2  LDA A DRA4       YES, GET KENNEDY STATUS
             AND A #$04       IS KENNEDY STILL BUSY?
             BNE BSY2         YES, WAIT IN LOOP
             LDA A #$0F       NO, GET "REWIND COMPLETE" CODE
             STA A OUTAC      STORE FOR MODEM OUTPUT
             JSR ACRDY        GO SEND IT
```

```
        RTS           RETURN
        SPC 1
*  WRITE END-OF-FILE SECTION
        SPC 1
EOF     LDA A DRB4    CHECK KENNEDY STATUS
        AND A #$01    IS WRITE MODE SELECTED?
        BNE BSY3      YES, CONTINUE
        JMP CMD       NO, CHECK FOR NEXT COMMAND
BSY3    LDA A DRA4    CHECK KENNEDY STATUS
        AND A #$04    IS KENNEDY BUSY?
        BNE BSY3      YES, WAIT IN LOOP
        LDA A #$03    NO, GET "EOFC AND WRITE SELECT" CODE
        STA A DRB4    SEND TO KENNEDY
        LDA A #$01    GET "WRITE SELECT" CODE
        STA A DRB4    SEND TO KENNEDY
BSY4    LDA A DRA4    CHECK KENNEDY STATUS
        AND A #$04    IS KENNEDY BUSY?
        BNE BSY4      YES, WAIT IN LOOP
        LDA A #$0F    NO, GET "EOF WRITTEN" CODE
        STA A OUTAC   STORE FOR MODEM OUTPUT
        JSR ACRDY     GO SEND IT
        JMP CMD       GO CHECK FOR COMMANDS AGAIN
        SPC 1
*  READ RECORD SECTION
        SPC 1
READ    JSR INTRD     GO INITIALIZE READ MODE
        TST $0061     IS "PREMATURE RETURN" TRAP SET?
        BNE NW1       YES, KENNEDY IN WRITE MODE, RETURN
        CLR DRB4      NO, RELEASE "HOLD" COMMAND
        JSR ROR       GO READ ONE RECORD
        TST $0061     IS "PREMATURE RETURN" TRAP SET?
        BNE NW1       YES, EOF ENCOUNTERED, RETURN
        JSR OTDT1     NO, GO OUTPUT ONE RECORD
NW1     JMP CMD       GO CHECK FOR COMMANDS
        SPC 1
*  RE-READ ONE RECORD SECTION
        SPC 1
RREAD   JSR INTRD     GO INITIALIZE READ MODE
        TST $0061     IS "PREMATURE RETURN" TRAP SET?
        BNE NW2       YES, KENNEDY IN WRITE MODE, RETURN
        LDA A #$08    NO, GET "HOLD" CODE
        STA A DRB4    SEND TO KENNEDY
        JSR ROR       GO READ ONE RECORD
        TST $0061     IS "PREMATURE RETURN" TRAP SET?
        BNE NW2       YES, EOF ENCOUNTERED, RETURN
        JSR OTDT1     NO, GO OUTPUT ONE RECORD
NW2     JMP CMD       GO CHECK FOR COMMANDS
        SPC 1
*  SKIP ONE RECORD SECTION
```

```
            SPC 1
      SKIP  INC $0060     SET "SKIP" TRAP
            JSR INTRD     GO INITIALIZE READ MODE
            TST $0061     IS "PREMATURE RETURN" TRAP SET?
            BNE NW3       YES, KENNEDY IN WRITE MODE, RETURN
            CLR DRB4      NO, RELEASE "HOLD" COMMAND
            JSR ROR       GO READ ONE RECORD
            TST $0061     IS "PREMATURE RETURN" TRAP SET?
            BNE NW3       YES, EOF ENCOUNTERED, RETURN
            LDA A DRA3    NO, CLEAR "END OF RECORD" FLAG
      ROOC  LDA A #$28    GET "ROOC AND HOLD" CODE
            LDA B #$08    GET "HOLD" CODE
            STA A DRB4    SEND TO KENNEDY
            STA B DRB4    SEND TO KENNEDY
            NOP           DELAY FOR "REOR" INTERRUPT
            LDA A CRA3    END OF RECORD REACHED?
            BPL ROOC      NO, LOOP
            LDA A DRA3    YES, CLEAR "END OF RECORD" FLAG
            JSR ACRDY     OUTPUT FINISHED CODE
      NW3   JMP CMD       GO CHECK FOR COMMANDS
            SPC 1
      *  INITIALIZE READ MODE SUBROUTINE
            SPC 1
      INTRD LDA A DRB4    CHECK KENNEDY STATUS
            AND A #$01    IS WRITE MODE SELECTED?
            BEQ RDA       NO, CONTINUE
            INC $0061     YES, SET "PREMATURE RETURN" TRAP
            BRA RT1       RETURN
      RDA   LDA A DRA4    CHECK FOR KENNEDY STATUS
            AND A #$08    IS READ DATA AVAILABLE?
            BEQ RDA       NO, WAIT IN LOOP
      RT1   RTS           RETURN
            SPC 1
      *  READ ONE RECORD SUBROUTINE
            SPC 1
      ROR   NOP           REQUIRED DELAY...
            NOP           ...FOR TRANSPORT TO
            NOP           ...START TRANSFERRING
            NOP           ...DATA FROM TAPE
      RBSY  LDA A DRA4    CHECK KENNEDY STATUS
            AND A #$04    IS MEMORY BEING FILLED?
            BEQ RBSY      YES, WAIT IN LOOP
            LDA A #$08    NO, GET "HOLD" CODE
            STA A DRB4    SEND TO KENNEDY
            LDA A DRA4    CHECK KENNEDY STATUS
            AND A #$10    WAS EOF READ?
            BEQ RBIE      NO, GO CHECK FURTHER
            LDA A #$0F    YES, GET "EOF READ" CODE
            STA A OUTAC   STORE FOR MODEM OUTPUT
```

```
             JSR ACRDY      GO SEND IT
             INC $0061      SET "PREMATURE RETURN" TRAP
             BRA RT2        RETURN
      RBIE   LDA A DRA4     CHECK KENNEDY STATUS
             AND A #$20     WAS READ BLOCK IN ERROR?
             BEQ NOER       NO, DATA IS OK
             LDA A #$FF     YES, GET "READ ERROR" CODE
             STA A OUTAC    STORE FOR MODEM OUTPUT
             TST $0060      IS "SKIP TRAP" SET?
             BNE RT2        YES, RETURN
             JSR ACRDY      NO, GO SEND IT
      RT2    RTS            RETURN
      NOER   LDA A #$00     GET "DATA OK" CODE
             STA A OUTAC    STORE FOR MODEM OUTPUT
             TST $0060      IS "SKIP TRAP" SET?
             BNE RT9        YES, RETURN
             JSR ACRDY      NO, GO SEND IT
      RT9    RTS            RETURN
             SPC 1
      *  OUTPUT ONE RECORD SUBROUTINE
             SPC 1
      OTDT1  CLR $0060      CLEAR FOR CHECKSUM
      IINC   LDA A DRA3     GET KENNEDY DATA
             STA A OUTAC    STORE FOR MODEM OUTPUT
             LDA B $60      GET LAST CHECKSUM
             ABA            ADD TO PRESENT CHECKSUM
             STA A $60      STORE CHECKSUM
             JSR ACRDY      SEND DATA
             LDA A #$28     GET "ROOC AND HOLD" COMMAND
             LDA B #$08     GET "HOLD" CODE
             STA A DRB4     SEND TO KENNEDY
             STA B DRB4     SEND TO KENNEDY
             NOP            DELAY FOR "REOR" INTERRUPT
             LDA A CRA3     END OF RECORD REACHED?
             BPL IINC       NO, OUTPUT MORE DATA
             LDA A DRA3     YES, CLEAR "END OF RECORD" FLAG
             LDA A $60      GET CHECKSUM
             STA A OUTAC    STORE FOR MODEM OUTPUT
             JSR ACRDY      SEND CHECKSUM
             CLR $0060      CLEAR CHECKSUM LOCATION
             RTS            RETURN
      *                VECTORED INTERRUPTS
             ORG $83F8
             FDB $8037      IRQ VECTOR
             ORG $83FC
             FDB $8037      NMI VECTOR
             FDB $8000      RES VECTOR
             SPC 1
             END
```

Source Code of Subroutine PLOT

```
ASMB,R,F
      HED  ** RT/DOS PLOT PACKAGE FOR TEK 4010 **
*
*
      NAM PLOT,7
*
*
      ENT WHERE,FACT,PLOT,PLTLU
      ENT TPLOT,CURSR,ERASE,HCOPY
*
*
      EXT .ENTR,EXEC,IFIX,FLOAT
*
*  THIS IS THE CENTRAL PROGRAM IN THE HP REAL-TIME/DISC
*  OPERATING SYSTEM PLOTTING PACKAGE.  IT PLOTS ON A
*  TEKTRONIX 4010 CATHODE RAY STORAGE TUBE.
*
*
*  WRITTEN BY JOHN CARLYLE
*
*
*************************
*
*
*   THERE ARE 8 SECTIONS TO THE PLOT PROGRAM
*
*      1-WHERE; ESTABLISHES WHERE PEN IS CURRENTLY.
*      2-FACT;  ESTABLISHES SCALING FACTOR OF PLOT
*      3-PLOT;  CONVERTS THE X,Y AND PEN DATA TO PLOT
*               COMMANDS.
*      4-PLTLU; ALLOWS THE USER TO DECLARE THE
*               LOGICAL UNIT NUMBER OF THE
*               PLOTTER UNIT. THIS ALLOWS THE
*               USE OF MORE THAN ONE PLOTTER.
*      5-TPLOT; TEKTRONIX 4010 CRT PLOTTING ROUTINE
*      6-CURSR; TEKTRONIX 4010 CRT CURSOR ACTIVATION
*      7-ERASE; TEKTRONIX 4010 CRT SCREEN ERASE
*      8-HCOPY; TEKTRONIX 4010 CRT HARDCOPY CREATION
*
*
*
*
      SKP
**************************
*
*
******* WHERE ****
*
*  THE -WHERE- CALL ALLOWS THE USER TO DETERMINE THE
```

```
*  CURRENT PLOTTER PEN POSITION.  THE NUMBERS PROVIDED
*  TO THE USER WILL BE IN FLOATING POINT.
*
* *   - FORTRAN LINKAGE -
*
*          CALL WHERE(X,Y)
*
*                 X  SPECIFIES THE 2 WORD BUFFER FOR X.
*                 Y  SPECIFIES THE 2 WORD BUFFER FOR Y.
*
*
* *
*
* *   -  CALLING SEQUENCE -
*
*           JSB WHERE    WHERE ROUTINE ORIGIN
*           DEF *+3      RETURN
*           DEF XC       LOCATION OF USER X 2 WD BUFFER
*           DEF YC       LOCATION OF USER Y 2 WD BUFFER
*
*
**************
*
*
XC     OCT 0         ADDRESS OF 2 WD BUFFER FOR X
YC     OCT 0         ADDRESS OF 2 WD BUFFER FOR Y
*
*
WHERE NOP
       JSB .ENTR
       DEF WHERE-2
       LDA XPEN      GET CURRENT X ORIGIN
       CMA,INA       NEGATE IT
       ADA IDX       CALCULATE CURRENT X POSITION
       JSB FLOAT     CONVERT FROM FIXED TO FLOATING
       FDV CFAC
       DST XC,I      STORE IN USERS BUFFER
*
       LDA YPEN      GET CURRENT Y ORIGIN
       CMA,INA       NEGATE IT
       ADA IDY       CALCULATE CURRENT Y POSITION
       JSB FLOAT     CONVERT FROM FIXED TO FLOATING
       FDV DFAC
       DST YC,I      STORE IN USERS BUFFER
       JMP WHERE,I   EXIT
*
*
*
*
```

Source Code of Subroutine PLOT

```
      SKP
*
******************
*
*
***** FACT ****
*
*
*  THE -FACT- CALL ALLOWS THE USER TO VARY THE SCALING
*  FACTOR USED FOR EACH PLOT.  THE SCALING FACTOR WILL
*  BE INITIALIZED AT  "1.0". THE FACTOR IS
*  MULTIPLIED BY 100.0 FOR USE WITH THE TEK 4010,
*  WHERE THE MAX LIMITS ARE (1023,1023).
*
* *   - FORTRAN LINKAGE -
*
*        CALL FACT(AX,AY)
*
*            AX = X PLOT FACTOR
*            AY = Y PLOT FACTOR
*
* *
*
* *   - CALLING SEQUENCE -
*
*           JSB FACT      FACTOR ROUTINE ORIGIN
*            DEF *+3
*            DEF FCT    LOC OF X PLOT FACTOR
*            DEF FCT+1   "  "  Y   "    "
*
*
******************
*
*
*
FCT   OCT 0         ADDRESS OF 2 WD FP FACTOR
      OCT 0
FACT  NOP
      JSB .ENTR
      DEF FACT-2
      DLD FCT,I
      FMP F100
      DST CFAC
      DLD FCT+1,I
      FMP F100
      DST DFAC
      JMP FACT,I
*
CFAC  DEC 100.0
```

```
DFAC  DEC 100.0
F100  DEC 100.0
*
*
      SKP
*****************************
*
*
***** PLOT ****
*
*
*  THE -PLOT- ROUTINE CONVERTS THE DEFINED X,Y
*  PARAMETERS TO PLOT INFORMATION THEN EXECUTES
*  THE PLOT.
*
** RESTRICTION--- NO PLOT LENGTH CAN EXCEED 16,383
*                INCREMENTS. (APPROXIMATELY 163 INCHES)
*
* *  - FORTRAN LINKAGE -
*
*          CALL PLOT(X,Y,IC)
*
*            -X,Y DEFINES THE NEW COORDINATE TO BE PLOTTED.
*
*            -IC  DEFINES THE PEN UP/DOWN COMMAND.
*
* *
*
* *  - CALLING SEQUENCE -
*
*          JSB  PLOT      PLOT ROUTINE ORIGIN
*          DEF  *+4
*          DEF  X         ADDRESS OF X COORDINATE.
*          DEF  Y         ADDRESS OF Y COORDINATE.
*          DEF  IC        ADDRESS OF PEN COMMAND.
**************
*
*
X     OCT 0          ADDRESS OF X PLOT DATA.
Y     OCT 0          ADDRESS OF Y PLOT DATA.
IC    OCT 0          ADDRESS OF PEN COMMAND.
*
PLOT  NOP
      JSB .ENTR
      DEF PLOT-3
*
*
      DLD X,I        LOAD X PLOT DATA
      JSB FPC        CONVERT AND FACTOR
```

```
      STA IX        STORE FIXED X MOVEMENT VALUE
*
      DLD Y,I       LOAD Y PLOT DATA
      JSB FPD       CONVERT AND FACTOR
      STA IY        STORE FIXED Y MOVEMENT VALUE
*
      DLD XPEN      LOAD OLD X,Y ORIGIN DATA
*
*       XPEN AND YPEN ARE IN 2 CONSECUTIVE
*       LOCATIONS FOR THIS DOUBLE LOAD.
*
*       THE PLOTTER DATA WILL BE
*       CALCULATED AS FOLLOWS:
*
*              IX + XPEN = IDX
*              IY + YPEN = IDY
*
*                WHERE IX = REQUIRED X MOVEMENT
*                WHERE IY = REQUIRED Y MOVEMENT
*                    XPEN = OLD X ORIGIN
*                    YPEN = OLD Y ORIGIN
*
      ADA IX        IX + XPEN
      ADB IY        IY + YPEN
      DST IDX       STORE ABSOLUTE PLOTTING DATA
*
*
*
*
*   DETERMINE PLOT MODE AND DRAW THE LINE....
*
      LDA IC,I     GET PEN COMMAND
      SSA,RSS      NEW ORIGIN?
      JMP PU.1     NO
      DLD IDX      YES, GET CURRENT POSITION
      DST XPEN     STORE IN ORIGIN AREA
      LDA IC,I     GET PEN COMMAND AGAIN
      CMA,INA      MAKE PEN COMMAND POSITIVE
PU.1  CPA C02      DOES PEN COMMAND = 2?
      JMP PU.2     YES
      CLA          NO, MOVE WITH PEN UP
      STA PENC
      JMP PU.3
PU.2  CLA,INA      MOVE WITH PEN DOWN
      STA PENC
PU.3  JSB TPLOT    DRAW THE LINE....
      DEF *+5
      DEF ILUN
      DEF PENC
```

```
      DEF IDX
      DEF IDY
      JMP PLOT,I
*
*
*
*  THIS ROUTINE MULTIPLIES THE PLOT CO-ORDINATE
*  BY THE SCALE FACTOR THEN CONVERTS FROM
*  FLOATING POINT TO FIXED.
*         A= X OR Y PLOT CO-ORDINATE ON ENTRY.
*
FPC   NOP
      FMP CFAC      (CO-ORDINATE)(PLOT FACTOR)
      FAD FD05
      JSB IFIX      CONVERT TO FIXED POINT
      JMP FPC,I     EXIT WITH A=FIXED PLOT #.
*
*
*
FPD   NOP
      FMP DFAC
      FAD FD05
      JSB IFIX
      JMP FPD,I
*
*
*
      SKP
*
********************
*
*** PLTLU ***
*
*
*  THE -PLTLU- CALL ALLOWS THE USER TO SET THE
* LOGICAL UNIT NUMBER FOR THE DESIRED PLOTTER.
* THIS CALL MUST BE MADE TO SET THE LU # BEFORE
* THE FIRST CALL TO -PLOT-; OTHERWISE THE SYSTEM
* WILL TERMINATE THE USER PROGRAM BECAUSE OF AN
* I/O REQUEST ERROR "LOGICAL UNIT = ZERO".
*
* * - FORTRAN LINKAGE -
*
*      CALL PLTLU(ILU)
*
*       THE LOGICAL UNIT # MUST BE INTEGER
*
* * - CALLING SEQUENCE :
*
```

```
*       JSB PLTLU     PLOT LU ROUTINE
*       DEF *+2       RETURN
*       DEF ILU       LOCATION OF INTEGER LU #
*
******************
*
*
*
ILU   BSS 1           STORAGE FOR LU # ADDRESS
*
*
PLTLU NOP
      JSB .ENTR       SET ADDRESS OF
      DEF PLTLU-1      PARAMETER IN "ILU".
*
      LDA ILU,I       SET LU #
      STA ILUN         IN LOCAL STORAGE.
*
      JMP PLTLU,I     RETURN
      SKP
*
*
*
************************
*
***** WORKING STORAGE ***
*
*
*  THE FOLLOWING GROUPS OF TWO WORDS MUST BE
*  IN 2 CONSECUTIVE MEMORY LOCATIONS.
*
IDX   OCT 0           ABSOLUTE X DATA FOR PLOTTER
IDY   OCT 0           ABSOLUTE Y DATA FOR PLOTTER
*
XPEN  OCT 0           STORAGE FOR X ORIGIN
YPEN  OCT 0           STORAGE FOR Y ORIGIN
*
IX    OCT 0           REQUIRED X MOVEMENT
IY    OCT 0           REQUIRED Y MOVEMENT
*
PENC  OCT 0           PEN COMMAND (MODE)
ILUN  OCT 0           LU # OF PLOTTER BEING USED
*
C02   OCT 2
FD05  DEC .5
      SKP
*
*  TEKTRONIX 4010 TERMINAL MANIPULATION SECTION
*
```

```
A      EQU 0           A-REGISTER DEFINITION
*
BAKAR OCT 137          BACK-ARROW TO SUPPRESS CR/LF FROM DRIVER
HBAKA OCT 57400        BACK-ARROW IN UPPER ASCII BYTE
ERAS  OCT 15414        ESC+FF CHARACTERS TO ERASE SCREEN
VECT  OCT 16537        GS + BACK-ARROW TO SET VECTOR MODE
ALCUR OCT 17433        US + ESC + SUB + BACK-ARROW TO RETURN TO
CUARO OCT 15137          ALPHA MODE THEN ENABLE GRAPHICS CURSOR
HCPY  OCT 15427        ESC+ETB CHARACTERS TO MAKE HARD COPY
ALPH  OCT 17537        US + BACK-ARROW TO SET ALPHA MODE
*
M2    OCT -2           ASCII CHARACTER COUNTS
M3    OCT -3
M4    OCT -4             FOR RTE/DOS EXEC CALLS
M5    OCT -5
B37   OCT 37           MASK FOR CURSOR-POSITION BYTE
B377  OCT 377          MASK FOR ASCII BYTE
HOBYT OCT 40           HIGH-ORDER BYTE TAG
LXBYT OCT 100          LOW-ORDER X-BYTE TAG
LYBYT OCT 140          LOW-ORDER Y-BYTE TAG
ICOD1 OCT 1            RTE/DOS EXEC-CALL READ CODE
ICOD2 OCT 2            RTE/DOS EXEC-CALL WRITE CODE
INDR  OCT 100000       INDIRECT BIT 15
*
IBUFR BSS 3            RTE/DOS EXEC-CALL BUFFER
IBUFL NOP              RTE/DOS EXEC-CALL BUFFER LENGTH
ICNWD NOP              RTE/DOS EXEC-CALL CONTROL WORD
ARGAD NOP              CALLER ARGUMENT-ADDRESS POINTER
RETAD NOP              CALLER RETURN-ADDRESS POINTER
XSTOR NOP              TEMPORARY X-COORDINATE STORAGE
YSTOR NOP              TEMPORARY Y-COORDINATE STORAGE
LOWX  NOP              TEMPORARY LOW-X BYTE STORAGE
TEMP  NOP              TEMPORARY STORAGE
MODE  NOP              POINT-PLOT MODE SWITCH
*
*
      HED TPLOT
*
*************************************************************
*************************************************************
**                                                         **
**    PLOTTING ROUTINE   "TPLOT"                           **
**                                                         **
**                                                         **
**    CALLING SEQUENCES :                                  **
**                                                         **
**      FORTRAN :   CALL TPLOT(LUN,MODE,IX,IY)             **
**                                                         **
**      ASMB    :   JSB TPLOT                              **
```

```
**                  DEF *+5                                 **
**                  DEF LUN                                 **
**                  DEF MODE                                **
**                  DEF IX                                  **
**                  DEF IY                                  **
**                                                          **
**                                                          **
**    WHERE : LUN  = LOGICAL UNIT NO. OF CRT                **
**            MODE = PLOTTING MODE                          **
**            IX   = X-COORDINATE , 0 TO 1023 MAX.          **
**            IY   = Y-COORDINATE , 0 TO 780 MAX.           **
**                                                          **
**                                                          **
**    PLOTTING MODES ARE AS FOLLOWS :                       **
**                                                          **
**     MODE = 0                                             **
**       THIS PUTS THE CRT INTO LINEAR-INTERPOLATE          **
**       MODE AND PLOTS A DARK VECTOR (INVISIBLE)           **
**       TO THE COORDINATES SPECIFIED .                     **
**       THIS MODE MUST ALWAYS BE CALLED TO PLOT            **
**       THE FIRST POINT OF ANY SEQUENCE WHICH              **
**       INVOLVES BRIGHT-VECTOR PLOTTING .                  **
**                                                          **
**     MODE > 0                                             **
**       THIS MODE DRAWS A BRIGHT LINEAR VECTOR             **
**       FROM ANY PREVIOUS POINT TO THE COORDINATES         **
**       SPECIFIED .  PRIOR TO USING THIS MODE ,            **
**       THE CRT MUST HAVE BEEN PUT IN VECTOR MODE          **
**       BY AN INITIAL MODE-0 PLOT .                        **
**                                                          **
**     MODE < 0                                             **
**       THIS MODE SIMULATES POINT PLOTTING BY              **
**       FIRST DRAWING A DARK VECTOR TO THE GIVEN           **
**       COORDINATES , AND THEN A BRIGHT VECTOR TO          **
**       THE SAME POINT , RESULTING IN A SINGLE             **
**       DOT ON THE SCREEN .                                **
**       MODE 0 NEED NOT BE USED PRIOR TO CALLING           **
**       POINT-PLOT .                                       **
**                                                          **
**                                                          **
**    THE CRT IS LEFT IN VECTOR MODE AFTER CALLING          **
**    ANY OF THESE PLOT ROUTINES .                          **
**                                                          **
**                                                          **
**    THIS ROUTINE CALLS THREE OTHER INTERNAL               **
**    SUBROUTINES :   'ENTRY'   'TKPLT'   'OUT'             **
**                                                          **
**************************************************************
**************************************************************
```

```
*
*
TPLOT NOP
      JSB ENTRY     SET UP THE POINTERS
      LDA ARGAD,I   PASS LOGICAL UNIT
      STA ICNWD       NUMBER TO EXEC CALL
      LDA M2        SET EXEC-CALL LENGTH
      STA IBUFL       TO TWO ASCII CHARACTERS
      ISZ ARGAD     ADVANCE ARGUMENT POINTER
      LDA ARGAD,I   GET THE NEXT ARGUMENT (MODE)
      SZA,RSS       CHECK FOR CASE 1, MODE = 0
      JMP DARK
      SSA           SKIP IF BRIGHT VECTOR
      JMP POINT     CASE 3, MODE < 0
      JMP BRITE     CASE 2, MODE > 0
*
*
*        CASE 1  -  DARK VECTOR
*
DARK  LDA VECT      GET CHARACTER FOR VECTOR MODE
      STA IBUFR       AND PASS IT TO EXEC CALL
      JMP INIT      INITIALIZE CRT
*
*
*        CASE 3  -  POINT-PLOT SIMULATION
*
POINT LDA VECT      GET CHARACTER FOR VECTOR MODE
      STA IBUFR       AND PASS IT TO EXEC CALL
      STA MODE      SET THE POINT-PLOT MODE SWITCH
INIT  JSB OUT       OUTPUT THE VECTOR-MODE CHARACTER
*
*
*        CASE 2  -  BRIGHT VECTOR
*
BRITE ISZ ARGAD     ADVANCE ARGUMENT POINTER
      LDA ARGAD,I   GET X-COORDINATE FROM CALLER
      STA XSTOR       AND SAVE IT LOCALLY
      ISZ ARGAD     ADVANCE ARGUMENT POINTER
      LDA ARGAD,I   GET Y-COORDINATE FROM CALLER
      STA YSTOR       AND SAVE IT LOCALLY
      JSB TKPLT     NOW PLOT THIS POINT
      LDA LOWX      GET LOW-X CURSOR BYTE AGAIN
      LSL 8         SHIFT INTO UPPER ASCII BYTE
      IOR BAKAR     ADD BACK-ARROW
      STA IBUFR       AND PASS IT TO EXEC CALL
      LDA M2        SET EXEC-CALL LENGTH
      STA IBUFL       TO TWO ASCII CHARACTERS
      LDA MODE      LOAD POINT-PLOT MODE SWITCH
      SZA             AND SKIP IF NOT POINT MODE
```

```
      JSB OUT       OUTPUT LOW-X BYTE AGAIN ,
      CLA             (TO PLOT SAME POINT AS BRIGHT)
      STA MODE      RESET POINT-PLOT MODE SWITCH
      JMP RETAD,I   RETURN
*
*
      HED CURSR
*
*****************************************************************
*****************************************************************
**                                                             **
**    CURSOR-COORDINATE ROUTINE    "CURSR"                     **
**                                                             **
**                                                             **
**    CALLING SEQUENCES :                                      **
**                                                             **
**      FORTRAN :   CALL CURSR(LUN,ICHAR,IX,IY)                **
**                                                             **
**      ASMB    :   JSB CURSR                                  **
**                  DEF *+5                                    **
**                  DEF LUN                                    **
**                  DEF ICHAR                                  **
**                  DEF IX                                     **
**                  DEF IY                                     **
**                                                             **
**                                                             **
**    WHERE : LUN   = LOGICAL UNIT NO. OF CRT                  **
**            ICHAR = KEYBOARD CHARACTER FROM CRT              **
**            IX    = CURSOR X-COORDINATE                      **
**            IY    = CURSOR Y-COORDINATE                      **
**                                                             **
**                                                             **
**    THIS ROUTINE PLACES THE CRT IN ALPHA MODE ,              **
**    TURNS ON THE CROSSHAIR CURSOR , AND WAITS                **
**    FOR THE OPERATOR TO ENTER ANY ALPHANUMERIC               **
**    CHARACTER + CARRIAGE-RETURN/LINEFEED .                   **
**                                                             **
**                                                             **
**    WHEN THE CROSSHAIR CURSOR APPEARS , THE                  **
**    OPERATOR ADJUSTS ITS POSITION AS REQUIRED ,              **
**    AND THEN TYPES ANY DESIRED ALPHANUMERIC                  **
**    CHARACTER + CRLF .  THE ASCII VALUE OF THE               **
**    KEYBOARD CHARACTER IS THEN RETURNED TO THE               **
**    CALLING PROGRAM (IN THE LOWER BYTE OF ICHAR) ,           **
**    ALONG WITH THE INTEGER VALUES OF THE X AND Y             **
**    COORDINATES OF THE CROSSHAIR INTERSECTION .              **
**                                                             **
**                                                             **
**    THE USE OF CTRL/A TO CHANGE THE KEYBOARD                 **
```

```
**     CHARACTER ENTRY IS ILLEGAL , SINCE THE DRIVER     **
**     WILL ALTER ONE OF THE COORDINATES INSTEAD .       **
**                                                       **
**                                                       **
**     THE CRT IS LEFT IN ALPHA MODE AFTER CALLING       **
**     THIS ROUTINE .                                    **
**                                                       **
**                                                       **
**     THIS ROUTINE CALLS THREE OTHER INTERNAL           **
**     SUBROUTINES :   'ENTRY'   'IN'   'OUT'            **
**                                                       **
***********************************************************
***********************************************************
*
*
CURSR NOP
      JSB ENTRY      SET UP THE POINTERS
      LDA ARGAD,I    PASS LOGICAL UNIT
      STA ICNWD        NUMBER TO EXEC CALL
      LDA M4         SET EXEC-CALL LENGTH
      STA IBUFL        TO FOUR ASCII CHARACTERS
      LDA ALCUR      PASS ALPHA-MODE ,
      STA IBUFR        CURSOR-ENABLE ,
      LDA CUARO        AND BACK-ARROW
      STA IBUFR+1      CHARACTERS TO EXEC CALL
      JSB OUT        OUTPUT THE CHARACTERS
*
      LDA M5         SET EXEC-CALL LENGTH
      STA IBUFL        TO FIVE ASCII CHARACTERS
      JSB IN           AND WAIT FOR THEM
      LDA IBUFR      GET FIRST WORD RECEIVED
      CLB            ISOLATE KEYBOARD CHARACTER BY
      LSR 8            DISCARDING LOW ASCII BYTE
      ISZ ARGAD      ADVANCE ARGUMENT POINTER
      STA ARGAD,I    RETURN CHARACTER TO CALLER
      LDA IBUFR      GET FIRST WORD AGAIN
      AND B37          AND ISOLATE HIGH-X CURSOR BYTE
      LSL 5          SHIFT IT INTO POSITION
      STA TEMP         AND SAVE IT TEMPORARILY
      LDA IBUFR+1    GET SECOND BUFFER WORD
      LSR 8          DISCARD LOWER ASCII BYTE
      AND B37        ISOLATE LOW-X CURSOR BYTE
      IOR TEMP       ADD HIGH-X BYTE
      ISZ ARGAD      ADVANCE ARGUMENT POINTER
      STA ARGAD,I      AND RETURN X-COORDINATE TO CALLER
      LDA IBUFR+1    GET SECOND BUFFER WORD AGAIN
      AND B37          AND ISOLATE HIGH-Y CURSOR BYTE
      LSL 5          SHIFT IT INTO POSITION
      STA TEMP         AND SAVE IT TEMPORARILY
```

```
      LDA IBUFR+2   GET THIRD BUFFER WORD
      LSR 8         DISCARD LOWER ASCII BYTE
      AND B37       ISOLATE LOW-Y CURSOR BYTE
      IOR TEMP      ADD HIGH-Y BYTE
      ISZ ARGAD     ADVANCE ARGUMENT POINTER
      STA ARGAD,I     AND RETURN Y-COORDINATE TO CALLER
      JMP RETAD,I   RETURN
*
*
      HED ERASE
*
*******************************************************
*******************************************************
**                                                   **
**    CRT SCREEN-ERASE ROUTINE   "ERASE"             **
**                                                   **
**                                                   **
**    CALLING SEQUENCES :                            **
**                                                   **
**      FORTRAN :   CALL ERASE(LUN)                  **
**                                                   **
**      ASMB    :   JSB ERASE                        **
**                  DEF *+2                          **
**                  DEF LUN                          **
**                                                   **
**    WHERE : LUN = LOGICAL UNIT NO. OF CRT          **
**                                                   **
**                                                   **
**    THIS ROUTINE CAUSES THE SCREEN OF THE CRT      **
**    SPECIFIED IN THE CALL TO BE ERASED , AND       **
**    LEAVES IT IN ALPHA MODE WITH THE CURSOR IN     **
**    THE 'HOME' POSITION .                          **
**                                                   **
**                                                   **
**    THIS ROUTINE CALLS TWO OTHER INTERNAL          **
**    SUBROUTINES :   'ENTRY'   'OUT'                **
**                                                   **
*******************************************************
*******************************************************
*
*
ERASE NOP
      JSB ENTRY     SET UP THE POINTERS
      LDA ARGAD,I   PASS LOGICAL UNIT
      STA ICNWD       NUMBER TO EXEC CALL
      LDA M3        SET EXEC-CALL LENGTH
      STA IBUFL       TO THREE ASCII CHARACTERS
      LDA ERAS      GET CHARACTERS TO ERASE SCREEN
      STA IBUFR       AND PASS TO EXEC CALL
```

```
      LDA HBAKA    GET UPPER BACK-ARROW CHARACTER
      STA IBUFR+1    AND PASS TO EXEC CALL
      JSB OUT      OUTPUT THE ERASE COMMAND
      JMP RETAD,I  RETURN
*
*
      HED HCOPY
*
*********************************************************
*********************************************************
**                                                     **
**    HARD-COPY PRODUCTION ROUTINE   "HCOPY"           **
**                                                     **
**                                                     **
**    CALLING SEQUENCES :                              **
**                                                     **
**      FORTRAN :   CALL HCOPY(LUN)                    **
**                                                     **
**      ASMB    :   JSB HCOPY                          **
**                  DEF *+2                            **
**                  DEF LUN                            **
**                                                     **
**                                                     **
**    WHERE : LUN = LOGICAL UNIT NO. OF CRT            **
**                                                     **
**                                                     **
**    THIS ROUTINE , WHICH WORKS ONLY WITH A           **
**    4010-1 TERMINAL EQUIPPED WITH A COPIER ,         **
**    CAUSES IT TO GENERATE ONE HARD COPY               **
**    FOR EACH CALL TO THE ROUTINE .                   **
**                                                     **
**                                                     **
**    AFTER EACH COPY CYCLE , THE TERMINAL IS LEFT     **
**    IN THE MODE IN WHICH THE CALLING PROGRAM         **
**    FOUND IT .                                       **
**                                                     **
**                                                     **
**    THIS ROUTINE CALLS TWO OTHER INTERNAL            **
**    SUBROUTINES :   'ENTRY'   'OUT'                  **
**                                                     **
*********************************************************
*********************************************************
*
*
HCOPY NOP
      JSB ENTRY    SET UP THE POINTERS
      LDA ARGAD,I  PASS LOGICAL UNIT
      STA ICNWD      NUMBER TO EXEC CALL
      LDA M3       SET EXEC-CALL LENGTH
```

```
      STA IBUFL        TO THREE ASCII CHARACTERS
      LDA HCPY       GET CHARACTERS TO MAKE HARD COPY
      STA IBUFR        AND PASS TO EXEC CALL
      LDA HBAKA      GET UPPER BACK-ARROW CHARACTER
      STA IBUFR+1      AND PASS TO EXEC CALL
      JSB OUT        OUTPUT THE COPY COMMAND
      JMP RETAD,I    RETURN
*
*
      HED TKPLT
*
*    THIS SUBROUTINE ASSEMBLES A COORDINATE PAIR AND
*    TRANSMITS IT TO THE TERMINAL , ALONG WITH A BACK-
*    ARROW TO SUPPRESS THE CRLF FROM THE DRIVER .
*
*
TKPLT NOP
      LDA YSTOR      GET THE Y-COORDINATE
      LSR 5          DISCARD THE LOW 5 BITS
      AND B37        ISOLATE HIGH-Y CURSOR BYTE
      IOR HOBYT      ADD HIGH-ORDER TAG BITS
      LSL 8          SHIFT INTO UPPER ASCII BYTE
      STA TEMP         AND SAVE TEMPORARILY
      LDA YSTOR      GET COORDINATE AGAIN
      AND B37        ISOLATE LOW-Y CURSOR BYTE
      IOR LYBYT      ADD LOW-Y TAG BITS
      IOR TEMP       ADD UPPER ASCII BYTE
      STA IBUFR        AND PASS TO EXEC CALL
      LDA XSTOR      GET THE X-COORDINATE
      LSR 5          DISCARD THE LOW 5 BITS
      AND B37        ISOLATE HIGH-X CURSOR BYTE
      IOR HOBYT      ADD HIGH-ORDER TAG BITS
      LSL 8          SHIFT INTO UPPER ASCII BYTE
      STA TEMP         AND SAVE TEMPORARILY
      LDA XSTOR      GET COORDINATE AGAIN
      AND B37        ISOLATE LOW-X CURSOR BYTE
      IOR LXBYT      ADD LOW-X TAG BITS
      STA LOWX       SAVE LOW-X CURSOR BYTE FOR POINT-PLOT
      IOR TEMP       ADD UPPER ASCII BYTE
      STA IBUFR+1      AND PASS TO EXEC CALL
      LDA HBAKA      GET UPPER BACK-ARROW CHARACTER
      STA IBUFR+2      AND PASS TO EXEC CALL
      LDA M5         SET EXEC-CALL LENGTH
      STA IBUFL        TO FIVE ASCII CHARACTERS
      JSB OUT          AND OUTPUT THE POINT
      JMP TKPLT,I    RETURN
*
*
      HED IN
```

```
*
IN     NOP
       JSB EXEC      CALL RTE/DOS EXEC FOR A READ
       DEF *+5         OPERATION
       DEF ICOD1
       DEF ICNWD
       DEF IBUFR
       DEF IBUFL
       JMP IN,I
*
*
       HED OUT
*
OUT    NOP
       JSB EXEC      CALL RTE/DOS EXEC FOR A WRITE
       DEF *+5         OPERATION
       DEF ICOD2
       DEF ICNWD
       DEF IBUFR
       DEF IBUFL
       JMP OUT,I
*
*
       HED ENTRY
*
*     THIS SUBROUTINE SETS UP POINTERS TO THE CALLING
*     PROGRAM'S RETURN ADDRESS AND ARGUMENT LIST .
*
*
ENTRY NOP
       LDA ENTRY     GET (ADDRESS+2) OF OUR CALLER
       ADA M2        SUBTRACT OFF THE TWO
       LDA A,I       FIND WHERE HE WAS CALLED FROM
       IOR INDR      ADD INDIRECT BIT
       STA RETAD       AND SAVE POINTER TO RETURN ADDRESS
       INA           ADVANCE POINTER TO ARGUMENT LIST
       STA ARGAD       AND SAVE FOR THE ROUTINE
       JMP ENTRY,I   RETURN TO LOCAL ROUTINE
*
*
       END
```

Source Code of Subroutine SYMB

```
ASMB,R,F
*
      HED ** REAL-TIME UTILITY ROUTINE - "SYMB" **
      NAM SYMB,7
*
      ENT SYMB
*
      EXT PLOT,SIN,COS,.ENTR,.FDV,ERRO
*
*
*  WRITTEN BY JOHN CARLYLE
*
*
****************************************************
*
* ROUTINE:  SYMB  (SYMBOL)
*
*          -FORTRAN LINKAGE-
*           CALL SYMB(X,Y,SIZE,BCD,THETA,N)
*
*          -CALLING SEQUENCE-
*             JSB SYMB
*             DEF *+7
*             DEF X
*             DEF Y
*             DEF SIZE
*             DEF BCD
*             DEF THETA
*             DEF N
*
*          WHERE  X AND Y ARE THE PAGE COORDINATES
*           OF THE LOWER LEFT CORNER OF THE FIRST
*           CHARACTER. SIZE IS THE DESIRED LETTER
*           HEIGHT. BCD IS THE LOCATION OF THE
*           ASCII ARRAY. THETA IS THE ANGLE OF
*           LETTERING WITH RESPECT TO THE  X-AXIS.
*           N IS THE NUMBER OF ASCII CHARACTERS TO
*           BE DRAWN (FROM THE ASCII ARRAY).
*
*           - X,Y,SIZE AND THETA ARE FLOATING POINT
*            NUMBERS. (THETA IS IN DEGREES).
*
*            N: 1. N IS A POSITIVE INTEGER DEFINING
*                  THE NUMBER OF ASCII CHARACTERS
*                  IN THE ARRAY -BCD-.  (THE ASCII
*                  CHARACTERS ARE PACKED 2 PER WORD
*                  IN THE ARRAY.
*
*               2. N = 0 TO DESIGNATE THAT ONLY ONE
```

```
*                  CHARACTER IS TO BE DRAWN. THE
*                  CHARACTER IS THE LOWER CHARACTER
*                  IN THE WORD SPECIFIED BY BCD.
*
*              3. N IS A NEGATIVE INTEGER TO MEAN
*                  THAT THE BCD VALUE IS AN INTEGER
*                  VALUE SPECIFYING A SPECIAL SYMBOL.
*                  (BCD) IS A POINTER TO THE SPECIAL
*                  SYMBOL TABLE (TAB2).
*
*                 N = -1  INDICATES PEN UP
*                 N < -1  INDICATES PEN DOWN TO
*                          DRAW A LINE FROM CURRENT
*                          POSITION TO POSITION (X,Y)
*
*******************************************************
*
X     DEF FL999    PARAMETER AREA
Y     DEF FL999     (SET BY .ENTR AFTER CALL)
SIZE  DEF OFCT      (INITIALIZED TO FIXED VALUES
BCD   DEF C.02       TO PROTECT ROUTINE FROM SHORT
THETA DEF OTHET      PARAMETER LIST).
N     DEF CM.8
*
*
SYMB  NOP
      JSB .ENTR     SET UP PARAMETER
      DEF SYMB-6     LINKAGE AREA
*
      LDA C.03     INITIALIZE PEN TO
      STA PEN        UP POSITION.
      LDA N,I      CHECK  -N-
      SSA,RSS       IF N >= 0, GO TO
      JMP S1         SET FOR ARRAY PLOT.
*
* SPECIAL CHARACTER   ( N < 0 )
*
      LDB C.02
      CMA,SZA   IF N<=-1 THEN SET PEN=2
      STB PEN       FOR PEN DOWN CONDITION.
      CCA          SET CHCNT = -1 FOR ONE CHAR
      STA CHCNT     TO BE DRAWN.
      LDA TAB2A    SET TABA TO REFERENCE TAB2 -
      STA TABA      SPECIAL CHARACTER TABLE.
      LDA BCD,I    GET CHARACTER VALUE, SAVE AS
      STA CHAR      INDEX TO TAB2.
      ADA CM15     SUBTRACT 15(8) TO CHECK FOR
      SSA,RSS       RANGE  0 TO 14 (CENTERED CHAR)
      JMP S2         -NORMAL OFFSET- (GT 14(8))
```

```
       LDA F4A       SET DIVISOR OF SIZE = 4
       JMP S2+1      GO TO CHECK  X,Y.
*
* ASCII CHARACTER PLOT (ARRAY OR SINGLE CHARACTER)
*
S1     CMA,INA       SET N NEGATIVE -
       STA B         (SAVE TEMPORARILY)
       SZA,RSS       IF N = 0 (SINGLE CHAR PLOT),
       CCA            SET  N = -1.
       STA CHCNT     SET N AS INDEX FOR CHAR. COUNT.
*
       LDA BCD     GET ARRAY ADDRESS - CONVERT TO
       RAL            CHAR. ADDRESS (UPPER CHAR)
       SZB,RSS       IF SINGLE CHAR. OUTPUT, SET ADDR.
       INA            TO LOWER (BIT 0 =1)
       STA ARRAD     SAVE ADDRESS.
       LDA TAB1A     SET TABLE ADDRESS = TAB1A TO
       STA TABA       REFERENCE ASCII SET TABLE.
*
S2     LDA F7A       SET DIVISOR OF SIZE = 7
       STA DIV
       DLD SIZE,I    GET SIZE PARAMETER, DIVIDE BY
       JSB .FDV       7 OR 4 (FLPT) FOR OFFSET.
DIV    NOP           (ADDR OF F7 OR F4 - SET AT S2+1)
       DST FCT       SET FACTOR  (SIZE/DIV).
*
* CHECK FOR NEW THETA (ROTATIONAL) PARAMETER
*
       DLD THETA,I   CHECK NEW THETA
       CPA OTHET      AGAINST OLD THETA VALUE
       RSS             (INITIALIZED TO 0-DEGREES.)
       JMP S3        -NEW-
       CPB OTHET+1
       JMP S4        -SAME AS OLD VALUE-
*
* CONVERT THETA TO RADIANS, COMPUTE SIN, COS
*
S3     DST OTHET     SAVE AS NEW OLD-THETA
       FMP RADN      CONVERT DEGREES TO RADIANS
       DST TEMP1
       JSB SIN       CALCULATE SINE
       JSB ERR0
       DST INCS
       DLD TEMP1
       JSB COS       CALCULATE COSINE
       JSB ERR0
       DST INCC
       DLD FCT
       JMP S5
```

```
*
* CHECK FOR NEW FACTOR PARAMETER (SIZE/DIV)
*
S4     DLD FCT     CHECK FOR CHANGE IN
       CPA OFCT        FACTOR
       RSS
       JMP S5        -NEW-
       CPB OFCT+1
       JMP S8       -SAME AS OLD VALUE
*
* CALCULATE POINT FACTORS FOR POINT (X1,Y1)
*
S5     DST OFCT     SET NEW VALUE AS OLD FACTOR
       FMP INCC     CALCULATE  XA1 = FCT * INCC
       DST XA1
       DLD OFCT
       FMP INCS     CALCULATE  YA1 = FCT * INCS
       DST YA1
*
* CALCULATE POINT FACTORS FOR 10X10 MATRIX (2 TO 9)
*
       LDA XA2A     SET ADDR. FOR
       STA TEMP1      XA(2)
       LDA CM.8     SET INDEX FOR RANGE
       STA TEMP2      XA(2)  TO  XA(9)
       DLD XA1      XA(I) = XA(1) + XA(I-1)
S6     FAD XA1
       DST TEMP1,I   SET  XA(I) FOR I = 2-9
       ISZ TEMP1     -SET ADDR.
       ISZ TEMP1           FOR NEXT FLPT NUMBER.
       ISZ TEMP2          INDEX FOR 2 TO 9
       JMP S6             -CONTINUE
*
       LDA YA2A          REPEAT
       STA TEMP1          ABOVE
       LDA CM.8            PROCESSING
       STA TEMP2            FOR
       DLD YA1               YA(2) TO YA(9)
S7     FAD YA1                ACCORDING TO:
       DST TEMP1,I
       ISZ TEMP1          YA(I) = YA(1) + YA(I-1)
       ISZ TEMP1
       ISZ TEMP2
       JMP S7
*
* PROCESS X,Y COORDINATES IN CALL
*
S8     DLD X,I      IF -X- IS GT OR = TO
       FSB FL999      999.0,
```

```
        SSA,RSS          THEN USE
        JMP S9            PREVIOUS X-ORIGIN
*
        DLD X,I       SET  X-ORIGIN:
        FSB XA2
        FAD YA2         XORG = X - XA(2) + YA(2)
        DST XORG
*
S9      DLD Y,I       IF -Y- IS GT OR = TO
        FSB FL999       999.0,
        SSA,RSS          THEN USE
        JMP S10           PREVIOUS Y-ORIGIN
*
        DLD Y,I       SET Y-ORIGIN:
        FSB XA2
        FSB YA2         YORG = Y - XA(2) - YA(2)
        DST YORG
*
S10     LDB N,I       IF N < 0, THEN SET
        LDA CHAR       (A) = CHAR INDEX
        SSB             AND GO TO
        JMP S12          GET CHAR. OFFSETS.
*
* EXTRACT CHAR FROM BCD ARRAY AND INDEX TO TABLES
*
S11     LDA ARRAD     GET CURRENT CHARACTER ADDRESS
        ISZ ARRAD      - SET FOR NEXT CHARACTER ADDR.-
        CLE,ERA       CONVERT TO WORD ADDR - POSITION
        LDA A,I         IN E.  GET WORD AND POSITION
        SEZ,RSS        UPPER (=0) OR LOWER (=1)
        ALF,ALF          CHARACTER
        AND M77           IN A. (USE ONLY LOW 6-BITS)
*
S12     ADA TABA      SET APPROPRIATE TABLE
        STA TEMP1      ADDRESS -
        LDA A,I       GET TABLE VALUE FOR -CHAR-
        AND M377      GET ADDR OF FIRST OFFSET WORD
        ADA TABLA      IN OFFSET TABLE - CONVERT TO
        RAL             UPPER POSITION
        STA OFFST        CHARACTER ADDRESS.
        LDA TEMP1,I   GET TABLE WORD AGAIN.
        SSA           IF BIT 15 = 1, SET OFFSET ADDRESS
        ISZ OFFST      TO LOWER POSITION.
        ALF,ALF       ROTATE OFFSET COUNT TO
        AND M177       LOW A (7-BITS) AND SET
        CMA,INA         NEGATIVE FOR
        STA OFFCT        INDEX FOR INDEX FACTORS
*
* EXTRACT AND PROCESS EACH OFFSET PAIR FOR CHARACTER
```

Source Code of Subroutine SYMB

```
*
S13    LDA OFFST    GET CURRENT OFFSET-PAIR CHARACTER
       ISZ OFFST     ADDRESS, SET FOR NEXT ADDRESS.
       CLE,ERA      CONVERT TO WORD ADDR, SET POSI-
       LDA A,I       TION IN E, GET OFFSET WORD.
       SEZ          SHIFT OFFSET PAIR TO UPPER A,
       ALF,ALF       (X,Y) OF 8-BITS.
       AND M1774    ISOLATE AND
       STA B         SAVE  X,Y.
       ALF          PUT X
       AND M17       IN LOW A,
       ALS            MULTIPLY BY 2
       STA TEMP1       AND SAVE FOR INDEX TO XA-ARRAY
       LDA B        PUT
       ALF,ALF       Y IN LOW A,
       AND M17        MULTIPLY
       ALS             BY 2
       STA TEMP2        AND SAVE FOR INDEX TO YA.
       LDA M36      IF X OFFSET = 17(8) FOR
       LDB C.03      PEN-UP, THEN
       CPA TEMP1      GO TO SET IC AND GET
       JMP S14         NEXT OFFSET PAIR.
*
       LDA XAD      COMPUTE ADDRESS OF
       ADA TEMP1      XA-ARRAY FOR X-OFFSET
       STA TEMP3
       LDA YAD      COMPUTE ADDRESS OF
       ADA TEMP2      YA-ARRAY FOR  Y-OFFSET
       STA TEMP4
       DLD XORG     COMPUTE:
       FAD TEMP3,I
       FSB TEMP4,I   XT = XORG + XA(KX) - YA(KY)
       DST XT
*
       LDA YAD      COMPUTE ADDRESS OF
       ADA TEMP1      YA-ARRAY FOR  X-OFFSET
       STA TEMP3
       LDA XAD      COMPUTE ADDRESS OF
       ADA TEMP2      XA-ARRAY FOR Y-OFFSET
       STA TEMP4
       DLD YORG     COMPUTE
       FAD TEMP3,I
       FAD TEMP4,I   YT = YORG + YA(KX) + XA(KY)
       DST YT
*
* CALL FOR PLOT FOR CURRENT XT,YT
*
       JSB PLOT
       DEF *+4
```

```
       DEF XT
       DEF YT
       DEF PEN
*
*
       LDB C.02     SET FOR PEN DOWN
S14    STB PEN
*
       ISZ OFFCT    INDEX CHARACTER OFFSET COUNT
       JMP S13       - MORE TO PROCESS -
*
* SET X-ORIGIN AND Y-ORIGIN FOR NEXT CHARACTER.
*
       DLD XORG
       FAD XA7      X-ORIGIN = X-ORIGIN + XA(7)
       DST XORG
*
       DLD YORG
       FAD YA7      Y-ORIGIN = Y-ORIGIN + YA(7)
       DST YORG
       LDA C.03
       STA PEN
*
       ISZ CHCNT    INDEX CHARACTER COUNTER
       JMP S11       - MORE TO PLOT -
*
* CALL TO SYMB COMPLETED
*
       JMP SYMB,I
*
*
* CONSTANT, FLAG AND STORAGE SECTION
*
A      EQU 0        A, B
B      EQU 1         REGISTERS
*
C.02   DEC 2
C.03   DEC 3
CM.8   DEC -8
CM15   DEC -15
*
M17    OCT 17
M36    OCT 36
M77    OCT 77
M177   OCT 177
M377   OCT 377
M1774  OCT 177400
*
FL999 DEC 999.0
```

```
*
F4A   DEF F4
F4    DEC 4.0
F7A   DEF F7
F7    DEC 7.0
*
PEN   NOP
*
CHCNT NOP
CHAR  NOP
OFFST NOP
OFFCT NOP
ARRAD NOP
*
TEMP1 NOP     TEMPORARY
TEMP2 NOP
TEMP3 NOP      STORAGE
TEMP4 NOP
*
INCS  DEC 0.
INCC  DEC 1.0
*
FCT   DEC 0.
OFCT  DEC .02  FOR .14 INCH INCREMENTS (.01 FOR .07)
*
OTHET DEC 0.   INITIALIZE TO ZERO DEGREES ROTATION
*
RADN  DEC .0174533  FACTOR FOR DEGREES TO RADIANS
*
*
*
XAD   DEF XA0
XA2A  DEF XA2
*
XA0   DEC .00      INITIAL
XA1   DEC .02       VALUES
XA2   DEC .04        SET
XA3   DEC .06         FOR
XA4   DEC .08          .14 INCH
XA5   DEC .10           INCREMENTS
XA6   DEC .12
XA7   DEC .14      (FOR .07 INCH INCREMENTS,
XA8   DEC .16        HALVE VALUES)
XA9   DEC .18
*
*
*
YAD   DEF YA0
YA2A  DEF YA2
```

```
*
YA0   DEC 0.
YA1   DEC 0.
YA2   DEC 0.
YA3   DEC 0.
YA4   DEC 0.
YA5   DEC 0.
YA6   DEC 0.
YA7   DEC 0.
YA8   DEC 0.
YA9   DEC 0.
*
*
*
XORG  DEC 0.
YORG  DEC 0.
*
XT    DEC 0.
YT    DEC 0.
*
*
TABA  NOP
*
TAB1A DEF TAB1
*
TAB2A DEF TAB2
*
*
* CHARACTER REFERENCE TABLES -
*
*  THE FOLLOWING TABLES (TAB1 AND TAB2) CONTAIN
*   THE INFORMATION TO ACCESS THE OFFSET TABLE
*   FOR EACH AVAILABLE CHARACTER.
*
*  EACH CHARACTER OR SPECIAL SYMBOL AVAILABLE
*   FOR PLOTTING IS ASSOCIATED WITH ONE UNIQUE
*   WORD IN ONE OF THE FOLLOWING TABLES.
*
*  EACH REFERENCE WORD CONTAINS THE FOLLOWING
*   INFORMATION:
*      1. RELATIVE ADDRESS OF WORD IN OFFSET TABLE
*          FOR START OF OFFSET STRING
*           (BITS 07-00)
*      2. NUMBER OF OFFSET PAIRS (8-BITS) IN STRING
*           (BITS 14-08)
*      3. STARTING POSITION OF STRING IN WORD,
*          0 MEANS UPPER, 1 MEANS LOWER.
*           (BIT  15)
*
```

```
*  TAB1  COMPRISES THE STANDARD CHARACTER SET
*  TAB2  COMPRISES SPECIAL CHARACTERS AND
*         CENTERED SYMBOLS WHICH CAN BE ACCESSED
*         BY POSITION WHEN PARAMETER N < 0, IN CALL.
*
*   TAB1 IS ORDERED BY POSITION DESIGNATED BY LOWER
*         6-BITS OF ASCII CODE  (E.G. A = 101 = 01)
*        - THIS TABLE IS LIMITED TO 64 ENTRIES - 00
*           TO 77.
*
*
*  POS CNT ADDR    CODE    CHARACTER
*  --- --- ----    ----    ---------
*
TAB2  OCT 103641   1   7   241     00
      OCT 106244   1  14   244     01
      OCT 003252   0   6   252     02
      OCT 003660   0   7   260     03
      OCT 103663   1   7   263     04
      OCT 003666   0   7   266     05
      OCT 003671   0   7   271     06
      OCT 004274   0  10   274     07
      OCT 005700   0  13   300     08
      OCT 003705   0   7   305     09
      OCT 007310   0  16   310     10
      OCT 006660   0  15   260     11
      OCT 103316   1   6   316     12
      OCT 002260   0   4   260     13
      OCT 006252   0  14   252     14
      OCT 101321   1   2   321     15
      OCT 101325   1   2   325     16
      OCT 102726   1   5   326     17
      OCT 103233   1   6   233     18
      OCT 104321   1  10   321     19
      OCT 002731   0   5   331     20
      OCT 102733   1   5   333     21
      OCT 103236   1   6   236     22
      OCT 001746   0   3   346     23
      OCT 004336   0  10   336     24
      OCT 004342   0  10   342     25
*
*
*
TAB1  OCT 110347   1  20   347     00          @
      OCT 004400   0  11     0     01          A
      OCT 106005   1  14     5     02          B
      OCT 104014   1  10    14     03          C
      OCT 103404   1   7     4     04          D
      OCT 003422   0   7    22     05          E
```

```
OCT 003022  0   6   22  06   F
OCT 006036  0  14   36  07   G
OCT 103025  1   6   25  10   H
OCT 003044  0   6   44  11   I
OCT 103047  1   6   47  12   J
OCT 003033  0   6   33  13   K
OCT 001425  0   3   25  14   L
OCT 102431  1   5   31  15   M
OCT 102030  1   4   30  16   N
OCT 004414  0  11   14  17   O
OCT 103453  1   7   53  20   P
OCT 006014  0  14   14  21   Q
OCT 104453  1  11   53  22   R
OCT 006460  0  15   60  23   S
OCT 102066  1   4   66  24   T
OCT 003447  0   7   47  25   U
OCT 001473  0   3   73  26   V
OCT 002452  0   5   52  27   W
OCT 102474  1   5   74  30   X
OCT 002477  0   5   77  31   Y
OCT 103467  1   7   67  32   Z
OCT 002156  0   4  156  33
OCT 001076  0   2   76  34
OCT 002160  0   4  160  35
OCT 002562  0   5  162  36
OCT 102564  1   5  164  37   _
OCT 100471  1   1   71  40
OCT 003574  0   7  174  41   !
OCT 004577  0  11  177  42   "
OCT 105603  1  13  203  43   #
OCT 006611  0  15  211  44   $
OCT 106217  1  14  217  45   %
OCT 105357  0  12  357  46   &
OCT 002177  0   4  177  47   '
OCT 002152  0   4  152  50   (
OCT 002154  0   4  154  51   )
OCT 005542  0  13  142  52   *
OCT 002542  0   5  142  53   +
OCT 103230  1   6  230  54   ,
OCT 101143  1   2  143  55   -
OCT 102630  1   5  230  56   .
OCT 101074  1   2   74  57   /
OCT 105013  1  12   13  60   0
OCT 102501  1   5  101  61   1
OCT 004504  0  11  104  62   2
OCT 006524  0  15  124  63   3
OCT 102110  1   4  110  64   4
OCT 105112  1  12  112  65   5
OCT 106113  1  14  113  66   6
```

```
      OCT 102521   1   5   121    67        7
      OCT 010524   0  21   124    70        8
      OCT 105534   1  13   134    71        9
      OCT 105625   1  13   225    72        :
      OCT 106225   1  14   225    73        ;
      OCT 001635   0   3   235    74        <
      OCT 102547   1   5   147    75        =
      OCT 001640   0   3   240    76        >
      OCT 007167   0  16   167    77        ?
*
*
*
*
* CHARACTER - OFFSET - TABLE
*   -EACH WORD CONTAINS 2 PAIRS OF X,Y  OFFSETS,
*       "X1Y1X2Y2", EACH PAIR IS 8-BITS AND 4
*       BITS IN EACH PAIR SPECIFY THE X AND Y POINT
*       FOR THE OFFSET.
*
* THE STRING OF OFFSET PAIRS FOR A CHARACTER MAY
*  START IN THE UPPER OR LOWER POSITION OF A
*  WORD.  THE STARTING LOCATION, POSITION INDICATOR
*  AND OFFSET COUNT FOR EACH CHARACTER IS CONTAINED
*  IN THE REFERENCE TABLES.
*
*
* PORTIONS OF OFFSET STRINGS MAY OVERLAP OTHER
*  STRINGS WHEN LINE SEGMENTS AMONG CHARACTERS
*  ARE IDENTICAL.
*
*
TABLA DEF TABLE    DEFINE STARTING ADDRESS OF TABLE
*
*  OCTAL PAIRS  ADDRESS SYMBOL
*
TABLE OCT 021045    2-2  2-5       00    +A
      OCT 062445    6-5  2-5
      OCT 024071    2-10 3-11
      OCT 054550    5-11 6-10
      OCT 061131    6-2  5-11            -D
      OCT 064143    6-10 6-3             -B
      OCT 051042    5-2  2-2
      OCT 024531    2-11 5-11
      OCT 064147    6-10 6-7       10
      OCT 053046    5-6  2-6
      OCT 053145    5-6  6-5
      OCT 061527    6-3  5-7             -0
      OCT 064143    6-10 6-3             +Q,+0,-C
      OCT 051062    5-2  3-2
```

```
OCT 021450   2-3  2-10
OCT 034531   3-11 5-11
OCT 064360   6-10 17-0     20
OCT 042142   4-4  6-2
OCT 064451   6-11 2-11          +E,+F
OCT 023126   2-6  5-6
OCT 023042   2-6  2-2
OCT 061042   6-2  2-2           +L,-H
OCT 024446   2-11 2-6
OCT 063151   6-6  6-11
OCT 061042   6-2  2-2      30   -N
OCT 024542   2-11 6-2           -M
OCT 064506   6-11 4-6
OCT 024442   2-11 2-2           +K
OCT 022551   2-5  6-11
OCT 033142   3-6  6-2
OCT 072525   7-5  5-5           +G
OCT 062543   6-5  6-3
OCT 051062   5-2  3-2      40
OCT 021450   2-3  2-10
OCT 034531   3-11 5-11
OCT 064147   6-10 6-7
OCT 051062   5-2  3-2           +I
OCT 041111   4-2  4-11
OCT 034531   3-11 5-11
OCT 024444   2-11 2-4           +U,-J
OCT 021462   2-3  3-2      50
OCT 051143   5-2  6-3
OCT 064542   6-11 6-2           +W
OCT 043042   4-6  2-2           -P,-R
OCT 024531   2-11 5-11
OCT 064147   6-10 6-7
OCT 053046   5-6  2-6
OCT 043142   4-6  6-2
OCT 022043   2-4  2-3      60   +S
OCT 031122   3-2  5-2
OCT 061545   6-3  6-5
OCT 053066   5-6  3-6
OCT 023450   2-7  2-10
OCT 034531   3-11 5-11
OCT 064102   6-10 4-2           -T
OCT 044451   4-11 2-11          -Z
OCT 064442   6-11 2-2      70
OCT 061360   6-2  17-0          -(PEN UP)
OCT 033126   3-6  5-6
OCT 024502   2-11 4-2           +V
OCT 064442   6-11 2-2           -X,-/
OCT 064760   6-11 17-0
OCT 024542   2-11 6-2           +
```

```
OCT 024506     2-11 4-6              +Y
OCT 041106     4-2  4-6       100
OCT 064522     6-11 5-2              -1
OCT 031102     3-2  4-2
OCT 044470     4-11 3-10
OCT 023450     2-7  2-10             +2
OCT 034531     3-11 5-11
OCT 064147     6-10 6-7
OCT 021442     2-3  2-2
OCT 061122     6-2  5-2       110    -4
OCT 054444     5-11 2-4
OCT 062151     6-4  6-11             -5
OCT 024446     2-11 2-6              -6
OCT 053145     5-6  6-5
OCT 061522     6-3  5-2
OCT 031043     3-2  2-3
OCT 022050     2-4  2-10
OCT 034531     3-11 5-11      120
OCT 064050     6-10 2-10             -7
OCT 024551     2-11 6-11
OCT 064102     6-10 4-2
OCT 024071     2-10 3-11             +8,+3
OCT 054550     5-11 6-10
OCT 063526     6-7  5-6
OCT 033126     3-6  5-6
OCT 062543     6-5  6-3       130
OCT 051062     5-2  3-2
OCT 021445     2-3  2-5
OCT 033047     3-6  2-7
OCT 024043     2-10 2-3              +9
OCT 031122     3-2  5-2
OCT 061550     6-3  6-10
OCT 054471     5-11 3-11
OCT 024046     2-10 2-6       140
OCT 032545     3-5  6-5
OCT 041507     4-3  4-7              ++,+*
OCT 042445     4-5  2-5              --
OCT 062505     6-5  4-5
OCT 021547     2-3  6-7
OCT 042447     4-5  2-7
OCT 061446     6-3  2-6              -=
OCT 063360     6-6  17-0      150
OCT 021543     2-3  6-3
OCT 041063     4-2  3-3              +(
OCT 034111     3-10 4-11
OCT 041123     4-2  5-3              +)
OCT 054111     5-10 4-11
OCT 051062     5-2  3-2              +[
OCT 034531     3-11 5-11
```

```
OCT 031122   3-2  5-2    160   +]
OCT 054471   5-11 3-11
OCT 041111   4-2  4-11         +
OCT 034130   3-10 5-10
OCT 044545   4-11 6-5
OCT 022466   2-5  3-6
OCT 032045   3-4  2-5
OCT 023450   2-7  2-10         +?
OCT 034531   3-11 5-11   170
OCT 064147   6-10 6-7
OCT 053106   5-6  4-6
OCT 042360   4-4  17-0
OCT 031122   3-2  5-2          +!
OCT 041462   4-3  3-2
OCT 170104   17-0 4-4
OCT 044507   4-11 4-7          +',+"
OCT 054511   5-11 4-11   200
OCT 170051   17-0 2-11
OCT 023471   2-7  3-11
OCT 024463   2-11 3-3          -#
OCT 033466   3-7  3-6
OCT 023146   2-6  6-6
OCT 053127   5-6  5-7
OCT 051524   5-3  5-4
OCT 062044   6-4  2-4    210
OCT 022063   2-4  3-3          +$
OCT 051544   5-3  6-4
OCT 062446   6-5  2-6
OCT 023470   2-7  3-10
OCT 054147   5-10 6-7
OCT 170111   17-0 4-11
OCT 041050   4-2  2-10         -%
OCT 034071   3-10 3-11   220
OCT 024360   2-10 17-0
OCT 021151   2-2  6-11
OCT 170142   17-0 6-2
OCT 061522   6-3  5-2
OCT 061107   6-2  4-7
OCT 043126   4-6  5-6
OCT 053507   5-7  4-7
OCT 170123   17-0 5-3
OCT 041504   4-3  4-4
OCT 052123   5-4  5-3
OCT 041043   4-2  2-3
OCT 061760   6-3  17-0
OCT 062046   6-4  2-6          +>
OCT 064043   6-10 2-3          -
OCT 061760   6-3  17-0
OCT 022146   2-4  6-6    240   +>
```

```
OCT 024042    2-10 2-2
OCT 042004    4-4  0-4
OCT 000100    0-0  4-0
OCT 042042    4-4  2-2
OCT 022024    2-4  1-4
OCT 001401    0-3  0-1
OCT 010060    1-0  3-0
OCT 040503    4-1  4-3       250
OCT 032044    3-4  2-4
OCT 021044    2-2  2-4
OCT 000501    0-1  4-1
OCT 022042    2-4  2-2
OCT 021403    2-3  0-3
OCT 020103    2-0  4-3
OCT 021442    2-3  2-2
OCT 021044    2-2  2-4       260
OCT 020042    2-0  2-2
OCT 001102    0-2  4-2
OCT 021004    2-2  0-4
OCT 040042    4-0  2-2
OCT 000104    0-0  4-4
OCT 021044    2-2  2-4
OCT 001040    0-2  2-0
OCT 041044    4-2  2-4       270
OCT 021002    2-2  0-2
OCT 022040    2-4  2-0
OCT 022102    2-4  4-2
OCT 021004    2-2  0-4
OCT 042042    4-4  2-2
OCT 000042    0-0  2-2
OCT 040042    4-0  2-2
OCT 021022    2-2  1-2       300
OCT 031042    3-2  2-2
OCT 042004    4-4  0-4
OCT 042000    4-4  0-0
OCT 040000    4-0  0-0
OCT 021004    2-2  0-4
OCT 021104    2-2  4-4
OCT 021040    2-2  2-0
OCT 021104    2-2  4-4       310
OCT 031423    3-3  1-3
OCT 002023    0-4  1-3
OCT 010400    1-1  0-0
OCT 010461    1-1  3-1
OCT 040061    4-0  3-1
OCT 031442    3-3  2-2
OCT 002104    0-4  4-4
OCT 000100    0-0  4-0       320
OCT 021042    2-2  2-2
```

```
      OCT 061360    6-2  17-0
      OCT 022545    2-5  6-5
      OCT 170050    17-0 2-10
      OCT 064051    6-10 2-11              -1,#16
      OCT 021111    2-2  4-11              -
      OCT 041063    4-2  3-3
      OCT 051502    5-3  4-2         330
      OCT 022545    2-5  6-5               +
      OCT 053124    5-6  5-4
      OCT 062562    6-5  7-2
      OCT 021126    2-2  5-6
      OCT 024571    2-11 7-11
      OCT 023146    2-6  6-6               +
      OCT 170043    17-0 2-3
      OCT 061760    6-3  17-0        340
      OCT 053462    5-7  3-2
      OCT 021543    2-3  6-3               +
      OCT 170046    17-0 2-6
      OCT 063106    6-6  4-6
      OCT 044104    4-10 4-4         345
      OCT 021507    2-3  4-7               +
      OCT 061544    6-3  6-4               -@
      OCT 051463    5-3  3-3         350
      OCT 022047    2-4  2-7
      OCT 034130    3-10 5-10
      OCT 063545    6-7  6-5
      OCT 052104    5-4  4-4
      OCT 032466    3-5  3-6
      OCT 043527    4-7 5-7
      OCT 063142    6-6 6-2
      OCT 033470    3-73-10
      OCT 044530    4-11 5-10
      OCT 022444    2-5 2-4
      OCT 031503    3-3 3-4
      OCT 062000    6-4
*
*
      END
```

Source Code of Program PLTME

```
FTN4
C
      PROGRAM PLTME
C
C
C  THIS PROGRAM WILL MAKE A TIME DOMAIN PLOT OF AN ACOUSTIC
C  EMISSION SIGNAL RECORDED ON THE KENNEDY 9000 TAPE DECK.
C  THE USER HAS THE OPTION OF VIEWING THE WAVEFORMS ONLY, OR
C  VIEWING AND WRITING GOOD WAVEFORM NUMBERS TO A DISC FILE.
C
C
C  WRITTEN BY JOHN CARLYLE
C
C
      DIMENSION LU(5),IREG(2),INBUF(36),IPBUF(10),IBUF(36)
      DIMENSION IDCB1(144),ITPNM(12),LVOLT(3),LTIME(6)
      DIMENSION TRX(2048),NTAPE(1024),IREC2(512)
      EQUIVALENCE (REG,IREG),(TRX(1537),NTAPE)
      EQUIVALENCE (NTAPE(513),IREC2)
      LOGICAL VIEW,EOF
      DATA ICNT/1/,IUSLA/17537B/,EOF/.FALSE./,VIEW/.TRUE./
      DATA LVOLT/2HVO,2HLT,2HS /,MINUS/26400B/
      DATA LTIME/2HMI,2HCR,2HOS,2HEC,2HON,2HDS/
C
C  RECOVER PARAMETERS, REWIND TAPE, AND DETERMINE MODE
C
      CALL RMPAR(LU)
      IF(LU(1).EQ.0) LU(1)=1
      ILU=LU(1)+400B
      CALL EXEC(3,410B)
      CALL PLTLU(LU(1))
      WRITE(LU(1),10)
   10 FORMAT("/PLTME: VIEW WAVEFORMS ONLY? _")
      READ(LU(1),20) IV
   20 FORMAT(A2)
      IF(IV.EQ.47117B) VIEW=.FALSE.
      IF(VIEW) GO TO 210
C
C  GET 'NAMR' INFORMATION AND CREATE FILE FOR NON-VIEW MODE
C
   30 WRITE(LU(1),40)
   40 FORMAT("/PLTME: ENTER 'NAMR' FOR DATA FILE: _")
      REG=EXEC(1,ILU,INBUF,-72)
      ISCHR=1
      IF(NAMR(IPBUF,INBUF,IREG(2),ISCHR)) 30,50
   50 IREG(1)=-1
      IREG(2)=0
      CALL CREAT(IDCB1,IERR,IPBUF,IREG,3,IPBUF(5),IPBUF(6))
      IF(IERR.GE.0) GO TO 70
```

```
      ITRY=ITRY+1
      IF(ITRY.GE.3) GO TO 110
      WRITE(LU(1),60) IERR
   60 FORMAT("/PLTME: FILE ERROR ",I4,".  TRY AGAIN!",/)
      GO TO 30
C
C GET HEADER DATA AND WRITE IT TO DATA FILE FOR NON-VIEW MODE
C
   70 WRITE(LU(1),80)
   80 FORMAT("/PLTME: TYPE IN ONE LINE OF HEADER DATA.",/)
      REG=EXEC(1,ILU,INBUF,36)
      CALL CODE(IREG(2)*2)
      READ(INBUF,*) (TRX(I),I=1,5)
      IF(TRX(1).NE.0.0) GO TO 140
      IF(ITRY.NE.0) GO TO 100
      DO 90 I=1,36
      IBUF(I)=INBUF(I)
   90 CONTINUE
      INDNT=(73-IREG(2)*2)*7
      ITRY=1
  100 CALL WRITF(IDCB1,IERR,INBUF,IREG(2))
      IF(IERR.GE.0) GO TO 70
  110 WRITE(LU(1),120) IERR
  120 FORMAT("/PLTME: FILE ERROR ",I4,".  ABORTING PROGRAM!",/)
  130 CALL PURGE(IDCB1,IERR,IPBUF,IPBUF(5),IPBUF(6))
      GO TO 620
  140 VOLTS=TRX(1)
      RATE=TRX(2)
      CALL WRITF(IDCB1,IERR,INBUF,IREG(2))
      IF(IERR.LT.0) GO TO 110
  150 WRITE(LU(1),160)
  160 FORMAT("/PLTME: ENTER TAPE FILE NUMBER: _")
      REG=EXEC(1,ILU,INBUF,36)
      CALL CODE(IREG(2)*2)
      READ(INBUF,*) IFILE
      IF(IFILE.LE.0) GO TO 150
      CALL WRITF(IDCB1,IERR,INBUF,IREG(2))
      IF(IERR.LT.0) GO TO 110
C
C POSITION TO PROPER TAPE FILE FOR BOTH MODES
C
  170 IF(ICNT.EQ.IFILE) GO TO 200
      ICNT=ICNT+1
      CALL EXEC(3,1310B)
      REG=EXEC(3,610B)
      IREG(1)=IAND(73B,IREG(1))
      IF(IREG(1).EQ.0) GO TO 170
  180 WRITE(LU(1),190) IREG(1)
  190 FORMAT("/PLTME: MAG TAPE STATUS = ",O3,"B.  ABORTING ",
```

```
      +"PROGRAM!",/)
       GO TO 130
   200 IF(VIEW) GO TO 250
       IWAVE=IWAVE+1
       GO TO 360
C
C  GET WAVEFORM DATA FOR VIEWING ONLY MODE
C
   210 WRITE(LU(1),220)
   220 FORMAT("/PLTME: ENTER GRAPH TITLE:")
       REG=EXEC(1,ILU,IBUF,-72)
       INDNT=(73-IREG(2))*7
       WRITE(LU(1),230)
   230 FORMAT("/PLTME: ENTER ATTENUATOR SETTING AND SAMPLING ",
      +"RATE: _")
       READ(LU(1),*) VOLTS,RATE
   240 WRITE(LU(1),160)
       READ(LU(1),*) IFILE
       IF(IFILE.LE.0) GO TO 240
       GO TO 170
   250 ICNT=0
   260 ICNT=ICNT+1
   270 WRITE(LU(1),280)
   280 FORMAT("/PLTME: ENTER WAVEFORM NUMBER  _")
       READ(LU(1),*) IWAVE
       IF(IWAVE.LE.0) GO TO 270
       IF(IWAVE-ICNT) 340,360,290
C
C  POSITION TO PROPER RECORD FOR VIEWING MODE
C
   290 IF(IWAVE.EQ.ICNT) GO TO 360
       ICNT=ICNT+1
       DO 300 I=1,2
       CALL EXEC(3,310B)
       REG=EXEC(3,610B)
       IREG(1)=IAND(373B,IREG(1))
       IF(IREG(1).EQ.200B) EOF=.TRUE.
       IF(IREG(1).LT.200B.AND.IREG(1).NE.0) GO TO 180
   300 CONTINUE
       IF(.NOT.EOF) GO TO 290
   310 WRITE(LU(1),320)
   320 FORMAT("/PLTME: WAVEFORM NUMBER TOO BIG!",/)
       EOF=.FALSE.
       DO 330 I=1,2
       CALL EXEC(3,1410B)
       REG=EXEC(3,610B)
       IREG(1)=IAND(73B,IREG(1))
       IF(IREG(1).NE.0) GO TO 180
   330 CONTINUE
```

```
      IF(IFILE.EQ.1) GO TO 250
      CALL EXEC(3,310B)
      GO TO 250
  340 IF(IWAVE.EQ.ICNT) GO TO 360
      ICNT=ICNT-1
      DO 350 I=1,2
      CALL EXEC(3,210B)
      REG=EXEC(3,610B)
      IREG(1)=IAND(373B,IREG(1))
      IF(IREG(1).NE.0) GO TO 180
  350 CONTINUE
      GO TO 340
C
C  READ IN DATA AND UNPACK IT FOR BOTH MODES
C
  360 CALL ERASE(LU(1))
      CALL EXEC(1,110B,NTAPE,512)
      REG=EXEC(3,610B)
      IREG(1)=IAND(373B,IREG(1))
      IF(IREG(1).EQ.200B) EOF=.TRUE.
      IF(IREG(1).LT.200B.AND.IREG(1).NE.0) GO TO 180
      IF(EOF) GO TO 370
      CALL EXEC(1,110B,IREC2,512)
      REG=EXEC(3,610B)
      IREG(1)=IAND(373B,IREG(1))
      IF(IREG(1).EQ.200B) EOF=.TRUE.
      IF(IREG(1).LT.200B.AND.IREG(1).NE.0) GO TO 180
      IF(.NOT.EOF) GO TO 380
  370 IF(VIEW) GO TO 310
      GO TO 570
  380 DO 390 L=1,2047,2
      LN=(L+1)/2
      L2=L+1
      IREG(2)=IAND(377B,NTAPE(LN))
      IREG(1)=JSHFT(NTAPE(LN),8)
      IREG(1)=IAND(377B,IREG(1))
      TRX(L)=FLOAT(IREG(1)-128)
      TRX(L2)=FLOAT(IREG(2)-128)
  390 CONTINUE
C
C  FIND MAX AND MIN OF DATA AND OBTAIN MAGNIFIER FOR BOTH MODES
C
      TMAX=-128
      TMIN=127
      DO 400 I=1,2048
      TMAX=AMAX1(TMAX,TRX(I))
      TMIN=AMIN1(TMIN,TRX(I))
  400 CONTINUE
      IF(TMAX.LE.64.0.AND.TMIN.GE.-64.0) GO TO 410
```

```
      IMAG=1
      GO TO 430
  410 IF(TMAX.LE.25.0.AND.TMIN.GE.-25.0) GO TO 420
      IMAG=2
      GO TO 430
  420 IMAG=5
C
C  DRAW AXES AND TICK MARKS FOR BOTH MODES
C
  430 CALL TPLOT(LU(1),0,137,137)
      CALL TPLOT(LU(1),1,937,137)
      CALL TPLOT(LU(1),1,937,637)
      CALL TPLOT(LU(1),1,137,637)
      CALL TPLOT(LU(1),1,137,137)
      DO 440 J=1,9
      IYP=J*50+137
      CALL TPLOT(LU(1),0,137,IYP)
      CALL TPLOT(LU(1),1,145,IYP)
      CALL TPLOT(LU(1),0,929,IYP)
      CALL TPLOT(LU(1),1,937,IYP)
  440 CONTINUE
      DO 450 J=1,9
      IXP=J*80+137
      CALL TPLOT(LU(1),0,IXP,137)
      CALL TPLOT(LU(1),1,IXP,145)
      CALL TPLOT(LU(1),0,IXP,629)
      CALL TPLOT(LU(1),1,IXP,637)
  450 CONTINUE
C
C  LABEL ORDINATE, ABSCISSA AND GRAPH FOR BOTH MODES
C
      DO 470 J=1,5
      IYP=J*100+80
      VMAX=VOLTS/FLOAT(IMAG)
      YABLE=ABS(VMAX-((VMAX/2.0)*(5.0-FLOAT(J))))
      CALL TPLOT(LU(1),0,70,IYP)
      CALL EXEC(2,LU(1),IUSLA,-2)
      WRITE(LU(1),460) YABLE
  460 FORMAT(F4.3)
  470 CONTINUE
      DO 490 J=1,2
      IYP=J*100+80
      CALL TPLOT(LU(1),0,56,IYP)
      CALL EXEC(2,LU(1),IUSLA,-2)
      WRITE(LU(1),480) MINUS
  480 FORMAT(A1)
  490 CONTINUE
      CALL SYMB(0.36,3.55,0.14,LVOLT,90.0,5)
      DO 500 J=0,5
```

```
      IXP=J*160+111
      XABLE=FLOAT(J)*RATE*409.6
      CALL TPLOT(LU(1),0,IXP,102)
      CALL EXEC(2,LU(1),IUSLA,-2)
      WRITE(LU(1),460) XABLE
  500 CONTINUE
      CALL TPLOT(LU(1),0,456,70)
      CALL EXEC(2,LU(1),IUSLA,-2)
      WRITE(LU(1),510) LTIME
  510 FORMAT(6A2)
      CALL TPLOT(LU(1),0,INDNT,750)
      CALL EXEC(2,LU(1),IUSLA,-2)
      WRITE(LU(1),520) IBUF
  520 FORMAT(36A2)
      CALL TPLOT(LU(1),0,350,725)
      CALL EXEC(2,LU(1),IUSLA,-2)
      WRITE(LU(1),530) IWAVE
  530 FORMAT("BIOMATION RECORDING ",I3)
C
C  PLOT WAVEFORM FOR BOTH MODES
C
      DO 550 I=1,2048
      IXP=FLOAT(I)*0.390625+137.0
      IYP=TRX(I)*1.5625*FLOAT(IMAG)+387.0
      IF(I.NE.1) GO TO 540
      CALL TPLOT(LU(1),0,IXP,IYP)
      GO TO 550
  540 CALL TPLOT(LU(1),1,IXP,IYP)
  550 CONTINUE
      CALL CURSR(LU(1),IQUIT,IXP,IYP)
      IF(.NOT.VIEW) GO TO 560
      CALL ERASE(LU(1))
      IF(IQUIT.NE.121B) GO TO 260
      GO TO 600
  560 IF(IQUIT.NE.107B) GO TO 200
C
C  WRITE GOOD WAVEFORMS TO DISK FOR NON-VIEWING MODE
C
      IPNT=IPNT+1
      ITPNM(IPNT)=IWAVE
      IF(IPNT.LT.15) GO TO 200
  570 CALL CODE
      WRITE(INBUF,580) (ITPNM(I),I=1,IPNT)
  580 FORMAT(15(I3," "))
      CALL WRITF(IDCB1,IERR,INBUF,IPNT*2)
      IF(IERR.LT.0) GO TO 110
      IPNT=0
      IF(.NOT.EOF) GO TO 200
C
```

```
C  RETURN UNUSED DISK SPACE AND QUIT
C
      CALL ERASE(LU(1))
      CALL LOCF(IDCB1,IERR,I,IREC,J,LEN)
      LEN=LEN/2-IREC-1
      CALL CLOSE(IDCB1,IERR,LEN)
      IF(IERR.GE.0) GO TO 600
      WRITE(LU(1),590) IERR,LEN
  590 FORMAT("/PLTME: ERROR ",I4," IN TRUNCATING DATA FILE BY ",
     +I6," BLOCKS!",/)
  600 WRITE(LU(1),610)
  610 FORMAT("/PLTME: FINISHED!",/)
  620 CONTINUE
      CALL EXEC(3,410B)
      END
```

Source Code of Function JSHFT

```
ASMB,R,F
      NAM JSHFT,7
      ENT JSHFT
      EXT .ENTR
*
*  FUNCTION JSHFT(IWORD,ICOUNT)
*
*   WHERE:   IWORD IS THE WORD TO BE SHIFTED
*            ICOUNT IS THE NUMBER OF BITS TO SHIFT
*            NEGATIVE ICOUNT SHIFTS THE WORD LEFT
*            POSITIVE ICOUNT SHIFTS THE WORD RIGHT
*
*
*  WRITTEN BY JOHN CARLYLE
*
*
WORD  NOP
COUNT NOP
JSHFT NOP
      JSB .ENTR     GET ADDRESSES OF PARAMETERS
      DEF WORD
      LDA WORD,I    GET THE WORD
      LDB COUNT,I   GET THE COUNT
      SZB,RSS       IS COUNT ZERO?
      JMP JSHFT,I   YES, RETURN
      SSB           NO, IS THE COUNT POSITIVE?
      JMP LEFT      NO, WILL SHIFT LEFT
RIGHT CMB,INB       YES, INITIALIZE FOR PLACE
      RAR           ROTATE RIGHT ONE PLACE
      INB,SZB       NUMBER OF SHIFTS COMPLETE?
      JMP *-2       NO, DO IT AGAIN
      JMP EXIT      YES, DONE
LEFT  RAL           ROTATE LEFT ONE PLACE
      INB,SZB       NUMBER OF SHIFTS COMPLETE?
      JMP *-2       NO, DO IT AGAIN
EXIT  JMP JSHFT,I   YES, RETURN
      END JSHFT
```

Source Code of Program AENOR

```
FTN4
C
      PROGRAM AENOR
C
C
C  THIS PROGRAM READS THE FILE CREATED BY <PLTME> AND CREATES
C  ANOTHER DISC FILE CONTAINING ALL OF THE HEADER INFORMATION
C  IN THE ORIGINAL FILE PLUS POWER SPECTRA DATA CALCULATED FROM
C  THE EXPERIMENTAL WAVEFORM TAPE USING THE WAVEFORM NUMBERS
C  IN THE <PLTME> FILE FOR POSITIONING.
C
C
C  WRITTEN BY JOHN CARLYLE
C
C
      DIMENSION LU(5),IREG(2),INBUF(36),IPBUF(10)
      DIMENSION IDCB1(144),IDCB2(144),ITPNM(36)
      DIMENSION TRX(2050),NTAPE(1024),IREC2(512)
      DIMENSION POWER(1025),DOUT(1027),DATA(18)
      EQUIVALENCE (REG,IREG),(DATA,ITPNM),(POWER,TRX)
      EQUIVALENCE (TRX(1537),NTAPE),(NTAPE(513),IREC2)
      EQUIVALENCE (POWER,DOUT(2))
      DATA ICNT/1/
C
C  RECOVER PARAMETERS
C
      CALL RMPAR(LU)
      IF(LU(1).EQ.0) LU(1)=1
      ILU=LU(1)+400B
C
C  GET 'NAMR' INFORMATION
C
   10 WRITE(LU(1),20) ICNT
   20 FORMAT("/AENOR: ENTER 'NAMR' FOR FILE #",I1,": _")
      REG=EXEC(1,ILU,INBUF,-72)
      ISCHR=1
      IF(NAMR(IPBUF,INBUF,IREG(2),ISCHR)) 10,30
   30 IF(ICNT.NE.1) GO TO 70
C
C  OPEN FILE #1
C
      CALL OPEN(IDCB1,IERR,IPBUF,0,IPBUF(5),IPBUF(6))
      IF(IERR.GE.0) GO TO 60
   40 WRITE(LU(1),50) IERR
   50 FORMAT("/AENOR: FILE ERROR ",I4,".  TRY AGAIN!",/)
      GO TO 10
C
C  CREATE FILE #2
C
```

```
   60 ICNT=2
      GO TO 10
   70 IREG(1)=-1
      IREG(2)=0
      CALL CREAT(IDCB2,IERR,IPBUF,IREG,3,IPBUF(5),IPBUF(6))
      IF(IERR.GE.0) GO TO 80
      ITRY=ITRY+1
      IF(ITRY.LT.3) GO TO 40
      GO TO 110
C
C  READ DATA IN CONTROL FILE
C
   80 ITRY=-1
   90 DO 100 L=1,36
      ITPNM(L)=0
  100 CONTINUE
      CALL READF(IDCB1,IERR,INBUF,36,LEN)
      IF(IERR.GE.0) GO TO 130
  110 WRITE(LU(1),120) IERR
  120 FORMAT("/AENOR: FILE ERROR ",I4,".  ABORTING PROGRAM!",/)
      GO TO 400
  130 IF(LEN.NE.-1) GO TO 160
      IF(ITRY) 140,140,360
  140 WRITE(LU(1),150)
  150 FORMAT("/AENOR: EOF IN CONTROL FILE.  ABORTING ",
     +"PROGRAM!",/)
      GO TO 400
C
C  TRANSFER HEADER DATA TO DATA FILE
C
  160 IF(ITRY) 170,190,190
  170 CALL CODE(LEN*2)
      READ(INBUF,*) (DATA(I),I=1,18)
      IF(DATA(1).NE.0.0) GO TO 180
      CALL WRITF(IDCB2,IERR,INBUF,LEN)
      IF(IERR.GE.0) GO TO 90
      GO TO 110
C
C  GET BIOMATION INPUT RANGE AND PROPER TAPE FILE
C
  180 VOLTS=DATA(1)*0.0078125
      CALL WRITF(IDCB2,IERR,INBUF,LEN)
      IF(IERR.LT.0) GO TO 110
      ITRY=0
      GO TO 90
  190 CALL CODE(LEN*2)
      READ(INBUF,*) (ITPNM(I),I=1,36)
      IF(ITRY) 200,200,260
  200 IFILE=ITPNM(1)
```

```
      ITRY=1
      IF(IFILE) 210,210,230
  210 WRITE(LU(1),220)
  220 FORMAT("/AENOR: INVALID MAG TAPE FILE.  ABORTING ",
     +"PROGRAM!",/)
      GO TO 400
C
C  POSITION MAG TAPE TO FILE AND INITIALIZE POINTERS
C
  230 ICNT=1
      CALL EXEC(3,410B)
  240 IF(ICNT.EQ.IFILE) GO TO 250
      ICNT=ICNT+1
      CALL EXEC(3,1310B)
      REG=EXEC(3,610B)
      IREG(1)=IAND(73B,IREG(1))
      IF(IREG(1).NE.0) GO TO 300
      GO TO 240
  250 IAE=1
      IREC=1
      CALL WRITF(IDCB2,IERR,INBUF,0)
      IF(IERR.GE.0) GO TO 90
      GO TO 110
C
C  POSITION TO GOOD AE WAVEFORM RECORD
C
  260 ICNT=1
  270 IF(ITPNM(ICNT).EQ.0) GO TO 90
  280 IF(ITPNM(ICNT).EQ.IREC) GO TO 290
      IREC=IREC+1
      CALL EXEC(3,310B)
      REG=EXEC(3,610B)
      IREG(1)=IAND(373B,IREG(1))
      IF(IREG(1).NE.0) GO TO 300
      CALL EXEC(3,310B)
      REG=EXEC(3,610B)
      IREG(1)=IAND(373B,IREG(1))
      IF(IREG(1).NE.0) GO TO 300
      GO TO 280
C
C  READ IN BIOMATION RECORD AND UNPACK IT
C
  290 CALL EXEC(1,110B,NTAPE,512)
      REG=EXEC(3,610B)
      IREG(1)=IAND(373B,IREG(1))
      IF(IREG(1).EQ.0) GO TO 320
  300 WRITE(LU(1),310) IREG(1)
  310 FORMAT("/AENOR: MAG TAPE STATUS = ",O3,"B.  ABORTING ",
     +"PROGRAM!",/)
```

```
      GO TO 400
  320 CALL EXEC(1,110B,IREC2,512)
      REG=EXEC(3,610B)
      IREG(1)=IAND(373B,IREG(1))
      IF(IREG(1).NE.0) GO TO 300
      DO 330 L=1,2047,2
      LN=(L+1)/2
      L2=L+1
      IREG(2)=IAND(377B,NTAPE(LN))
      IREG(1)=JSHFT(NTAPE(LN),8)
      IREG(1)=IAND(377B,IREG(1))
      TRX(L)=FLOAT(IREG(1)-128)*VOLTS
      TRX(L2)=FLOAT(IREG(2)-128)*VOLTS
  330 CONTINUE
C
C  OBTAIN NORMALIZED POWER SPECTRUM REF. 1 MW INTO 50 OHMS
C  VALUES HAVE BEEN DOUBLED FOR FREQUENCIES OTHER THAN DC
C
      CALL FOUR2(TRX,2048,1,-1,0)
      TOTN=0.0
      DO 340 L=1,2049,2
      LN=(L+1)/2
      TRX(L)=TRX(L)/2048.0
      TRX(L+1)=TRX(L+1)/2048.0
      POWER(LN)=TRX(L)*TRX(L)+TRX(L+1)*TRX(L+1)
      POWER(LN)=POWER(LN)*20.0
      IF(LN.NE.1) POWER(LN)=POWER(LN)*2.0
      TOTN=TOTN+POWER(LN)
  340 CONTINUE
      IF(IAE.NE.1) GO TO 350
      TOTO=TOTN
  350 DOUT(1)=TOTO/TOTN
      DOUT(1027)=FLOAT(ITPNM(ICNT))
C
C  WRITE NORMALIZING FACTOR AND SPECTRUM TO DISC
C
      CALL WRITF(IDCB2,IERR,DOUT,2054)
      IF(IERR.LT.0) GO TO 110
      ICNT=ICNT+1
      IREC=IREC+1
      IAE=IAE+1
      GO TO 270
C
C  RETURN UNUSED DISC SPACE AND QUIT
C
  360 CALL LOCF(IDCB2,IERR,ICNT,IREC,L,LEN)
      LEN=LEN/2-IREC-1
      CALL CLOSE(IDCB2,IERR,LEN)
      IF(IERR.GE.0) GO TO 380
```

```
      WRITE(LU(1),370) IERR,LEN
  370 FORMAT("/AENOR: ERROR ",I4," IN DELETING FILE2 BY ",I6,
     +" BLOCKS!",/)
  380 WRITE(LU(1),390)
  390 FORMAT("/AENOR: FINISHED!",/)
      GO TO 410
  400 CALL PURGE(IDCB2,IERR,IPBUF,IPBUF(5),IPBUF(6))
  410 CALL CLOSE(IDCB1,IERR)
      END
```

```
FTN4
      SUBROUTINE FOUR2 (DATA,N,NDIM,ISIGN,IFORM)
C     COOLEY-TUKEY FAST FOURIER TRANSFORM IN USASI BASIC
C     FORTRAN.  MULTI-DIMENSIONAL TRANSFORM, EACH DIMENSION
C     A POWER OF TWO, COMPLEX OR REAL DATA.
C     TRANSFORM(K1,K2,...) = SUM(DATA(J1,J2,...)*EXP(ISIGN*2*PI
C     *SQRT(-1)*((J1-1)*(K1-1)/N(1)+(J2-1)*(K2-1)/N(2)+...))),
C     SUMMED FOR ALL J1 AND K1 FROM 1 TO N(1), J2 AND K2 FROM
C     TO N(2) ETC. FOR ALL NDIM SUBSCRIPTS.  NDIM MUST BE
C     POSITIVE AND EACH N(IDIM) MUST BE A POWER OF TWO.  ISIGN
C     IS +1 OR -1.  LET NTOT = N(1)*N(2)*...*N(NDIM).  THEN A -1
C     TRANSFORM FOLLOWED BY A +1 ONE (OR VICE VERSA) RETURNS
C     NTOT TIMES THE ORIGINAL DATA.  IFORM = 1, 0 OR -1, AS DATA
C     IS COMPLEX, REAL OR THE FIRST HALF OF A COMPLEX ARRAY.
C     TRANSFORM VALUES ARE RETURNED TO ARRAY DATA.  THEY ARE
C     COMPLEX, REAL OR THE FIRST HALF OF A COMPLEX ARRAY, AS
C     IFORM = 1, -1 OR 0.  THE TRANSFORM OF A REAL ARRAY (IFORM
C     = 0) DIMENSIONED N(1) BY N(2) BY ... WILL BE RETURNED IN
C     THE SAME ARRAY, NOW CONSIDERED TO BE COMPLEX OF DIMENSIONS
C     N(1)/2+1 BY N(2) BY ....  NOTE THAT IF IFORM = 0 OR -1,
C     N(1) MUST BE EVEN, AND ENOUGH ROOM MUST BE RESERVED.  THE
C     MISSING VALUES MAY BE OBTAINED BY COMPLEX CONJUGATION.
C     THE REVERSE TRANSFORMATION, OF A HALF COMPLEX ARRAY DIMEN-
C     SIONED N(1)/2+1 BY N(2) BY ..., IS ACCOMPLISHED BY SETTING
C     IFORM TO -1.  IN THE N ARRAY, N(1) MUST BE THE TRUE N(1),
C     NOT N(1)/2+1.  THE TRANSFORM WILL BE REAL AND RETURNED TO
C     THE INPUT ARRAY.  RUNNING TIME IS PROPORTIONAL TO NTOT*
C     LOG2(NTOT), RATHER THAN THE NAIVE NTOT**2.  FURTHERMORE,
C     LESS ERROR IS BUILT UP.  WRITTEN BY NORMAN BRENNER OF MIT
C     LINCOLN LABORATORY, JANUARY 1969.  SEE-- IEEE AUDIO
C     TRANSACTIONS (JUNE 1967), SPECIAL ISSUE ON FFT.
      DIMENSION DATA(1), N(1)
      NTOT=1
      DO 10 IDIM=1,NDIM
   10 NTOT=NTOT*N(IDIM)
      IF (IFORM) 70,20,20
   20 NREM=NTOT
      DO 60 IDIM=1,NDIM
      NREM=NREM/N(IDIM)
      NPREV=NTOT/(N(IDIM)*NREM)
      NCURR=N(IDIM)
      IF (IDIM-1+IFORM) 30,30,40
   30 NCURR=NCURR/2
   40 CALL BITRV (DATA,NPREV,NCURR,NREM)
      CALL COOL2 (DATA,NPREV,NCURR,NREM,ISIGN)
      IF (IDIM-1+IFORM) 50,50,60
   50 CALL FIXRL (DATA,N(1),NREM,ISIGN,IFORM)
      NTOT=(NTOT/N(1))*(N(1)/2+1)
   60 CONTINUE
```

```
      RETURN
   70 NTOT=(NTOT/N(1))*(N(1)/2+1)
      NREM=1
      DO 100 JDIM=1,NDIM
      IDIM=NDIM+1-JDIM
      NCURR=N(IDIM)
      IF (IDIM-1) 80,80,90
   80 NCURR=NCURR/2
      CALL FIXRL (DATA,N(1),NREM,ISIGN,IFORM)
      NTOT=NTOT/(N(1)/2+1)*N(1)
   90 NPREV=NTOT/(N(IDIM)*NREM)
      CALL BITRV (DATA,NPREV,NCURR,NREM)
      CALL COOL2 (DATA,NPREV,NCURR,NREM,ISIGN)
  100 NREM=NREM*N(IDIM)
      RETURN
      END
      SUBROUTINE COOL2 (DATA,NPREV,N,NREM,ISIGN)
C     DISCRETE FOURIER TRANSFORM OF LENGTH N.  IN-PLACE COOLEY-
C     TUKEY ALGORITHM, BIT-REVERSED TO NORMAL ORDER, SANDE-TUKEY
C     PHASE SHIFTS.
C     DIMENSION DATA(NPREV,N,NREM)
C     COMPLEX DATA
C     DATA(J1,K4,J5) = SUM(DATA(J1,J4,J5)*EXP(ISIGN*2*PI*I*
C     (J4-1)*(K4-1)/N)), SUMMED OVER J4 = 1 TO N FOR ALL J1 FROM
C     1 TO NPREV, K4 FROM 1 TO N AND J5 FROM 1 TO NREM.  N MUST
C     BE A POWER OF TWO.  METHOD--LET IPREV TAKE THE VALUES 1, 2
C     OR 4, 4 OR 8, ..., N/16, N/4, N.  THE CHOICE BETWEEN 2 OR
C     4, ETC., DEPENDS ON WHETHER N IS A POWER OF FOUR.  DEFINE
C     IFACT = 2 OR 4, THE NEXT FACTOR THAT IPREV MUST TAKE, AND
C     IREM = N/(IFACT*IPREV).  THEN--
C     DIMENSION DATA(NPREV,IPREV,IFACT,IREM,NREM)
C     COMPLEX DATA
C     DATA(J1,J2,K3,J4,J5) = SUM(DATA(J1,J2,J3,J4,J5)*EXP(ISIGN*
C     PI*I*(K3-1)*((J3-1)/IFACT+(J2-1)/(IFACT*IPREV)))), SUMMED
C     J3 = 1 TO IFACT FOR ALL J1 FROM 1 TO NPREV, J2 FROM 1 TO
C     IPREV, K3 FROM 1 TO IFACT, J4 FROM 1 TO IREM AND J5 FROM 1
C     TO NREM.  THIS IS A PHASE-SHIFTED DISCRETE FOURIER TRANS-
C     FORM OF LENGTH IFACT.  FACTORING N BY FOURS SAVES ABOUT
C     TWENTY FIVE PERCENT OVER FACTORING BY TWOS.  DATA MUST BE
C     BIT-REVERSED INITIALLY.  IT IS NOT NECESSARY TO REWRITE
C     THIS SUBROUTINE INTO COMPLEX NOTATION SO LONG AS THE
C     FORTRAN COMPILER USED STORES REAL AND IMAGINARY PARTS IN
C     ADJACENT STORAGE LOCATIONS.  IT MUST ALSO STORE ARRAYS
C     WITH THE FIRST SUBSCRIPT INCREASING FASTEST.
      DIMENSION DATA(1)
      TWOPI=6.2831853071786*FLOAT(ISIGN)
      IP0=2
      IP1=IP0*NPREV
      IP4=IP1*N
```

```
      IP5=IP4*NREM
      IP2=IP1
C     IP2=IP1*IPROD
      NPART=N
   10 IF (NPART-2) 60,30,20
   20 NPART=NPART/4
      GO TO 10
C     DO A FOURIER TRANSFORM OF LENGTH TWO
   30 IF (IP2-IP4) 40,160,160
   40 IP3=IP2*2
C     IP3=IP2*IFACT
      DO 50 I1=1,IP1,IP0
C     I1 = 1+(J1-1)*IP0
      DO 50 I5=I1,IP5,IP3
C     I5 = 1+(J1-1)*IP0+(J4-1)*IP3+(J5-1)*IP4
      I3A=I5
      I3B=I3A+IP2
C     I3 = 1+(J1-1)*IP0+(J2-1)*IP1+(J3-1)*IP2+(J4-1)*IP3+
C          (J5-1)*IP4
      TEMPR=DATA(I3B)
      TEMPI=DATA(I3B+1)
      DATA(I3B)=DATA(I3A)-TEMPR
      DATA(I3B+1)=DATA(I3A+1)-TEMPI
      DATA(I3A)=DATA(I3A)+TEMPR
   50 DATA(I3A+1)=DATA(I3A+1)+TEMPI
      IP2=IP3
C     DO A FOURIER TRANSFORM OF LENGTH FOUR (FROM BIT
C     REVERSED ORDER)
   60 IF (IP2-IP4) 70,160,160
   70 IP3=IP2*4
C     IP3=IP2*IFACT
C     COMPUTE TWOPI THRU WR AND WI IN DOUBLE PRECISION, IF
C     AVAILABLE.
      THETA=TWOPI/FLOAT(IP3/IP1)
      SINTH=SIN(THETA/2.)
      WSTPR=-2.*SINTH*SINTH
      WSTPI=SIN(THETA)
      WR=1.
      WI=0.
      DO 150 I2=1,IP2,IP1
C     I2 = 1+(J2-1)*IP1
      IF (I2-1) 90,90,80
   80 W2R=WR*WR-WI*WI
      W2I=2.*WR*WI
      W3R=W2R*WR-W2I*WI
      W3I=W2R*WI+W2I*WR
   90 I1MAX=I2+IP1-IP0
      DO 140 I1=I2,I1MAX,IP0
C     I1 = 1+(J1-1)*IP0+(J2-1)*IP1
```

```
      DO 140 I5=I1,IP5,IP3
C     I5 = 1+(J1-1)*IP0+(J2-1)*IP1+(J4-1)*IP3+(J5-1)*IP4
      I3A=I5
      I3B=I3A+IP2
      I3C=I3B+IP2
      I3D=I3C+IP2
C     I3 = 1+(J1-1)*IP0+(J2-1)*IP1+(J3-1)*IP2+(J4-1)*IP3+
C          (J5-1)*IP4
      IF (I2-1) 110,110,100
C     APPLY THE PHASE SHIFT FACTORS
  100 TEMPR=DATA(I3B)
      DATA(I3B)=W2R*DATA(I3B)-W2I*DATA(I3B+1)
      DATA(I3B+1)=W2R*DATA(I3B+1)+W2I*TEMPR
      TEMPR=DATA(I3C)
      DATA(I3C)=WR*DATA(I3C)-WI*DATA(I3C+1)
      DATA(I3C+1)=WR*DATA(I3C+1)+WI*TEMPR
      TEMPR=DATA(I3D)
      DATA(I3D)=W3R*DATA(I3D)-W3I*DATA(I3D+1)
      DATA(I3D+1)=W3R*DATA(I3D+1)+W3I*TEMPR
  110 T0R=DATA(I3A)+DATA(I3B)
      T0I=DATA(I3A+1)+DATA(I3B+1)
      T1R=DATA(I3A)-DATA(I3B)
      T1I=DATA(I3A+1)-DATA(I3B+1)
      T2R=DATA(I3C)+DATA(I3D)
      T2I=DATA(I3C+1)+DATA(I3D+1)
      T3R=DATA(I3C)-DATA(I3D)
      T3I=DATA(I3C+1)-DATA(I3D+1)
      DATA(I3A)=T0R+T2R
      DATA(I3A+1)=T0I+T2I
      DATA(I3C)=T0R-T2R
      DATA(I3C+1)=T0I-T2I
      IF (ISIGN) 120,120,130
  120 T3R=-T3R
      T3I=-T3I
  130 DATA(I3B)=T1R-T3I
      DATA(I3B+1)=T1I+T3R
      DATA(I3D)=T1R+T3I
  140 DATA(I3D+1)=T1I-T3R
      TEMPR=WR
      WR=WSTPR*TEMPR-WSTPI*WI+TEMPR
  150 WI=WSTPR*WI+WSTPI*TEMPR+WI
      IP2=IP3
      GO TO 60
  160 RETURN
      END
      SUBROUTINE FIXRL (DATA,N,NREM,ISIGN,IFORM)
C     FOR IFORM = 0, CONVERT THE TRANSFORM OF A DOUBLED-UP REAL
C     ARRAY, CONSIDERED COMPLEX, INTO ITS TRUE TRANSFORM.
C     SUPPLY ONLY THE FIRST HALF OF THE COMPLEX TRANSFORM, AS
```

```
C     THE SECOND HALF HAS CONJUGATE SYMMETRY.  FOR IFORM = -1,
C     CONVERT THE FIRST HALF OF THE TRUE TRANSFORM INTO THE
C     TRANSFORM OF A DOUBLED-UP ARRAY.  N MUST BE EVEN.
C     USING COMPLEX NOTATION AND SUBSCRIPTS STARTING AT ZERO,
C     THE TRANSFORMATION IS--
C     DIMENSION DATA(N,NREM)
C     ZSTP = EXP(ISIGN*2*PI*I/N)
C     DO 10 I2=0,NREM-1
C     DATA(0,I2) = CONJ(DATA(0,I2))*(1+I)
C     DO 10 I1=1,N/4
C     Z = (1+(2*IFORM+1)*I*ZSTP**I1)/2
C     I1CNJ = N/2-I1
C     DIF = DATA(I1,I2)-CONJ(DATA(I1CNJ,I2))
C     TEMP = Z*DIF
C     DATA(I1,I2) = (DATA(I1,I2)-TEMP)*(1-IFORM)
C 10  DATA(I1CNJ,I2) = (DATA(I1CNJ,I2)+CONJ(TEMP))*(1-IFORM)
C     IF I1=I1CNJ, THE CALCULATION FOR THAT VALUE COLLAPSES
C     INTO A SIMPLE CONJUGATION OF DATA(I1,I2).
      DIMENSION DATA(1)
      TWOPI=6.2831853071786*FLOAT(ISIGN)
      IP0=2
      IP1=IP0*(N/2)
      IP2=IP1*NREM
      IF (IFORM) 10,70,70
C     PACK THE REAL INPUT VALUES (TWO PER COLUMN)
   10 J1=IP1+1
      DATA(2)=DATA(J1)
      IF (NREM-1) 70,70,20
   20 J1=J1+IP0
      I2MIN=IP1+1
      DO 60 I2=I2MIN,IP2,IP1
      DATA(I2)=DATA(J1)
      J1=J1+IP0
      IF (N-2) 50,50,30
   30 I1MIN=I2+IP0
      I1MAX=I2+IP1-IP0
      DO 40 I1=I1MIN,I1MAX,IP0
      DATA(I1)=DATA(J1)
      DATA(I1+1)=DATA(J1+1)
   40 J1=J1+IP0
   50 DATA(I2+1)=DATA(J1)
   60 J1=J1+IP0
   70 DO 80 I2=1,IP2,IP1
      TEMPR=DATA(I2)
      DATA(I2)=DATA(I2)+DATA(I2+1)
   80 DATA(I2+1)=TEMPR-DATA(I2+1)
      IF (N-2) 200,200,90
   90 THETA=TWOPI/FLOAT(N)
      SINTH=SIN(THETA/2.)
```

```
      ZSTPR=-2.*SINTH*SINTH
      ZSTPI=SIN(THETA)
      ZR=(1.-ZSTPI)/2.
      ZI=(1.+ZSTPR)/2.
      IF (IFORM) 100,110,110
  100 ZR=1.-ZR
      ZI=-ZI
  110 I1MIN=IP0+1
      I1MAX=IP0*(N/4)+1
      DO 190 I1=I1MIN,I1MAX,IP0
      DO 180 I2=I1,IP2,IP1
      I2CNJ=IP0*(N/2+1)-2*I1+I2
      IF (I2-I2CNJ) 150,120,120
  120 IF (ISIGN*(2*IFORM+1)) 130,140,140
  130 DATA(I2+1)=-DATA(I2+1)
  140 IF (IFORM) 170,180,180
  150 DIFR=DATA(I2)-DATA(I2CNJ)
      DIFI=DATA(I2+1)+DATA(I2CNJ+1)
      TEMPR=DIFR*ZR-DIFI*ZI
      TEMPI=DIFR*ZI+DIFI*ZR
      DATA(I2)=DATA(I2)-TEMPR
      DATA(I2+1)=DATA(I2+1)-TEMPI
      DATA(I2CNJ)=DATA(I2CNJ)+TEMPR
      DATA(I2CNJ+1)=DATA(I2CNJ+1)-TEMPI
      IF (IFORM) 160,180,180
  160 DATA(I2CNJ)=DATA(I2CNJ)+DATA(I2CNJ)
      DATA(I2CNJ+1)=DATA(I2CNJ+1)+DATA(I2CNJ+1)
  170 DATA(I2)=DATA(I2)+DATA(I2)
      DATA(I2+1)=DATA(I2+1)+DATA(I2+1)
  180 CONTINUE
      TEMPR=ZR-.5
      ZR=ZSTPR*TEMPR-ZSTPI*ZI+ZR
  190 ZI=ZSTPR*ZI+ZSTPI*TEMPR+ZI
C     RECURSION SAVES TIME, AT A SLIGHT LOSS IN ACCURACY.  IF
C     AVAILABLE, USE DOUBLE PRECISION TO COMPUTE ZR AND ZI.
  200 IF (IFORM) 270,210,210
C     UNPACK THE REAL TRANSFORM VALUES (TWO PER COLUMN)
  210 I2=IP2+1
      I1=I2
      J1=IP0*(N/2+1)*NREM+1
      GO TO 250
  220 DATA(J1)=DATA(I1)
      DATA(J1+1)=DATA(I1+1)
      I1=I1-IP0
      J1=J1-IP0
  230 IF (I2-I1) 220,240,240
  240 DATA(J1)=DATA(I1)
      DATA(J1+1)=0.
  250 I2=I2-IP1
```

```
      J1=J1-IP0
      DATA(J1)=DATA(I2+1)
      DATA(J1+1)=0.
      I1=I1-IP0
      J1=J1-IP0
      IF (I2-1) 260,260,230
  260 DATA(2)=0.
  270 RETURN
      END
      SUBROUTINE BITRV (DATA,NPREV,N,NREM)
C     SHUFFLE THE DATA BY BIT REVERSAL.
C     DIMENSION DATA(NPREV,N,NREM)
C     COMPLEX DATA
C     EXCHANGE DATA(J1,J4REV,J5) WITH DATA(J1,J4,J5) FOR ALL J1
C     FROM 1 TO NPREV, ALL J4 FROM 1 TO N (WHICH MUST BE A POWER
C     OF TWO), AND ALL J5 FROM 1 TO NREM.  J4REV-1 IS THE BIT
C     REVERSAL OF J4-1, E.G., SUPPOSE N = 32.  THEN FOR J4-1 =
C     10011, J4REV-1 = 11001, ETC.
      DIMENSION DATA(1)
      IP0=2
      IP1=IP0*NPREV
      IP4=IP1*N
      IP5=IP4*NREM
      I4REV=1
C     I4REV = 1+(J4REV-1)*IP1
      DO 60 I4=1,IP4,IP1
C     I4 = 1+(J4-1)*IP1
      IF (I4-I4REV) 10,30,30
   10 I1MAX=I4+IP1-IP0
      DO 20 I1=I4,I1MAX,IP0
C     I1 = 1+(J1-1)*IP0+(J4-1)*IP1
      DO 20 I5=I1,IP5,IP4
C     I5 = 1+(J1-1)*IP0+(J4-1)*IP1+(J5-1)*IP4
      I5REV=I4REV+I5-I4
C     I5REV = 1+(J1-1)*IP0+(J4REV-1)*IP1+(J5-1)*IP4
      TEMPR=DATA(I5)
      TEMPI=DATA(I5+1)
      DATA(I5)=DATA(I5REV)
      DATA(I5+1)=DATA(I5REV+1)
      DATA(I5REV)=TEMPR
   20 DATA(I5REV+1)=TEMPI
C     ADD ONE WITH DOWNWARD CARRY TO THE HIGH ORDER BIT
C     OF J4REV-1.
   30 IP2=IP4/2
   40 IF (I4REV-IP2) 60,60,50
   50 I4REV=I4REV-IP2
      IP2=IP2/2
      IF (IP2-IP1) 60,40,40
   60 I4REV=I4REV+IP2
```

```
      RETURN
      END
```

Source Code of Program GASJT

```
FTN4
C
      PROGRAM GASJT
C
C
C  THIS PROGRAM READS AN EXPERIMENTAL TAPE CONTAINING GAS JET
C  RECORDINGS, CALCULATES A POWER SPECTRUM FOR EACH RECORDING,
C  AVERAGES THE SPECTRA, AND PRODUCES A DISC FILE CONTAINING
C  HEADER INFORMATION AS WELL AS THE AVERAGE POWER SPECTRUM.
C
C
C  WRITTEN BY JOHN CARLYLE
C
C
      DIMENSION LU(5),IREG(2),INBUF(36),IPBUF(10)
      DIMENSION IDCB1(144),TRX(2050),NTAPE(1024),IREC2(512)
      DIMENSION POWER(1025),CUM(1025),DOUT(1027),IFILE(2)
      EQUIVALENCE (IREG,REG),(CUM,DOUT(2)),(POWER,TRX)
      EQUIVALENCE (TRX(1537),NTAPE),(NTAPE(513),IREC2)
      DATA IFILE/-1,0/
      CALL RMPAR(LU)
      IF(LU(1).EQ.0) LU(1)=1
      ILU=LU(1)+400B
C
C  GET 'NAMR' AND CREATE DATA FILE
C
   10 WRITE(LU(1),20)
   20 FORMAT("/GASJT: ENTER 'NAMR' FOR DATA FILE: _")
      REG=EXEC(1,ILU,INBUF,-72)
      ISCHR=1
      IF(NAMR(IPBUF,INBUF,IREG(2),ISCHR)) 10,30
   30 CALL CREAT(IDCB1,IERR,IPBUF,IFILE,3,IPBUF(5),IPBUF(6))
      IF(IERR.GE.0) GO TO 50
      WRITE(LU(1),40) IERR
   40 FORMAT("/GASJT: FILE ERROR ",I4,".  TRY AGAIN!",/)
      GO TO 10
C
C  GET HEADER DATA AND WRITE IT TO DATA FILE
C
   50 WRITE(LU(1),60)
   60 FORMAT("/GASJT: TYPE IN ONE LINE OF HEADER DATA.",/)
      REG=EXEC(1,ILU,INBUF,36)
      CALL CODE(IREG(2)*2)
      READ(INBUF,*) (POWER(I),I=1,5)
      IF(POWER(1).NE.0.0) GO TO 100
      CALL WRITF(IDCB1,IERR,INBUF,IREG(2))
      IF(IERR.GE.0) GO TO 50
   70 WRITE(LU(1),80) IERR
   80 FORMAT("/GASJT: FILE ERROR ",I4,".  ABORTING PROGRAM!",/)
```

```
   90 CALL PURGE(IDCB1,IERR,IPBUF,IPBUF(5),IPBUF(6))
      GO TO 250
  100 VOLTS=POWER(1)*0.0078125
      CALL WRITF(IDCB1,IERR,INBUF,IREG(2))
      IF(IERR.LT.0) GO TO 70
      CALL WRITF(IDCB1,IERR,INBUF,0)
      IF(IERR.LT.0) GO TO 70
C
C  GET TAPE FILE NUMBER AND POSITION MAG TAPE
C
  110 WRITE(LU(1),120)
  120 FORMAT("/GASJT: TAPE FILE NUMBER? _")
      READ(LU(1),*) IFILE(1)
      IF(IFILE(1).LE.0) GO TO 110
      ICNT=1
      CALL EXEC(3,410B)
  130 IF(ICNT.EQ.IFILE(1)) GO TO 160
      ICNT=ICNT+1
      CALL EXEC(3,1310B)
      REG=EXEC(3,610B)
      IREG(1)=IAND(73B,IREG(1))
      IF(IREG(1).EQ.0) GO TO 130
  140 WRITE(LU(1),150) IREG(1)
  150 FORMAT("/GASJT: MAG TAPE STATUS = ",O3,"B.  ABORTING ",
     +"PROGRAM!",/)
      GO TO 90
C
C  READ IN BIOMATION RECORD AND UNPACK IT
C
  160 IAE=1
  170 CALL EXEC(1,110B,NTAPE,512)
      REG=EXEC(3,610B)
      IREG(1)=IAND(373B,IREG(1))
      IF(IREG(1).EQ.200B) GO TO 200
      IF(IREG(1).NE.0) GO TO 140
      CALL EXEC(1,110B,IREC2,512)
      REG=EXEC(3,610B)
      IREG(1)=IAND(373B,IREG(1))
      IF(IREG(1).NE.0) GO TO 140
      DO 180 L=1,2047,2
      LN=(L+1)/2
      L2=L+1
      IREG(2)=IAND(377B,NTAPE(LN))
      IREG(1)=JSHFT(NTAPE(LN),8)
      IREG(1)=IAND(377B,IREG(1))
      TRX(L)=FLOAT(IREG(1)-128)*VOLTS
      TRX(L2)=FLOAT(IREG(2)-128)*VOLTS
  180 CONTINUE
C
```

```
C  CALCULATE POWER SPECTRUM REF. 1 MW INTO 50 OHMS
C  VALUES HAVE BEEN DOUBLED FOR FREQUENCIES OTHER THAN DC
C  CALCULATE AVERAGE IN ARRAY 'CUM'
C
        CALL FOUR2(TRX,2048,1,-1,0)
        DO 190 L=1,2049,2
        LN=(L+1)/2
        TRX(L)=TRX(L)/2048.0
        TRX(L+1)=TRX(L+1)/2048.0
        POWER(LN)=TRX(L)*TRX(L)+TRX(L+1)*TRX(L+1)
        POWER(LN)=POWER(LN)*20.0
        IF(LN.NE.1) POWER(LN)=POWER(LN)*2.0
        CUM(LN)=POWER(LN)+CUM(LN)
    190 CONTINUE
        IAE=IAE+1
        GO TO 170
C
C  WRITE OUT AVERAGED POWER SPECTRUM WHEN EOF ENCOUNTERED
C
    200 IAE=IAE-1
        DO 210 I=1,1025
        CUM(I)=CUM(I)/FLOAT(IAE)
    210 CONTINUE
        DOUT(1)=1.00
        DOUT(1027)=FLOAT(IAE)
        CALL WRITF(IDCB1,IERR,DOUT,2054)
        IF(IERR.LT.0) GO TO 70
        CALL LOCF(IDCB1,IERR,ICNT,IREC,L,LEN)
        IF(IERR.LT.0) GO TO 70
        LEN=LEN/2-IREC-1
        CALL CLOSE(IDCB1,IERR,LEN)
        IF(IERR.GE.0) GO TO 230
        WRITE(LU(1),220) IERR,LEN
    220 FORMAT("/GASJT: ERROR ",I4," IN TRUNCATING FILE BY ",I6,
       +" BLOCKS!",/)
    230 WRITE(LU(1),240)
    240 FORMAT("/GASJT: FINISHED!",/)
    250 CONTINUE
        END
```

Source Code of Program PLFFT

```
FTN4
C
      PROGRAM PLFFT
C
C
C  THIS PROGRAM WILL MAKE A FREQUENCY DOMAIN PLOT OF ACOUSTIC
C  EMISSION SIGNALS USING THE DATA PRODUCED BY <AENOR> AND
C  <GASJT>.  THE USER HAS THE OPTION OF NORMALIZING THE PLOTS
C  USING THE GAS JET DATA FOR THE EXPERIMENT, AND CAN ALSO
C  EXAMINE SHAPE CHANGES THROUGH CONSTANT ENERGY PLOTS.
C
C
C  WRITTEN BY JOHN CARLYLE
C
C
      DIMENSION LU(5),IREG(2),INBUF(36),IPBUF(10),TBUF(18)
      DIMENSION IDCB1(144),DATA(1028),HBUF(18),IDATA(2056)
      DIMENSION IBUF1(6),IBUF2(8),IBUF3(10)
      DIMENSION IDCB2(144),GAS(1028)
      EQUIVALENCE (REG,IREG),(INBUF,HBUF),(DATA,IDATA)
      EQUIVALENCE (DATA(1011),TBUF)
      DATA ICNT/1/,IUSLA/17537B/,ITRY/-1/,IMAG/1/
      DATA IBUF1/2HPO,2HWE,2HR ,2H(D,2HBM,2H) /
      DATA IBUF2/2HFR,2HEQ,2HUE,2HNC,2HY ,2H(M,2HHZ,2H) /
      DATA IBUF3/2HRE,2HLA,2HTI,2HVE,2H P,2HOW,2HER,
     +2H (,2HDB,2H) /
C
C  RECOVER PARAMETERS
C
      CALL RMPAR(LU)
      IF(LU(1).EQ.0) LU(1)=1
      ILU=LU(1)+400B
C
C  GET 'NAMR' INFORMATION
C
      CALL PLTLU(LU(1))
   10 WRITE(LU(1),20) ICNT
   20 FORMAT("/PLFFT: ENTER 'NAMR' FOR FILE #",I1,": _")
      REG=EXEC(1,ILU,INBUF,-72)
      ISCHR=1
      IF(NAMR(IPBUF,INBUF,IREG(2),ISCHR)) 10,30
   30 IF(ICNT.NE.1) GO TO 80
C
C  OPEN FILE #1
C
      CALL OPEN(IDCB1,IERR,IPBUF,0,IPBUF(5),IPBUF(6))
      IF(IERR.GE.0) GO TO 60
   40 WRITE(LU(1),50) IERR
   50 FORMAT("/PLFFT: FILE ERROR ",I4,".  TRY AGAIN!",/)
```

```
      GO TO 10
C
C  OPEN FILE #2 AND READ GAS JET DATA
C
   60 WRITE(LU(1),70)
   70 FORMAT("/PLFFT: PLOT WAVEFORMS NORMALIZED BY GAS JET? _")
      READ(LU(1),190) IGAS
      IF(IGAS.NE.54505B) GO TO 150
      ICNT=2
      GO TO 10
   80 CALL OPEN(IDCB2,IERR,IPBUF,0,IPBUF(5),IPBUF(6))
      IF(IERR.GT.0) GO TO 90
      ITRY=ITRY+1
      IF(ITRY.LT.2) GO TO 40
      GO TO 220
   90 ITRY=-1
  100 CALL READF(IDCB2,IERR,GAS,2056,LEN)
      IF(LEN.LT.0.OR.IERR.LT.0) GO TO 220
      IF(LEN.NE.0.AND.ITRY.GT.0) GO TO 110
      IF(LEN.NE.0) GO TO 100
      ITRY=1
      GO TO 100
  110 IF(LEN.EQ.2054) GO TO 120
      GO TO 320
  120 DO 140 I=2,1026
      IF(GAS(I).GT.0.0) GO TO 130
      GAS(I)=-99.0
      GO TO 140
  130 GAS(I)=ALOGT(GAS(I))
  140 CONTINUE
C
C  READ DATA IN PLOT FILE
C
  150 ICNT=-1
      ITRY=-1
  160 WRITE(LU(1),170)
  170 FORMAT("/PLFFT: WHICH BIOMATION RECORDING DO YOU WANT? _")
      READ(LU(1),*) INUM
      IF(ICNT.NE.-1) GO TO 200
      WRITE(LU(1),180)
  180 FORMAT("/PLFFT: PLOT WAVEFORMS WITH CONSTANT ENERGY? _")
      READ(LU(1),190) ICAL
  190 FORMAT(A2)
  200 CALL ERASE(LU(1))
  210 CALL READF(IDCB1,IERR,DATA,2056,LEN)
      IF(IERR.GE.0) GO TO 240
  220 WRITE(LU(1),230) IERR
  230 FORMAT("/PLFFT: FILE ERROR ",I4,".  ABORTING PROGRAM!",/)
      GO TO 630
```

```
  240 IF(LEN.NE.-1) GO TO 260
      WRITE(LU(1),250)
  250 FORMAT("/PLFFT: EOF ENCOUNTERED.  FINISHED!")
      GO TO 630
  260 IF(ICNT) 270,300,310
  270 CALL CODE(LEN*2)
      READ(IDATA,*) (TBUF(I),I=1,18)
      IF(TBUF(1).NE.0.0) GO TO 290
      IF(ITRY.GE.0) GO TO 210
      DO 280 I=1,18
      HBUF(I)=DATA(I)
  280 CONTINUE
      INDNT=(73-LEN*2)*7
      ITRY=1
      GO TO 210
  290 TIME=TBUF(2)
      BNDWT=1.0/(TIME*2.048)
      ICNT=0
      GO TO 210
  300 IF(LEN.NE.0) GO TO 210
      ICNT=1
      GO TO 210
  310 IF(LEN.EQ.2054) GO TO 340
  320 WRITE(LU(1),330) LEN
  330 FORMAT("/PLFFT: IMPOSSIBLE LENGTH = ",I5,".  ABORTING ",
     +"PROGRAM!",/)
      GO TO 630
  340 IF(IFIX(DATA(1027)).LT.INUM) GO TO 210
C
C  OBTAIN LOG OF DATA AND GET MAX VALUE
C
D     IMAG=1
      DMAX=-99.0
      DO 370 I=2,1026
      IF(ICAL.EQ.54505B) DATA(I)=DATA(I)*DATA(1)
  350 IF(DATA(I).GT.0.0) GO TO 360
      DATA(I)=-99.0
      GO TO 370
  360 DATA(I)=ALOGT(DATA(I))
      IF(IGAS.EQ.54505B) DATA(I)=DATA(I)-GAS(I)
      DMAX=AMAX1(DMAX,DATA(I))
  370 CONTINUE
      IMAX=IFIX(DMAX)
      IF(DMAX.GE.0.0) IMAX=IMAX+1
C
C  DRAW AXES AND TICK MARKS
C
  380 CALL TPLOT(LU(1),0,137,137)
      CALL TPLOT(LU(1),1,937,137)
```

```
      CALL TPLOT(LU(1),1,937,637)
      CALL TPLOT(LU(1),1,137,637)
      CALL TPLOT(LU(1),1,137,137)
      DO 390 J=1,9
      IYP=J*50+137
      CALL TPLOT(LU(1),0,137,IYP)
      CALL TPLOT(LU(1),1,145,IYP)
      CALL TPLOT(LU(1),0,929,IYP)
      CALL TPLOT(LU(1),1,937,IYP)
  390 CONTINUE
      DO 400 J=1,9
      IXP=J*80+137
      CALL TPLOT(LU(1),0,IXP,137)
      CALL TPLOT(LU(1),1,IXP,145)
      CALL TPLOT(LU(1),0,IXP,629)
      CALL TPLOT(LU(1),1,IXP,637)
  400 CONTINUE
C
C  LABEL ORDINATE, ABSCISSA, AND GRAPH
C
      DO 420 J=0,5
      IYP=J*100+130
      LABEL=(IMAX-5+J)*10
      CALL TPLOT(LU(1),0,70,IYP)
      CALL EXEC(2,LU(1),IUSLA,-2)
      WRITE(LU(1),410) LABEL
  410 FORMAT(I4)
  420 CONTINUE
      IF(IGAS.NE.54505B) GO TO 430
      CALL SYMB(0.50,2.57,0.14,IBUF3,90.0,19)
      GO TO 440
  430 CALL SYMB(0.50,3.13,0.14,IBUF1,90.0,11)
  440 DO 460 J=0,5
      IXP=J*160+118
      XABLE=FLOAT(J)/(10*TIME*FLOAT(IMAG))
      CALL TPLOT(LU(1),0,IXP,102)
      CALL EXEC(2,LU(1),IUSLA,-2)
      WRITE(LU(1),450) XABLE
  450 FORMAT(F3.2)
  460 CONTINUE
      CALL TPLOT(LU(1),0,INDNT,750)
      CALL EXEC(2,LU(1),IUSLA,-2)
      WRITE(LU(1),470) INBUF
  470 FORMAT(36A2)
      IF(ICAL.NE.54505B) GO TO 490
      CALL TPLOT(LU(1),0,441,650)
      CALL EXEC(2,LU(1),IUSLA,-2)
      WRITE(LU(1),480)
  480 FORMAT("NOT CALIBRATED")
```

```
 490 IF(IGAS.NE.54505B) GO TO 510
     CALL TPLOT(LU(1),0,329,700)
     CALL EXEC(2,LU(1),IUSLA,-2)
     WRITE(LU(1),500)
 500 FORMAT(26H"NORMALIZED USING GAS JET")
 510 CALL TPLOT(LU(1),0,435,70)
     CALL EXEC(2,LU(1),IUSLA,-2)
     WRITE(LU(1),520) IBUF2
 520 FORMAT(8A2)
     CALL TPLOT(LU(1),0,0,0)
     CALL EXEC(2,LU(1),IUSLA,-2)
     ICNT=DATA(1027)
     WRITE(LU(1),530) ICNT
 530 FORMAT(" BIOMATION RECORDING ",I3)
     CALL TPLOT(LU(1),0,780,0)
     CALL EXEC(2,LU(1),IUSLA,-2)
     WRITE(LU(1),540) BNDWT
 540 FORMAT("BANDWIDTH ",F3.2," KHZ")
C
C  PLOT POWER SPECTRUM IN DECIBEL FORMAT
C
     DO 600 I=1,1025/IMAG
     IXP=FLOAT(I)*0.78125*FLOAT(IMAG)+137.0
     IYP=(DATA(I+1)-FLOAT(IMAX))*100.0+637.0
     IF(IYP-637) 560,560,550
 550 IYP=637
     GO TO 580
 560 IF(IYP-137) 570,580,580
 570 IYP=137
 580 IF(I.NE.1) GO TO 590
     CALL TPLOT(LU(1),0,IXP,IYP)
     GO TO 600
 590 CALL TPLOT(LU(1),1,IXP,IYP)
 600 CONTINUE
     CALL CURSR(LU(1),IQUIT,IXP,IYP)
     CALL ERASE(LU(1))
     ICNT=ICNT+1
     IF(IQUIT.EQ.43B) GO TO 160
     IF(IQUIT.EQ.121B) GO TO 630
     IF(IQUIT.EQ.115B) GO TO 610
     GO TO 210
 610 WRITE(LU(1),620)
 620 FORMAT("/PLFFT: MAGNIFY BY 1,2, OR 5? _")
     READ(LU(1),*) IMAG
     IF(IMAG.LT.1) IMAG=1
     IF(IMAG.GT.2) IMAG=5
     CALL ERASE(LU(1))
     GO TO 380
C
```

```
C  QUIT
C
  630 CALL CLOSE(IDCB1,IERR)
      IF(IGAS.EQ.54505B) CALL CLOSE(IDCB2,IERR)
      END
```

Source Code of Program AECNF

```
FTN4
C
      PROGRAM AECNF
C
C
C  THIS PROGRAM AVERAGES THE POWER SPECTRA IN THE FILE CREATED
C  UNDER <AENOR> AND THEN PLOTS THE AVERAGED POWER SPECTRUM
C  ALONG WITH THE CONFIDENCE LIMITS SPECIFIED BY THE USER.
C  THE USER CAN NORMALIZE THE AVERAGE POWER SPECTRUM USING
C  THE GAS JET DATA CALCULATED WITH <GASJT>.
C
C
C  WRITTEN BY JOHN CARLYLE
C
C
      DIMENSION LU(5),IREG(2),INBUF(36),IPBUF(10),TBUF(18)
      DIMENSION IDCB1(144),DATA(1028),HBUF(18),IDATA(2056)
      DIMENSION IBUF1(6),IBUF2(8),IDCB2(144),GAS(1028)
      DIMENSION AVE(1026),VAR(1025),IBUF3(10)
      EQUIVALENCE (REG,IREG),(INBUF,HBUF),(DATA,IDATA)
      EQUIVALENCE (DATA(1011),TBUF),(TAVE,AVE)
      DATA ICNT/1/,IUSLA/17537B/,ITRY/-1/,IMAG/1/,IPASS/-1/
      DATA IBUF1/2HPO,2HWE,2HR ,2H(D,2HBM,2H) /
      DATA IBUF2/2HFR,2HEQ,2HUE,2HNC,2HY ,2H(M,2HHZ,2H) /
      DATA IBUF3/2HRE,2HLA,2HTI,2HVE,2H P,2HOW,2HER,
     +2H (,2HDB,2H) /
C
C  RECOVER PARAMETERS
C
      CALL RMPAR(LU)
      IF(LU(1).EQ.0) LU(1)=1
      ILU=LU(1)+400B
C
C  GET 'NAMR' INFORMATION
C
      CALL PLTLU(LU(1))
   10 WRITE(LU(1),20) ICNT
   20 FORMAT("/AECNF: ENTER 'NAMR' FOR FILE #",I1,": _")
      REG=EXEC(1,ILU,INBUF,-72)
      ISCHR=1
      IF(NAMR(IPBUF,INBUF,IREG(2),ISCHR)) 10,30
   30 IF(ICNT.NE.1) GO TO 90
C
C  OPEN FILE #1
C
      CALL OPEN(IDCB1,IERR,IPBUF,0,IPBUF(5),IPBUF(6))
      IF(IERR.GE.0) GO TO 60
   40 WRITE(LU(1),50) IERR
   50 FORMAT("/AECNF: FILE ERROR ",I4,".  TRY AGAIN!",/)
```

```
      GO TO 10
C
C  OPEN FILE #2
C
   60 WRITE(LU(1),70)
   70 FORMAT("/AECNF: PLOT WAVEFORMS NORMALIZED BY GAS JET? _")
      READ(LU(1),80) IGAS
   80 FORMAT(A2)
      IF(IGAS.NE.54505B) GO TO 100
      ICNT=2
      GO TO 10
   90 CALL OPEN(IDCB2,IERR,IPBUF,0,IPBUF(5),IPBUF(6))
      IF(IERR.GT.0) GO TO 100
      ITRY=ITRY+1
      IF(ITRY.LT.2) GO TO 40
      GO TO 130
C
C  READ DATA IN PLOT FILE
C
  100 CALL ERASE(LU(1))
  110 ICNT=-1
      ITRY=-1
  120 CALL READF(IDCB1,IERR,DATA,2056,LEN)
      IF(IERR.GE.0) GO TO 150
  130 WRITE(LU(1),140) IERR
  140 FORMAT("/AECNF: FILE ERROR ",I4,".  ABORTING PROGRAM!",/)
      GO TO 760
  150 IF(LEN.NE.-1) GO TO 180
      IF(ICNT.GT.0) GO TO 170
      WRITE(LU(1),160)
  160 FORMAT("/AECNF: EOF ENCOUNTERED. ABORTING PROGRAM!",/)
      GO TO 760
  170 IF(IPASS) 300,340,340
  180 IF(ICNT) 190,230,240
  190 CALL CODE(LEN*2)
      READ(IDATA,*) (TBUF(I),I=1,18)
      IF(TBUF(1).NE.0.0) GO TO 210
      IF(ITRY.GE.0.OR.IPASS.GT.0) GO TO 120
      DO 200 I=1,18
      HBUF(I)=DATA(I)
      INDNT=(73-LEN*2)*7
      ITRY=1
  200 CONTINUE
      GO TO 120
  210 IF(IPASS.GT.0) GO TO 220
      TIME=TBUF(2)
      BNDWT=1.0/(TIME*2.048)
  220 ICNT=0
      GO TO 120
```

```
  230 IF(LEN.NE.0) GO TO 120
      ICNT=1
      GO TO 120
  240 IF(LEN.EQ.2054) GO TO 270
  250 WRITE(LU(1),260) LEN
  260 FORMAT("/AECNF: IMPOSSIBLE LENGTH = ",I5,".  ABORTING ",
     +"PROGRAM!",/)
      GO TO 760
C
C  CALCULATE AVERAGE OF NORMALIZED AE WAVEFORMS
C
  270 IF(IPASS) 280,320,320
  280 NWAVE=NWAVE+1
      DO 290 I=2,1026
      DATA(I)=DATA(I)*DATA(1)
      AVE(I)=DATA(I)+AVE(I)
  290 CONTINUE
      TAVE=TAVE+DATA(1)
      GO TO 120
  300 CALL RWNDF(IDCB1,IERR)
      IF(IERR.LT.0) GO TO 130
      TAVE=TAVE/FLOAT(NWAVE)
      DO 310 I=2,1026
      AVE(I)=AVE(I)/FLOAT(NWAVE)
  310 CONTINUE
      IPASS=1
      GO TO 110
C
C  CALCULATE VARIANCE OF NORMALIZED AE WAVEFORMS
C
  320 DO 330 I=2,1026
      DATA(I)=DATA(I)*DATA(1)
      VAR(I-1)=(DATA(I)-AVE(I))*(DATA(I)-AVE(I))+VAR(I-1)
  330 CONTINUE
      GO TO 120
  340 NDEGF=NWAVE-1
      DO 350 I=1,1025
      VAR(I)=SQRT(VAR(I)/(FLOAT(NWAVE)*FLOAT(NDEGF)))
  350 CONTINUE
C
C  READ GAS JET DATA
C
      ITRY=-1
      IF(IGAS.NE.54505B) GO TO 410
  360 CALL READF(IDCB2,IERR,GAS,2056,LEN)
      IF(LEN.LT.0.OR.IERR.LT.0) GO TO 130
      IF(LEN.NE.0.AND.ITRY.GT.0) GO TO 370
      IF(LEN.NE.0) GO TO 360
      ITRY=1
```

```
      GO TO 360
  370 IF(LEN.EQ.2054) GO TO 380
      GO TO 250
  380 DO 400 I=2,1026
      IF(GAS(I).GT.0.0) GO TO 390
      GAS(I)=-99.0
      GO TO 400
  390 GAS(I)=ALOGT(GAS(I))
  400 CONTINUE
C
C  GET PROPER "T" VALUE AND CONFIDENCE LIMITS
C
  410 WRITE(LU(1),420) NDEGF
  420 FORMAT("/AECNF: ENTER 'T' VALUE AND CONFIDENCE LIMITS ",
     +"FOR ",I3," DF: _")
      READ(LU(1),*) TVAL,ICONF
      CALL ERASE(LU(1))
      IMAG=1
C
C  OBTAIN LOG OF DATA AND FIND MAX FOR PLOT
C
  430 IPASS=-1
  440 IF(IPASS) 450,480,480
  450 DMAX=-99.0
      DO 470 I=2,1026
      DATA(I)=(AVE(I)+TVAL*VAR(I-1))/TAVE
      IF(DATA(I).GT.0.0) GO TO 460
      DATA(I)=-99.0
      GO TO 470
  460 DATA(I)=ALOGT(DATA(I))
      IF(IGAS.EQ.54505B) DATA(I)=DATA(I)-GAS(I)
      DMAX=AMAX1(DMAX,DATA(I))
  470 CONTINUE
      IMAX=IFIX(DMAX)
      IF(DMAX.GE.0.0) IMAX=IMAX+1
      GO TO 510
  480 DO 500 I=2,1026
      DATA(I)=(AVE(I)-FLOAT(IPASS)*TVAL*VAR(I-1))/TAVE
      IF(DATA(I).GT.0) GO TO 490
      DATA(I)=-99.0
      GO TO 500
  490 DATA(I)=ALOGT(DATA(I))
      IF(IGAS.EQ.54505B) DATA(I)=DATA(I)-GAS(I)
  500 CONTINUE
      GO TO 670
C
C  DRAW AXES AND TICK MARKS
C
  510 CALL TPLOT(LU(1),0,137,137)
```

```
      CALL TPLOT(LU(1),1,937,137)
      CALL TPLOT(LU(1),1,937,637)
      CALL TPLOT(LU(1),1,137,637)
      CALL TPLOT(LU(1),1,137,137)
      DO 520 J=1,9
      IYP=J*50+137
      CALL TPLOT(LU(1),0,137,IYP)
      CALL TPLOT(LU(1),1,145,IYP)
      CALL TPLOT(LU(1),0,929,IYP)
      CALL TPLOT(LU(1),1,937,IYP)
  520 CONTINUE
      DO 530 J=1,9
      IXP=J*80+137
      CALL TPLOT(LU(1),0,IXP,137)
      CALL TPLOT(LU(1),1,IXP,145)
      CALL TPLOT(LU(1),0,IXP,629)
      CALL TPLOT(LU(1),1,IXP,637)
  530 CONTINUE
C
C  LABEL ORDINATE, ABSCISSA, AND GRAPH
C
      DO 550 J=0,5
      IYP=J*100+130
      LABEL=(FLOAT(IMAX)-5.0+FLOAT(J))*10.0
      CALL TPLOT(LU(1),0,70,IYP)
      CALL EXEC(2,LU(1),IUSLA,-2)
      WRITE(LU(1),540) LABEL
  540 FORMAT(I4)
  550 CONTINUE
      IF(IGAS.NE.54505B) GO TO 560
      CALL SYMB(0.50,2.57,0.14,IBUF3,90.0,19)
      GO TO 570
  560 CALL SYMB(0.50,3.13,0.14,IBUF1,90.0,11)
  570 DO 590 J=0,5
      IXP=J*160+118
      XABLE=FLOAT(J)/(10.0*TIME*FLOAT(IMAG))
      CALL TPLOT(LU(1),0,IXP,102)
      CALL EXEC(2,LU(1),IUSLA,-2)
      WRITE(LU(1),580) XABLE
  580 FORMAT(F3.2)
  590 CONTINUE
      CALL TPLOT(LU(1),0,INDNT,750)
      CALL EXEC(2,LU(1),IUSLA,-2)
      WRITE(LU(1),600) INBUF
  600 FORMAT(36A2)
      CALL TPLOT(LU(1),0,364,725)
      CALL EXEC(2,LU(1),IUSLA,-2)
      WRITE(LU(1),610) ICONF
  610 FORMAT(I2,"% CONFIDENCE LIMITS")
```

```
      IF(IGAS.NE.54505B) GO TO 630
      CALL TPLOT(LU(1),0,329,700)
      CALL EXEC(2,LU(1),IUSLA,-2)
      WRITE(LU(1),620)
  620 FORMAT(26H"NORMALIZED USING GAS JET")
  630 CALL TPLOT(LU(1),0,435,70)
      CALL EXEC(2,LU(1),IUSLA,-2)
      WRITE(LU(1),640) IBUF2
  640 FORMAT(8A2)
      CALL TPLOT(LU(1),0,0,0)
      CALL EXEC(2,LU(1),IUSLA,-2)
      WRITE(LU(1),650) NWAVE
  650 FORMAT(I3," SPECTRA AVERAGED")
      CALL TPLOT(LU(1),0,780,0)
      CALL EXEC(2,LU(1),IUSLA,-2)
      WRITE(LU(1),660) BNDWT
  660 FORMAT("BANDWIDTH ",F3.2," KHZ")
C
C  PLOT POWER SPECTRUM IN DECIBEL FORMAT
C
  670 DO 730 I=1,1025/IMAG
      IXP=FLOAT(I)*0.78125*FLOAT(IMAG)+137.0
      IYP=(DATA(I+1)-FLOAT(IMAX))*100.0+637.0
      IF(IYP-637) 690,690,680
  680 IYP=637
      GO TO 710
  690 IF(IYP-137) 700,710,710
  700 IYP=137
  710 IF(I.NE.1.AND.IPASS.NE.0) GO TO 720
      CALL TPLOT(LU(1),-1,IXP,IYP)
      GO TO 730
  720 CALL TPLOT(LU(1),1,IXP,IYP)
  730 CONTINUE
      IPASS=IPASS+1
      IF(IPASS.LE.1) GO TO 440
      CALL CURSR(LU(1),IQUIT,IXP,IYP)
      CALL ERASE(LU(1))
      IF(IQUIT.EQ.115B) GO TO 740
      IF(IQUIT.EQ.124B) GO TO 410
      GO TO 760
  740 WRITE(LU(1),750)
  750 FORMAT("/AECNF: MAGNIFY BY 1,2, OR 5? _")
      READ(LU(1),*) IMAG
      IF(IMAG.LT.1) IMAG=1
      IF(IMAG.GT.2) IMAG=5
      CALL ERASE(LU(1))
      GO TO 430
C
C  QUIT
```

```
C
  760 CALL CLOSE(IDCB1,IERR)
      IF(IGAS.EQ.54505B) CALL CLOSE(IDCB2,IERR)
      END
```

Source Code of Program DBSVR

```
FTN4
C
      PROGRAM DBSVR
C
C
C  THIS PROGRAM WILL SAVE THE DISC DATA FILES CREATED USING
C  <AENOR> AND <GASJT> ON TAPE AND VERIFY THEM.  THE USER
C  CAN ALSO RESTORE THE DATA FILES TO DISC.
C
C
C  WRITTEN BY JOHN CARLYLE
C
C
      DIMENSION LU(5),IREG(2),INBUF(36),IPBUF(10)
      DIMENSION IDCB1(144),IDATA(2056),ICOMP(2056),IDEOF(6)
      EQUIVALENCE (REG,IREG)
      DATA IDEOF/401B,77577B,77577B,401B,100000B,1B/
C
C  RECOVER PARAMETERS
C
      CALL RMPAR(LU)
      IF(LU(1).EQ.0) LU(1)=1
      IF(LU(2).EQ.0) LU(2)=8
      CALL EXEC(3,400B+LU(2))
C
C  DETERMINE MODE
C
      WRITE(LU(1),10)
   10 FORMAT("/DBSVR:  IS THIS A RESTORE OPERATION? _")
      READ(LU(1),20) IREST
   20 FORMAT(A2)
      IF(IREST.EQ.54505B) GO TO 250
C
C  POSITION MAG TAPE FOR SAVE
C
      WRITE(LU(1),30)
   30 FORMAT("/DBSVR:  IS ARCHIVE TAPE BLANK? _")
      READ(LU(1),20) IVIRG
      IF(IVIRG.EQ.54505B) GO TO 50
   40 CALL EXEC(3,1300B+LU(2))
      REG=EXEC(1,LU(2),INBUF,36)
      IF(IAND(IREG(1),200B).EQ.0) GO TO 40
      CALL EXEC(3,1400B+LU(2))
C
C  SAVE FILE OPENING SECTION
C
   50 WRITE(LU(1),60)
   60 FORMAT("/DBSVR:  ENTER NAME OF FILE TO BE SAVED: _")
      REG=EXEC(1,400B+LU(1),INBUF,-72)
```

```
      ISCHR=1
      IF(NAMR(IPBUF,INBUF,IREG(2),ISCHR)) 50,70
   70 CALL OPEN(IDCB1,IERR,IPBUF,0,IPBUF(5),IPBUF(6))
      IF(IERR.GE.0) GO TO 100
   80 WRITE(LU(1),90) IERR
   90 FORMAT("/DBSVR:  FILE ERROR ",I4,".  TRY AGAIN!",/)
      GO TO 50
C
C  SAVE DATA TRANSFER SECTION
C
  100 CALL READF(IDCB1,IERR,IDATA,2056,LEN)
      IF(IERR.GE.0) GO TO 130
  110 WRITE(LU(1),120) IERR
  120 FORMAT("/DBSVR:  FILE ERROR ",I4,".  ABORTING PROGRAM!",/)
      GO TO 210
  130 IF(LEN.NE.-1) GO TO 150
      WRITE(LU(1),140)
  140 FORMAT("/DBSVR:  EOF ENCOUNTERED.  FILE ON MAG TAPE!",/)
      CALL EXEC(3,100B+LU(2))
      GO TO 220
  150 IF(LEN) 160,180,160
  160 CALL EXEC(2,LU(2),IDATA,LEN)
  170 REG=EXEC(3,600B+LU(2))
      IREG(1)=IAND(IREG(1),73B)
      IF(IREG(1).NE.0) GO TO 190
      GO TO 100
  180 CALL EXEC(2,LU(2),IDEOF,6)
      GO TO 170
  190 WRITE(LU(1),200) IREG(1)
  200 FORMAT("/DBSVR:  MAG TAPE STATUS = ",O3,"B.  ABORTING ",
     +"PROGRAM!",/)
  210 IF(IREST.EQ.54505B) GO TO 490
      CALL EXEC(3,1400B+LU(2))
      CALL EXEC(3,300B+LU(2))
      CALL EXEC(3,100B+LU(2))
      GO TO 490
  220 IOK=IVRFY(IDCB1,IDATA,ICOMP,LU(2),IVIRG)
      IF(IOK.EQ.1) GO TO 230
      WRITE(LU(1),460)
      GO TO 210
  230 CALL CLOSE(IDCB1,IERR)
      WRITE(LU(1),240)
  240 FORMAT("/DBSVR:  SAVE ANOTHER FILE? _")
      IVIRG=47117B
      READ(LU(1),20) IMORE
      IF(IMORE.EQ.54505B) GO TO 50
      CALL EXEC(3,100B+LU(2))
      GO TO 510
C
```

```
C  FILE POSITIONING FOR RESTORE
C
  250 WRITE(LU(1),260)
  260 FORMAT("/DBSVR:  ENTER FILE NUMBER: _")
      READ(LU(1),*) IFILE
      ICNT=1
      IF(IFILE) 270,270,290
  270 WRITE(LU(1),280)
  280 FORMAT("/DBSVR:  INVALID MAG TAPE FILE.  TRY AGAIN!",/)
      GO TO 250
  290 IF(IFILE.EQ.1) GO TO 310
  300 CALL EXEC(3,1300B+LU(2))
      ICNT=ICNT+1
      IF(ICNT.LT.IFILE) GO TO 300
      GO TO 320
  310 IVIRG=54505B
  320 WRITE(LU(1),330)
  330 FORMAT("/DBSVR:  FILE ID IS:")
      REG=EXEC(1,LU(2),IDATA,2056)
      CALL EXEC(2,LU(1),IDATA,IREG(2))
      WRITE(LU(1),340)
  340 FORMAT("/DBSVR:  OK TO RESTORE? _")
      READ(LU(1),20) IYEP
      IF(IYEP.EQ.54505B) GO TO 350
      CALL EXEC(3,400B+LU(2))
      IVIRG=0
      GO TO 250
  350 CALL EXEC(3,200B+LU(2))
      ITRY=0
C
C  RESTORE FILE CREATION SECTION
C
  360 WRITE(LU(1),370)
  370 FORMAT("/DBSVR:  ENTER FILE NAME FOR DATA STORAGE: _")
      REG=EXEC(1,400B+LU(1),INBUF,-72)
      ISCHR=1
      IF(NAMR(IPBUF,INBUF,IREG(2),ISCHR)) 360,380
  380 IREG(1)=-1
      IREG(2)=0
      CALL CREAT(IDCB1,IERR,IPBUF,IREG,3,IPBUF(5),IPBUF(6))
      IF(IERR.GE.0) GO TO 390
      ITRY=ITRY+1
      IF(ITRY.GE.3) GO TO 110
      WRITE(LU(1),90) IERR
      GO TO 360
C
C  RESTORE DATA TRANSFER SECTION
C
  390 REG=EXEC(1,LU(2),IDATA,2056)
```

```
      IF(IAND(IREG(1),200B).GT.0) GO TO 420
      IREG(1)=IAND(IREG(1),73B)
      IF(IREG(1).NE.0) GO TO 190
      IF(IREG(2).NE.6) GO TO 410
      DO 400 I=1,6
      IF(IDATA(I).NE.IDEOF(I)) GO TO 410
  400 CONTINUE
      IREG(2)=0
  410 CALL WRITF(IDCB1,IERR,IDATA,IREG(2))
      IF(IERR.LT.0) GO TO 110
      GO TO 390
  420 CALL LOCF(IDCB1,IERR,ICNT,IREC,L,LEN)
      LEN=LEN/2-IREC-1
      CALL CLOSE(IDCB1,IERR,LEN)
      IF(IERR.GE.0) GO TO 440
      WRITE(LU(1),430) IERR,LEN
  430 FORMAT("/DBSVR:  ERROR ",I4," IN TRUNCATING FILE BY ",I6,
     +" BLOCKS!",/)
      GO TO 500
  440 CALL OPEN(IDCB1,IERR,IPBUF,0,IPBUF(5),IPBUF(6))
      WRITE(LU(1),450)
  450 FORMAT("/DBSVR:  EOF ENCOUNTERED.  FILE ON DISC!",/)
      IOK=IVRFY(IDCB1,IDATA,ICOMP,LU(2),IVIRG)
      IF(IOK.EQ.1) GO TO 470
      WRITE(LU(1),460)
  460 FORMAT("/DBSVR:  VERIFICATION ERROR.  ABORTING ",
     +"PROGRAM!",/)
      GO TO 500
  470 CALL CLOSE(IDCB1,IERR)
      WRITE(LU(1),480)
  480 FORMAT("/DBSVR:  RESTORE ANOTHER FILE? _")
      READ(LU(1),20) IMORE
      IF(IMORE.NE. 54505B) GO TO 510
      CALL EXEC(3,400B+LU(2))
      IVIRG=0
      GO TO 250
C
C  QUIT
C
  490 IF(IREST.EQ.54505B) GO TO 500
      CALL CLOSE(IDCB1,IERR)
      GO TO 510
  500 CALL PURGE(IDCB1,IERR,IPBUF,IPBUF(5),IPBUF(6))
  510 CALL EXEC(3,400B+LU(2))
      END
      FUNCTION IVRFY(IDCB1,IDATA,ICOMP,LU,IVIRG)
      DIMENSION IDCB1(1),IDATA(1),ICOMP(1),IREG(2)
      EQUIVALENCE (REG,IREG)
      CALL RWNDF(IDCB1,IERR)
```

```
      CALL EXEC(3,1400B+LU)
      CALL EXEC(3,1400B+LU)
      IF(IVIRG.EQ.54505B) GO TO 10
      CALL EXEC(3,300B+LU)
   10 REG=EXEC(1,LU,ICOMP,2056)
      CALL READF(IDCB1,IERR,IDATA,2056,LEN)
      IF(IERR.LT.0.OR.IAND(IREG(1),73B).NE.0) GO TO 40
      IF(LEN.EQ.-1.OR.IAND(IREG(1),200B).NE.0) GO TO 30
      IF(LEN.EQ.0) GO TO 10
      IF(IREG(2).NE.LEN) GO TO 40
      DO 20 I=1,LEN
      IF(IDATA(I).NE.ICOMP(I)) GO TO 40
   20 CONTINUE
      GO TO 10
   30 IF(LEN.EQ.-1.AND.IAND(IREG(1),200B).NE.0) GO TO 50
   40 IVRFY=-1
      RETURN
   50 IVRFY=1
      RETURN
      END
```

REFERENCES

1. Carlyle, J.M., and Scott, W.R., "Acoustic Emission Fatigue Analyzer", Experimental Mechanics, 16, 10, 369-372 (1976)

2. Scott, W.R., and Carlyle, J.M., U.S. Patent 4089224 (1978)

3. Carlyle, J.M., Acoustic Emission in Fiber Reinforced Composites, M.Tech. Thesis, Brunel University, London (1974)

4. Kaiser, J., Untersuchungen uber das auftreten Gerauschen beim Zugversuch, Ph.D. Thesis, Technische Hochschule, Munich (1950)

5. Portevin, A., and LeChatelier, F., "Sur un Phenomene Observe lors de l'Essai de Traction d'Alliages en Cours de Transformation", Comptes Rendus Hebdomadaires des Seances de l'Academie des Sciences, 176, 507-510 (1923)

6. Joffe, A., The Physics of Crystals, McGraw-Hill, New York (1928)

7. Mason, W.P., McSkimin, H.J., and Shockley, W., "Ultrasonic Observation of Twinning in Tin", Physical Review, 73, 10, 1213-1214 (1948)

8. Dunegan, H.L., and Tatro, C.A., "Passive Pressure Transducer Utilizing Acoustic Emission", Review of Scientific Instruments, 38, 8, 1145-1147 (1967)

9. Pollock, A.A., and Smith, B., "Acoustic Emission Monitoring of a Military Bridge", Non-destructive Testing, 5, 6, 348-353 (1972)

10. Lean, J.B., Plateau, J., Bachet, C., and Crussard, C., "Sur la Formation d'Ondes Sonores, au Cours d'Essais de Traction, dan des Eprouvettes Metalliques", Comptes Rendus Hebdomadaires des Seances de l'Academie des Sciences, 246, 2845-2848 (1958)

11. Schofield, B.H., Bareiss, R.A., and Kyrala, A.A., Acoustic Emission Under Applied Stress, ASTIA Document AD 155674, WADC Technical Report 58-194, Wright Air Development Center, Dayton, Ohio, April 1958

12. Tatro, C.A., Sonic Techniques in the Detection of Crystal Slip in Metals, Progress Report, Engineering Experiment Station, College of Engineering, Michigan State University, East Lansing, Michigan, January 1959

13. Schofield, B.H., Acoustic Emission Under Applied Stress, ASD-TDR-63-509, Wright-Patterson Air Force Base, Dayton, Ohio, Part I, April 1963, Part II, May 1964

14. Tatro, C.A., and Liptai, R.G., "Acoustic Emission from Crystalline Substances", Proceedings of the Symposium on Physics and Nondestructive Testing, Southwest Research Institute, San Antonio, Texas, October 1962

15. Hardy, H.R., Jr., "Applications of Acoustic Emission Techniques to Rock Mechanics Research", 41-83, Acoustic Emission, ASTM STP 505, American Society for Testing and Materials, Philadelphia (1972)

16. Green, A.T., Lockman, C.S., and Steele, R.K., "Acoustic Verification of Structural Integrity of Polaris Chambers", Modern Plastics, 41, 11, 137-139 (1964)

17. Speich, G.R., and Fisher, R.M., "Acoustic Emission During Martensite Formation", 140-151, Acoustic Emission, ASTM STP 505, American Society for Testing and Materials, Philadelphia (1972)

18. Gerberich, W.W., and Hartbower, C.E., "Some Observations on Stress Wave Emission as a Measure of Crack Growth", International Journal of Fracture Mechanics, 3, 3, 185-192 (1967)

19. Fisher, R.M., and Lally, J.S., "Microplasticity Detected by an Acoustic Technique", Canadian Journal of Physics, 45, 2, 1147-1159 (1967)

20. James, D.R., and Carpenter, S.H., "Relationship Between Acoustic Emission and Dislocation Kinetics in Crystalline Solids", Journal of Applied Physics, 42, 12, 4685-4697 (1971)

21. Hartbower, C.E., Gerberich, W.W., and Crimmins, P.P., "Monitoring Subcritical Crack Growth by Detection of Elastic Stess Waves", The Welding Journal, 47, 1, 1-18 (1968)

22. Dunegan, H.L, Harris, D.O., and Tatro, C.A., "Fracture Analysis by Use of Acoustic Emission", Engineering Fracture Mechanics, 1, 1, 105-122 (1968)

23. Anderson, T.T., Gavin, A.P., Karvinen, J.R., Price, C.C., and Reimann, K.J., "Detecting Acoustic Emission in Large Metal Cooled Fast Breeder Reactors", 250-269, Acoustic Emission, ASTM STP 505, American Society for Testing and Materials, Philadelphia (1972)

24. Parry, D.L., "Nondestructive Flaw Detection in Nuclear Power Installations", 107-126, Incipient Failure Diagnosis, U.S. Atomic Energy Commission Conference 671011, Gatlinburg, Tennessee, November 1967

25. Jolly, W.D., "The Application of Acoustic Emission to In-Process Weld Inspection", Materials Evaluation, 28, 6, 135-139 (1970)

26. Prine, D.W., NDT of Welds by Acoustic Emission, Technical Report DE 73-X, Dunegan/Endevco Co., San Juan Capistrano, California (1973)

27. Hutton, P.H., "Acoustic Emission Applied Outside the Laboratory", 114-128, Acoustic Emission, ASTM STP 505, American Society for Testing and Materials, Philadelphia (1972)

28. Rathbun, D.K., Beattie, A.G., and Hiles, L.A., Filament Wound Materials Evaluation with Acoustic Emission, Report SCL-DC-70-260, Sandia Laboratories, Livermore, California, April 1971

29. Liptai, R.G., "Acoustic Emission from Composite Materials", 285-298, Composite Materials: Testing and Design, ASTM STP 497, American Society for Testing and Materials, Philadelphia (1972)

30. Pattnaik, A., and Lawley, A., Role of Microstructure on Acoustic Emission in the Deformation of Al-$CuAl_2$ Composites, Technical Report 10, Contract N00014-67-A-0406-0001, Office of Naval Research, Arlington, Virginia, April 1973

31. Harris, D.O., Tetelman, A.S., and Darwish, F.A., "Detection of Fiber Cracking by Acoustic Emission", 238-249, Acoustic Emission, ASTM STP 505, American Society for Testing and Materials, Philadelphia (1972)

32. Balderston, H.L., "The Broad Range Detection of Incipient Failure Using the Acoustic Emission Phenomenon", 297-317, Acoustic Emission, ASTM STP 505, American Society for Testing and Materials, Philadelphia (1972)

33. Carlyle, J.M., "Imminent Fracture Detection in Graphite/Epoxy Using Acoustic Emission", Experimental Mechanics, 18, 5, 191-195 (1978)

34. Mullin, J.V., and Mehan, R.L., "Evaluation of Composite Failures Through Fracture Signature Analysis", Journal of Testing and Evaluation, 1, 3, 215-219 (1973)

35. Speake, J.H., and Curtis, G.J., "Characterization of the Fracture Processes in CFRP Using Spectral Analysis of the Acoustic Emission Arising from the Application of Stress", Paper 29, International Conference on Carbon Fibers, sponsored by the Plastics Institution, London, February 1974

36. Ono, K., Huang, G., Kawamoto, A., Anisotropic Acoustic Emission Behavior of HSLA Steels, ONR 78-01, Contract N00014-75-C-0419, Office of Naval Research, Washington, D.C., January 1978

37. Kiesewetter, N., and Schiller, P., "The Acoustic Emission From Moving Dislocations in Aluminum", Physica Status Solidi (A), 38, 2, 569-576 (1976)

38. Frederick, J.R., Use of Acoustic Emission in Nondestructive Testing, AFML-TR-72-114, Wright-Patterson Air Force Base, Dayton, Ohio, December 1971

39. Tandon, K.N., and Tangri, K., "Acoustic Emissions During Deformation of Polycrystalline Silicon-Iron", Materials Science and Engineering, 20, 1, 47-54 (1975)

40. Carpenter, S.H., and Heiple, C.R., "Acoustic Emission Generated by Dislocation Mechanisms During the Deformation of Metals", 49-104, Fundamentals of Acoustic Emission, K. Ono, editor, University of California, Los Angeles (1979)

41. Wadley, H.N.G., Scruby, C.B., and Speake, J.H., "Acoustic Emission for Physical Examination of Metals", International Metals Review, 25, 2, 41-64 (1980)

42. Scruby, C.B., Wadley, H.N.G., Rusbridge, K., and Stockham-Jones, D., The Influence of Microstructure on Acoustic Emission During the Deformation of Aluminum Alloys, AERE-R-10069, Atomic Energy Research Establishment, Harwell, Oxfordshire, October 1981

43. Scruby, C.B., Wadley, H.N.G., and Sinclair, J.E., The Origin of Acoustic Emission During Deformation of Aluminum and an Aluminum-Magnesium Alloy, AERE-R-9643, Atomic Energy Research Establishment, Harwell, Oxfordshire, June 1980

44. Burridge, R., and Knopoff, L., "Body Force Equivalents for Seismic Dislocation", Bulletin of the Seismological Society of America, 54, 6, 1875-1888 (1964)

45. Cousland, S.McK., and Scala, C.M., "Acoustic Emission and Microstructure in the Aluminum Alloys 7075 and 7050", Metal Science, 15, 609-614 (1981)

46. Byerlee, J.D., and Peselnick, L., "Elastic Shocks and Earthquakes", Naturwissenschaften, 57, 2, 82-85 (1970)

47. McBride, S.L., MacLachlan, J.W., and Paradis, B.P., "Acoustic Emission and Inclusion Fracture in 7075 Aluminum Alloys", Journal of Nondestructive Evaluation, 2, 1, 35-41 (1981)

48. Nozue, A., and Kishi, T., "An Acoustic Emission Study of the Intergranular Cracking of AISI 4340 Steel", Journal of Acoustic Emission, 1, 1, 1-6 (1982)

49. Stone, D.E.W., and Dingwall, P.F., "Acoustic Emission Parameters and Their Interpretation, *NDT International*, 10, 2, 51-62 (1977)

50. Pollock, A.A., "Acoustic Emission Amplitudes", *Non-destructive Testing*, 6, 5, 264-269 (1973)

51. Stephens, R.W.B., and Pollock, A.A., "Waveforms and Frequency Spectra of Acoustic Emissions", *Journal of the Acoustical Society of America*, 50, 3, 904-910 (1971)

52. Ono, K., "Acoustic Emission Arising from Plastic Deformation and Fracture", 167-207, *Fundamentals of Acoustic Emission*, K. Ono, editor, University of California, Los Angeles (1979)

53. Malen, K., and Bolin, L., "A Theoretical Estimate of Acoustic Emission Stress Amplitudes", *Physica Status Solidi (B)*, 61, 2, 637-645 (1974)

54. Pao, Y.H., Gajewski, R.R., and Ceranoglu, A.N., "Acoustic Emission and Transient Waves in an Elastic Plate", *Journal of the Acoustical Society of America*, 65, 1, 96-105 (1979)

55. Lamb, H., "On the Propagation of Tremors Over the Surface of an Elastic Solid", *Philosophical Transactions of the Royal Society*, A203, 1-42 (1904)

56. Breckenridge, F.R., Tschiegg, C.E., and Greenspan, M., "Acoustic Emission: Some Applications of Lamb's Problem", *Journal of the Acoustical Society of America*, 57, 3, 626-631 (1975)

57. Hsu, N., and Hardy, S., "Experiments in Acoustic Emission Waveform Analysis for Characterization of AE Sources, Sensors and Structures", 85-106, *Elastic Waves and Nondestructive Testing of Materials*, AMD Vol. 29, Y.H. Pao, editor, American Society of Mechanical Engineers, New York (1978)

58. Wadley, H.N.G., Scruby, C.B., and Shrimpton, G., *Quantitative Acoustic Emission Source Characterization During Low Temperature Cleavage and Intergranular Fracture*, AERE-R-9644, Atomic Energy Research Establishment, Harwell, Oxfordshire, December 1979

59. Kinsler, L.E., and Frey, A.R., *Fundamentals of Acoustics*, Wiley, New York (1965)

60. Bhatia, A.B., *Ultrasonic Absorption*, Oxford University Press, London (1967)

61. Blitz, J., *Fundamentals of Ultrasonics*, Butterworths, London (1967)

62. Hochschild, R., "Microwave Nondestructive Testing in One (Not-So-Easy) Lesson", Materials Evaluation, 26, 1, 35A-42A (1968)

63. Filipczynski, L., Pawlowski, Z., and Wehr, J., Ultrasonic Methods of Testing Materials, Butterworths, London (1966)

64. Stephens, R.W.B., and Bates, A.E., Acoustics and Vibrational Physics, Arnold, London (1966)

65. Krautkramer, J., and Krautkramer, H., Ultrasonic Testing of Materials, Springer-Verlag, New York (1969)

66. Elsley, R., and Graham, L., Rockwell International, Thousand Oaks, California, private communication, August 1981

67. Kino, G.S., "Broadband Acoustic Emission Transducers", Appendix G, A Review of Advanced Acoustic Emission Transducers, D.K. Lemon, Report NADC-81087-60, Naval Air Development Center, Warminster, Pennsylvania, April 1981

68. Frederick, J.R., Ultrasonic Engineering, Wiley, New York (1965)

69. Hueter, T.F., and Bolt, R.H., Sonics, Wiley, New York (1962)

70. Mason, W.P., Piezoelectric Crystals and Their Application to Ultrasonics, Van Nostrand, New York (1950)

71. Vahaviolos, S.J., Energy-Signal Processing for High Frequency Failure Mode Analysis, Ph.D. Thesis, Columbia University, New York (1976)

72. Reid, A., "The Manufacture of Probes", 213-222, Non-destructive Testing, H.B. Egerton, editor, Oxford University Press, London (1969)

73. Sachse, W., and Hsu, N., "Ultrasonic Transducers for Materials Testing and Their Characterization", 277-406, Physical Acoustics Vol. 14, W.P. Mason, editor, Academic Press, New York (1979)

74. Bobber, R.J., Underwater Electroacoustic Measurements, Naval Research Laboratories, Washington, DC (1970)

75. Leschek, W.C., "Acoustic Emission Transducer Calibrator", Materials Evaluation, 33, 2, 41-48 (1975)

76. Hatano, H., and Mori, E., "Acoustic Emission Transducer and Its Absolute Calibration", Journal of the Acoustical Society of America, 59, 2, 344-349 (1976)

77. McBride, S.L., and Hutchison, T.S., "Helium Gas Jet Spectral Calibration of Acoustic Emission Transducers and Systems", Canadian Journal of Physics, 54, 17, 1824-1830 (1976)

78. Hsu, N., and Breckenridge, F.R., "Characterization and Calibration of Acoustic Emission Sensors", Materials Evaluation, 39, 1, 60-68 (1981)

79. Pekeris, C.L., "The Seismic Surface Pulse", Proceedings of the National Academy of Sciences, 41, 469-480 (1955)

80. Breckenridge, F.R., National Bureau of Standards, Washington, DC, private communication, March 1982

81. Hsu, N.N., Acoustic Emission Simulator, U.S. Patent 4018084 (1977)

82. Scruby, C.B., Wadley, H.N.G., Dewhurst, R.J., Hutchins, D.A., and Palmer, S.B., A Laser Generated Standard Acoustic Emission Source, AERE-R-10003, Atomic Energy Research Establishment, Harwell, Oxfordshire (1981)

83. Bentley, M.N., and Green, G.A., "A Method of Calibration for Acoustic Emission Measurements", Proceedings of the Institute of Acoustics, London, December 1976

84. Green, G.A., and Dingwall, P.F., "The Use of the Helium Gas Jet in the Analysis of Acoustic Emissions", NDT International, 11, 4, 175-178 (1978)

85. Acquaviva, S.J., Birchon, D., Carlyle, J.M., Faller, J.G., Graham, L.J., Hart, S.D., McBride, S.L., Scott, I.G., Stone, D.E.W., and Vanderveldt, H.H., "Interlaboratory Comparisons of Acoustic Emission Spectra", NDT International, 13, 5, 230-234 (1980)

86. Otnes, R.K., and Enochson, L., Digital Time Series Analysis, Wiley, New York (1972)

87. Beauchamp, K.G., Signal Processing Using Analog and Digital Techniques, Wiley, New York (1973)

88. Ramirez, R.W., The FFT: Fundamentals and Concepts, Tektronix, Beaverton, Oregon (1975)

89. Fundamentals of Signal Analysis, HP Application Note 243, Hewlett-Packard Co., Palo Alto California (1981)

90. Brigham, E.O., The Fast Fourier Transform, Prentice-Hall, Englewood Cliffs, New Jersey (1974)

91. Skolnik, M.I., Introduction to Radar Systems, McGraw-Hill, New York (1962)

92. RTE-IVB System Manager's Manual, HP Manual 92068-90006, Hewlett-Packard Co., Cupertino, California (1980)

93. RTE-IVB Terminal User's Reference Manual, HP Manual 92068-90002, Hewlett-Packard Co., Cupertino, California (1980)

94. RTE-IVB Programmer's Reference Manual, HP Manual 92068-90004, Hewlett-Packard Co., Cupertino, California (1980)

95. DOS-RTE Relocatable Library Reference Manual, HP Manual 24998-90001, Hewlett-Packard Co., Cupertino, California (1980)

96. RTE-IV Assembler Reference Manual, HP Manual 92067-90003, Hewlett-Packard Co., Cupertino, California (1980)

97. Seely, S., Dynamic Systems Analysis, Reinhold Publishing Co, New York (1964)

98. Spectrum Analysis . . . Pulsed RF, HP Application Note 150-2, Hewlett-Packard Co., Palo Alto, California (1971)

99. Spectrum Analysis . . . Noise Measurements, HP Application Note 150-4, Hewlett-Packard Co., Palo Alto, California (1973)

100. McBride, S.L., and Hutchison, T.S., Normalization of Impulse Stress Events by the Helium Gas Jet Method, Bulletin No. 7, Royal Military College, Kingston, Ontario (1978)

101. Kanninen, M.F., "An Augmented Double Cantilever Beam Model for Studying Crack Propagation and Arrest", International Journal of Fracture, 9, 1, 83-92 (1973)

102. Wadley, H.N.G., Furze, D.C., Scruby, C.B., and Eyre, B.L., The Effect of Isothermal Tempering upon the Acoustic Emission During Ductile Fracture of a Low Alloy Steel, AERE-R-9034, Atomic Energy Research Establishment, Harwell, Oxfordshire, September 1978

103. Wadley, H.N.G., and Scruby, C.B., Quantitative Acoustic Emission Studies During Deformation and Fracture: A Review, AERE-R-10353, Atomic Energy Research Establishment, Harwell, Oxfordshire, December 1981

104. Cooley, J.W., and Tukey, J.W., "An Algorithm for Machine Calculation of Complex Fourier Series", Mathematics of Computation, 19, 90, 297-301 (1965)